R-00-40

# Nuclear data for accelerator-driven transmutation

## Annual Report 1999/2000

A Atac, J Blomgren, C Johansson,
J Klug, N Olsson, P-U Renberg

Department of Neutron Research
and The Svedberg Laboratory
Uppsala University

September 2000

**Svensk Kärnbränslehantering AB**
Swedish Nuclear Fuel
and Waste Management Co
Box 5864
SE-102 40 Stockholm Sweden
Tel 08-459 84 00
+46 8 459 84 00
Fax 08-661 57 19
+46 8 661 57 19

ISSN 1402-3091
SKB Rapport R-00-40

# Nuclear data for accelerator-driven transmutation

## Annual Report 1999/2000

A Ataç, J Blomgren, C Johansson,
J Klug, N Olsson, P-U Renberg

Department of Neutron Research
and The Svedberg Laboratory
Uppsala University

September 2000

# Contents

VI. S. Dangtip, A. Ataç, B. Bergenwall, J. Blomgren, K. Elmgren, C. Johansson, J. Klug, N. Olsson, G. Alm Carlsson, J. Söderberg, O. Jonsson, L. Nilsson, P.-U. Renberg, P. Nadel-Turonski, C. Le Brun, F.-R. Lecolley, J.-F. Lecolley, C. Varignon, Ph. Eudes, F. Haddad, M. Kerveno, T. Kirchner and C. Lebrun, A facility for measurements of nuclear cross sections for fast neutron cancer therapy, *Nucl. Instr. Meth.* **A452** (2000) 484–504.

VII. S. Dangtip, N. Olsson, A. Ataç, B. Bergenwall, J. Blomgren, K. Elmgren, C. Johansson, J. Klug, G. Alm Carlsson, J. Söderberg, P. Nadel-Turonski, O. Jonsson, L. Nilsson, P.-U. Renberg, J.-F. Lecolley, F.-R. Lecolley, C. Varignon, M. Kerveno, F. Haddad and T. Kirchner, Partial and total kerma coefficients for carbon deduced from experimental double-differential cross sections at 95 MeV, (submitted to *Phys. Med. Biol.*)

VIII. Summary Record of the Twelfth Meeting of the Working Party on International Evaluation Co-operation (WPEC), JAERI, June 20 – 21, 2000, *OECD/NEA Report NEA/SEN/NSC/WPEC(2000)2.*

IX. Minutes of the 23rd Meeting of the International Nuclear Data Committee (INDC), IAEA, Vienna, May 24 – 26, 2000, *IAEA Report INDC/P(00)-15.*

# 1 Background

The present project, supported as a research task agreement by Statens Kärnkraftsinspektion (SKI), Svensk Kärnbränslehantering AB (SKB), Barsebäck Kraft AB (BKAB) and Vattenfall AB, started 1998-07-01. From 1999-01-01 the project also receives support from Försvarets forskningsanstalt (FOA). The primary objective from the supporting organizations is to promote research and research education of relevance for development of the national competence within nuclear energy.

The aim of the project is in short to:

- promote development of the competence within nuclear physics and nuclear technology by supporting licenciate and PhD students,
- push forward the international research front regarding fundamental nuclear data within the presently highlighted research area "accelerator-driven transmutation",
- strengthen the Swedish influence within the mentioned research area by expanding the international contact network,
- constitute a basis for Swedish participation in the nuclear data activities at IAEA and OECD/NEA.

The project is run by the Department of Neutron Research (INF) at Uppsala University, and is utilizing the unique neutron beam facility at the national The Svedberg Laboratory (TSL) at Uppsala University.

In this document, we give a status report after the second year (1999-07-01–2000-06-30) of the project.

# 2 Introduction

Transmutation techniques in accelerator-driven systems (ADS) involve high-energy neutrons, created in the proton-induced spallation of a heavy target nucleus. The existing nuclear data libraries developed for reactors of today go up to about 20 MeV, which covers all available energies for that application; but with a spallator coupled to a core, neutrons with energies up to $1 - 2$ GeV will be present. Although a large majority of the neutrons will be below 20 MeV, the relatively small fraction at higher energies still has to be characterized. Above $\sim$ 200 MeV, direct reaction models work reasonably well, while at lower energies nuclear distortion plays a non-trivial role. This makes the $20 - 200$ MeV region the most important for new experimental cross section data.

Very little high-quality neutron-induced data exist in this energy domain. Only the total cross section (Finlay et al., 1993) and the *np* scattering cross section have been investigated extensively. Besides this, there are data on neutron elastic scattering from UC Davis at 65 MeV on a few nuclei (Hjort et al., 1994). Programmes to measure neutron elastic scattering have been proposed or begun at Los Alamos (Rapaport and Osborne) and IUCF (Finlay et al., 1992), with the former resulting in a thesis on data in the $5° - 30°$ range on a few nuclei.

The situation is similar for (n,xp) reactions, where programmes have been run at UC Davis (Ford et al., 1989), Los Alamos (Rapaport and Sugarbaker, 1994) and TRIUMF

(Alford and Spicer, 1998), but with limited coverage in secondary particle energy and angle. Better coverage has been obtained by the Louvain-la-Neuve group up to 70 MeV (Slypen et al., 1994).

Thus, there is an urgent need for neutron-induced cross section data in the region around 100 MeV, which is an area where very few facilities in the world can give contributions. By international collaboration within an EU supported Concerted Action, which will be followed by the full scale project HINDAS, the level of ambition for the present project has been increased, and the potential of the unique neutron beam facility at The Svedberg Laboratory in Uppsala can be fully exploited.

# 3 Experimental setup and techniques

## 3.1 The TSL neutron beam facility

At TSL, quasi-monoenergetic neutrons are produced by the reaction $^7$Li(p,n)$^7$Be in a $^7$Li target bombarded by $50-180$ MeV protons from the cyclotron, as is illustrated in Fig. 1 (Condé et al., 1990, Klug et al., 2000). After the target, the proton beam is bent by two

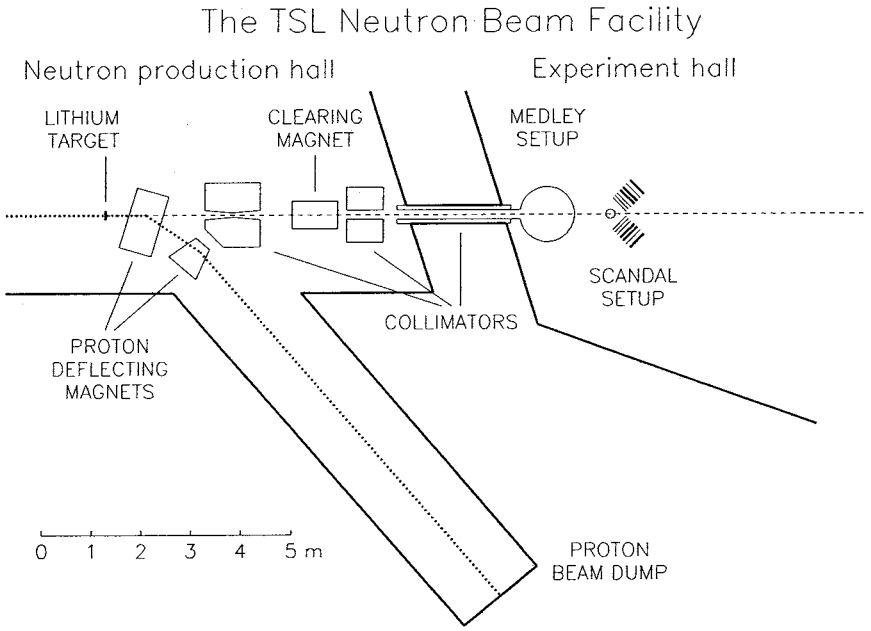


Figure 1: The TSL neutron beam facility.

dipole magnets into an 8 m long concrete tunnel, where it is focused and stopped in a well-shielded Faraday cup, which is used to measure the proton beam current. A narrow neutron beam is formed in the forward direction by a system of three collimators, with a total thickness of more than four metres.

The energy spectrum of the neutron beam consists of a high-energy peak, having approximately the same energy as the incident proton beam, and a low-energy tail. About half of all neutrons appear in the high-energy peak, while the rest are roughly equally distributed in energy, from the maximum energy and down to zero. The thermal contribution is small. The low-energy tail of the neutron beam can be reduced using

time-of-flight (TOF) techniques over the long distance between the neutron source and the reaction target (about 8 m).

The relative neutron beam intensity is monitored by integrating the charge of the primary proton beam, as well as by using thin film breakdown counters, placed in the neutron beam, measuring the number of neutron-induced fissions in $^{238}$U (Prokofiev et al., 1999).

Two multi-purpose experimental setups are semi-permanently installed at the neutron beam line, namely MEDLEY and SCANDAL. These will be described below.

## 3.2 The MEDLEY setup

The MEDLEY detector array (Dangtip et al., 2000), shown in Fig. 2, is designed for measurements of neutron-induced light-ion production cross sections of relevance for

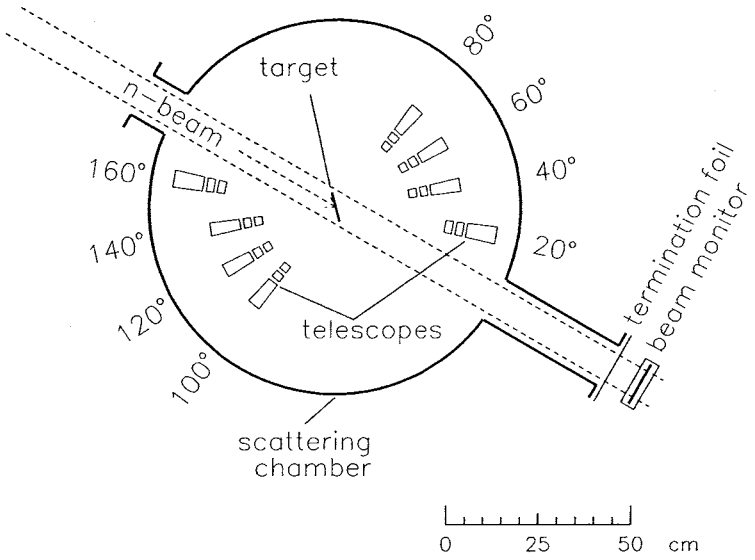


Figure 2: The MEDLEY detector array.

applications within ADS and fast-neutron cancer therapy and related dosimetry. It consists of eight particle telescopes, installed at scattering angles of 20° – 160° with 20° separation, in a 1 m diameter scattering chamber, positioned directly after the last neutron collimator. All the telescopes are fixed on a turnable plate at the bottom of the chamber, which can be rotated without breaking the vacuum.

Each telescope (Fig. 3) is a $\Delta E - \Delta E - E$ detector combination, where the $\Delta E$ detectors are silicon surface barrier detectors with thicknesses of 50 or 60 $\mu$m and 400 or 500 $\mu$m, respectively, while the $E$ detector is a 50 mm long inorganic CsI(Tl) crystal, tapered over the last 20 mm to fit the 18 × 18 mm photodiode readout. $\Delta E - \Delta E$ or $\Delta E - E$ techniques are used to identify light charged particles (p, d, t, $^3$He, $\alpha$). The chosen design gives a sufficient dynamic range to distinguish all charged particles from a few MeV up to more than 100 MeV.

The solid angle of the telescopes is defined by active collimators, designed as thin hollow plastic scintillator detectors, mounted on small photomultiplier tubes. A signal

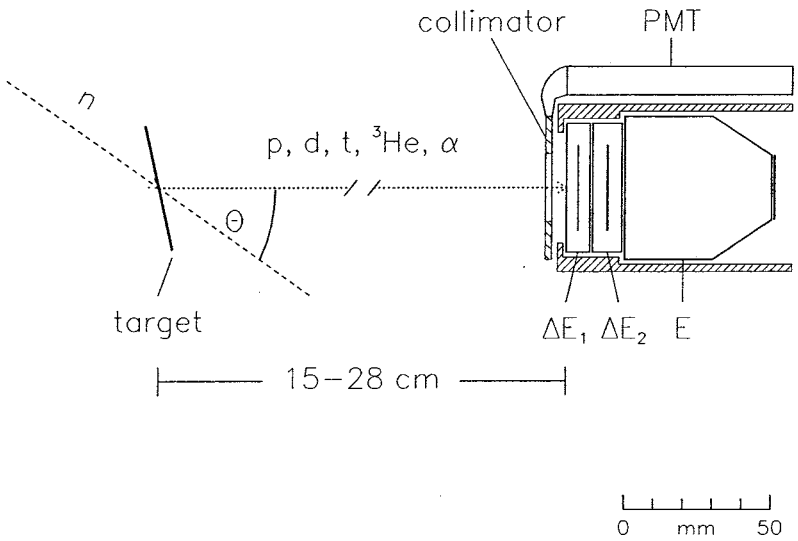


Figure 3: A MEDLEY telescope.

from such a detector is used to veto the corresponding event, thereby ensuring that only particles that pass inside the collimator are registered.

Energy calibration of the silicon detectors is performed by determining the pulse height for the various particles at the point where they start to punch through the detectors, with the assumption of linear correspondence between pulse height and energy. Alpha particles from a $^{241}$Am source are used to check the calibration curve for the first, thin $\Delta E$ detector. For the CsI detectors, the linear response assumption is no longer valid, and the calibration curve is determined particle by particle by plotting the calculated energy, derived from the energy deposited in the second silicon $\Delta E$ detector and standard stopping power data, versus the measured pulse height. The obtained calibration is checked by comparing with pulse heights of resolved states in, e.g., $^{12}$C(n,p) and (n,d) reactions, for which the energies are known. Adding the energy losses in the three detectors gives the incident energy for each charged particle. The energy resolution is typically about 2 MeV at 80 MeV.

Absolute cross section normalization is obtained by comparison with free $np$ scattering, using a $CH_2$ target. After proper subtraction of target-out and $^{12}$C(n,xp) background contributions, the cross section per count can be determined from the $np$ scattering peak, using data previously taken at a similar energy (Rönnqvist et al., 1992, Olsson et al., 2000). The normalization coefficient is then applied to the data for the target under study to get the absolute cross section.

## 3.3 The SCANDAL setup

The SCANDAL setup (Klug et al., 2000) is primarily intended for studies of elastic neutron scattering, i.e., (n,n) reactions. Neutron detection is accomplished via conversion to protons by the H(n,p) reaction. In addition, (n,xp) reactions in nuclei can be studied by direct detection of protons. This feature is also used for calibration, and the setup has therefore been designed for a quick and simple change from one mode to the other.

The device is illustrated in Fig. 4. It consists of two identical systems, in most cases located on each side of the neutron beam. The design allows the neutron beam to pass

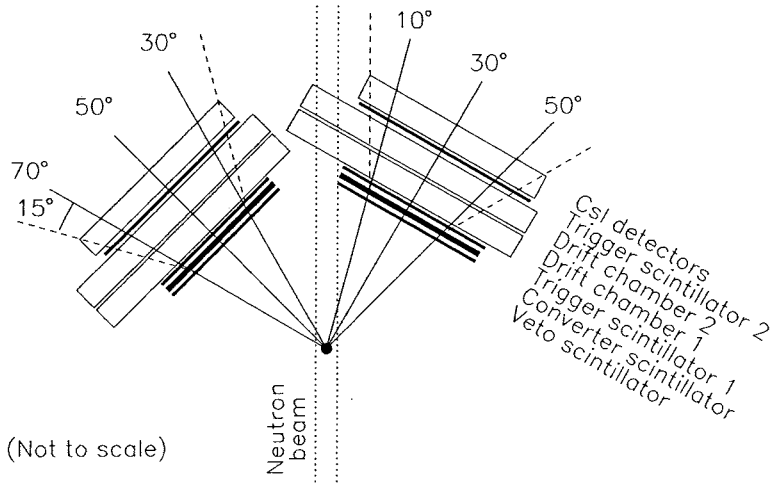


Figure 4: The SCANDAL setup

through the drift chambers of the right-side setup, making low-background measurements close to zero degrees feasible.

In neutron detection mode, each arm consists of a 2 mm thick veto scintillator for fast charged-particle rejection, a neutron-to-proton converter which is a 10 mm thick plastic scintillator, a 2 mm thick plastic scintillator for triggering, two drift chambers for proton tracking, a 2 mm thick $\Delta E$ plastic scintillator, which is also part of the trigger, and an array of 12 large CsI detectors for energy determination. The trigger is provided by a coincidence of the two trigger scintillators, vetoed by the front scintillator. The compact geometry allows a large solid angle for protons emitted from the converter. Recoil protons are selected using the $\Delta E$ and $E$ information from the plastic scintillators and the CsI detectors, respectively.

The response of the equipment has been carefully studied using carbon (March 1999) and $CH_2$ (November 1999) targets. The energy resolution is about 3.7 MeV (FWHM), which is sufficient to resolve elastic and inelastic scattering in several nuclei. The angular resolution is calculated to be about 1.4° (rms) when using a cylindrical scattering sample of 5 cm diameter.

When SCANDAL is used for (n,xp) studies, the veto and converter scintillators are removed. A multitarget arrangement can be used to increase the target content without impairing the energy resolution, which is typically 2.5 MeV (FWHM). This multitarget box allows up to seven targets to be mounted simultaneously, interspaced with multiwire proportional counters (MWPC). In this way it is possible to determine in which target layer the reaction took place, and corrections for energy loss in the subsequent targets can be applied (Thun et al., 2000). In addition, different target materials can be studied simultaneously, thus facilitating absolute cross section normalization by filling a few of the multitarget slots with $CH_2$ targets. The first two slots are normally kept empty, and used to identify charged particles contaminating the neutron beam.

The response in (n,xp) mode was tested in March 2000 by measuring *np* scattering, using $CH_2$ targets. The result is shown in Fig. 5, where it can be compared to a previous measurement of that cross section with a magnetic spectrometer (Rönnqvist

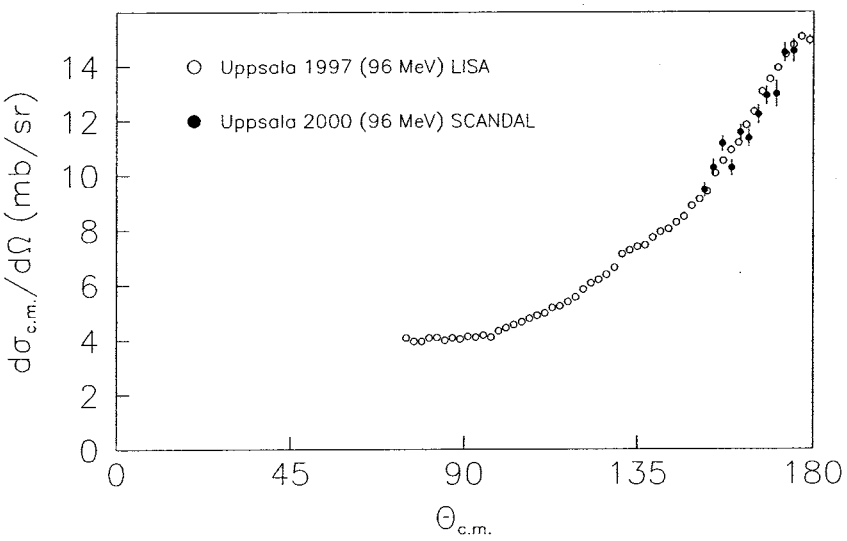


Figure 5: Backward *np* scattering cross sections as determined with the LISA magnetic spectrometer and with SCANDAL.

et al., 1992, Olsson et al., 2000). As can be seen, the data sets agree well within the statistical uncertainties.

# 4 Results and analysis

## 4.1 Elastic scattering

Elastic scattering of neutrons on $^{208}$Pb was studied in May, 2000. Since natural lead only contains about 50% $^{208}$Pb, we acquired an amount of thorium ore, highly enriched in $^{232}$Th, on the international market. In this radioactive ore, $^{208}$Pb is the end product of $^{232}$Th decay. To extract a pure sample of lead, a contract was signed between STCU and Institute of Colloid and Water Chemistry in Ukraine, and Uppsala University, in which the Ukrainian partners took on responsibility to process the ore. Thus, in early May we received about 400 g of lead, enriched to 88% in $^{208}$Pb. The material was casted in the shape of a cylinder, to be useful in the scattering measurements.

Data were collected for about one week of beam time, which was used for measurement with the lead target, but also $CH_2$ and carbon targets were used for absolute cross section determination. In addition, sample-out background measurements were performed. The two arms of SCANDAL were placed to cover the angular ranges $10° - 50°$ and $30° - 70°$, respectively.

The analysis of the scattering data has recently started, and angular distributions are not yet available. However, a preliminary energy spectrum of neutrons scattered at 9° is shown in Fig. 6. The tail on the right side of the elastic peak is not only the result of inelastic scattering, but is also affected by the response of the converter scintillator. The dotted curve illustrates the sample-out background, normalized to the same incident neutron flux as the lead data. As can be seen, this background is very small.

Some work remains before a complete angular distribution in the region $10° - 70°$ can be presented. Since the cross section falls off several orders of magnitude within this

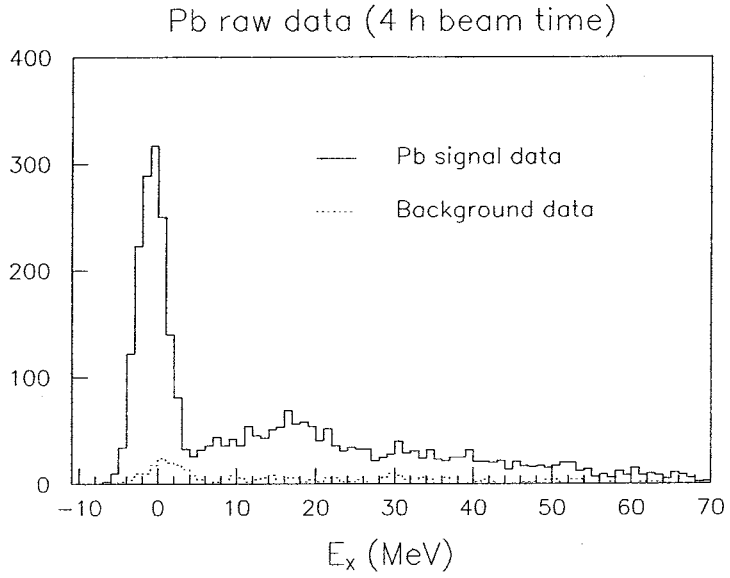


Figure 6: Double-differential cross section for the $^{208}$Pb(n,n) reaction at $E_n = 96.5$ MeV and $\theta = 9°$ (solid line). The corresponding background is also indicated (dotted line).

interval, it might be necessary to complement the data with a new measurement for the largest angles. It will be very interesting to see how well these data can be described by recent optical model representations (Koning).

## 4.2 (n,xlcp) reactions

In April 1999 and February 2000, we performed experiments to measure double differential cross sections $d^2\sigma/d\Omega dE$ for protons and other light charged particles (d, t, $^3$He, $\alpha$) emitted in reactions of 100 MeV neutrons on enriched $^{208}$Pb targets.

The charged particles were detected using MEDLEY, which allowed to measure continuum energy distributions in the forward direction ($10° - 80°$). At larger angles, in view of the relatively low intensity of the neutron beam and of the estimated small cross sections, only the low-energy part of the spectra could be measured ($E_p \leq 40$ MeV at $\theta = 160°$). To improve the counting rate at backward angles, at least for protons, we also used the multitarget arrangement together with the two arms of SCANDAL, which covered the angular range $10° - 140°$ in two settings. With this setup, the high-energy part ($E_p > 30$ MeV) of the proton spectra could be measured also at backward angles.

For the MEDLEY measurements, we used a 25 mm diameter by 0.5 mm thick lead target, enriched to 88% in $^{208}$Pb. Figs. 7a and b show typical $\Delta E_1 - \Delta E_2$ and $\Delta E_2 - E$ scatter plots, respectively, from 96.5 MeV neutron-induced charged-particle production reactions in lead at 20°. The energy threshold of the telescopes was about $2 - 3$ MeV for the hydrogen isotopes and about 9 MeV for the helium isotopes. Preliminary results from MEDLEY are presented in Figs. 8 and 9. The analysis is in progress. Fig. 8 shows the double differential cross section for protons emitted at 20° (filled circles) and 40° (open circles), while Fig. 9 displays the double differential cross section for protons (filled circles), deuterons (filled squares) and tritons (open circles) emitted at 20°.

In the SCANDAL measurement the multitarget contained five lead foils (each 220

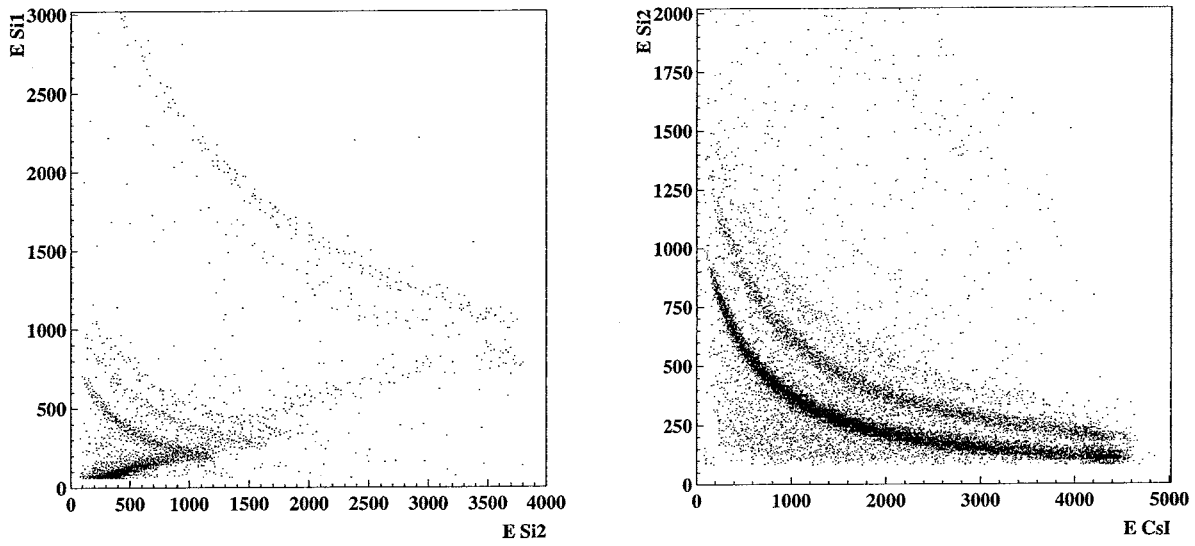


Figure 7: (a) $\Delta E$ vs. $\Delta E$ and (b) $\Delta E$ vs. $E$ scatter plots for $^{208}$Pb(n,xlcp) reactions at 96.5 MeV.

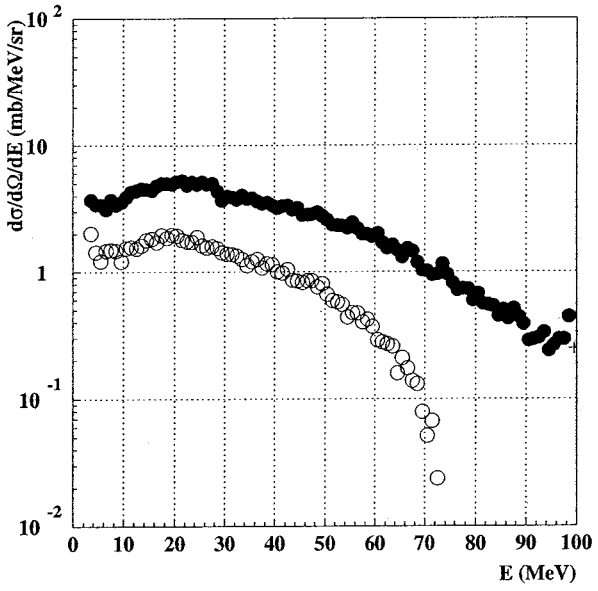


Figure 8: Preliminary double-differential cross section for the $^{208}$Pb(n,xp) reaction with $E_n$ = 96.5 MeV, and at 20° (filled circles) and 40° (open circles).

$\mu$m thick), one carbon foil (360 $\mu$m) and one $CH_2$ foil (360 $\mu$m). The carbon target was used to subtract the background contribution of protons from quasi-free neutron scattering in the carbon of $CH_2$. In addition to normalization, the *np* scattering data allowed to calibrate the CsI detectors using the well-defined two-body kinematics of that process. With the simultaneous measurement of the *np* scattering and Pb(n,xp) processes, the detection efficiency problem is in principle avoided. One needs, however, to evaluate the solid angle of the CsI detectors viewing the different finite targets. For

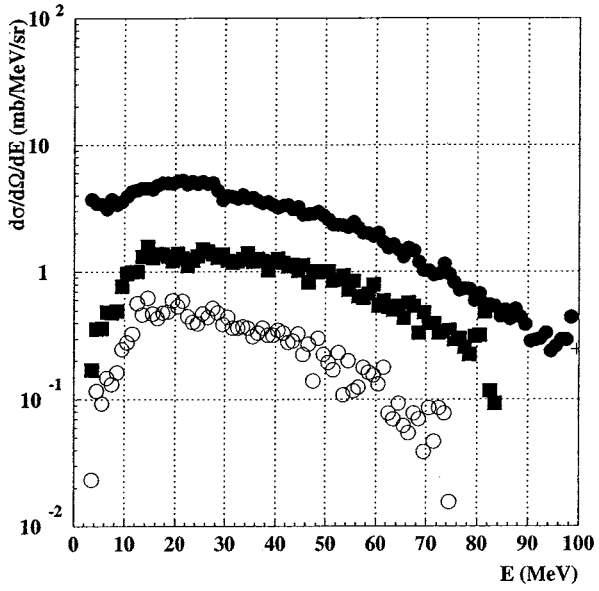


Figure 9: Preliminary double-differential cross section for $^{208}$Pb(n,xp) (filled circles), $^{208}$Pb(n,xd) (filled squares) and $^{208}$Pb(n,xt) (open circles) reactions at $\theta = 20°$.

these evaluations, we performed a simulation of the setup using the GEANT code of CERNLIB. Preliminary results of proton production above 35 MeV in lead are given for the scattering angles 18°, 24°, 35° and 55° in Fig. 10.

Similar measurements have been performed for $^{56}$Fe(n,$X$) at 100 MeV, using both SCANDAL (February 2000) and MEDLEY (May 2000). These data will be analysed after the corresponding work on the lead data has been completed.

# 5 International activities

## 5.1 Collaboration

The Uppsala group participates since 1998-08-01 in a CEC supported two-year Concerted Action, called "Physical aspects of lead as a neutron-producing target for accelerator transmutation devices". The aim of the project is to collect and structure available information on lead, and to make suggestions on what additional data are needed for this target material. The project is organized in ten work packages, of which our group is fully or partly involved in four.

The third and the fourth (and last) semi-annual meetings with the partners of the Concerted Action were held in Brussels 2000-01-28–29 and 2000-06-23–24, respectively, with Nils Olsson representing the Uppsala group. Progress reports were given by the various groups, and during the last meeting a final project report was drafted. This report will be delivered to the CEC in September.

The Concerted Action has been followed up by a proposal for a European collaboration on nuclear data for ADT, which was submitted to the 5th CEC program on October 4. The proposal, "High- and Intermediate Energy Nuclear Data for Accelerator-Driven Systems (HINDAS)", involves 16 European institutions from Belgium, France, Germany,

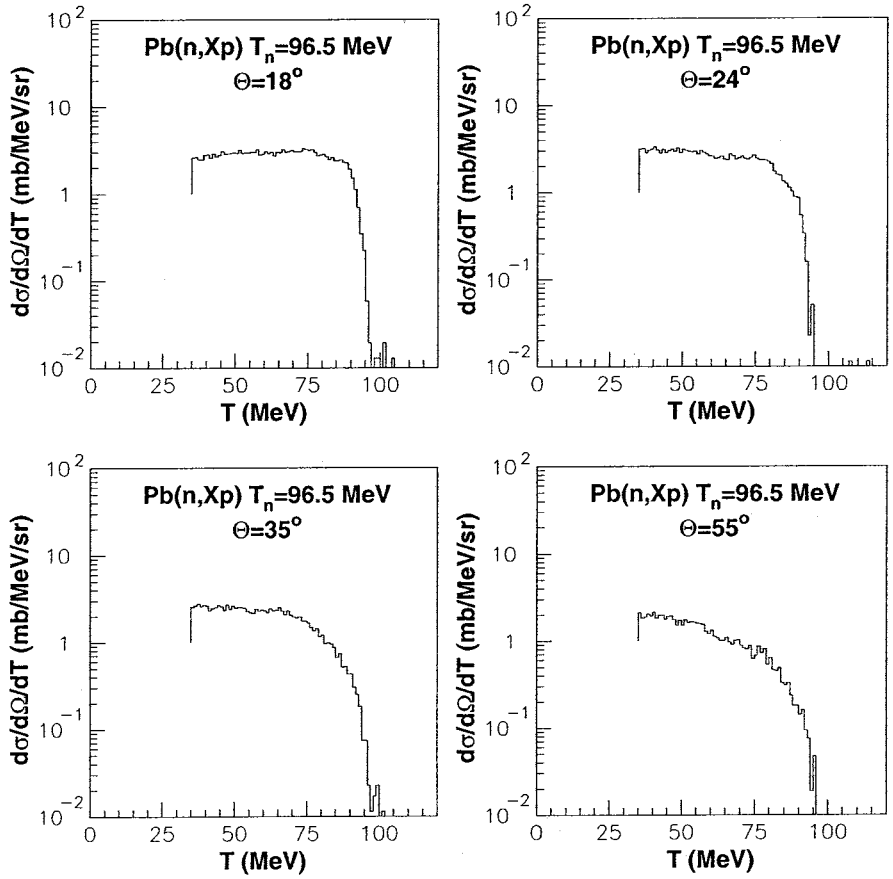


Figure 10: Preliminary double-differential cross section for the $^{208}$Pb(n,xp) reactions at $E_n$ = 96.5 MeV and $\theta$ = 18°, 24°, 35° and 55°.

The Netherlands, Spain, Sweden and Switzerland, and the experimental work will be performed at six European laboratories (UCL in Louvain-la-Neuve, TSL in Uppsala, KVI in Groningen, PSI in Villigen, COSY at Jülich and GSI in Darmstadt). Work on the theoretical interpretation of the experimental results is also included. The project is coordinated by Prof. Jean-Pierre Meulders, Louvain-la-Neuve, Belgium.

HINDAS was positively received by the CEC, and was approved at a level of 2.1 MEUR. Of this, 210 kEUR falls on the Uppsala partner, while the collaborators that use the TSL neutron facility will get: Subatech, Nantes (150 kEUR), LPC, Caen (150 kEUR), ZSR, Hannover (150 kEUR), PTB, Braunschweig (36 kEUR). Most of the money is intended for PhD students or postdocs. This means an increasing engagement for the Uppsala group and TSL, but also more focus on the activities here.

The project will start 2000-09-01 with the kick-off meeting in Brussels 2000-10-09, and run over three years.

For the Uppsala partner, a substantial fraction of the grant will be used to employ a postdoc, who can act as liaison between the Uppsala group and the collaborating groups. However, he/she will also strengthen the experimental competence in Uppsala, and be a complement to the existing supervisors at INF.

To our judgement, the proposal is well organized and focused. It involves a major part of the competence and equipment available in Europe, and will also contribute to

the development of nuclear data activities in Europe, by bringing new scientists into this area.

During August and December 1999, Jan Blomgren and four students, including Cecilia Johansson and Joakim Klug, participated in an experiment at Indiana University Cyclotron Facility, located in Bloomington, Indiana, USA. The experiment concerns neutron-proton scattering, which is closely related to our own activities, but with a rather different experimental technique. Such journeys are very beneficial for the students, who learn a lot by participating in the setting up of a complicated experiment, and also get experience of work in an international environment.

## 5.2 Meetings and conferences

Accelerator-based research in Uppsala celebrated its 50th anniversary on December 8, with a half-day symposium and a dinner. The celebration attracted some 200 participants. The symposium included talks on historical views, but also five talks about present and future research. One of these, "Applied neutron physics", was given by Nils Olsson.

The International Nuclear Data Committee (INDC) of the Nuclear Data Section (NDS) at IAEA held its 23rd meeting in Vienna 2000-05-24–26. During the meeting, the performance of the NDS was reviewed, and proposals for Co-ordinated Research Projects (CRP) and other data development projects were discussed. Among the eight projects recommended by the INDC, one was related to creating a nuclear reaction data base for accelerator applications. During the meeting, Nils Olsson gave a report on the Nuclear Data Research Activities in Sweden.

# 6 Administrative matters

## 6.1 Personnel and PhD students

From 2000-01-01 the Department of Neutron Research (INF) got a new research group, specialized on studies of nuclear structure and gamma-ray detection. This group is headed by Johan Nyberg, who has received a six-year position as senior researcher from NFR. The group includes a junior researcher, Matthias Weiszflog, also sponsored by NFR, and a PhD student. With this group, INF strengthens its competence in the mentioned areas of research.

In May, the professors chair in applied nuclear physics at INF was finally filled, after a vacancy period of five years. The new professor is Jan Källne, who is leading a large group in neutron diagnostics of fusion plasmas. This is a great step forward for the department, and it means that the subject of applied nuclear physics now is fully accepted and recognized at the university.

INF has had two PhD dissertations during the year, namely Marco Tardocchi who has worked with neutron diagnostics of fusion plasmas, and Anders Axelsson who spent his research efforts on nuclear structure. In September 2000, Somsak Dangtip will defend his thesis, which is related to cross section measurements of medical relevance, measured using MEDLEY.

The supervision within the present project is performed to limited extent by the project leader, Nils Olsson, and to a larger extent by Ayşe Ataç and Jan Blomgren. In the fall of 2000, a postdoc will also by employed using resources within the HINDAS project. Two PhD students are directly connected to and financed by the present project, namely Cecilia Johansson and Joakim Klug, which both are connected to the research school AIM (Advanced Instrumentation and Measurements). Two other students, Bel Bergenwall who is financed by AIM, and Udomrat Tippawan with a schoolarship from Thailand, have tasks strongly related to the present project, and especially to the line of development emerging from the collaboration with the French groups within HINDAS.

Members of our group participate in several courses on nuclear physics as well as on energy technology. Some of these include problems related to transmutation. Also more outreach talks, seminars, articles and interviews related to this project have been given.

## 6.2 Reference group

The third and fourth reference group meetings, with participation by Per-Eric Ahlström (SKB), Benny Sundström (SKI), Thomas Lefvert (Vattenfall AB), Fredrik Winge (BKAB) and Anders Ringbom (FOA), were held at SKB in Stockholm 2000-01-14, and in Uppsala 2000-06-15, respectively. Scientific and administrative reports on the progress of the project were given at these meetings.

In addition to the meetings, the progress of the work is continously communicated to the reference group members by short, written, quarterly reports.

# References


Alford W.P. and Spicer B.M., 1998, Nucleon charge-exchange reactions at intermediate energy, Advances in Nuclear Physics 24, 1.

Condé H., Hultqvist S., Olsson N., Rönnqvist T., Zorro R., Blomgren J., Tibell G., Håkansson A., Jonsson O., Lindholm A., Nilsson L., Renberg P.-U., Brockstedt A., Ekström P., Österlund M., Brady P., Szeflinski Z., 1990, A facility for studies of neutron induced reactions in the 50 - 200 MeV range, Nucl. Instr. Meth. A292, 121.

Dangtip S., Ataç A., Bergenwall B., Blomgren J., Elmgren K., Johansson C., Klug J., Olsson N., Alm Carlsson G., Söderberg J., Jonsson O., Nilsson L., Renberg P.-U., Nadel-Turonski P., Le Brun C., Lecolley F.-R., Lecolley J.-F., Varignon C., Eudes Ph., Haddad F., Kerveno M., Kirchner T., Lebrun C., 2000, A facility for measurements of nuclear cross sections for fast neutron cancer therapy, Nucl. Instr. Meth., in press.

Finlay R., Abfalterer W.P., Fink G., Montei E., Adami T., Lisowski P.W., Morgan G.L., Haight R.C., 1993, Neutron total cross sections at intermediate energies, Phys. Rev. C47, 237.

Finlay R., 1992, Proposal to the NSF for support of CHICANE/Spectrometer System for the IUCF Cooler Ring.

Ford T.D., Brady F.P., Castaneda C.M., Drummond J.R., McEachern B., Romero J.L., Sorenson D.S., 1989, A large dynamic range detector for measurement of neutron-induced charged particle spectra down to zero degrees, Nucl. Instr. Meth. A274, 253.

Hjort E.L., Brady F.P., Romero J.L, Drummond J.R., Sorenson D.S., Osborne J.H., McEachern B., 1994, Measurements and analysis of neutron elastic scattering at 65 MeV, Phys. Rev. C50, 275.

Klug J., Blomgren J., Ataç A., Bergenwall B., Dangtip S., Elmgren K., Johansson C., Olsson N., Rahm J., Jonsson O., Nilsson L., Renberg P.-U., Nadel-Turonski P., Ringbom A., Oberstedt A., Tovesson F., Le Brun C., Lecolley J.-F., Lecolley F.-R., Louvel M., Marie N., Schweitzer C., Varignon C., Eudes Ph., Haddad F., Kerveno M., Kirchner T., Lebrun C., Stuttgé L., Slypen I., Prokofiev A., Smirnov A., Michel R., Neumann S., Herpers U., 2000, SCANDAL - A facility for elastic neutron scattering studies in the $50 - 130$ MeV range, to be published.

Koning A., private communication.

Olsson N., Blomgren J., Condé H., Dangtip S., Elmgren K., Rahm J., Rönnqvist T., Zorro R., Jonsson O., Nilsson L., Renberg P.-U., Ringbom A., Tibell G., Ericson T.E.O., Loiseau B., 2000, Uppsala neutron-proton scattering measurements and the $\pi NN$ coupling constant, Physica Scripta T87, 7.

Prokofiev A.V., Smirnov A.N., Renberg P.-U., 1999, A monitor for intermediate-energy neutrons based on thin film breakdown counters, Report TSL/ISV-99-0203, Uppsala University.

Rapaport J. and Sugarbaker E., 1994, Isovector excitations in nuclei, Annu. Rev. Nucl. Part. Sci. 44, 109.

Rapaport J., private communication, and Osborne J., thesis, unpublished.

Rönnqvist T., Condé H., Olsson N., Zorro R., Blomgren J., Tibell G., Jonsson O., Nilsson L., Renberg P.-U., van der Werf S.Y., 1992, Backward angle $np$ differential cross sections at 96 MeV, Phys. Rev. C45, R496.

Slypen I., Corcalciuc V., Ninane A., Meulders J.P., 1994, Charged particles produced in fast neutron induced reactions on $^{12}$C in the $45 - 80$ MeV energy range, Nucl. Instr. Meth. A337, 431.

Thun J., Källne J., Varignon C., Blomgren J., Borne F., Elmgren K., Jonsson O., Lecolley J.-F., Ledoux X., Lefebvres F., Olsson N., Patin Y., Renberg P.-U., 2000, The response of a liquid scintillator detector to neutrons of energies between 21 and 100 MeV, to be published.

# Appendix I

ELSEVIER

Nuclear Physics A654 (1999) 939c–942c

NUCLEAR PHYSICS A

www.elsevier.nl/locate/npe

# Precise strength of the $\pi$NN coupling constant

T. E. O. Ericson*[,a,b], B. Loiseau[c], J. Rahm[a], J. Blomgren[a], N. Olsson[a] and A. W. Thomas[d]

[a]The Svedberg Laboratory, Box 533, S-75121 Uppsala, Sweden

[b]CERN, CH-1211 Geneva 23, Switzerland

[c]Université Pierre et Marie Curie, L.P.T.P.E., F-75252 Paris, France

[d]Special Research Center for the Subatomic Structure of Matter, University of Adelaide, Adelaide 5005, Australia

Abstract. We report here a preliminary value for the $\pi NN$ coupling constant deduced from the Goldberger-Miyazawa-Oehme sum rule for forward $\pi N$ scattering. As in our previous determination from np backward differential scattering cross sections we give a critical discussion of the analysis with careful attention not only to the statistical, but also to the systematic uncertainties. Our preliminary evaluation gives $g_c^2 = 13.99(24)$.

## 1. INTRODUCTION

The crucial coupling of low energy hadron physics is the $\pi NN$ coupling constant, which for the pseudoscalar interaction of a charged pion has the approximate value $g_c^2 \simeq 14$. One would like this quantity to be determined experimentally to a precision of about 1% for accurate tests of chiral symmetry predictions, such as the Goldberger-Treiman relation. Determinations of the coupling constant in later years are given in Table 1.

The Nijmegen group pointed out some years ago that the earlier determinations from the 1980's had important systematic uncertainties and they have since advocated values about 5% lower than the previous ones, mainly based on their analysis of $NN$ interactions [1]. However, these later determinations are, in general, not transparently linked to the underlying data and the systematic errors in the analysis are unknown. An exception is the GMO analysis by Arndt et al. [2]. Important physical constants are generally determined directly from experimental data with transparent, refutable procedures. The $\pi NN$ coupling constant should be no exception. We have therefore started a program of such determinations [3,4]. A first approach is based on single energy backward np differential cross sections, dominated by pion pole contributions. Following an old idea of Chew, the extrapolation to the pion pole at $t = -\mathbf{q}^2 = m_\pi^2$ gives directly $g^4$. But,

- previous data were not precise enough and in particular lacked absolute normalization,

*This work was partly done at the Research Center for the Subatomic Structure of Matter in Adelaide.

Table 1
Some important determinations of the pion-nucleon coupling constant

| Source | Year | System | $g^2_{\pi NN}$ | Reference |
|---|---|---|---|---|
| Karlsruhe-Helsinki | 1980 | $\pi$p | 14.28(18) | Nucl. Phys. **A336**, 331 (1980). |
| Kroll et al. | 1981 | pp | 14.52(40) | Physics Data **22-1**(1981). |
| Nijmegen [1] | 1993 | pp, np | 13.58(5) | Phys. Rev. C **47**, 512 (1993). |
| VPI | 1994 | pp, np | 13.7 | Phys. Rev. C **50**, 2731 (1994). |
| Nijmegen | 1997 | pp, np | 13.54(5) | ΠN Newsletter **13**, 96 (1997). |
| Timmermans | 1997 | $\pi^+$p | 13.45(14) | ΠN Newsletter **13**, 80 (1997). |
| VPI [2] | 1994 | GMO, $\pi$p | 13.75(15) | Phys. Rev. C **49**, 2729 (1994). |
| Uppsala [3] | 1995 | np→pn | 14.62(30) | Phys. Rev. Lett. **75**, 1046 (1995). |
| Uppsala [4] | 1998 | np→pn | 14.52(26) | Phys. Rev. C **57**, 1077 (1998). |

- the original extrapolation method requires a polynomial expansion with a large number of terms, which makes systematics in the extrapolation obscure.

These deficiencies have been largely eliminated [3,4]. High precision absolutely normalized differential np cross sections have recently been measured at 96 and 162 MeV by the Uppsala neutron group. Furthermore, we have replaced the original Chew method by a Difference Method for which the extrapolation is required only for the difference between the actual cross section and value for the coupling constant. The extrapolation now only concerns a correction and can be done with far greater simplicity and confidence. Figure 1 demonstrates concretely how we make such an extrapolation. Note the strong improvement in the quality of the experimental data from the older Bonner [5] data to the new Uppsala data at the same energy.

How good is this method? We have tested it using over 10000 pseudoexperiments generated from models with known coupling constant with 'experimental' points equivalent to actual observed ones. The original coupling constants are regenerated with an accuracy of about $\pm 1\%$. The method is therefore well under control.

The experimental differential cross sections have closely similar shape over a wide band of energies and any energy is as good as another for extrapolation purposes. The experimental data from Uppsala have been obtained in dedicated measurements, in contrast with previous data. They agree accurately with the shape of similar experiments at other energies by the PSI group [6], but differ in shape with data, mainly from Los Alamos [5]. This discrepancy is presently not fully resolved. (For a different opinion on the Uppsala data and the extrapolation procedure, see the Comment by de Swart et al. and our rebuttal, in Phys. Rev. Letters **81** issue 22, November 30, 1998). A critical discussion of the experimental situation has been made by Blomgren et al. [7]. Using the most recent Uppsala data gives $g_c^2 = 14.52(26)$ [4].

## 2. THE GOLDBERGER-MIYAZAWA-OEHME RELATION

In order to obtain additional model-independent information we (T. E. O. Ericson, B. Loiseau, A. W. Thomas) evaluate at present the Goldberger-Miyazawa-Oehme (GMO)

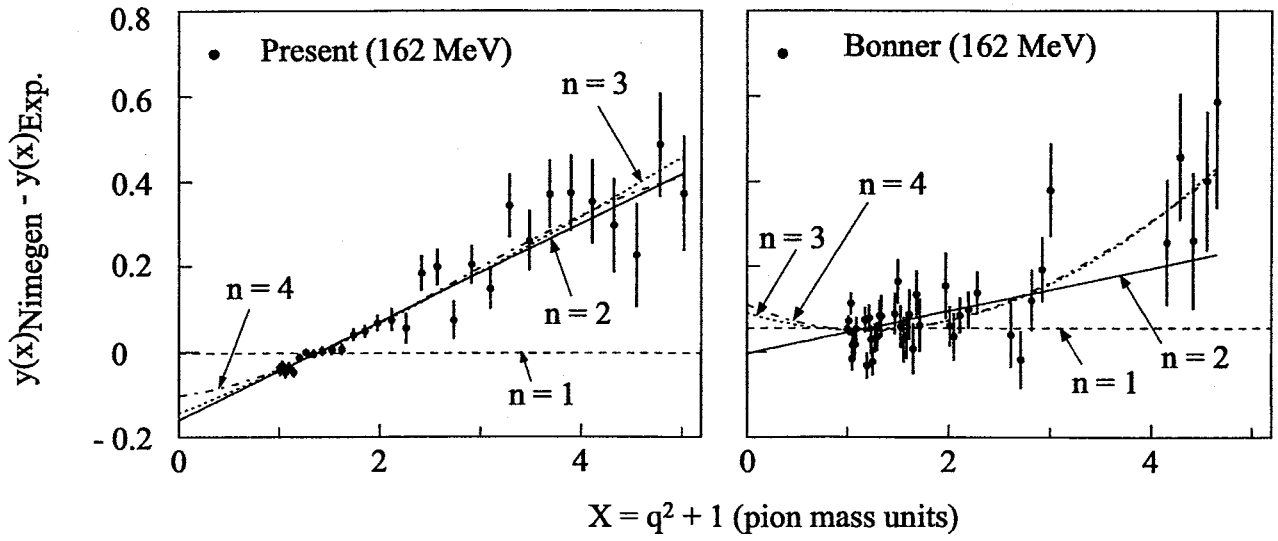


Figure 1. Extrapolations of the Chew function $y(q^2)$ to the pion pole at 162 MeV with the Difference Method using Nijmegen 93 as comparison model and different polynomial order n. Left figure Uppsala data, right figure Bonner data. For n=2 $g_c^2$(Uppsala)=14.52(26); for n=3 $g_c^2$(Bonner)=12.95(37); the Bonner data are normalized to SM95.

sumrule for $\pi$N forward scattering [8] in terms of the $\pi N$ scattering lengths and total cross sections. Assuming only charge symmetry:

$$g_c^2 = -4.50J^- + 103.3(\frac{a_{\pi^-p} - a_{\pi^+p}}{2}). \quad (1)$$

Here $J^-$ is given in $mb$ by the integral $J^- = -(1/4\pi^2)\int_0^\infty(\sigma^T_{\pi^+p} - \sigma^T_{\pi^-p})/\sqrt{k^2+m_\pi^2}dk$ and $a_{\pi^\pm p}$ are expressed in units of $m_{\pi^+}^{-1}$.

Everything is in principle measurable to good precision. Still this expression has not been too useful in the past because the scattering lengths were theoretically constructed from the analysis of scattering at higher energies. Recent splendid experiments at PSI determine the $\pi^-$p and $\pi^-$d energy shifts and widths in pionic atoms and from that the corresponding scattering lengths follow accurately [9]. We have critically examined the situation with careful attention to errors. In particular, we have examined the accuracy of the constraints due to pion-deuteron data.

In order to get a robust evaluation we write the relation as

$$g_c^2 = -4.50J^- + 103.3a_{\pi^-p} - 103.3(\frac{a_{\pi^-p} + a_{\pi^+p}}{2}). \quad (2)$$

Using $J^- = -1.077(47)$ $mb$ [10,11] and the experimental $\pi^-$p scattering length [9]

$$g_c^2 = 4.85(22) + 9.12(8) - 103.3(\frac{a_{\pi^-p} + a_{\pi^+p}}{2}) = 13.97(23) - 103.3(\frac{a_{\pi^-p} + a_{\pi^+p}}{2}). \quad (3)$$

Here the last term is a small quantity which we can evaluate with small statistical and systematic uncertainties from the experimental $\pi^-$d scattering length. The cross section

integral $J^-$ is presently the largest source of error. Uncertainties from the small deuteron term will not have a major impact on the result which is stable. Evaluating this last term from the impulse approximation only would increase $g_c^2$ by 1.25(5). However, double s wave scattering decreases $g_c^2$ by $-1.08$, while smaller correction terms come from the p wave Fermi motion (+0.24), the dispersive correction from absorption ($-0.18(4)$) [12] and the s-p wave double scattering interference term ($-0.21$) [13]. To exploit the present experimental precision the dominant double scattering term must be controlled to better than 10%, while other corrections require little more than estimates. Of these terms the s-p interference term is presently not fully elucidated. It depends on short range behavior and may be partly spurious. Using the correction terms from refs. [12] and [13] we find a preliminary value $g_c^2 = 13.99(24)$ including the s-p interference term and 14.20(24) excluding it.

In conclusion, we have now two independent methods with controllable errors for the coupling constant. The Difference Method gives 14.52(26) or a 2% error. Its future expected improvements are a) a full angular range, which will give normalization to $\pm 1\%$ (now $\pm 2\%$) and b) several incident neutron energies (which in principle should contain very similar information) from which the future precision is expected to reach $\pm 1.5\%$. The GMO relation gives the preliminary value 13.99(24) or $\pm 2\%$. The expected improvements are in the dispersion integral evaluation, now $\pm 4.6\%$ to $\pm 2$ to 3%, which leads to a precision in the coupling constant of $\pm(1$ to $1.5)\%$.

In summary, the two model independent methods which have been critically examined here provide no support for the low value for the coupling constant, close to 13.5, which has been advocated elsewhere. The lower value cannot be completely excluded at present, but better data and careful analysis should settle the issue.

## REFERENCES


1. V. Stoks, R. Timmermans, and J.J. de Swart, Phys. Rev. C **47**, 512 (1993).
2. R.A. Arndt, R.L. Workman, and M.M. Pavan, Phys. Rev. C **49**, 2729 (1994).
3. T.E.O. Ericson, B. Loiseau, J. Nilsson, N. Olsson, J. Blomgren, et al., Phys. Rev. Lett. **75**, 1046 (1995).
4. J. Rahm, J. Blomgren, H. Condé, *et al.*, Phys. Rev. C **57**, 1077 (1998).
5. B.E. Bonner, J.E. Simmons, C.L. Hollas, et al., Phys. Rev. Lett. **41**, 1200 (1978).
6. W. Hürster, T. Fischer, G. Hammel, K. Kern, M. Kleinschmidt, et al., Phys. Lett. **B90**, 367 (1980) and private communication.
7. J. Blomgren, N. Olsson, and J. Rahm, "The $\pi NN$ Coupling Constant and the Shape and Normalization of *np* Scattering Cross Sections," to be published.
8. M. L. Goldberger, H. Miyazawa, and R. Oehme, Phys. Rev. **99** (1955) 986.
9. D. Chatellard, J.-P. Egger, E. Jeannet, *et al.*, Nucl. Phys. **A625** (1997) 310.
10. R. Koch, Karlsruhe preprint TKP85-5 (1985).
11. Preliminary evaluations by R. Arndt, private communication, and by ourselves give similar values.
12. I. R. Afnan and A. W. Thomas, Phys. Rev. C **10** (1974) 109.
13. V. V. Baru and A. E. Kudryatsev, Phys. Atom. Nucl. **60** (1997) 1475 and private communication.

# Appendix II

Physica Scripta. Vol. T87, 7–13, 2000

# Uppsala Neutron-Proton Scattering Measurements and the πNN Coupling Constant

N. Olsson[1], J. Blomgren[1], H. Condé[1], S. Dangtip[1], K. Elmgren[1], J. Rahm[1], T. Rönnqvist[1], R. Zorro[1], O. Jonsson[2], L. Nilsson[2], P.-U. Renberg[2], A. Ringbom[3], G. Tibell[3], T. E. O. Ericson[4] and B. Loiseau[5]

[1] Department of Neutron Research, Uppsala University, Box 535, S-75121 Uppsala, Sweden
[2] The Svedberg Laboratory, Uppsala University, Box 533, S-75121 Uppsala, Sweden
[3] Department of Radiation Sciences, Uppsala University, Box 535, S-75121 Uppsala, Sweden
[4] CERN, CH-1211 Geneva 23, Switzerland, and The Svedberg Laboratory, Uppsala University, Box 533, S-75121 Uppsala, Sweden
[5] Laboratoire de Physique Nucléaire et de Hautes Energies et Laboratoire de Physique Théorique des Particules Élémentaires, Universités D. Diderot et P. & M. Curie, 4 Place Jussieu, 75252 Paris Cedex 05, France

*Received October 8, 1999; accepted November 1, 1999*

PACS Ref: 13.75.Cs, 13.75.Gx, 21.30.-x

**Abstract**

The differential np scattering cross section has been measured at 96 MeV and 162 MeV at backward angles at the neutron beam facility of the The Svedberg Laboratory in Uppsala. The angular distributions have been normalized to the experimental total np cross section. Between 150° and 180°, the angular distributions are steeper than for most previous measurements and nucleon-nucleon potential predictions, but for all the angular range covered, the data agree very well in shape with the recent PSI data. At 180°, the difference versus older data amounts to about 10%, implying serious consequences because of the fundamental importance of this cross section. Values of the charged πNN coupling constant have been extracted from the data.

## 1. Introduction

The interest in cross section measurements involving high-energy neutrons is increasing rapidly. This is motivated by a number of emerging applications, such as fast neutron cancer therapy, accelerator-driven transmutation technologies, dose delivery to airfare crew, and the very rapidly growing problem with electronics failures induced by high-energy cosmic-ray neutrons. For all these areas, neutrons in the few ten to few hundred MeV energy range play key roles.

The np scattering cross section has a large impact on all these applications. The reason is that the np cross section is used as a primary standard for measurements of other neutron-induced cross sections in the $0-350$ MeV region [1], i.e., those other cross sections are normalized to that of np scattering. In particular the 180° np cross section, i.e., the H(n,p) cross section at 0°, is used for normalization purposes. This cross section therefore has to be known to high precision, *irrespective of its theoretical interpretation.*

In the present situation, with significant discrepancies in the experimental data base (see the contribution by Blomgren *et al.* elsewhere in these proceedings), and conflicting results after theoretical analysis of the data, we have concluded that our first priority should be to try to establish new data with good control of systematic uncertainties. The present work represents such an attempt. This paper will therefore be concentrated on experimental and analysis aspects, and be more brief on the interpretation of the data.

Although the main motivation of the present work is of applied character, these data are also of interest in investigations of the fundamental properties of the NN interaction. Data on np scattering have also been used to extract a value of the πNN coupling constant. Presently, there is an intense debate on the actual value of this constant, but also on which techniques to employ in its determination. The conflicting results of different approaches have forced a critical reappraisal of the entire reasoning on which the previous values were based. It has therefore become of interest to determine $g^2_{\pi^\pm}$ and $g^2_{\pi^0}$ to high precision, convincingly and model-independently [2].

## 2. Experimental arrangement

The experimental setup and procedure have been described in detail recently [3,4], and therefore only a brief summary will be given here. The 162 MeV results have been published recently by Rahm *et al.* [3], while part of the results at 96 MeV have been published by Rönnqvist *et al.* [5], and the remaining 96 MeV data are to be published [6].

The TSL neutron beam facility is shown in Fig. 1. Protons from the cyclotron impinge on the neutron production target from the left in the figure. Neutrons are produced by the $^7$Li(p,n)$^7$Be reaction, using a 214, 427 or 821 mg/cm$^2$ thick lithium target (depending on incident energy and angular range to be studied), enriched to 99.98% in $^7$Li. After the target, the proton beam is bent into a well-shielded beam

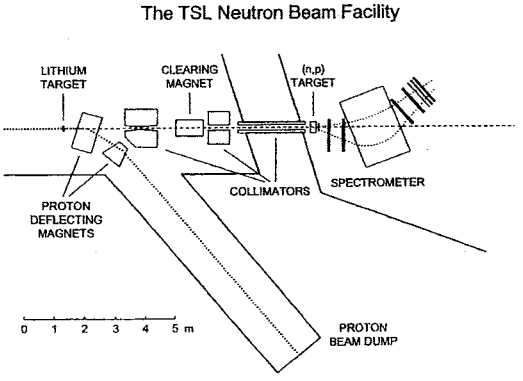


*Fig. 1.* Overview of the Uppsala neutron beam facility. The neutron production, shielding and collimation are shown, as well as the magnetic spectrometer arrangement.

dump. The neutron beam is defined by a 1.1 m long iron collimator, with two other collimators serving as beam scrapers. The vacuum system is terminated after the first collimator with a 1 mm thick aluminium plate. Charged particles produced in this plate are deflected by a clearing dipole magnet. The diameter of the neutron beam at the np target position, 8 m from the neutron production target, is about 7 cm. The neutron yield is in the order of $10^5 - 10^6$ $s^{-1}$ over the full target area. The centroid of the full energy peak in the neutron spectrum is determined to $96 \pm 0.5$ MeV and $162 \pm 1$ MeV. The total energy spread in the peak is estimated to be 0.9 MeV (FWHM) at 96 MeV, and 1.3 and 2.3 MeV at 162 MeV, for which two lithium target thicknesses are used.

To maximize the count rate without impairing the energy resolution, a sandwiched multi-target system is used. It consists of thin target layers interspaced by nine multi-wire proportional chambers (MWPCs), each having an efficiency of $\geq 99\%$. In this way, it is possible to determine in which target the scattering or reaction takes place, so that corrections for energy losses in the subsequent targets can be applied. The first two MWPCs provides veto signals for rejection of the few charged particles that contaminate the neutron beam. The target box contains five 35/100 mg/cm$^2$ thick $CH_2$ targets and two 85/185 mg/cm$^2$ $^{12}C$ targets for the 96/162 MeV measurements. The carbon targets are used for subtraction of the carbon contribution to the $CH_2$ spectra. The targets are stacked in the following (downstream) order: 2 $CH_2$, 2 carbon and 3 $CH_2$ layers.

The momentum determination of the charged particles emitted from the targets is performed with a spectrometer consisting of a dipole magnet and four drift chambers (DCHs) [7], two in front of and two behind the magnet. The scattering angle is determined by the trajectory through the first two DCHs. The detection efficiency for a drift chamber plane is typically $\geq 98\%$. To minimize the multiple scattering of charged particles in air, the space between the first two DCHs and the volume in the pole gap is filled with helium gas.

The trigger signal is generated by a small 1 mm thick plastic scintillator, located immediately after the multi-target box and an array of large plastic scintillators, positioned behind the last DCH. These large plastic scintillators are of thicknesses 2, 4 and 10 mm, respectively. Different trigger conditions were used for different energies and angular ranges. The relatively low counting rate allowed very generous trigger conditions to be used for all settings, thereby diminishing the risk of inadvertently rejecting good events.

The entire setup can be rotated around a pivot point, located below the centre of the multi-target box. With one position and one magnetic field setting, the spectrometer has a horizontal angular acceptance of about 15° in the laboratory system. Measurements are performed with up to five different settings of the spectrometer position. The angular regions covered were $\theta_{CM} = 168 - 180°$, 148 – 180°, 148–174°, 128 – 158° and 116 – 154° in the previous measurement at 96 MeV by Rönnqvist *et al.*, 98 – 128° and 74 – 110° in the recent 96 MeV measurement, and 152–180°, 136 – 168°, 118 – 154°, 88 – 130° and 72 – 108° in the 162 MeV measurement. The data have been binned into two-degree intervals. The energy resolution in the measured spectra is typically in the range 3 – 7 MeV (FWHM). The angular resolution due to multiple scattering is estimated to be 0.3° – 1.3° (rms). The best energy and angular resolutions are obtained in the 140 – 180° range.

## 3. Data analysis

### 3.1. *Data reduction and corrections*

The data are analyzed off-line on an event-by-event basis. Before an event is accepted, a number of tests is applied. A brief summary of the analysis procedure is given below. More detailed information about the data reduction has been given in Ref. [3].

Events originating from charged particles contaminating the neutron beam, or from charged-particle production in the thin scintillator just after the target system, are rejected. The scattering angle is determined by calculating the particle trajectory through the first two DCHs, using both the horizontal and vertical coordinate information. The particle momentum is determined by a ray-tracing procedure, using magnetic field maps and position information from the DCHs. Three DCHs are required for this purpose. The use of the fourth DCH offers a possibility for a redundancy check. The few events with dubious energy determination, or with a trajectory outside the magnetic field limits or an origin outside the neutron beam spot are rejected. To avoid vertical acceptance corrections, a narrow software gate of typically ±0.8° is applied on the vertical scattering angle, ensuring that no events are lost in the magnetic gap. For the largest magnetic fields, there is a stronger vertical focusing, which allows slightly larger gates, up to ±1.2°, to be used. The momentum information, in combination with the pulse heights from two of the large scintillators, is used to discriminate between protons and other charged particles (almost exclusively deuterons).

All accepted events are stored in matrices with angular and energy binning in the laboratory system of 1° and 0.25 MeV, respectively. Before extracting the hydrogen peak content, the carbon contribution to the $CH_2$ spectra is subtracted.

The np scattering peak contents are determined by integration. Since the energy resolution varies with angle, different integration windows are used. These are defined in a consistent way, and the final peak contents are determined by integrating the data in a region of $\pm\Delta E$ around the centroid, where $\Delta E$ is the peak FWHM. With this definition, the carbon background amounts to maximum 25% of the hydrogen peak for the largest recoil angles.

The variation of the width of the np peak with angle also causes an angular dependence in the background contribution from the low-energy continuum of the $^7Li(p,n)$ reaction. The data are corrected for this effect by using experimental neutron spectra from this reaction determined by Byrd and Sailor [8] at $E_p = 90.1$ MeV and 139.9 MeV. To simulate the finite resolution of our experiment, the Byrd and Sailor spectra, which have a much better resolution than in the present experiment, are folded with Gaussian resolution functions. From these folded spectra, the neutron continuum contribution to the peak, as defined above, can be determined as a function of peak width, and appropriate relative correction factors (< 5%) can be determined.

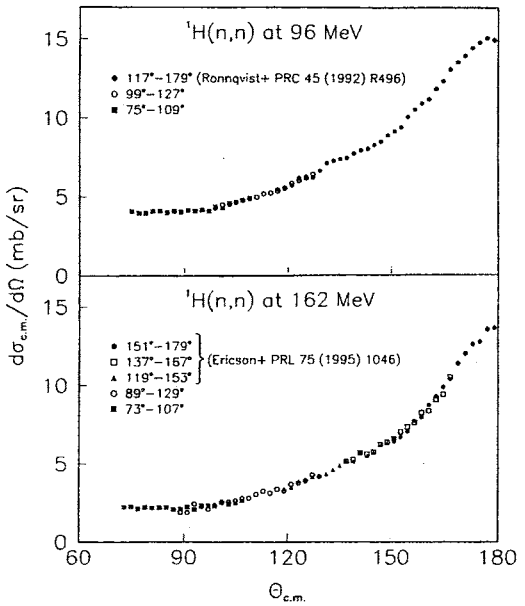


*Fig. 2.* Relative differential np scattering cross sections at 96 and 162 MeV. The data sets were normalized to each other in the overlapping regions.

Since the energy of the recoil protons varies with scattering angle, the variation of the proton absorption with energy in the detector system has to be taken into account. To first order, elastic in- and out-scattering of protons cancel, and thus only non-elastic losses have to be considered. We have calculated these losses in the targets, detectors and helium gas, using the total reaction cross sections given by Carlson [9]. The proton attenuation gives non-negligible corrections only in the angular region below $\theta_{c.m.} = 110°$, and the maximum correction amounts to 1.8%.

### 3.2. *Relative cross sections and uncertainties*

The relative cross section data from the different spectrometer settings, all treated as relative cross sections, are matched pairwise in the overlapping regions using a minimum $\chi^2$ criterion [3]. The $\chi^2$ per degree of freedom is typically around 1. The result of this matching is shown in the c.m. system in Fig. 2. As can be seen, the agreement in shape in the overlapping regions is very good. Final relative np scattering cross sections are obtained by averaging the data from the different data sets in each 2° (c.m) angular bin.

A good test of the reliability of this procedure is provided by the Rönnqvist 96 MeV data, where part of the data were obtained with a different spectrometer configuration, resulting in many overlapping sets. Also in this case the $\chi^2$ per degree of freedom is about 1 for all overlapping regions. Furthermore, there is no systematic shape difference between distributions with similar angular coverage, which is also verified by the small $\chi^2$'s mentioned above.

At the time of these experiments, no external monitor was available, and we have therefore normalized the relative data by this overlap technique. (Such a monitor has recently been installed, and will be used for future measurements.) Even if such a monitor were at hand, this overlap technique had to be used anyway, because these angular distributions were recorded in separate runs, spanning over several years.

Many sources of uncertainties contribute to the total error in the relative cross section. These errors are of both random and systematic character. Since the measurement is relative, only those systematic errors that affect the shape of the angular distribution have to be considered.

The random error is dominated by counting statistics, giving a contribution in the range 1.0% to 3.8% per point. The smaller value is valid for the data at most backward angles. Another small, random error contribution is due to bin truncation when integrating the np peak. This error is at most 0.6% per point.

The most important contribution to the systematic error is related to the subtraction of the carbon background in the $CH_2$ energy spectra. Above about 145° the hydrogen peak is well separated from the carbon spectrum (*Q-value* = −12.6 MeV), and below 125° the hydrogen peak is superimposed on a flat carbon continuum. In the latter region the uncertainty in the relative thickness of the $CH_2$ and pure carbon targets introduces an error in the np cross section. With an estimated relative thickness uncertainty of 5%, the error in the angular region 75° – 125°/73° – 135° (96/162 MeV) is less than 0.7% and 1.0%, respectively.

In the angular range 125° – 145°/135° – 155° (96/162 MeV) the hydrogen peak interferes with the rising slope of the carbon background. Hence, a small error in the relative energy loss corrections for the $CH_2$ and carbon spectra, respectively, affects the background subtraction. This causes an error in the determined np cross section of < 2%, using an estimated relative energy uncertainty of ±1 MeV. The problems arising from this effect can be seen in the 96 MeV data around 133°. Since the effect occurs in the middle of one of the angular settings, it is not expected to contribute significantly to a possible progressive shape uncertainty arising from the overlap normalization procedure.

The correction (< 5%) for the contribution from the low-energy continuum of the $^7$Li(p,n) spectrum to the np scattering peak introduces a systematic error that varies with the peak width and thus with the angle. Assuming a relative uncertainty of 10% in the correction, an error in the data of at most 0.5% arises.

The error from the small correction due to the energy-dependent attenuation of the protons is estimated to be less than 0.6%.

When adding the various systematic uncertainties quadratically, the total systematic error varies from 0.3% to 2.0% in the full angular region. The largest errors are found in the range $\theta_{c.m.} = 125° – 145°/135° – 155°$ (96/162 MeV).

In addition to the random and systematic errors discussed, the shape of the full angular distribution is affected by the matching of the data sets. A quadratic addition of the uncertainties in the fitted coefficients, emerging mainly from the finite counting statistics, results in a shape error between the most forward and most backward data sets, i.e., in the 75°/73° to 179° cross section ratio (96/162 MeV). This error is ±2.1% and ±2.6% for the 96 and 162 MeV data, respectively.

There could in principle be additional slope errors caused by small inhomogenities in the drift chamber efficiencies, which could be amplified from one setting to the next one. This does not seem probable, however, because these

chambers have shown a very uniform efficiency in a number of experiments. In addition, about 75% of the angular distribution, i.e., from 75°/73° to 153°, is extremely well described by a few recent partial-wave analyses (PWA). The $\chi^2$ per degree of freedom, after optimum fitting, is 0.95/2.54 and 1.27/1.19 (96/162 MeV) with respect to the NI93 [10] and SM95 [11] PWA's, respectively. Deviation from these models is found only beyond 155°, which is within one of the angular settings, and more or less outside the overlap region for the next setting.

Thus, all the deviation from the PWA's are within one setting, and this deviation in shape is about 10%. The drift chamber average efficiency is 98%, which means that if there would be a linear variation with position (which is highly unlikely), it could at most be 100% at one end and 96% at the other, which would not account for more than part of the effect.

### 3.3. *Normalization procedure*

Absolute np scattering cross sections are obtained by normalization to the total np cross section, which can be done since other reaction channels are negligible below 270 MeV. The total cross section $\sigma_T$ has been experimentally determined around 100–160 MeV by several groups, and is considered to be well known. If the entire angular range, i.e., from 0° to 180°, had been measured in the present experiment, it would have been possible to normalize the data to the total cross section directly by integration. Since that is not the case, we consider our angular distribution as a measurement of a *fraction* of the total cross section, i.e., the part between 74°/72° and 180°. By using a number of PWA's or potential models, it is possible to estimate the magnitude $F$ of this fraction, to which the data should be normalized. Thus, we require that the integral over the solid angle of our data should be equal to

$$\sigma_{74°/72°-180°} = \int_{74°/72°}^{180°} \frac{d\sigma}{d\Omega} d\Omega = F\sigma_T^{exp}, \quad (1)$$

where

$$F = \sigma^{PWA}_{74°/72°-180°}/\sigma_T^{PWA}. \quad (2)$$

To obtain $\sigma_T^{exp}$, we have used the Los Alamos data of Lisowski *et al.* [12], the Harvard data of Measday and Palmieri [13], and the PSI data of Grundies *et al.* [14]. The total error of these data sets is below 1%, about 4%, and less than 1.5%, respectively, and they are in very good agreement.

The total cross section is determined by fitting the absolute scale of the Nijmegen energy-dependent PWA NI93 [10] to the experimental data in the energy region 80 – 250 MeV. A slight renormalization of 0.995 is needed to obtain an optimum fit. Also other PWA's and potentials have been tested, but it is found that NI93 gives the best description of the energy dependence of $\sigma_T^{exp}$. The uncertainty from this procedure has two sources; the 1% systematic error of the experimental data, and the ±0.5/ ± 1.0 MeV uncertainty in the neutron beam energy, which affects the total cross section determination because it has a slope of about 1.1%/MeV at 96 MeV and 0.5%/MeV at 162 MeV.

The fraction $F$ of the total cross section covered in the present experiment is determined from the PWA's

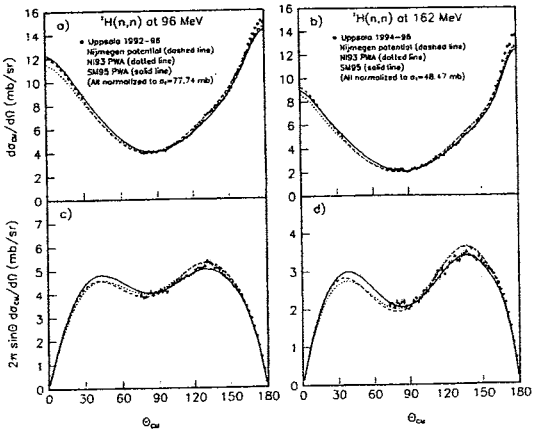


*Fig. 3.* Angular distributions for the SM95 [11], VZ40 [15] and NI93 [27] PWA's, and the present experimental data (filled circles) at 96 and 162 MeV. (Upper panels) Differential cross sections for np scattering. (Lower panels) Differential np scattering cross sections multiplied by the solid angle element $2\pi \sin\theta$.

SM95 [11], VL40 [1] and VZ40 [15] of VPI, and NI93 of Nijmegen [10]. VL40, VZ40 and NI93 are energy-dependent PWA's based on data in the 0 to 350 or 400 MeV region, while SM95 was obtained by fitting up to 1.6 GeV. For the final value of $F$ we take the average of the four mentioned PWA's. Also potential models were investigated, but are not included in the determination, because we believe that the PWA's are more reliable since they describe the total cross section better. Thus, the integrated np scattering data have been normalized to

$$\sigma^{exp}_{74°/72°-180°} = F\sigma_T^{exp}. \quad (3)$$

The result is shown in Fig. 3, where the upper panels display the differential cross sections, and the lower panels show the same differential cross sections multiplied with the solid angle element $2\pi \sin\theta$. In this representation, each angle bin directly shows its contribution to the total cross section. Also shown in the figure are the PWA's used to determine $F$, after normalization to the experimental total cross section. As was discussed in the previous section, the data are well represented by any of the PWA's in most of the covered angular region. Deviations occur only at the extreme backward angles which, however, carry only small contributions to the total cross section.

The spread in $F$ for the various PWA's and NN potential models can be used to estimate the precision of this normalization procedure. The maximum deviation from the average value is about 3%. From this comparison, we estimate the normalization uncertainty to at worst ±2.0%. In addition, we have the intrinsic uncertainty in $\sigma_T^{exp}$ of about 1%. Summing these effects yields a total normalization uncertainty of ±1.9% and ±2.3% at 96 and 162 MeV, respectively. However, a word of caution should be given here: The estimated uncertainty relies on the assumption that the various models give a reasonable account of the main characteristics of the angular distribution. If the balance between the two humps at about 40° and 130° seen in Fig. 3 is considerably different, our normalization would of course be affected. If, e.g., the cross

section in the forward hemisphere is larger than predicted by the models, this has to be compensated by lower backward cross sections to conserve the total cross section, and in this case our normalization would have to be lower.

The forward np data situation at our energies provides little guidance. There is only one large data set, by Bersbach *et al.* [16], for which the uncertainties are too large to draw conclusions at this level of confidence. At much higher energies, there are more precise data by Terrien *et al.* [17]. It can be noted that the lowest energy data by Terrien at 378 MeV lies about 15 – 20% above the SM99 solution by Arndt *et al.* If such a situation would be present at our energies, the consequences for the back-angle cross section, and thereby also for the extraction of the πNN coupling constant could be significant. A modification of the forward (0 – 60°) cross section up by 20% corresponds to lowering the remaining angular distribution by about 10% for a conserved total cross section. This would reduce the value of the *πNN* coupling constant by about 5%. We are planning a measurement of the remaining part of the angular distribution at 96 MeV to investigate this possibility further.

## 4. Experimental results

The final experimental differential cross sections are shown as filled circles in Fig. 4. The errors given are the quadratic sums of the statistical and systematic uncertainties of the relative cross sections discussed above. They do not include, however, the normalization uncertainty and the shape uncertainty between the most forward and backward data sets, i.e., in the 75°/73° to 179° cross section ratio.

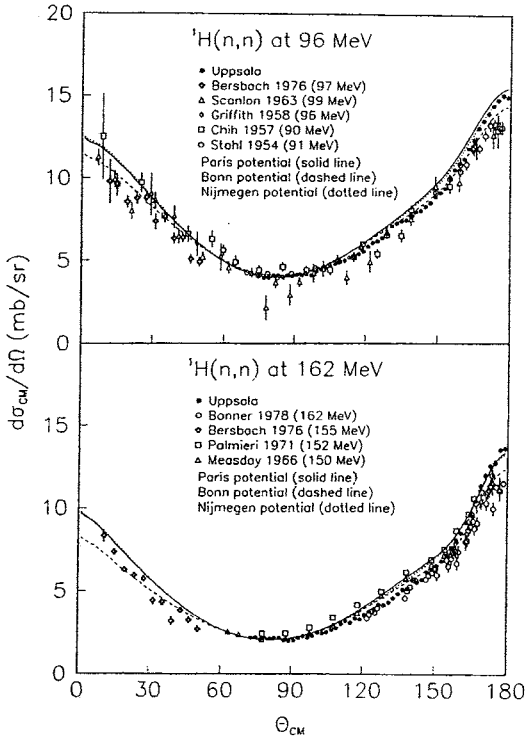


*Fig. 4.* Differential np scattering cross sections of the present work (filled circles). Also plotted are other data from the literature at energies close to 96 MeV (Upper panel) and 162 MeV (Lower panel). The lines show predictions for the Paris [25] (solid), Bonn (dashed) and Nijmegen (dotted) NN potentials.

The present data are compared with other experimental data from measurements performed close to that energy in Fig. 4. Thus, we give in the figure the data of Stahl and Ramsey [18], Chih and Powell [19], Scanlon *et al.* [20], Bersbach *et al.* [16], Bonner *et al.* [21], Palmieri and Wolfe [22], and Measday [23]. Although these older data show a larger spread than the present ones, it is obvious that the new data are at least 10% higher at the most backward angles.

As could be seen in Fig. 3, the data are steeper than the PWA's in the 154° – 180° region, while they are well described at smaller angles, as has been discussed earlier. As can be expected from the figure, and as has been mentioned in Ref. [24], the Uppsala data lead to a very high $\chi^2$ for the PWA NI93 [10].

In Fig. 4, the present data are compared with three NN potential models, namely the Paris [25], Bonn [26] and Nijmegen [27] potentials. The angular distributions of the Paris and Nijmegen potentials are rather similar, and describe the data reasonably well in the 160° – 180° region, while a 7% overprediction is seen in the 110° – 160° region. One should keep in mind, however, that both the Paris and Nijmegen potentials overpredict the total cross section by 3 – 5%. It is interesting to note that although the Nijmegen potential and the present data do not agree over the entire interval studied, the 90°-to-180° cross section ratio is in good agreement. The Bonn potential describes the data fairly well in the 74° – 150° region, while it underpredicts them by 6% at 180°. This potential gives, on the other hand, a total np cross section which is in good agreement with the experimental one.

To be able to compare the present results with data at other energies, the differential cross sections $d\sigma/d\Omega$ have been converted into $d\sigma/dt$, where $t$ is the Mandelstam variable, corresponding to the square of the c.m. charge exchange momentum transfer. If $p_n$ denotes the neutron incident laboratory momentum, the product,

$$p_n^2 \frac{d\sigma}{dt}, \tag{4}$$

when plotted versus $t$, should look the same for all data sets if only the pion pole term plays a significant role. Deviations from such a universal behaviour could be attributed to, e.g., effects of other interactions, such as multiple pion exchange. Since a majority of the data sets have either a floating normalization, or a large uncertainty in the absolute scale, we have renormalized the different data sets to agree at $t = 0$, which corresponds to np scattering at 180°. This was done by fitting the data according to an empirical two-exponential form [28],

$$\frac{d\sigma}{dt} = \alpha_1 e^{\beta_1 t} + \alpha_2 e^{\beta_2 t}, \tag{5}$$

which has been frequently used in the past when comparing different data sets.

A few data sets are plotted in this way together with our data at 162 MeV in Fig. 5. The plots cover the range up to $t = 0.06$ (GeV/c)$^2$, corresponding to np scattering angles of about 127° at 160 MeV and 153° at 580 MeV. The fit to the present 162 MeV data is shown as a solid line, whereas

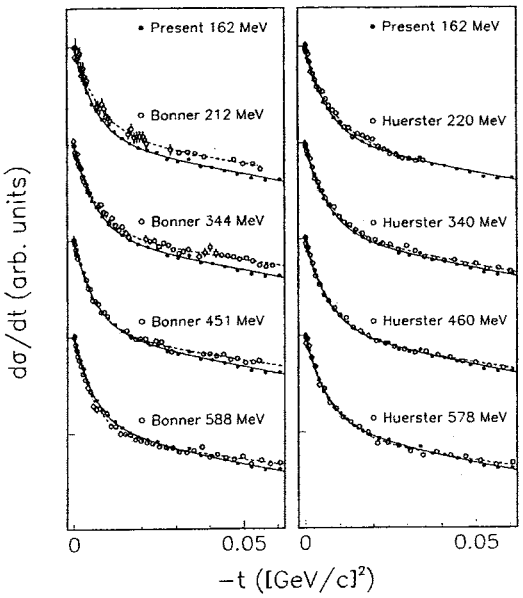


*Fig. 5.* Differential np scattering cross sections for data at various energies plotted as $d\sigma/dt$ versus $t$. The different data sets were normalized to each other at $t = 0$.

the fits to other data are represented by dashed lines. All the fits were performed up to $t = 0.08$ (GeV/c)$^2$. The left panel shows data of Bonner *et al.* [21] from 212 to 588 MeV. At the lower energies, these data are less steep than the present data set, just as was the case at 162 MeV (Fig. 4). The deviation is of the order of 15%. The agreement improves, however, when going to higher energies. The 451 MeV data set agrees well with the present one up to $t = 0.03$ (GeV/c)$^2$, and at 588 MeV the Bonner data set is even steeper than ours at small $t$. The right panel shows data of Hürster *et al.* [29] at approximately the same energies. These data show a remarkable agreement with the present ones at all energies, with shape deviations within a few percent. The Hürster data, which originally covered the angular range 144° – 180°, have recently been extended down to 80°, and are published by Franz *et al.* elsewhere in these proceedings.

The striking similarity in shape with the Hürster/Franz data can be illustrated in another way. We have used the phenomenological two-exponential fits above to the Hürster/Franz data, and compared these with the present 162 MeV data, allowing only the absolute scale to be re-normalized. For the lowest Hürster/Franz energy, 200 MeV, we obtain $\chi^2 = 1.2$ (/d.o.f.), the average of all fits in the 200–300 MeV region is 1.6 and for the full range, 200–580 MeV, it is still only 3.4. This is in contrast with the Bonner data, where we find $\chi^2 = 12.3$ (/d.o.f.) at 162 MeV.

## 5. Determination of the πNN coupling constant

Our primary aim is to achieve normalized np cross sections. We now briefly explore the impact these data have on the discussion of the πNN coupling constant. The procedure has previously been discussed in our work at 162 MeV to which we refer for details [3]. The analysis is based on the fact that the charged pion exchange contributes importantly to the np charge exchange at small momentum transfers. This was realized already in 1958 by Chew, who suggested a model-independent extrapolation to the pion pole for the determination of the coupling constant.

The Chew extrapolation procedure [30,31] is based on a polynomial expansion in the square of the momentum transfer, $q^2$. The technique used to extrapolate to the pion pole is to first construct a smooth physical function, the Chew function, by multiplying the cross section by $(q^2 + m_\pi^2)^2$, which removes the pole term, after which the extrapolation can be made far more safely and controlled. More exactly, in the physical region the function $y(x)$ is defined by:

$$y(x) = \frac{sx^2}{m_\pi^4 g_R^4} \frac{d\sigma}{d\Omega}(x) = \sum_{i=0}^{n-1} a_i x^i. \tag{6}$$

Here $s$ is the square of the total energy and $x = q^2 + m_\pi^2$. At the pion pole $x = 0$, the Chew function gives

$$y(0) \equiv a_0 \equiv g_{\pi^\pm}^4 / g_R^4 \tag{7}$$

in terms of the pseudoscalar coupling constant $g_{\pi^\pm}^2 \simeq 14$. The quantity $g_R^2$ is a reference scale for the coupling chosen for convenience. It is important to realize that the model-independent extrapolation requires accurate data with absolute normalization of the differential cross section. If the differential cross section is incorrectly normalized by a factor $N$, the extrapolation gives $\sqrt{N} g_{\pi^\pm}^2$. This is one of the most important sources of uncertainty in the practical extrapolation from data.

An improvement of this rather slowly converging expansion is the difference method introduced in our previous work at 162 MeV [3,32], and has subsequently been applied also to np data at 96 MeV [6] and $\bar{p}p$ charge exchange [33]. The difference method is also described in detail in the contribution by Loiseau *et al.* in these proceedings. The difference method applies the Chew method to the difference between the function $y(x)$ obtained from a model with exactly known coupling constant and from the experimental data, i.e.,

$$y_M(x) - y_{exp}(x) = \sum_{i=0}^{n-1} d_i x^i \tag{8}$$

with $g_R$ of Eqs. (6) and (7) replaced by the model value $g_M$. At the pole

$$y_M(0) - y_{exp}(0) \equiv d_0 \equiv \frac{g_M^4 - g_{\pi^\pm}^4}{g_M^4}. \tag{9}$$

This procedure should diminish systematic extrapolation errors and remove a substantial part of the irrelevant information at large momentum transfers.

We apply the difference method using four comparison models, i.e., the Nijmegen [27] and Bonn B [26] potentials, the Nijmegen energy-dependent PWA NI93 [10], and the VPI energy-dependent PWA SM95 [11]. In our analysis, the difference method requires only a few terms in the polynomial expansion, and this gives a small, statistical extrapolation error. Averaging the values from the extrapolations, we find $g_{\pi^\pm}^2 = 14.73 \pm 0.14$ (extrapolation and statistical) $\pm 0.23$ (systematic) $\pm 0.15$ (normalization) $= 14.73 \pm 0.31$

at 96 MeV, and $g^2_{\pi^\pm} = 14.52 \pm 0.13$ (extrapolation and statistical) $\pm 0.15$ (systematic) $\pm 0.17$ (normalization) $= 14.52 \pm 0.26$ at 162 MeV.

## 6. Summary and Conclusions

The np differential cross section has been measured at 96 and 162 MeV using the neutron beam facility at the The Svedberg Laboratory in Uppsala. The data were normalized using the total np cross section, which has been experimentally determined with high precision. Since our data do not cover the full angular range, the experiment was considered as a measurement of a fraction of the total cross section. This fraction was determined by using the angular shape of a number of energy-dependent PWA's. The data were normalized to the average fraction, obtained from those PWA's, multiplied with the experimental total cross section. We estimate the normalization error to about $\pm 2\%$.

A general feature is that our data are about 10% higher at 180° and have a steeper slope in the 150° – 180° angular region than most of the older data in the same energy region. As a consequence, the slope is also steeper than several of the current PWA's and NN potential models. A similar situation is also present at higher energies, where large data sets disagree significantly in shape. The shape of the present data is, however, in very good agreement with the new Franz *et al.* data, presented elsewhere in these proceedings.

The np scattering cross section at 180° is used as a primary standard for normalization of most other neutron-induced cross sections. Uncertainties of the order of 10% in this cross section are therefore unacceptable. Remeasuring the absolute np scattering cross sections with high precision and at several energies should be of high priority.

As a by-product of the present investigation, we have obtained extrapolated values $g^2_{\pi^\pm} = 14.73 \pm 0.31$ ($f^2_{\pi^\pm} = 0.0813 \pm 0.0017$) at 96 MeV and $g^2_{\pi^\pm} = 14.52 \pm 0.26$ ($f^2_{\pi^\pm} = 0.0803 \pm 0.0014$) at 162 MeV for the charged πNN coupling constant using the difference method, presented in the contribution by Loiseau *et al.* elsewhere in these proceedings.

Our future plans include measurements of np scattering between 10° and 170° (c.m) at a few energies in the 50 – 180 MeV range. To this end, the new SCANDAL (SCAttered Nucleon Detection AssembLy) setup will be used. The new detector system has been designed to detect either recoil protons or scattered neutrons. In this manner, it will be possible to cover both the backward angles by detecting the recoil protons and the forward angles by detecting the scattered neutrons. In particular, we plan to extend the data we have at 96 and 162 MeV to cover the full angular range, i.e., also the forward angles $\theta_{\text{c.m.}} = 10° - 70°$. By including these forward-angle data, we could normalize our angular distributions to the total np cross section directly, without any assumptions about the angular shape. In addition, a re-examination of the backward-angle cross section at 96 MeV is being planned.

## Acknowledgements

We thank The Svedberg Laboratory crew for careful operation of the cyclotron. We are also grateful to M. Lacombe for discussions on contributions to the cross sections for the Paris potential, and to W.R. Gibbs for advice on producing pseudo-data from models. TE acknowledges an interesting discussion with M. Rentmeester and BL the hospitality of the The Svedberg Laboratory.

This work was financially supported by the Swedish Natural Science Research Council, the CNRS French-Swedish Bilateral Cooperation Program, Vattenfall AB, Swedish Nuclear Fuel and Waste Management Company, Swedish Nuclear Power Inspectorate, Barsebäck Power AB, and the Swedish Defense Research Establishment.

## References

1. Arndt, R. and Workman, R. L., "Nuclear Data Standards for Nuclear Measurements," (edited by H. Condé), NEANDC-311 "U"/INDC(SEC)-101 (OECD, Paris, 1992) p. 17; Carlson, A. D., Chiba, S., Hambsch, F.-J., Olsson, N. and Smirnov, A. N., "Update to Nuclear Data Standards for Nuclear Measurements," (edited by H. Wienke), INDC(NDS)-368 (IAEA, Vienna, 1997) p. 9. Data as given by SAID (see Ref. [11]).
2. Ericson, T. E. O., Nucl. Phys. A **543**, 409c (1992).
3. Rahm, J. *et al.*, Phys. Rev. C **57**, 1077 (1998).
4. Condé, H. *et al.*, Nucl. Instr. Meth. A **292**, 121 (1990).
5. Rönnqvist, T. *et al.*, Phys. Rev. C **45**, R496 (1992).
6. Rahm, J. *et al.*, to be published.
7. Höistad, B. *et al.*, Nucl. Instr. Meth. A **295**, 172 (1990).
8. Byrd, R. C. and Sailor, W. C., Nucl. Instr. and Meth. A **264**, 494 (1989).
9. Carlson, R. F., At. Data Nuc. Data Tables **63**, 93 (1996).
10. Stoks, V. G. J., Klomp, R. A. M., Rentmeester, M. C. M. and de Swart, J. J., Phys. Rev. C **48**, 792 (1993). Data as given by SAID (see Ref. [11]).
11. Arndt, R. A., Strakovsky, I. I. and Workman, R. L., Phys. Rev. C **52**, 2246 (1995). Data as given by Scattering Analysis Interactive Dial-Up (SAID), Virginia Polytechnic Institute, Blackburg, VA, USA (R.A. Arndt, private communication).
12. Lisowski, P. W. *et al.*, Phys. Rev. Lett. **49**, 255 (1982).
13. Measday, D. F. and Palmieri, J. N., Nucl. Phys. **85**, 142 (1966).
14. Grundies, V., Franz, J., Rössle, E. and Schmitt, H., Phys. Lett. B **158**, 15 (1985).
15. Arndt, R. A., Strakovsky, I. I. and Workman, R. L., Phys. Rev. C **50**, 2731 (1994).
16. Bersbach, A. J., Mischke, R. E. and Devlin, T. J., Phys. Rev. D **13**, 535 (1976).
17. Terrien, Y. *et al.*, Phys. Rev. Lett. **59**, 1534 (1987).
18. Stahl, R. H. and Ramsey, N. F., Phys. Rev. **96**, 1310 (1954).
19. Chih, C. Y. and Powell, W. M., Phys. Rev. **106**, 539 (1957).
20. Scanlon, J. P., Stafford, G. H., Thresher, J. J., Bowen, P. H. and Langsford, A., Nucl. Phys. **41**, 401 (1963).
21. Bonner, B. E. *et al.*, Phys. Rev. Lett. **41**, 1200 (1978).
22. Palmieri, J. N. and Wolfe, J. P., Phys. Rev. C **3**, 144 (1971).
23. Measday, D. F., Phys. Rev. **142**, 584 (1960).
24. Rentmeester, M. C. M., Klomp, R. A. M. and de Swart, J. J., Phys. Rev. Lett. **81**, 5253 (1998).
25. Lacombe, M. *et al.*, Phys. Rev. C **21**, 861 (1980).
26. Machleidt, R., Holinde, K. and Elster, Ch., Phys. Rep. **149**, 1 (1987), and R. Machleidt, private communication.
27. Stoks, V. G. J., Klomp, R. A. M., Terheggen, C. P. F. and de Swart, J. J., Phys. Rev. C **49**, 2950 (1994). Data as given by SAID (see Ref. [11]).
28. Wilson, R., Ann. Phys. **32**, 193 (1965).
29. Hürster, W. *et al.*, Phys. Lett. B **90**, 367 (1980).
30. Chew, G. F., Phys. Rev. **112**, 1380 (1958).
31. Cziffra, P. and Moravcsik, M. J., Phys. Rev. **116**, 226 (1959).
32. Ericson, T. E. O. *et al.*, Phys. Rev. Lett. **75**, 1046 (1995).
33. Ericson, T. E. O. and Loiseau, B., Phys. Lett. B **393**, 167 (1996).

# Appendix III

Physica Scripta. Vol. T87, 33–46, 2000

# How Strong is the Strong Interaction? The πNN Coupling Constant and the Shape and Normalization of np Scattering Cross Sections

J. Blomgren, N. Olsson and J. Rahm

Department of Neutron Research, Uppsala University, Box 535, S-75121 Uppsala, Sweden

*Received October 8 1999; accepted November 9, 1999*

PACS Ref: 23.75.Cs, 65.43.y

**Abstract**

The world data base on np scattering differential cross section data from 100 to 1000 MeV incident neutron energy has been reviewed. In addition, the status of the np total cross section and the pp $\rightarrow$d$\pi^+$ total cross section is discussed, as these have frequently been used to normalize np scattering data. It appears that the shapes of the largest np data sets tend to fall into two groups, with different steepness at backward angles. Also, it seems as the two major techniques for normalizing data yield incompatible results. Both these effects have consequences when using np data to determine the pion-nucleon coupling constant, $g^2_{\pi NN}$, which is currently under debate.

## 1. Introduction

The absolute strength of the strong interaction in the nuclear sector is commonly expressed by the pion-nucleon coupling constant, $g^2_{\pi NN}$. The πNN coupling constant is not directly accessible by experiments; it is a deduced parameter. A variety of methods to obtain a value of $g^2_{\pi NN}$ have emanated over time*. For a review, see Ref. [1].

Neutron–proton (np) scattering – as well as proton-proton scattering – have been extensively used for such determinations. If np scattering were due to one-pion exchange only, the determination of $g^2_{\pi NN}$ should be rather straight forward. This is illustrated in Fig. 1. The coupling in each vertex is given by $g_{\pi NN}$, and since the coupling comes in twice, the amplitude is $g^2_{\pi NN}$. The differential cross section is the amplitude squared, and thus the cross section is proportional to $g^4_{\pi NN}$. In reality, other processes are also present, like two-pion exchange, and therefore the picture above is oversimplified. However, if one-pion exchange is present in np scattering, a component of the cross section proportional to $g^4_{\pi NN}$ could be expected.

Returning to the simple picture, we note that the differential cross section for np scattering decreases with increasing momentum transfer, i.e., with increasing angle, assuming the interaction to be mediated by the uncharged pion, $\pi^0$, and the characteristic scale of how rapidly the cross section decreases is given by the pion mass. However, in addition to this pure scattering process, there is the possibility of charge exchange, where a charged pion ($\pi^\pm$) is mediating the interaction, thus altering the identity of the two particles. This process has its minimum momentum transfer at 180° in the centre-of-mass (c.m.) system, and should therefore to first order look like a mirror image of $\pi^0$ exchange. This simple picture resembles reality, as illustrated in Fig. 2, but this is partly a coincidence.

This rise in cross section at backward c.m. angles is one of the best known signs of the exchange character of the nuclear force. It is interesting to note that this feature looks similar over a very broad energy interval, from 100 MeV incident neutron energy up to several GeV.

The actual value of the πNN coupling constant is canonically quoted at the pion pole, i.e., at the momentum transfer $q^2 = -m^2_\pi$, where the form factor vanishes. This makes $g^2_{\pi NN}$ ultimately unavailable for direct experimental measurements. However, at 180° np scattering, the momentum transfer is small and hence the situation is rather close to this limit, and therefore backward np scattering data have been frequently used to extract $g^2_{\pi NN}$. It is evident from

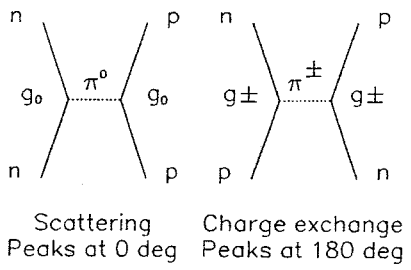


*Fig. 1.* Simplified diagrams of the one-pion contributions to the np scattering cross section.

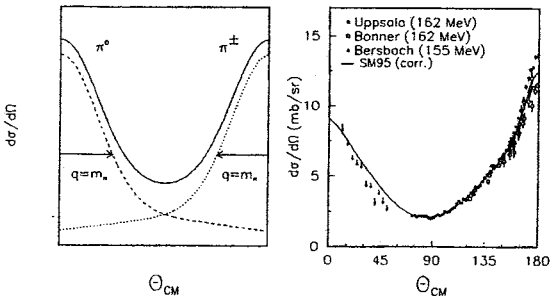


*Fig. 2.* Left panel: the expected shape of the np cross section from very simple assumptions, as described in the text. Right panel: the data situation at around 160 MeV. The solid line is the global partial-wave analysis SM95, renormalized to the experimental total cross section.

* Two different definitions of the coupling strength are frequently used, with different notation. The pseudovector coupling $f^2 \sim 0.08$ and the pseudoscalar $g^2 \sim 14$, are related by a multiplicative factor; $g^2 \equiv f^2(2M_p/m_{\pi^\pm})^2$, where $M_p$ and $m_{\pi^\pm}$ are the proton and charged pion masses, respectively. To be strictly correct, the pseudoscalar notation, which we use throughout this article, should be written $g^2/4\pi$, but the $1/4\pi$ factor is often omitted.

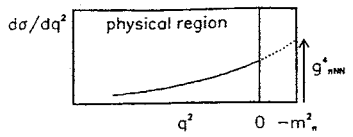


*Fig. 3.* An illustration of the relation between np scattering data and the coupling constant. Note that the value of $g^2$ is sensitive to both the shape and the normalization of the data.

Fig. 3 that both the *shape* and the *normalization* of the data contribute in such a determination. Remembering that the cross section is proportional to $g^4_{\pi NN}$, it is obvious that the value of $g^2_{\pi NN}$ goes as the square root of the normalization.

The precise value of the $\pi$NN coupling constant has consequences for the quantitative discussion of a large number of phenomena in hadron and nuclear physics. This involves predictions by low-energy theorems of pion photo- and leptoproduction, as well as the Goldberger-Treiman relation, which relates the axial vector coupling constant of beta decay with the decay rate of pions, just to mention a few. Moreover, its strength governs the properties of the deuteron to a very high degree. If all other nucleon-nucleon (NN) potential information were known, the value of $g^2_{\pi NN}$ could be determined very accurately, because then a difference of only a few percent in its value would be sufficient to either unbind the deuteron or to produce a bound diproton, in both cases with major consequences for the world as we know it.

Around 1980, it was believed that the $\pi$NN coupling constant was well known. Koch and Pietarinen [2] obtained a value of the charged pion coupling constant, $g^2_{\pi^\pm} = 14.28 \pm 0.18$, from $\pi^\pm$p scattering data. Kroll [3] determined the neutral pion coupling constant to $g^2_{\pi^0} = 14.52 \pm 0.4$, from analysis of pp scattering data by means of forward dispersion relations.

In the early 1990's, the Nijmegen group [4–6] found substantially smaller values for the coupling constants, on the basis of extensive and global partial-wave analyses (PWA) of *NN* scattering data. The obtained values were $g^2_{\pi^0} = 13.47 \pm 0.11$ and $g^2_{\pi^\pm} = 13.54 \pm 0.05$. Similar coupling constants, with values around $g^2_\pi = 13.7$, have been found also by the Virginia Tech group [7–9] from analysis of both $\pi^\pm$N and NN data. These results have stimulated an intense debate, and they have forced a critical reappraisal of the entire reasoning on which the previous values were based. Reviewing this issue, it has become evident that the basis for the standard text book value, with respect to both the np scattering data base and the analysis tools, is weaker than previously thought. It has therefore become urgent to determine $g^2_{\pi NN}$ to high precision, convincingly and model-independently [1].

Recently, high-precision np scattering experiments at 96 MeV [10,11] and 162 MeV [12,13] were presented. A novel technique to determine $g^2_{\pi NN}$ from these data was employed, resulting in values of $14.73 \pm 0.31$ and $14.52 \pm 0.26$ at the two energies, respectively, i.e., discrepant from the global NN analyses above, but in agreement with the values obtained from $\pi$N scattering and pp forward dispersion relations. The results, as well as the data and the method, have been strongly critizised and debated [14,15].

In this paper, we present a review of the world data base on np scattering differential cross sections from 100 to 1000 MeV incident neutron energy. In addition, the status of the np total cross section and of the pp $\rightarrow$ d$\pi^+$ total cross section is discussed, since these have frequently been used to normalize np scattering data. We have found two major problematic features of the data base. First, it appears that the large data sets tend to fall into two groups, characterized by a different steepness at backward angles. Consequently, significantly different values of $g^2_{\pi NN}$ have been suggested. Second, the two major techniques for normalizing data yield incompatible results.

It is difficult to overemphasize the importance of knowing the np scattering cross section precisely. Besides providing a testing ground for the pion-nucleon coupling constant, the np scattering cross section – in particular at 180° – is of utmost importance for many applications of today, including medical applications, studies of electronics failures induced by cosmic-ray neutrons, and accelerator-driven transmutation of nuclear waste and energy production technologies. The reason is that this cross section is frequently used to normalize measurements of other neutron-induced cross sections. Large uncertainties for such an important cross section are therefore unacceptable.

This paper is an evaluation work in the sense that it does not contain any new experimental or theoretical information. It is focused on investigating the data base, with the objective to supply information needed to understand the present experimental situation and its theoretical consequences. During the work, we have found several surprising contradictions and inconsistencies in the data base, both with regard to the angular distribution and to the absolute normalization. To our knowledge, this is the first time that all available experimental data in the 100 – 1000 MeV range are critically examined and compared on the same footing. This is in sharp contrast to the situation at lower energies (< 20 MeV), where the important nuclear energy applications have enforced many careful evaluations of nuclear data.

The outline of the paper is as follows; first the data base is inspected and its main features are discussed in Section 2. In Section 3, the different cross section shapes are studied, and Section 4 deals with the normalization problem. Finally, summary, conclusions and outlook are given in Section 5.

## 2. Brief survey of the np scattering data base

Our study is limited to the differential np scattering cross section data only, in the energy region 100 – 1000 MeV. Of all np scattering data in this energy range, the differential cross section data dominate heavily, and are more numerous than all other data combined (such as measurements of e.g. spin degrees of freedom). For our investigations, we have used the Nijmegen data base which is essentially complete in the 100 – 1000 MeV range. This data base is easily accessed over www [16]. For a list of references, see, e.g., Ref. [17]. Our investigation was terminated in January 1999 and covers data up to this date.

A summary of the differential cross section data is presented in Table I, with references and some angular coverage characteristics. The total number of data points is 5511. The largest data sets are due to Bonner *et al.* (2004 data

Table I. *Summary of the np differential cross section data base in the 100-1000 MeV range.*

| Data set | No of data points in angular interval 0°–180° | 0°–120° | 120°–150° | 150°–180° | Ref. |
|---|---|---|---|---|---|
| All data | 5511 | 1424 | 1429 | 2653 | |
| Bonner | 2004 | 149 | 754 | 1101 | [18] |
| Evans | 145 | 82 | 29 | 34 | [21,22] |
| Jain | 140 | 69 | 32 | 39 | [23] |
| Northcliffe | 189 | 105 | 35 | 49 | [24] |
| Bonner setup | 2478 | 405 | 850 | 1223 | |
| Bizard | 900 | 0 | 266 | 634 | [19] |
| Rahm | 54 | 24 | 15 | 15 | [13] |
| Hürster | 720 | 0 | 134 | 586 | [20] |
| Keeler | 279 | 142 | 69 | 68 | [38] |
| Terrien | 498 | 498 | 0 | 0 | [25] |
| Bersbach | 162 | 162 | 0 | 0 | [26] |
| Others | 420 | 193 | 95 | 132 | |

points) [18], Bizard *et al.* (900) [19] and Hürster *et al.* (720) [20]. The data sets by Evans *et al.* (145) [21,22], Jain *et al.* (140) [23] and Northcliffe *et al.* (189) [24] were all obtained with essentially the same setup as the Bonner data and with almost the same collaborators. When discussing systematic effects, it makes sense to group all these data together, which we refer to as Bonner setup data, summing to 2478 data points, i.e., almost half the data base.

Another way of comparing the data sets is via their statistical weight. In number of data points the Bonner group, Bizard and Hürster data comprise 45%, 16% and 13%, respectively, but in statistical weight the numbers are 44%, 10% and 28%, respectively. In addition, Terrien *et al.* [25] and Bersbach *et al.* [26] have published 498 and 162 data points, respectively, all at small angles, which are beyond the scope of this article, because it is focused on the impact on the charged coupling constant.

Since the work of Hürster *et al.* was published, the group has performed further measurements at PSI extending the angular range to 80° – 180°. These data are presented in the contribution by Franz *et al.* [27] to these proceedings. With this extension, the data set now contains 2223 data points, including the 720 Hürster points. Once these data are published, and thus included in the data bases, they will constitute 32% by number of the world data on np scattering cross sections, reducing the impact of the Bonner group and Bizard data to 35% and 13%, respectively. In statistical weight this will correspond to 66%, 21% and 5% for the Franz, Bonner and Bizard data, respectively.

## 3. The np scattering angular distribution

As discussed in the introduction, the most striking feature of the np scattering cross section is the pronounced peak in the backward direction, which is present from below 100 MeV to above 10 GeV incident energy. This has been ranked as one of the best examples of the presence of pions in the nuclear interaction [28]. If there were no other contributions to the cross section, the shape would be independent of incident energy, and the normalization should scale with the square of the incoming momentum. Therefore, the quantity

$$p_n^2 \frac{d\sigma}{dt}, \tag{1}$$

where $p_n$ is the neutron incident laboratory momentum and $t$ is the Mandelstam variable, i.e., the c.m. momentum transfer squared, should look the same for all data sets if only the pion pole term plays a significant role [29]. Deviations from a universal behaviour could then be attributed to effects of other interactions, like multiple pion exchange.

For comparisons of different data sets, we have taken ourselves the liberty to use our data at 162 MeV [12,13] as a reference.

### 3.1. *Direct comparison of different data sets*

To be able to compare data at different energies, we present the data in the c.m. system, plotted as $d\sigma/dt$ versus $t$; see Figs. 4 and 5. A majority of the data sets have either a floating normalization, or a large uncertainty in the absolute scale. Therefore, we have renormalized the different data sets to agree at $t = 0$ for the presentation below. To make this normalization in a reasonable way, we have fitted the data according to a two-exponential shape,

$$\frac{d\sigma}{dt} = \alpha_1 e^{\beta_1 t} + \alpha_2 e^{\beta_2 t}, \tag{2}$$

which has been frequently used by previous authors when comparing different data sets [30]. The fit to the Uppsala data is shown as a solid line, whereas the fits to other data are represented by dashed lines. The fits were performed

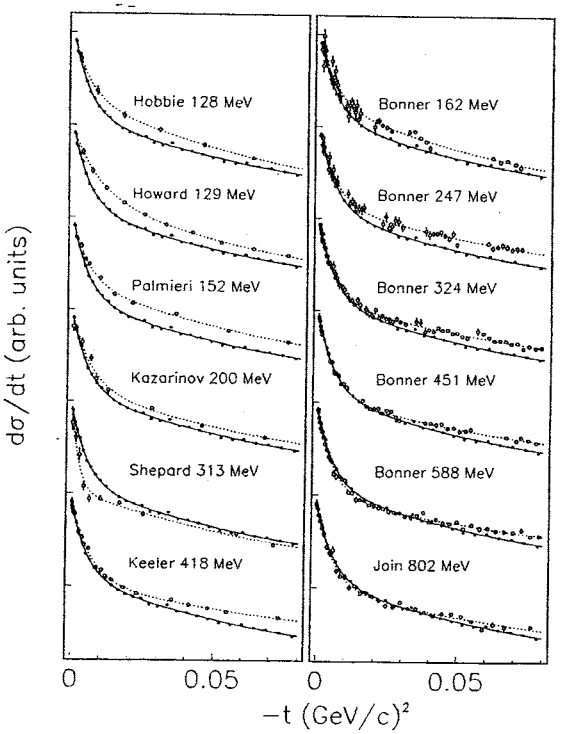


*Fig. 4.* Data of Bonner, Hobbie, Howard, Palmieri, Kazarinov, Shepard and Keeler plotted as $d\sigma/dt$ versus $t$ for a few energies. The Uppsala data at 162 MeV are shown for reference. (Linear scale).

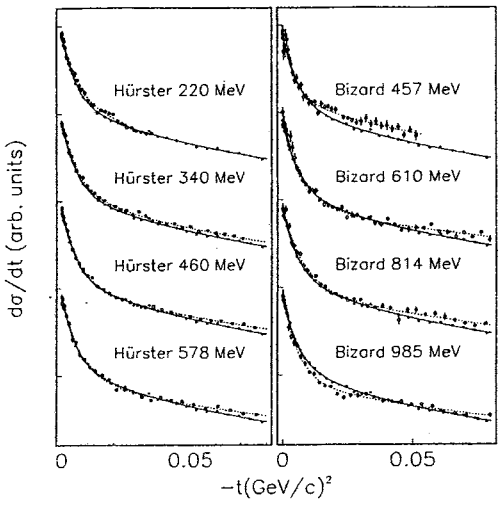


*Fig. 5.* Data of Hürster and Bizard plotted as $d\sigma/dt$ versus $t$ for a few energies. The Uppsala data at 162 MeV are shown for reference. (Linear scale).

up to $t = 0.08$ (GeV/c)$^2$, regardless of how far out in angle the data extend. The reason for this choice is somewhat arbitrary, but is not crucial; using a moderately wider range does not influence the conclusions of this study.

As can be seen in Fig. 4, the data of Hobbie (128 MeV) [31], Howard (129 MeV) [32] and Palmieri (152 MeV) [33] all show flatter distributions for small $t$. The data of Measday (129 and 150 MeV) [34] were obtained with the same setup as the Palmieri data, and indeed they display a similar shape. The data of Randle (130 MeV) [35] are too scarce to draw any conclusions. Several of the data sets mentioned have, however, very few data points close to $t = 0$, which makes the extrapolation to $t = 0$, and thus the normalization, uncertain. The Kazarinov data at 200 MeV [36] can be made compatible with our data if the point at the smallest $t$ is taken out and the remaining data are normalized again, resulting in a reduction of about 10%. The data of Shepard [37] have distributions that are steeper than ours at all their energies (182 – 378 MeV), whilst the data of Keeler [38] (212 – 418 MeV) seem to be flatter.

A few of the data sets of Bonner are shown in the same figure. At low energies, the Bonner data are flatter than the Uppsala data, but this discrepancy decreases gradually in magnitude with increasing energy, and the Jain data at 802 MeV (obtained with the Bonner setup) are in reasonably good agreement with the Uppsala 162 MeV data. At lower energies, the individual points scatter substantially. Above 400 MeV, the scatter in the individual points is smaller, indicating a better precision in the data.

A similar comparison with the Hürster(/Franz) data from 220 to 578 MeV is shown in Fig. 5. At all energies the agreement with the Uppsala data is good, at least up to $t = 0.05$ (GeV/c)$^2$. It is interesting to note that in the range $t = 0 - 0.03$ (GeV/c)$^2$, which corresponds to the angular region where the Uppsala data deviate the most from the Bonner data, the agreement with the Hürster/Franz data is almost perfect.

The Bizard data, displayed in the same figure, show a more complex pattern. At their lowest energies, they are much flatter than the Uppsala data, while being steeper at their highest energies (around 1 GeV). The transition is not very smooth; instead the steepness jumps from one energy to the next.

In previous work, it has been common to express the shape of the np cross section by the parameter $\beta = (\alpha_1\beta_1 + \alpha_2\beta_2)/(\alpha_1 + \alpha_2)$ [20], which corresponds to the logarithmic derivative at $t = 0$ of the two-exponential expression above*. In Fig. 6, such a plot is presented for the three largest data sets (Bizard, Bonner and Hürster) together with the Uppsala data, and for the Virginia partial-wave analysis (PWA) SM95 [42] as well as the Nijmegen PWA NI93 [17]. As can be seen, almost all data are in agreement with each other, in spite of the significant differences displayed in the $d\sigma/dt$ plots. The spread of the data points and the errors are, however, comparatively large. It seems therefore as if $\beta$ is not a very sensitive measure of the shape of the cross section.

We have attempted another method to illustrate the steepness of the cross section. In Fig. 7, we have plotted the ratios $(d\sigma/dt)_{t=0}/(d\sigma/dt)_{t=0.02}$ and $(d\sigma/dt)_{t=0}/(d\sigma/dt)_{t=0.04}$, respectively. In such a plot, if the reaction mechanism is dominated by one-pion exchange, the data should appear as straight horizontal lines irrespective of at which value of $t$ the comparison is being made. It can be noted that the Hürster/Franz data actually display such a rather flat behaviour. The Bonner data, on the other hand, display more of an energy dependence. At higher energies, all the three largest sets agree well. The previous observation that the steepness of the Bizard data seems to vary from point to point is corroborated by this figure.

In addition to the data, the predictions by the Virginia PWA SM95 and the Nijmegen PWA NI93 are shown. They both fall close to the Bonner data, which is not surprising. The Nijmegen group have rejected all Hürster data from their analysis [17], and the Hürster data have never been entered into the Virginia data base. Both analyses are therefore heavily dominated by the Bonner group data.

### 3.2. *Comparison of data with PWAs*

The sharp disagreement between the Uppsala and Hürster/Franz data on one hand, and the Virginia and Nijmegen PWAs on the other hand, has prompted us to make an investigation of some aspects of these PWAs.

A comparison [39] with the Nijmegen PWA NI93 yields a $\chi^2$ for the 31 Uppsala data points at 162 MeV in the 120° – 180° range [12] of about 290. For the rest of the accepted data, i.e., about 60% of the data base, the $\chi^2$ is close to one per point. (Notably, the Hürster data, whose shape is in much better agreement with the Uppsala data than the Bonner data, have been rejected in the Nijmegen analysis.) Inclusion of the Uppsala data in the analysis reduces the $\chi^2$ to about 265 only. Remarkably, when both the Bonner data are excluded and the Uppsala data at 96 MeV (32 points; Ref. [10]) and 162 MeV are included, the analysis still yields a $\chi^2$ for the Uppsala 162 MeV data of 246! This is surprising, since there is now almost no other differential cross section data left in the 150° – 180° range. In the last comparison, a PWA of np data only, covering the range 0 – 500 MeV, is used. All differential cross sections with

* In the present work, where we have fitted data renormalized to $d\sigma/dt = 1$ at $t = 0$, this expression simplifies to $\beta = \alpha_1\beta_1 + \alpha_2\beta_2$ because $\alpha_1 + \alpha_2 \equiv 1$.

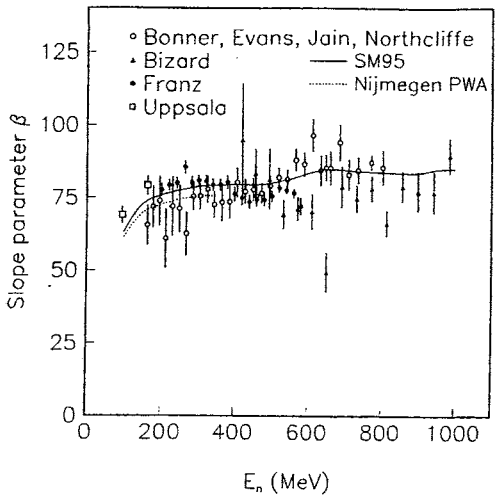


*Fig. 6.* The slope parameter $\beta$, i.e., the logarithmic derivative at $t = 0$.

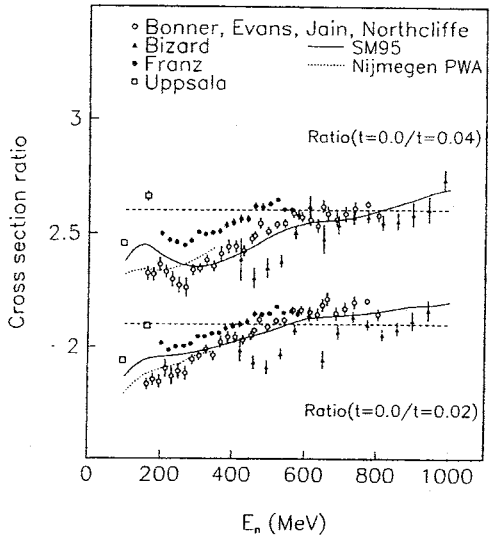


*Fig. 7.* The ratio of $d\sigma/dt$ at $(t = 0.00)/(t = 0.02)$, and $(t = 0.00)/(t = 0.04)$, respectively. The dashed horizontal lines are to guide the eye. If the np scattering process were due to one-pion exchange only, the data should fall on such straight lines.

$\theta > 119°$ are dropped, and the Uppsala 162 MeV data are included. The $\chi^2$ for our 31 data points is then 174.

The corresponding comparisons with the Virginia PWAs yield the following. The $\chi^2$ for the 31 Uppsala data points at 162 MeV compared to SM95 (0 – 1600 MeV) is 158, which is already less than that obtained by Nijmegen after dropping all cross sections with $\theta > 119°$! For the low-energy PWA, VZ40 (0 – 400 MeV), the $\chi^2$ is 238, i.e., comparable to that of the Nijmegen group. The C150 (125 – 174 MeV) PWA yields $\chi^2 = 379$. It should be pointed out here that the Virginia group does not reject data in the fitting on the same strict criteria as the Nijmegen group. On the other hand, the Virginia group have not included the Hürster data into their data base.

A common feature of all the comparisons is that the Uppsala data, both at 96 and 162 MeV, are steeper than the PWAs for $\theta > 150°$. It is interesting to note, however, that the best agreement is obtained when comparing the Uppsala data with the SM95 PWA, which has a relatively large weight for data at higher energies. The worst result, on the other hand, is found using the C150 solution, which is based on data in a very restricted energy region.

Previously, the shape of the data was investigated by plotting the ratio of $d\sigma/dt$ for two different momentum transfers $t$, as was shown in Fig. 7. The energy dependence of the PWAs can also be studied by this method. In the same figure, two examples, for $t = 0.02$ and 0.04, are presented. A striking feature is the dip-bump structure in the 100 – 400 MeV region. At larger $t$ than plotted here, this structure gets even more pronounced.

### 3.3 *Comparison of data using the extracted coupling constant*

Recently, the novel difference method [12,13] for extraction of the coupling constant from np scattering data was applied by Arndt *et al.* to the Virginia data base [40]. This provides a consistency check on large data sets, where the extracted coupling constant can be inspected over a wide energy range.

The result of this survey for the Bonner and Bizard data is displayed in Fig. 8. The dotted lines indicate the weighted averages of this analysis, which are $13.62 \pm 0.04$ and $13.02 \pm 0.09$ for the Bonner and Bizard data, respectively. These results are in agreement with the coupling constants provided by the Virginia PWAs, and are thus a support for the difference method as such. What is more noteworthy is the apparent energy dependence of the result for both these data sets. The coupling constant obtained from the Bonner data seems to increase roughly linearly with bombarding energy, while the Bizard data show a parabolic behavior. The solid lines in Fig. 8 are first- and second-order fits to the extracted coupling constants for the Bonner and Bizard data, respectively. The $\chi^2/(d.o.f.)$ for a uniform coupling constant is 2.9 and 4.2 for the Bonner and Bizard data,

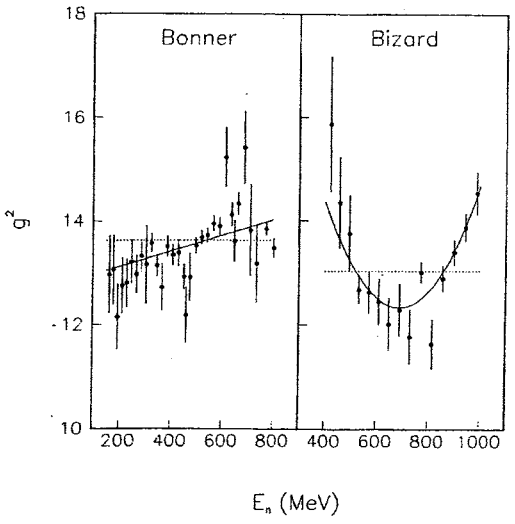


*Fig. 8.* The $\pi$NN coupling constant resulting from a difference method analysis by Arndt *et al.* [40] for the Bonner and Bizard data. The solid lines are first and second order fits to the data, respectively, while the dotted lines are weighted averages.

respectively, while it is 2.0 and 1.5, respectively, for the solid lines.

It is interesting to compare the cross section shape analysis presented in Fig. 7 with the apparent energy dependence of the coupling constant for the Bonner data in Fig. 8. In the former, it seems as the shape of the backward-angle cross section gets gradually steeper with increasing energy. A steeper backward-angle cross section should be linked to a higher coupling constant, as is indeed seen in the latter. Thus, the two pictures are qualitatively consistent.

The analysis was performed in two versions by Arndt *et al.*; one with the original normalization, and a second one with the absolute scale obtained by a renormalization to SM95. The energy dependence looks very similar in the two cases, but the absolute magnitude of $g^2$ is slightly different. It is the first of these versions that is shown in Fig. 8.

## 4. Normalization of np scattering data

As was pointed out above, the largest data sets are due to Bizard, Bonner and Hürster. In addition, the experiments by Northcliffe, Evans and Jain belong to the Bonner setup group. All these experiments were normalized by measuring np scattering simultaneously with the pion-production reaction $np \rightarrow d\pi^0$, when above threshold. This reaction has never been measured on an absolute scale directly, but it is linked to the $pp \rightarrow d\pi^+$ reaction via isospin invariance. Keeler and Uppsala have normalized to the total cross section, which can be done by integrating the differential cross section, given that the inelastic channels are small or can be corrected for.

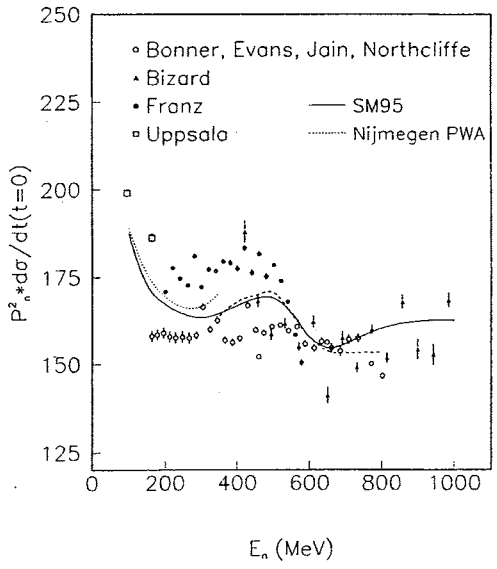


*Fig. 9.* The $t = 0$ cross section with its original normalization, obtained by fitting the data with a two-exponential expression. Note that the vertical scale has been suppressed. The deviating Uppsala points at 96 and 162 MeV were normalized using the total cross section, while all other data points were normalized by pion production techniques or by fits to a partial-wave analysis. The regular behaviour of the Bonner data below 300 MeV is because they were normalized to PWAs from VPI. The dashed line is explained in Section 5 of the text.

At energies below the pion threshold, many data sets were measured as relative data only, but have subsequently been normalized by different techniques before being tabulated. Notably, some of them have been normalized to PWAs, and thereby implicitly to older data. This is the case for the Measday and Bonner data below the pion-production threshold, which have been normalized to the PWA YLAN4MP [41] and Virginia PWAs [42], respectively.

It is apparent already from the data base that normalization of np scattering data is difficult. In Fig. 9, the $t = 0$ cross section obtained from the two-parameter fit described in section 3.1 is displayed. The original normalizations have been used. It can be noted that most of the data scatter substantially. In contrast, the Bonner data below 300 MeV display a regular behaviour, but this is artificial. These data were measured as relative points only, but have later been normalized to a PWA of the Virginia group. Also, the predictions by the Nijmegen PWA NI93 and the Virginia PWA SM95 are shown. It should be noted that neither of the two put a large emphasis on the original normalization of data. (The dashed line is explained in Section 5.)

### 4.1. *Normalization using the* $np \rightarrow d\pi^0$ *reaction*

As was mentioned above, the standard method to normalize np scattering cross sections above 275 MeV incident energy has been to make a measurement relative to the $np \rightarrow d\pi^0$ cross section, by a simultaneous detection of deuterons in the same spectrometer. This cross section is in turn related to the $pp \rightarrow d\pi^+$ cross section by a factor 2 from isospin invariance, and a correction of a few percent from Coulomb force differences [43].

The normalization involves a few ingredients:

(1) Energy transformation from the np to the pp system. The $np \rightarrow d\pi^0$ and $pp \rightarrow d\pi^+$ cross sections should be compared at the same invariant energy. Following a text book derivation [44], the c.m. cross section close to threshold has the general behaviour

$$\sigma \propto \frac{p_\pi^2}{v_{\pi d} v_{NN}}, \tag{3}$$

where $p_\pi$ is the c.m. momentum of the outgoing pion, and $v_{\pi d}$ and $v_{NN}$ are the c.m. relative velocities of the outgoing pion and deuteron, and the incoming nucleons, respectively.

(2) Correction for the Coulomb force. The np and pp entrance channels differ by the Coulomb repulsion in the latter, and that is also the case for the $d\pi^0$ and $d\pi^+$ exit channels. This effect can be calculated and compensated for. A commonly used simple analytic expression for the approximate correction is

$$G = \frac{2\pi\gamma}{e^{2\pi\gamma} - 1}, \tag{4}$$

where $\gamma = \alpha\mu/p$, $\alpha = 1/137.06$, $\mu$ is the reduced mass and $p$ is the c.m. momentum of the incoming proton or outgoing pion. It should be noted that there are corrections both in the entrance and exit channels [45], but the pp channel correction has been omitted in several papers on the $pp \rightarrow d\pi^+$ reaction and its time reversal. The exit channel correction goes to infinity at threshold, while it is 3 – 5%

in the 400 – 600 MeV region. The entrance channel correction is about 2% in the same region.

Recently, a theoretical investigation of the combined effect of the Coulomb interaction and the mass difference in the two systems has been undertaken by Niskanen and Vestama [46]. They found that the effect on the transition amplitudes from the fact that these reactions proceed via an intermediate Δ resonance, which has a different mass in the two cases, is far from negligible. The correction when comparing the two different total cross sections is several percent, and varies with energy in a non-monotonous fashion. Exactly at threshold, it is infinite, at 300 MeV neutron energy, just above the $np \rightarrow d\pi^0$ threshold, it is about +10%, falling to about −2% at 500 MeV, and then rising rapidly up to about +8% at about 600 MeV, above which it stays constant up to 800 MeV, which was the highest energy investigated. This dip structure was attributed to the intermediate Δ excitation. These numbers translate directly to the absolute scale of np scattering cross sections, normalized with this technique. It is interesting to note that with such renormalizations, the discrepancy between the total cross section and pion-production methods decreases substantially, and the absolute scale increases for the latter. Furthermore, it should be pointed out that this correction is about as large as the uncertainty in the $pp \rightarrow d\pi^+$ cross section data, and it has not been taken into account in any np scattering work in the past using the pion normalization technique. To our knowledge, the Franz *et al.* [27] data published in these proceedings are the first where this effect has been included.

(3) Determination of the $pp \rightarrow d\pi^+$ cross section. This is a difficult task because of a number of reasons. First, the data situation is complicated. There are large discrepancies in some regions, and data have also changed systematically and significantly over time. Therefore, some np data sets ought to be renormalized, since they have been normalized to a $pp \rightarrow d\pi^+$ cross section which is now believed to be incorrect. Second, the techniques to estimate the cross section are not without problems, and third, the resonant shape of the $pp \rightarrow d\pi^+$ cross section as such induces complications. These aspects will be elaborated below.

4.1.1. *How large is actually the* $pp \rightarrow d\pi^+$ *cross section?* We have studied four different analytic expressions for the total $pp \rightarrow d\pi^+$ cross section up to 1 GeV. These are due to Richard-Serre *et al.* (1970) [47], Spuller and Measday (1975) [48], Bystricky *et al.* (1987) [49], and Ritchie (1991) [50].

Richard-Serre *et al.* made a three-parameter fit to the $pp \rightarrow d\pi^+$ cross section up to $E_p = 500$ MeV. This approach was elaborated by Spuller and Measday, who added two more terms to the Richard-Serre expression. These two parameterizations agree reasonably well with each other, and with the data situation at that time. In addition, these two groups have made fits covering a larger energy region, adding more terms to the expressions. Richard-Serre *et al.* goes up to $E_p = 700$ MeV and Spuller-Measday to $E_p = 1100$ MeV. Bystricky *et al.* fitted the data with an expansion into a series of functions, related to Laguerre polynomials. The published fit uses 10 parameters up to 4.2 GeV. In 1991, Ritchie fitted a sum of two Lorentzians plus a linear and a square root term to the data up to $E_p = 1700$ MeV. The two latter are probably the most useful ones when establishing the present cross section, while the two former are of interest because they were used to estimate cross sections for normalization of the large np data sets, i.e., the Bizard, Bonner and Hürster sets.

To extract a "best cross section" for the normalization reaction $pp \rightarrow d\pi^+$, we have investigated the phenomenological fits by Richard-Serre *et al.*, Spuller and Measday, and Ritchie, using the $pp \rightarrow d\pi^+$ data base of the Virginia group (a complete reference list is given in Ref. [42]). There are 52 different data sets in this energy region, with in total 191 data points. Of these, 6 sets with in total 19 points have been rejected by the Virginia group, i.e., 46 sets with a total of 172 points remain. We have only used data accepted by the Virginia group. (Most of the rejected points have large error bars, so an erroneous omission would still not significantly change the conclusions below.) Both $pp \rightarrow d\pi^+$ cross section data and the inverse reaction $d\pi^+ \rightarrow pp$ have been utilized, converted by detailed balance.

Our first observation was that data have changed significantly over time. In Fig. 10, data before and after 1975 are displayed*. It can be noted that the new data deviate substantially from the old data in the $E_p = 400$ to 600 MeV region. In the lower panel, the relative difference of data after 1975 versus the Richard-Serre high-energy fit is plotted. Data with relative errors larger than 7% have been omitted to avoid difficulties in reading the graph. The deviation in the 400 – 600 MeV region is obvious. It can also be noted that the data below 400 MeV scatter significantly. A conclusion from this investigation is that np scattering data produced between 1975 and 1980, i.e., the three largest data sets; Bizard, Bonner and Hürster, might need re-normalizations upwards by about 10% in the 400 – 600 MeV range. This should be taken into account when performing analyses of the np scattering data base.

As a second step, we have tried to estimate the precision in the $pp \rightarrow d\pi^+$ cross section of today. In Fig. 11, all data are displayed together with the Ritchie fit from 1991. This fit represents the most recent estimate of the cross section [51]. It can be noted that although the general description is reasonably good, the scattering of the data is not negligible. The precision in the cross section determination is to our judgement in the 5 – 10% range at energies above 400 MeV. Below that energy, the uncertainty is even larger; the cross section does not seem to be known to better than ±15%.

There are several reasons why the $pp \rightarrow d\pi^+$ cross section is not a very good reference. First, the cross section as such is not known to better than 5% anywhere from threshold and up to 1 GeV. It is probably known *now* to better than 10% above 400 MeV, but not much better. Note that it has changed by 10% in the 400 – 600 MeV energy region since 1980. Second, the cross section shape as such induces additional problems. The cross section increases rapidly from the threshold and up to a maximum at about 600 MeV, and then it goes down steeply again. This was discussed in the Northcliffe paper, where it was concluded that

* The reason for this division is that the three largest data sets, i.e., Bizard, Bonner and Hürster, were all published between 1975 and 1980. During this period, only 6 accepted $pp \rightarrow d\pi^+$ data were published, so putting the cut at 1975 should be a rather good illustration.

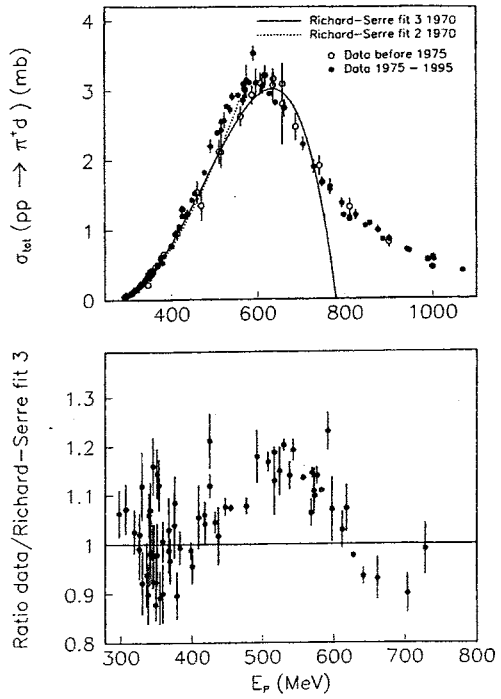


*Fig. 10.* Upper panel: The pp → dπ⁺ cross section data before and after 1975, together with the Richard-Serre *et al.* fits to the data 1970. Lower panel: All data 1995 relative to the Richard-Serre *et al.* fit 3 of 1970. This plot indicates the relative shifts in the data base since 1975.

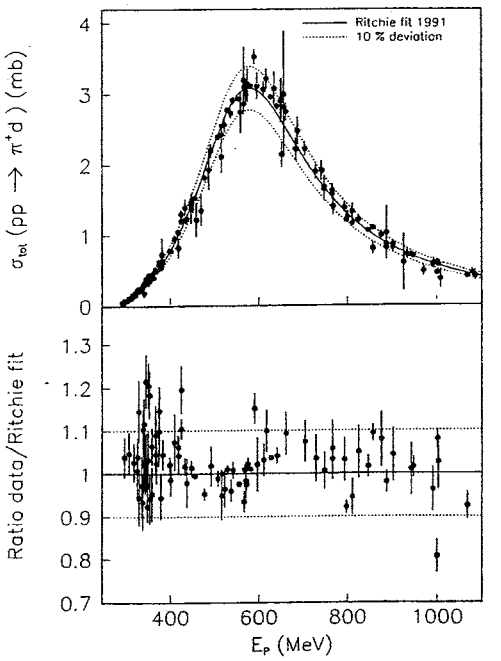


*Fig. 11.* Upper panel: The present data of the pp → dπ⁺ reaction together with the Ritchie fit to the data 1991. Dotted lines indicate the fit ±10%. Lower panel: All data 1995 relative to the Ritchie fit 1991. Data with relative errors larger than 7% have been omitted in the plot.

a ±3 MeV uncertainty in the absolute neutron energy corresponds to a ±6% uncertainty in the cross section at the energy of their experiment (459 MeV) from the steepness of the cross section alone [52]. At lower incident energies, the uncertainty arising from this effect is even larger. Finally, this normalization relies on that isospin invariance holds for the pp → dπ⁺ and np → dπ⁰ reactions. As was mentioned in section 4.1, a recent theoretical investigation [46] indicates deviations on the several percent level because of, e.g., mass differences in the two channels. These deviations are difficult to verify experimentally, and they have not been taken into account by any previous author.

Recently, Heimberg *et al.* have measured the pp → dπ⁺ analyzing power, and the total and differential cross sections very close to threshold at the IUCF cooler ring [53], and Drochner *et al.* have measured the total and differential cross sections in the same energy range, however not as close to the threshold, at COSY [54]. These two measurements differ substantially in absolute scale, with the IUCF data being about 20% larger in magnitude than the COSY data. In a recent publication, however, an improved analysis of the COSY data [55] resulted in slightly higher cross sections, which agree rather well with those of Heimberg *et al.*

The recent COSY cross section data [55], as well as the Heimberg *et al.* data [53], are in reasonable agreement with the old Rose data [56], which dominated this region previously, and with the np → dπ⁰ cross section by Hutcheon *et al.* [57], after corrections for isospin and Coulomb differences. This agreement should not be overinterpreted, though, as has been discussed in a comment and reply to the COSY publication [58,59]. It has been suggested that comparisons of the pp → dπ⁺ and np → dπ⁰ cross sections should allow tests of charge independence. However, the np → dπ⁰ data were normalized to np scattering, using a PWA from Virginia. The dominating data set in the Virginia data base in this energy interval is the Bonner data, which were normalized to pp → dπ⁺ data. (The only such data in this energy interval until recently were from the measurement by Rose [56].) Thus, the data are interdependent in a non-trivial manner, and tests of charge independence might therefore not be very reliable.

4.1.2. *Experimental data normalized to pion production.* Bizard *et al.* normalized their experiment by the pion production technique, but do neither give the used pp → dπ⁺ cross section, nor do they give a reference. Since the publication, the data have been re-normalized twice by others (see, e.g., Ref. 6 in [24]), before being tabulated in 1982 [60]. Since then, the pp → dπ⁺ cross section has changed significantly in part of the energy region studied (see Section 4.1.1), and therefore a re-normalization might be needed.

Hürster *et al.* fitted pp → dπ⁺ cross section data to a phenomenological expression suggested by Spuller and Measday [48]. Since then, the group has extended the measurements to cover a much wider angular range, where the previous data is a subset. In connection with this, the group has undertaken a thorough re-normalization [27], and we have therefore not investigated this data set further.

Bonner *et al.* do not tell explicitly how data were normalized, but refer to the well-known pp → dπ⁺ cross section, with a reference to Richard-Serre *et al.* [47]. However, they actually used a fit of Spuller and Measday (fit F), but without Coulomb corrections [61].

It is difficult to attempt a renormalization of previous data, since too much information has been lost over time. This is, however, not the case for the recent Northcliffe experiment, which was carried out at 459 MeV neutron energy. The normalization was not performed by the prescription in Section 4.1, but at the same total c.m. energy for the np and pp systems, i.e., at 462 MeV proton energy (although the proton energy was mistakenly taken to be 464 MeV). The correct normalization energy should rather be 467 MeV, if following the prescription from Section 4.1. The Northcliffe approach is obviously invalid, which is easily realized from the fact that for some total c.m. energies, the np channel has opened, but the pp channel is still below threshold. We conclude from the text in section II of their paper that there was no Coulomb correction, since $\sigma_p$ and $\sigma_n$ differ by exactly a factor 2. Using the prescription above, we end up with a renormalization upwards of 8%. The PSI group has made a similar estimation, resulting in a normalization upwards by 12% [62]. The difference between the two results is partly due to different extractions of the $pp \rightarrow d\pi^+$ cross section, and partly because the PSI group included the Niskanen-Vestama correction.

The Evans and Jain data were normalized with very similar techniques. In both papers the corresponding proton energy is calculated using the same deuteron c.m. momentum. No Coulomb corrections were applied. If applying the Niskanen-Vestama correction, the cross section would increase by 8%. On the other hand, Evans assumed a proton cross section of $\sigma_{pp\rightarrow d\pi^+} = 2.86$ mb, which is substantially higher than the Ritchie value of $\sigma_{pp\rightarrow d\pi^+} = 2.59$ mb. It should be noted that the proton cross section is difficult to extract in this energy region, so the large deviation is not surprising. (The Ritchie fit seems to be lower than data in the 600 – 800 MeV region, which can be seen in the lower panel of Fig. 11. There all data with relative errors less than 7% are plotted as the ratio to the Ritchie fit. Almost all data fall above the fit.)

### 4.2. *Normalization using the total* np *cross section*

If the entire angular distribution were experimentally known at a certain energy, normalization to the total cross section would be trivial. There are two main sources of uncertainties when using the total cross section for normalization. First, the entire angular distribution is not measured in most cases, and assumptions have to be made about the undetected part. Second, if above the pion-production threshold, the integrated differential elastic scattering cross section does not correspond to the experimental total cross section, but corrections must be applied for inelastic channels. A third uncertainty could be ascribed to how well the total cross section is known. All these effects are discussed below.

In most experiments only a part of the angular distribution is measured. The reliability of the total cross section normalization technique depends in such cases on the extrapolation techniques used for the unmeasured region. This has been studied by the Uppsala group, which has used different PWAs when normalizing the same data [10,12,13]. The distribution of the results has been used to estimate the uncertainty in this procedure. At 96 and 162 MeV, when covering the 120° – 180° angular region, a normalization uncertainty of 4% was given. After having extended the data sets to covering 74° – 180°, the normalization uncertainty was estimated to 2%.

The total cross section is dominated by elastic scattering, but in addition inelastic effects contribute. Below the pion-production threshold, the two largest are capture and np bremsstrahlung. The $np \rightarrow d\gamma$ cross section is rather well known, particularly from data on the inverse $\gamma d \rightarrow np$ reaction. The total cross section for this reaction is below 100 μb in the energy interval of this paper, and is thereby accounting for a sub-percent correction. The $np \rightarrow np\gamma$ cross section is much less well known, but new data are underway [63]. The $pp \rightarrow pp\gamma$ reaction has been studied, and its cross section is typically four orders of magnitude smaller than the elastic cross section. There are reasons to believe that the $np\gamma$ cross section is an order of magnitude larger than for $pp\gamma$, but this would still make the total bremsstrahlung cross section three orders of magnitude smaller than the elastic cross section. Thus, both these two inelastic processes impose sub-percent effects, which are negligible with present experimental precision.

Above the pion-production threshold at 275 MeV, the total cross section has to be corrected for contributions from pion-producing reactions, such as the $np \rightarrow d\pi^0$, $np \rightarrow nn\pi^+$, $np \rightarrow np\pi^0$, and $np \rightarrow pp\pi^-$ reactions. At even higher energies, two-pion production has significant contributions. If such a correction could be made accurately, the total cross section data could be used for normalization also above the pion-production threshold.

In the region rather close to the threshold, i.e., the 275 – 500 MeV domain, the correction required to use the total cross section normalization should be fairly well known. Bystricky *et al.* [49] have made an investigation of pion production in NN interactions. In Table VII of that paper, a phenomenological fit describing the total inelastic cross section in np scattering is presented, with errors on the sub-percent level all the way up to about 1.5 GeV. This indicates that the required correction could be made with very high accuracy. The authors pointed out, however, that this surprisingly small uncertainty could be smaller than the confidence level of $1\sigma$ because of correlation of parameters.

A more direct approach would be to look at reaction cross section data. The reaction cross section excluding $np \rightarrow d\pi^0$ has been measured to $11.0 \pm 0.8$ mb at 795 MeV [64]. The $np \rightarrow d\pi^0$ cross section can be estimated using the Ritchie parameterization of the $pp \rightarrow d\pi^+$ cross section and Coulomb corrections, resulting in $0.8 \pm 0.1$ mb. Combining these results yield a reaction cross section of $11.8 \pm 0.8$ mb, i.e., a 7% uncertainty. At the highest energy where the total cross section is precisely known, 770 MeV, it is $38.3 \pm 0.2$ mb. A correction for the reaction cross section obtained above, results in an elastic cross section of $26.5 \pm 0.8$ mb, i.e., a 3% uncertainty. It seems therefore not unlikely that such a procedure can be as precise as normalization by simultaneous pion detection.

4.2.1. *Total cross section data base.* In the energy region within the scope of this article, 100 – 1000 MeV, we are aware of 12 np total cross section data sets. These are listed in Table II, and the most important data sets are plotted in Fig. 12.

Table II. *Summary of the* np *total cross section data base in the 100-1000 MeV range.*

| Data set | Energy span (MeV) | No of data points | Ref. |
|---|---|---|---|
| Ashmore | 351 | 1 | [71] |
| Bowenz | 15–120 | 63 | [67] |
| Chen | 380 | 1 | [72] |
| Culler | 93–107 | 4 | [68] |
| Devlin | 247–2469 | 26 | [70] |
| Grundies | 126–577 | 24 | [66] |
| Kazarinov | 200 | 1 | [36] |
| Keeler | 212–495 | 6 | [38] |
| Lisowski | 39–770 | 112 | [65] |
| Measday | 88–151 | 7 | [69] |
| Palevsky | 730 | 1 | [73] |
| Shapiro | 125–168 | 2 | [74] |

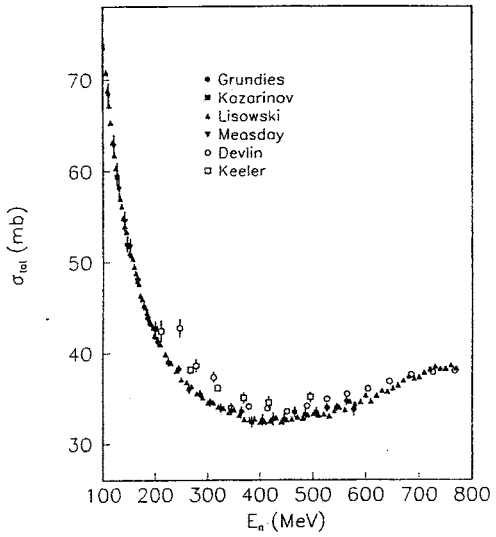


*Fig. 12.* The np total cross section.

There are two large high-accuracy data sets available, by Lisowski *et al.* [65] from Los Alamos, and by Grundies *et al.* [66] from PSI. These two sets are in perfect agreement all over their common energy domain, i.e., 125 – 580 MeV, and are supported by the measurements of Bowen *et al.* [67], Culler *et al.* [68], Kazarinov *et al.* [36], and Measday *et al.* [69]. The data of Keeler *et al.* [38] and Devlin *et al.* [70] are both systematically above the Grundies-Lisowski data (up to about 6%). This is true also for one datum point by Ashmore *et al.* [71]. The measurement by Chen *et al.* [72] is $1\sigma$ below the Grundies-Lisowski result. The Palevsky *et al.* [73] and Shapiro *et al.* [74] results both lie slightly below the Grundies-Lisowski result, but with large error bars. Neither the Palevsky nor the Shapiro results are due to direct np total cross section measurements, but are deduced from combinations of pp and *pd* measurements.

It has been claimed by Bugg and Machleidt [75] that the total cross section is uncertain. They point out that the Lisowski and Grundies data sets lie systematically below several measurements with monoenergetic neutron beams and liquid hydrogen targets, which they consider a more attractive technique as regards absolute normalization. In a total cross section measurement, the dominating uncertainties are statistics and the precision in determining the target properties, i.e., the number of target nuclei and the physical extent of the target. Both the Lisowski and the Grundies measurements have statistics superior compared to any other data set. Concerning knowledge of the target properties, using solid polythene targets, which was done by Lisowski, allows good control of systematic effects. As an example, this group has made extensive investigations of their targets, including X-ray scanning to find cavities, and state-of-the-art techniques to find impurities and to determine the densities accurately. The group of Grundies also used a hydrocarbon target; in their case it consisted of liquid cyclohexane contained in an aluminium box. Such targets are easier to use and control than cryogenic liquid hydrogen targets. In fact, the technique of using a $CH_2$-vs-C difference was originally motivated by the difficulties in determining liquid hydrogen target characteristics.

It is notable that the reasonably precise measurements using the $CH_2$-vs-C difference technique (Culler, Grundies, Kazarinov, Lisowski and Measday) all agree very well. Of these, Grundies and Lisowski use white neutron beams and the others use quasi-monoenergetic beams. Measday used both the $CH_2$-vs-C difference technique and $LH_2$ with agreement to better than 2%, which was limited by statistics. Finlay *et al.* [76] have made total cross section measurements on a series of nuclei, with varying target techniques. They claim agreement to better than 1% for these two target techniques, however for other target materials.

It has also been suggested by Bugg [77] that wrap-around effects could be a potential hazard in the Lisowski experiment. This is difficult to believe. The micropulse separation of LAMPF is typically of the order of microseconds. This combined with a typical flight path of 20 – 100 m, indicates that wrap-around neutrons have energies of a few MeV, which are easy to discriminate. In fact, wrap-around effects are probably more important, however still negligible, in so-called monoenergetic experiments. The much smaller micropulse separation, 50 – 100 ns at typical cyclotrons, results in wrap-around neutrons at much higher energies. In a carefully conducted experiment, however, this should not be a problem.

The measurements differing from these internally consistent data sets are due to Devlin, Keeler and one datum point by Ashmore. The single Ashmore point is $2\sigma$ above the Grundies-Lisowski data, and its statistical weight is not very large.

There are a few questions around the Devlin experiment. Neutrons were produced by an internal target in the Princeton–Pennsylvania Accelerator (PPA), but without explicit reference to which target material was used. In two other neutron experiments at PPA [26,37], platinum targets were used, which might have been the case also here. Neutrons emitted at 20° were collimated to a narrow beam. At these angles, the beam has a polarization which was not corrected for in the data. In a study on np scattering using a similar neutron production at a larger angle (38°), a beam polarization of 4.7% was identified [37]. It is not evident what effect the neutron beam polarization has on the total cross section data, and it might be wise to give these data lower significance when discussing the total cross section.

The Devlin experiment has been characterized as a monoenergetic neutron beam experiment, but this is a truth with qualification. The technique actually resembles a white source measurement. The intrinsic width of the neutron energy distribution is not explicitly given in the publication, but from Fig. 7 of the paper, we have deduced a very uncertain FWHM of about 20 MeV. Using time-of-flight (TOF) techniques, the energy resolution was reduced to about 4 MeV at 230 MeV, which is substantially worse than the resolution of the Grundies and Lisowski experiments.

The Keeler experiment used the D(p,n) reaction for neutron production. We are not aware of any experimental problems, but it can be noted in Fig. 2 of the paper that there might be a second peak at around 16 ns in the TOF spectrum. If this is actually a beam contamination, the results could be affected. It can be noted that both the Keeler and the Devlin data lie above the Grundies-Lisowski data in the region around 400 MeV, where the total cross section displays a minimum. If there was any contamination of neutrons at other energies in the former experiments, such a filling of the minimum could result.

To summarize the situation: two recent high-quality measurements agree perfectly (Grundies, Lisowski), with four older data sets supporting them (Bowen, Culler, Kazarinov, Measday). One data set is different from this (Keeler), and a few others either have too poor statistics to make a strong impact (Ashmore, Chen, Palevsky) or can be suspected to contain systematic errors (Devlin, Palevsky, Shapiro). We have chosen to adopt the Grundies-Lisowski result when normalizing our np data. Lechanoine-LeLuc and Lehar has made a review of the data situation, coming to the same conclusion [78].

4.2.2. *Experimental data normalized to the total cross section.* Keeler *et al.* [38] measured the np scattering cross section at 212, 319, 418 and 493 MeV. This experiment represents the only measurement of the full angular distribution after 1975. It was performed using two rather similar setups, one for detecting the scattered neutron at forward angles, and one for proton detection at backward angles. These two systems had an overlap to allow consistency checks. A system of monitors allowed the neutron detector efficiencies to be calibrated by putting the detector in the direct beam. The data were finally normalized to the total cross section by making a PWA of the differential cross section and integrating the solution over all angles.

The total cross section data lie systematically a few percent above the data sets of Lisowski and Grundies (see above). If the Lisowski data are used for cross section normalization, the Keeler data should be multiplied by 0.962, 0.945, 0.942 and 0.945 at 212, 319, 417 and 495 MeV, respectively. These factors are in reasonably good agreement with what the technique to be described in section 4.3 suggests, which is not surprising.

Rönnqvist *et al.* [10] and Ericson *et al.* [12] measured the np scattering cross section at 96 and 162 MeV, respectively, obtaining their normalization from the total cross section by extrapolating the experimental data using PWAs for the unmeasured angular region 0° – 120°. The uncertainty of this technique was estimated to 4% when applied to 96 and 162 MeV data covering 120° – 180°. The precision in this normalization was improved in the recently extended measurements [11,13], which cover a continuous angular range from about 70° to 180° (c.m.), using a slightly different approach. The contribution to the total cross section from the detected part of the angular distribution was determined by direct integration of the experimental data. This was compared with the corresponding fraction of the total cross section for several PWAs. An average value was used, and the spread in this contribution was used to estimate the uncertainty in the procedure. Finally, the angular distribution was normalized to the experimental total cross section of Lisowski *et al.*, multiplied with this fractional factor. With the data sets extended to 70° – 180°, the normalization uncertainty has dropped to 2%. The new normalizations are within the quoted uncertainty of the previous values.

4.2.3. *How should differential cross-section data be normalized to the total cross section?* This issue might seem innocent, but it is not self-evident how such a normalization procedure should be carried out. We have illustrated the problem in Fig. 13, where the solid line is the Virginia PWA SM95 at 200 MeV, and the data points are pseudodata, generated by multiplying SM95 with a parabola to simulate a steeper cross section at the forward and backward directions. The error bars were generated by a mathematical function to resemble a realistic case. In the upper panel, the pseudodata have been normalized to SM95 by minimization of $\chi^2$, which is a typical procedure used by PWA groups. In the lower panel, the contribution to the total cross section from each angular bin above is displayed, by plotting $2\pi \sin\theta d\sigma/d\Omega$, i.e., the differential cross section multiplied with the solid angle element. It is evident that the pseudodata and SM95 correspond to very different total cross sections (in this case by 20%). Thus, a $\chi^2$

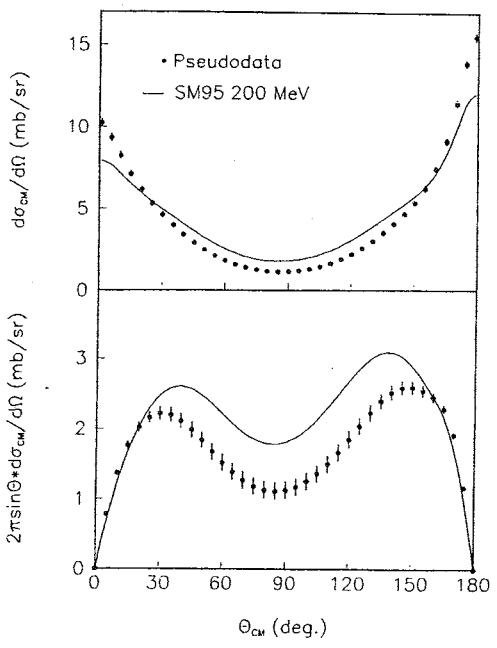


*Fig. 13.* Pseudodata normalized to SM95 by minimizing $\chi^2$ (upper panel), resulting in different total cross sections by about 20% (indicated in the lower panel). See the text for details.

normalization of differential cross section data does not necessarily result in the same total cross section.

### 4.3. *Cross-check of the total cross-section and pion-production normalizations*

At energies just above the pion-production threshold, a very small fraction of the total cross section comes from pion-production reactions. Therefore, normalizations using the total cross section and the $np \rightarrow d\pi^0$ reaction can be compared. To do this, a correction of the total cross section is required, as described in Section 4.2. This correction is rather small for the first 200 MeV above the threshold. We have made such a comparison using the Franz *et al.* data at 320 MeV [27].

In Fig. 14, the Franz data with their original normalization, obtained from the $np \rightarrow d\pi^0$ cross section, are shown in the upper left panel. In addition, the Keeler small-angle data at 319 MeV are plotted, also with their original normalization. In the lower left panel, the cross section multiplied with the solid angle element $2\pi \sin\theta$ is given, thus displaying how much each scattering angle contributes to the total cross section. It is evident that the two data sets are not in mutual agreement. We have taken ourselves the liberty to renormalize them to agree internally, applying Legendre polynomial fits to the two data sets and joining the fits in the overlap region. Finally, the combined set was normalized to the experimental total cross section by Lisowski *et al.*, with a 3% correction for the inelasticities obtained from SM95. The resulting set is presented in the right panels.

The renormalization factors are rather large. The Keeler set had to be reduced by 13%. However, the Keeler data were normalized to their own total cross section measurement, which is about 6% higher than the Lisowski and Grundies

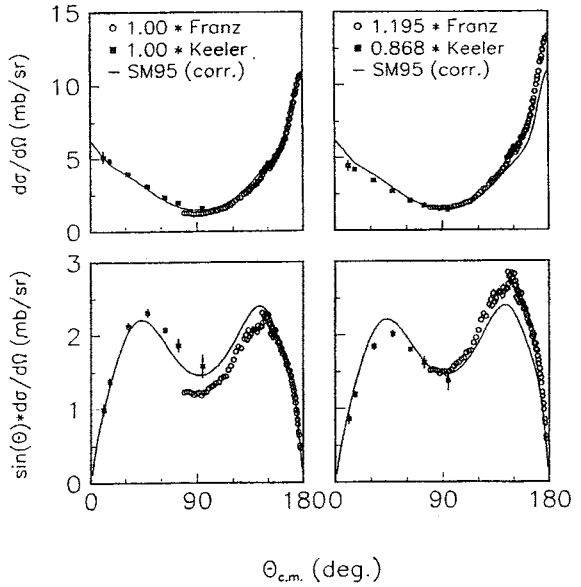


*Fig. 14.* Cross-check of the pion-production and total cross-section normalization methods. Upper left: the Keeler and Franz data with their original normalization. Lower left: the same data, but multiplied with the solid angle element $2\pi \sin\theta$. Right: the same data but renormalized to the total cross section. The PWA SM95 has been renormalized to the experimental total cross section. See the text for details.

data. Our renormalization therefore accounts for additionally 7%. The Franz data need to be renormalized upwards by almost 20%! Apparently, the pion production and total cross section normalizations are inconsistent. The inconsistency is even larger than what can be explained from the previous systematic shift of the $pp \rightarrow d\pi^+$ cross section. It is evident from Fig. 14 that there are large uncertainties involved in this procedure, because of the small overlap between the two data sets, and the large error bars of the Keeler data at about 90°. Nevertheless, it seems as relatively large renormalizations are required to bring the differential and total cross section data into agreement.

### 4.4. *Conclusion and discussion on normalization techniques*

We find it evident that normalization using pion production has an inherent uncertainty on the 5 – 10% level from the $pp \rightarrow d\pi^+$ data situation only. In addition, there are other complications, like the precision in absolute neutron energy and the conversion from $pp \rightarrow d\pi^+$ to $np \rightarrow d\pi^0$. Our conclusion is that it is presently impossible to normalize to better than 10% with this technique. This has profound consequences for the debate on the pion-nucleon coupling constant, $g^2_{\pi NN}$. The difference between the values 14.4 and 13.6 is about 6%, which corresponds to 12% in normalization (recall that the coupling constant scales to first order with the normalization $N$ of the differential cross section as $\sqrt{N}$). With present techniques, data normalized with the pion production method cannot distinguish between these two values.

When using the total cross section for normalization, substantially better precision is reached if a wide-angle data set is used. With reasonable assumptions about the uncertainty in the angular distribution of the undetected region, an uncertainty in the normalization of the order of 2 – 4% has been reached in a few recent experiments, which is sufficiently precise to distinguish the 13.6 and 14.4 values of $g^2_{\pi NN}$.

Our conclusion is that the total cross section is a more reliable technique than pion-production normalization. The total cross section is known with a precision superior to any other neutron-induced cross section. We believe that one of the best ways of avoiding the present normalization difficulties is to measure relative, differential np scattering cross sections, covering the full angular distribution, and normalize the result to the total cross section. Thus, an unambiguous normalization could be performed. Such experimental efforts are underway [79].

A novel and promising approach is attempted at IUCF (see the contribution by T. Peterson in these proceedings). The idea is to use a tagged neutron beam to measure the absolute scale of the cross section at backward angles. This requires good absolute knowledge of virtually every component in the detection system, but if this can be achieved, it would open a new possibility to resolve the normalization discrepancy.

## 5. Summary, discussion and outlook

In this paper, we have examined the world data base on np differential scattering cross section data from 100 to 1000 MeV incident neutron energy. In addition, the status of the np total cross section and the $pp \rightarrow d\pi^+$ total cross sec-

tion has been reviewed, because these have frequently been used to normalize np scattering data.

We have found two major problematic features of the data base. First, it appears that the shape of the large data sets tend to fall into either one of two mutually incompatible groups, with different steepness at backward angles. Second, it is not only the shape of the data that is under debate, but also the absolute scale. There are two major techniques for normalizing data, which yield incompatible results. Both these effects have implications for the determination of the pion-nucleon coupling constant, $g^2_{\pi NN}$, and not surprisingly, different opinions about its value appear.

It is tempting to speculate about some features of the data and the theoretical analyses of them. The Bonner and the Hürster/Franz data, which heavily dominate the data base in the 200 – 500 MeV range, are definitely incompatible in this energy interval, while the disagreement at higher energies is not as large. The Hürster/Franz data look rather similar to what could be expected if one-pion charge exchange dominates the cross section over a wide energy range, making the cross section almost insensitive to energy in the 100 – 1000 MeV interval. If these data are correct, it seems not unlikely that a simpler interpretation could be made, being more "one-pionlike". Could it be that some of the theoretical models of today are misguided by the difficult data situation, and thus too complicated?

By the publication of the Franz data [27], the input to PWA becomes rather different. The relative statistical weights for the Bonner group, Bizard and Hürster data are today 44%, 10% and 28%, respectively, but with the Franz data replacing the Hürster data, these numbers will change to 21%, 5% and 66%, respectively, thus the PSI data will dominate heavily. It will be very interesting to follow this development.

One striking feature in some PWAs, e.g, SM95, is the wiggly behaviour around 600 MeV. This is obvious in Fig. 9, but it can also be seen in Fig. 7, and possibly also in Fig. 6. It is noteworthy that this shows up at the maximum of the $np \rightarrow d\pi^0$ cross section, i.e., at the $\Delta$ resonance. If there are experimental problems associated with this, e.g., a normalization problem tending to push the cross section up before the maximum and below after or vice versa, wiggles could be produced.

The np data on which SM95 is based were almost exclusively normalized by pion production techniques. Not one single experiment has taken the large ($\sim 8\%$) correction factor emanating from the $\Delta$ resonance into account in the calculation of the $np \rightarrow d\pi^0$ cross section from the $pp \rightarrow d\pi^+$ cross section. If the np scattering process were governed by one-pion exchange only, the data would fall on a horizontal line in Fig. 9. The dashed line is such a horizontal line, corrected for charge symmetry breaking effects, as calculated by Niskanen and Vestama [46]. The close similarity with the SM95 solution calls for a discussion. Could it possibly be that the physics might be simpler than indicated by the Virginia analysis, but that the data are jeopardized by not taking the Niskanen-Vestama effect into account in the normalization process?

One of our conclusions after this investigation is that there is still a great need for new, precision data, especially in the low energy range, i.e., up to 500 MeV or so. In particular, the available data at backward angles for energies below 200 MeV are very scarce, and new data in this range should therefore be given high priority.

Normalization has been a problem for a long time, manifested in that some theoretical analyses are performed using floating normalization. This approach has made sense when using data with very unreliable absolute scale, but, evidently, important physics information has been lost in the process. Finding techniques to obtain precise, reliable normalization should therefore be given high priority. Our conclusion is that normalization to the total cross section has the best potential in this respect. Measurements covering the entire angular distribution would be of particular value for this purpose.

Furthermore, efforts should be put into a more elaborate evaluation of the existing data. By careful analysis of the experimental conditions, it might be possible to find systematic problems that can explain the deviations.

## Acknowledgements

Numerous stimulating discussions with Torleif Ericson and Benoît Loiseau are gratefully acknowledged. We want to thank the The Svedberg Laboratory and the Uppsala neutron collaboration for its support, J.A. Niskanen for valuable discussions, and the PSI group for supplying data prior to publication. This work was supported by the Swedish Natural Science Research Council, Vattenfall AB, Swedish Nuclear Fuel and Waste Management Company, Swedish Nuclear Power Inspectorate, Barsebäck Power AB, and the Swedish Defense Research Establishment.

## References

1. Ericson, T. E. O., Nucl. Phys. A **543**, 409c (1992).
2. Koch, R. and Pietarinen, E., Nucl. Phys. A **336**, 331 (1980).
3. Kroll, P., Physics Data **22-1**, (ed. H. Behrens and G. Ebel), (Fachinformationszentrum, Karlsruhe, 1981).
4. Bergervoet, J. R. *et al.*, Phys. Rev. C **41**, 1435 (1990).
5. Klomp, R. A. M., Stoks, V. G. J. and de Swart, J. J., Phys. Rev. C **44**, R1258 (1991).
6. Stoks, V., Timmermans, R. and de Swart, J. J., Phys. Rev. C **47**, 512 (1993).
7. Arndt, R. A., Li, Z., Roper, D. and Workman, R. L., Phys. Rev. Lett. **65**, 157 (1990).
8. Arndt, R. A., Strakovsky, I. I. and Workman, R. L., Phys. Rev. C **50**, 2731 (1994).
9. Arndt, R. A., Workman, R. L. and Pavan, M. M., Phys. Rev. C **49**, 2729 (1994).
10. Rönnqvist, T. *et al.*, Phys. Rev. C **45**, R496 (1992).
11. Rahm, J. *et al.*, Phys. Rev. C (submitted).
12. Ericson, T. E. O. *et al.*, Phys. Rev. Lett. **75**, 1046 (1995).
13. Rahm, J. *et al.*, Phys. Rev. C **57**, 1077 (1998).
14. Rentmeester, M. C. M., Klomp, R. A. M. and de Swart, J. J., Phys. Rev. Lett. **81**, 5253 (1998).
15. Ericson, T. E. O. *et al.*, Phys. Rev. Lett. **81**, 5254 (1998).
16. The Nijmegen data base is easily accessed over www at http://nn-online.sci.kun.nl/. A listing of the data is found in Ref. [17]. The selection criteria for data in the Nijmegen data base are that they have been published after January 1, 1955 in a regular journal. Data from conference proceedings or quasi-elastic data are not used. We have found some publications fulfilling these criteria, but not present in the data base. These are de Pangher, J. Phys. Rev. **99**, 1447 (1955); Golovin, B. M., Dzhelepov, V. P., Katyshev, Yu.V. Konin, A. D. and Medved, S. V., Sov. Phys. JETP **36**, 516 (1959); Amaglobeli, N. S. and Kazarinov, Iu. M., Sov. Phys. JETP **34**, 37 (1958); Kazarinov, Iu. M. and Simonov, Iu. N., Sov. Phys. JETP **4**, 161 (1957); and Amaglobeli, N. S. and Kazarinov, Yu. M., Sov. Phys. JETP **37**, 1125 (1960). None of these articles contain data changing the conclusions in this paper. It should be noticed that only the first one falls within the energy window of the Nijmegen analyses (up to 350 MeV).
In addition, we would like to issue a warning for the data by Murray, T.

A. *et al.*, Nuovo Cim. **49**, 261 (1967). These data are not on free np scattering, but quasi-elastic scattering on deuterium. However, this data set is not used in the Nijmegen analyses anyway because of its high energy.
17. Stoks, V. G. J., Klomp, R. A. M., Rentmeester, M. C. M. and de Swart, J. J., Phys. Rev. C 48, 792 (1993).
18. Bonner, B. E. *et al.*, Phys. Rev. Lett. **41**, 1200 (1978).
19. Bizard, G. *et al.*, Nucl. Phys B **85**, 14 (1975).
20. Hürster, W. *et al.*, Phys. Lett. B **90**, 367 (1980).
21. Evans, M. L. *et al.*, Phys. Rev. Lett. **36**, 497 (1976).
22. Evans, M. L. *et al.*, Phys. Rev. C **26**, 2525 (1982).
23. Jain, Mahavir *et al.*, Phys. Rev. C **30**, 566 (1984).
24. Northcliffe, L. C. *et al.*, Phys. Rev. C 47, 36 (1993).
25. Terrien, Y. *et al.*, Phys. Rev. Lett. **59**, 1534 (1987).
26. Bersbach, A. J., Mischke, R. E. and Devlin, T. J., Phys. Rev. D **13**, 535 (1976).
27. Franz, J., Rössle, E., Schmitt, H. and Schmitt, L., published elsewhere in these proceedings.
28. Ericson, T. E. O., Prog. Part. Nucl. Phys. **11**, 245 (1983).
29. Loiseau, B., private communication.
30. Wilson, R., Ann. Phys. **32**, 193 (1965).
31. Hobbie, R. K. and Miller, D., Phys. Rev. **120**, 2201 (1960).
32. Howard, V. J. *et al.*, Nucl. Phys. A **218**, 140 (1974).
33. Palmieri, J. N. and Wolfe, Janet P., Phys. Rev. C **3**, 144 (1971).
34. Measday, D. F., Phys. Rev. **142**, 584 (1960).
35. Randle, T. C. *et al.*, Proc. Phys. Soc. A **69**, 760 (1956).
36. Kazarinov, Y. M. and Simonov, Y. N., Sov. Phys. JETP **16**, 24 (1963).
37. Shepard, P. F., Devlin, T. J., Mischke, R. E. and Solomon, J., Phys. Rev. D **10**, 2735 (1976).
38. Keeler, R. K. *et al.*, Nucl. Phys. A **377**, 529 (1982).
39. de Swart, J. J., private communication.
40. Arndt, R. A., Strakovsky, I. I. and Workman, R. L., Phys. Rev. C **52**, 2246 (1995).
41. Breit, G., Christakis, A. M., Hull, M. H., Ruppel, H. M. and Seamon, R. E., Bull. Am. Phys. Soc. **9**, 378 (1964).
42. Arndt, R. A., Strakovsky, I. I. and Workman, R. L., Phys. Rev. C **48**, 1926 (1993). The data base can be reached via www at http://said.phys.vt.edu/.
43. Reitan, A., Nucl. Phys. B **11** (1969) 170.
44. Segrè, E., "Nuclei and Particles," (Benjamin/Cummings, Reading, Massachusetts, 1977).
45. Karlsson, B., private communication.
46. Niskanen, J. and Vestama, M., Phys. Lett. B **394**, 253 (1997).
47. Richard-Serre, C. *et al.*, Nucl. Phys. B **20**, 413 (1970).
48. Spuller, J. and Measday, D. F., Phys. Rev. D **12**, 3550 (1975).
49. Bystricky, J. *et al.*, J. Physique **48**, 1901 (1987).
50. Ritchie, B. G., Phys. Rev. C **44**, 533 (1991).
51. Measday, D. F., private communication.
52. In the Northcliffe *et al.* paper [24], it was quoted as ±3% error in energy. We assume that this is a misprint, based on comparisons with Fig. 5 in their paper, and the Ritchie fit. If it were indeed a ±3% uncertainty, we get a ±14% error in the cross section.
53. Heimberg, P. *et al.*, Phys. Rev. Lett. **77**, 1012 (1996).
54. Drochner, M. *et al.*, Phys. Rev. Lett. **77**, 454 (1996).
55. Drochner, M. *et al.*, Nucl. Phys. A **643**, 55 (1998).
56. Rose, Carl M. Jr., Phys. Rev. **154**, 1305 (1967).
57. Hutcheon, D. A., Nucl. Phys. A **535**, 618 (1991).
58. Blomgren, J. and Olsson, N., Phys. Rev. Lett. **83**, 1692 (1999).
59. Drochner, M. *et al.*, Phys. Rev. Lett. **83**, 1693 (1999).
60. Bystricky, J. and Lehar, F., "Physics Data," No. 11-1 parts I and II, 1978, and No. 11–2 and 11–3, 1982, N – N Data (Fachinformationszentrum, Karlsruhe, 1982).
61. Glass, G., private communication.
62. Schmitt, L., private communication.
63. Wender, S. A., private communication.
64. Glass, G. *et al.*, Phys. Rev. C **28**, 1045 (1983).
65. Lisowski, P. W. *et al.*, Phys. Rev. Lett. **49**, 255 (1982).
66. Grundies, V., Franz, J., Rössle, E. and Schmitt, H., Phys. Lett. B **158**, 15 (1985).
67. Bowen, P. H., Scanlon, J. P., Stafford, G. H., Thresher, J. J. and Hodgson, P. E., Nucl. Phys. **22**, 640 (1961).
68. Culler, V. and Waniek, R. W., Phys. Rev. **99**, 740 (1955).
69. Measday, D. F. and Palmieri, J. N., Nucl. Phys. **85**, 142 (1966).
70. Devlin, T. J. *et al.*, Phys. Rev. D **8** (1973) 136.
71. Ashmore, A., Jarvis, R. G., Mather, D. S. and Sen, S. K., Proc. Phys. Soc. A **70**, 745 (1957).
72. Chen, F. F., Leavitt, C. P. and Shapiro, A. M., Phys. Rev. **103** 211 (1956).
73. Palevsky, H., Friedes, J. L., Sutter, R. J., Chrien, R. E. and Muether, H. R., in Proc. Int. Congress on Nuclear Physics, Paris, 1964, (ed. P. Gugenberger), (Centre National de la Recherche Scientifique, Paris, France, 1964), p. 162.
74. Widgoff Shapiro M., Cormack, A. M. and Koehler, A. M., Phys. Rev. **138B**, 823 (1965).
75. Bugg, D. V. and Machleidt, R., Phys. Rev. C **52**, 1203 (1995).
76. Finlay, R., private communication.
77. Bugg, D. V., comments to TSL proposal F66, private communication.
78. Lechanoine-LeLuc, C. and Lehar, F., Rev. Mod. Phys. **65**, 47 (1993).
79. Blomgren, J., Olsson, N. and the Uppsala neutron collaboration, TSL experiment FA113.

# Appendix IV

ELSEVIER

Nuclear Physics A 677 (2000) 3–24

NUCLEAR PHYSICS A

www.elsevier.nl/locate/npe

# The $^{9}$Be(n,p)$^{9}$Li reaction and the Gamow–Teller unit cross section

S. Dangtip [a], J. Blomgren [a,*], N. Olsson [a], H. Condé [a], K. Elmgren [a], J. Rahm [a], A. Ringbom [b], G. Tibell [b], O. Jonsson [c], L. Nilsson [c], P.-U. Renberg [c], S.Y. van der Werf [d]

[a] *Department of Neutron Research, Uppsala University, Box 535, S-75121 Uppsala, Sweden*
[b] *Department of Radiation Sciences, Uppsala University, Box 535, S-75121 Uppsala, Sweden*
[c] *The Svedberg Laboratory, Uppsala University, Box 533, S-75121 Uppsala, Sweden*
[d] *Kernfysisch Versneller Instituut, Zernikelaan 25, 9747 AA Groningen, The Netherlands*

Received 25 February 2000; revised 17 April 2000; accepted 1 May 2000

**Abstract**

Double differential cross sections of the $^{9}$Be(n,p)$^{9}$Li reaction have been measured at 96 MeV in the angular range 0°–27° up to about 20 MeV excitation energy. In addition, the $^{12}$C(n,p)$^{12}$B reaction has been measured in the same angular and excitation energy range. Cross sections for reactions leading to the ground state and the first excited state (2.69 MeV) of $^{9}$Li have been analysed using peak-fitting techniques. The data have been compared with cross sections obtained from distorted-wave Born approximation calculations. A Gamow–Teller (GT) unit cross section for the ground state transition of $7.4 \pm 1.2$ mb/sr was determined from the identified GT strength. Discrepancies in the Gamow–Teller unit cross sections for different (n,p) and (p,n) transitions from the $^{9}$Be ground state, resembling the situation for $^{13}$C, have been found. 

*PACS:* 24.50.+g; 25.40.-h; 25.40.Kv; 27.20.+n
*Keywords:* NUCLEAR REACTION $^{9}$Be(n,p), $^{12}$C(n,p), $E = 96$ MeV; Measured $\sigma(E_p, \theta)$; DWBA calculations; Deduced Gamow–Teller strength

## 1. Introduction

The (p,n) reaction has been the subject of intensive experimental effort during the last twenty years. Now a very rich data base exists, where the main excitations — with special emphasis on Gamow–Teller (GT) strength — can be studied versus, e.g., projectile energy and target mass [1,2].

* Corresponding author. E-mail: jan.blomgren@tsl.uu.se

0375-9474/00/$ – see front matter 
PII: S0375-9474(00)00284-0

It has been found that the GT unit cross section, $\hat{\sigma}_{GT}$, varies smoothly as a function of mass $A$, at a given energy, and that it is slightly larger for odd than for even nuclei. This unit cross section is given by

$$\hat{\sigma}_{GT} = \sigma_{GT}/B_{GT}, \tag{1}$$

where $\sigma_{GT}$ is the experimental GT cross section at 0°, corrected for optical model distortions and the finite momentum and energy transfer in the reaction, and $B_{GT}$ is the strength obtained from the corresponding $\beta$ decay.

The unit cross section for odd nuclei is systematically 20–30% larger than for even. This behaviour is not fully understood. Furthermore, for some odd nuclei, e.g., $^{13}$C and $^{15}$N (and possibly $^{35}$Cl), the GT unit cross section for the ground state transition is 30–40% larger than a smooth trend through the data points for other odd nuclei would indicate. In contrast, the transition to the 15.1 MeV state in the $^{13}$C(p,n)$^{13}$N reaction does not show any such effects.

A number of possible explanations have been discussed in the literature. Taddeucci et al. [1] suggested that optical potential parameter differences between odd and even nuclei could lead to uncertainties in distorted wave calculations. Systematic studies of optical potentials, especially for nonzero-spin targets, are thus motivated.

The unit cross section proportionality (Eq. (1)) relies on the dominance of central interactions and direct reaction mechanisms. Possible contributions from non-central interactions and non-direct reaction mechanisms as a reason for such effects have been discussed [1,3].

Another possibility of why the unit cross sections differ is because of problems with the axial vector current $g_A$. The Gamow–Teller transition in nuclear $\beta$ decay is determined by $(g_A/g_V)^2 B_{GT}$, while $\hat{\sigma}_{GT}$ is a function of $B_{GT}$ and $A$ only. It has been found that in the nuclear medium, the value of $g_A$ for the free neutron is reduced to an effective value of $(g_A)_{eff} = (0.8 - 0.9)g_A$, resulting in quenching values $[(g_A)_{eff}/g_A]^2$ of 60–80% [2]. In addition, the importance of heavy-meson exchange for GT matrix elements has been pointed out [4,5], which could possibly have some implications for the value of $g_A$. It is not known whether such effects could be different for odd and even nuclei.

Lack of data prevents systematic studies of such effects by the (n,p) reaction. Although with fewer data points available, the data base on unit cross sections for (n,p) on even nuclei shows a trend similar to that of (p,n) data. For odd nuclei, there are only two cases where the corresponding $B_{GT}$ is known; $^3$He from TRIUMF [6], and $^{13}$C from LAMPF [7] and TRIUMF [8].

Hence, further (n,p) reaction studies on nuclei, where corresponding data on (p,n) at about the same energy are available, should be most useful. One of the best cases among several candidates is $^9$Be (see Fig. 1a). The residual isotope $^9$Li has its first excited state as high as 2.7 MeV, which can be resolved from the ground-state with our present setup. Measurements on the corresponding $\beta^-$ decay from $^9$Li have been carried out [9–14], and this decay is also included in a recent review of log $ft$ values in $\beta$ decay [15]. Furthermore, the $^9$Be(p,n)$^9$B reaction has been studied by Pugh et al. [16] at 135 MeV at IUCF. Its ground-state transition was reported with good precision. In addition, the transition leading

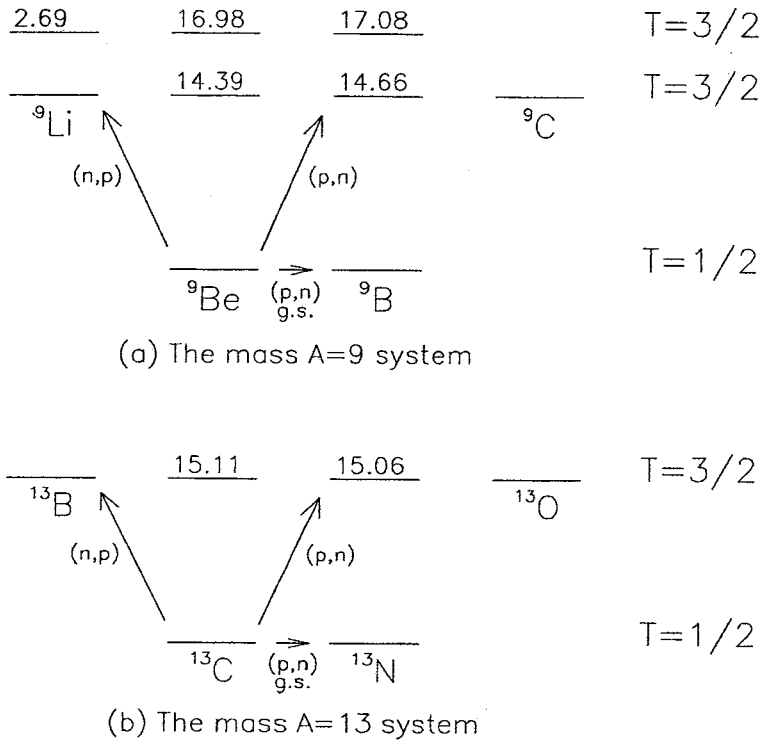


Fig. 1. Isobar diagrams of the mass (a) $A = 9$ and (b) $A = 13$ systems.

to the 14.6 MeV excited state of $^{9}$B, which is a member of the isospin $T = \frac{3}{2}$ multiplet, has been studied in the same work, and can be compared directly with the transition to the same isospin state (the ground state of $^{9}$Li) by the $^{9}$Be(n,p)$^{9}$Li reaction.

We have measured double-differential cross sections of the $^{9}$Be(n,p)$^{9}$Li reaction at 96 MeV using the TSL neutron facility, which is described in Section 2. The data reduction and experimental results are presented in Section 3, while details of the data analysis are found in Section 4. The results are discussed in Section 5, and finally, a summary and the conclusions are given in Section 6.

## 2. Experimental apparatus and procedure

The experiment presented in this paper was performed at the neutron facility of The Svedberg Laboratory in Uppsala, Sweden. The equipment (see Fig. 2) has been described in detail in Ref. [17], and only a brief summary is given here. The $95.8 \pm 0.5$ MeV neutrons were produced by the $^{7}$Li(p,n)$^{7}$Be reaction, using a 110 mg/cm$^{2}$ thick disc of lithium, enriched to 99.98% in $^{7}$Li. After the target, the proton beam was bent into a well-shielded beam dump. A narrow neutron beam in the forward direction was defined by a system of three collimators. The vacuum system was terminated with a 1 mm thick aluminium plate after the first collimator. Charged particles produced in this plate and along the collimator channel were deflected by a clearing magnet. The diameter of the neutron beam at the (n,p) target position, 8 m from the neutron production target, was about 7 cm. The neutron beam was dumped in a tunnel about 10 m after the spectrometer.

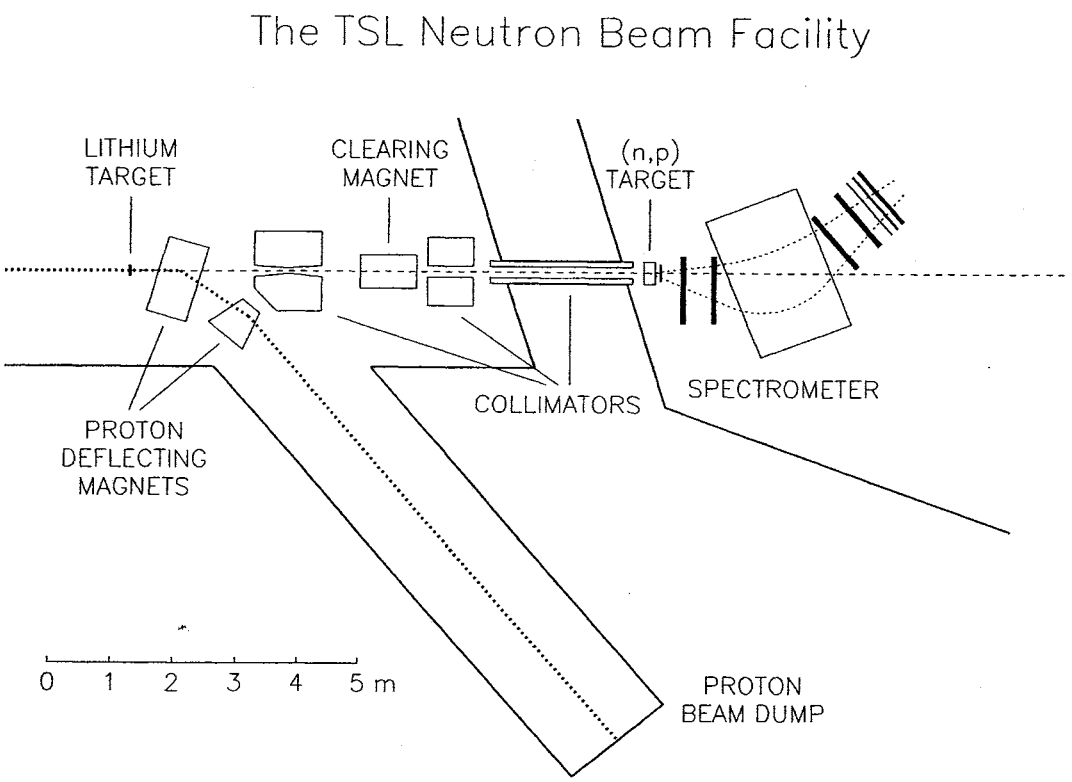


Fig. 2. The Uppsala (n,p) facility.

The sandwiched multi-target system used in the present study was filled with a 85 mg/cm$^2$ carbon foil, five 180–190 mg/cm$^2$ beryllium discs and a 50 mg/cm$^2$ $CH_2$ reference foil. The targets were interspaced by multi-wire proportional chambers (MWPC), allowing identification of the target, in which the reaction occurred. Before the target planes, two MWPC's were used to reject charged particles contaminating the beam. Spectra were also recorded with no beryllium targets mounted in the multi-target box to determine the small instrumental background. With a 3.0 μA proton beam incident on the $^7$Li target, the neutron yield was about $3.0 \times 10^5$ s$^{-1}$ in the solid angle defined by the collimator.

The momentum determination of the charged particles emitted from the reaction target was performed with a spectrometer consisting of a dipole magnet and four drift chambers, two in front of and two behind the magnet. The scattering angle was determined by the trajectory through the first two drift chambers. The spectrometer was operated slightly different than in our previous experiments; it was hooked onto a pivot point in order to simplify the positioning of the spectrometer. This was done at the cost of a reduced momentum bite.

The data were taken with the spectrometer magnet at three different positions, covering the scattering angle regions 0°–10°, 7°–17°, and 17°–27°, respectively. The magnetic field strength was kept at 1.0 T for all settings. The energy resolution was about 2.7 MeV (FWHM).

A trigger signal for the data acquisition system was generated by a triple coincidence between two large plastic scintillators, located behind the last drift chamber, and a thin scintillator, positioned immediately after the multi-target box. The neutron time-of-flight (TOF)

was measured using the thin-scintillator signal and the cyclotron RF as start and stop signals of a time-to-digital converter (TDC), respectively. This information was used to reject events from low-energy neutrons in the tail of the neutron spectrum. Together with information on the particle momentum, the pulse heights from the two large scintillators were used for particle identification, enabling separation of protons from other charged particles.

The data acquisition system was based on a VME-bus configuration in conjunction with CAMAC and NIM electronic modules. For each event the time information from the drift chambers and the MWPCs of the multi-target box, together with the linear signals from the scintillators and the neutron TOF, were stored on magnetic tape. In addition, preliminary spectra could be monitored on-line.

## 3. Data reduction and experimental results

The data were analysed off line on an event-by-event basis. The target plane in which the reaction took place was first identified. Events caused by charged particles contaminating the neutron beam, or produced in the thin plastic scintillator by (n,p) reactions, were identified and rejected. A neutron TOF criterion was applied, by which only charged particles associated with full energy neutrons were accepted. For the remaining events, energies were determined by ray-tracing through the magnet. This was done twice; first drift chamber one, two, and four were used. A second determination was made with the third instead of the fourth drift chamber. If the results obtained from the two combinations were too different, the event was rejected and so were events whose trajectory was outside the magnetic field boundaries. As the next step, particle identification was performed by an energy loss measurement in the scintillator telescope together with the momentum information obtained from the ray-tracing. The accepted beryllium or carbon data events were stored as relative double-differential cross sections in matrices with angular and energy bin widths of 1° and 0.5 MeV, respectively.

The background data, dominated by *np* scattering in the MWPC foils of the multi-target system, were treated in a similar way, and were subsequently subtracted from the beryllium and carbon data.

Also the data from the $CH_2$ foil, providing the normalization of the cross section scale, were analysed in an similar manner. A gaussian distribution was fitted to the hydrogen peak in the energy spectrum for each angular bin. The cross section scale was obtained by normalizing the angular distribution of the hydrogen-peak contents to that of a previous *np* scattering measurement [18]. This normalization was done by integrating the area under the angular distributions in the same angular region as covered by the present experiment.

Due to the finite width of the micropulses from the cyclotron (3–4 ns), the TOF rejection of low-energy neutrons was not complete. The remaining tail of low-energy neutrons was therefore subtracted from the beryllium spectra using an unfolding technique. The tail below the peak in the proton spectrum was divided into bins, where the contents were compared with the total hydrogen spectrum. Scaled by this ratio, a shifted beryllium spectrum was subtracted from the full spectrum for each bin. The effect of this correction is small, and in the main region of interest for this work, it is negligible.

Acceptance corrections were determined experimentally by making narrow software cuts on the vertical scattering angle to allow only trajectories almost parallel to the median plane, i.e., unperturbed by the pole faces of the magnet. By comparing the energy spectra and angular distributions obtained with different vertical angle cuts, the required correction factors could be extracted.

Examples of experimentally determined double-differential cross sections in the centre-of-mass (c.m.) system, grouped in 1° bins, are shown in Fig. 3 for carbon (left panel) and beryllium (right panel). The error bars represent the statistical uncertainties only. In addition, the cross section scale has a systematic error which is dominated by the 4% uncertainty in the *np* scattering cross section. The data at the very forward angles cover up to a few MeV of excitation energy only. The region covered is, however, wide enough to allow us to study the ground state transition. This can be verified by comparing with the data obtained from the carbon foil, which were analysed in parallel, because the $Q$-values are very similar. The carbon cross section data are in good agreement with our previously published data [19]. The ground state cross sections for $^{9}$Be(n,p) were determined by two different approaches; by an absolute determination using *np* scattering as cross section reference, and by a relative comparison with the $^{12}$C(n,p) ground state transition, using cross sections from Ref. [19]. The two methods agree well with each other.

## 4. Data analysis

The experimental data obtained in this work are expected to correspond to a mixture of transitions of different multipolarities to states of different degrees of collectivity and possibly, due to the nature of inclusive proton measurements, contributions from other reaction channels with (at least) one proton in the exit channel. In contrast to the studies of medium-weight and heavy nuclei [20–22], multistep contributions are expected to be negligible for light nuclei, because of the much lower level densities. That this is indeed the case has been verified by a calculation using a computer code by Bonetti and Chiesa [23,24], based on the Feshbach–Kerman–Koonin theory for statistical multistep direct reactions [25].

To extract the contribution from GT strength, as well as from other multipolarities, the energy distribution at each angular bin of 1° was fitted with a number of gaussian peaks, located where some structure is visible. The angular distribution of the gaussian peaks were subsequently compared with those obtained from distorted-wave Born approximation (DWBA) calculations, using wave functions from shell-model calculations for light nuclei. At higher excitation energies, the measured energy spectra were compared directly, i.e., without peak fitting, with spectra generated from the shell-model and DWBA calculations.

In the following subsections, the different steps of the analysis are described in some detail. The results are discussed and compared with theoretical studies.

### *4.1. Peak fitting*

To extract information on the various structures seen in the spectra, the data were decomposed into gaussian peaks, each representing a known level or resonance in the

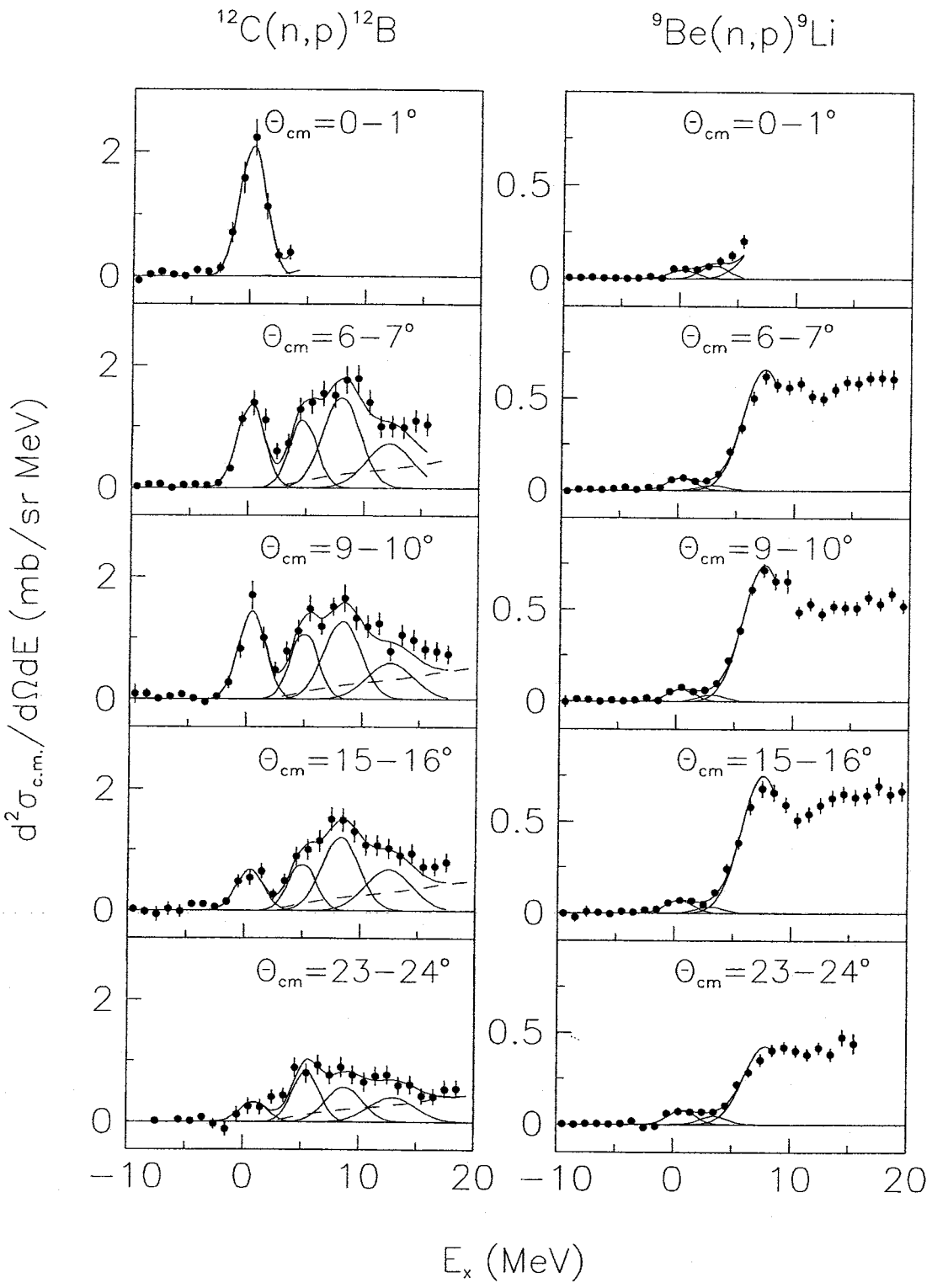


Fig. 3. Experimental double differential cross sections of the $^{12}C(n,p)^{12}B$ reaction (this work; left), and the $^{9}Be(n,p)^{9}Li$ reaction (right) at $E_n = 96$ MeV, projected into energy spectra with angular bins of 1°. Solid lines represent the gaussian peaks used to fit the data. In the case of $^{12}C$ also a phase-space continuum was introduced in the analysis. The sum of the curves is shown as a solid line close to the data points.

Table 1
Parameters of the gaussian peaks used to fit the carbon spectra in Fig. 3

| $E_x$ (MeV) | $\Gamma^a$ (MeV) | $\Gamma^b$ (MeV) |
|---|---|---|
| 0 | 2.7 | 0 |
| 4.5 | 2.7 | 0 |
| 7.8 | 3.7 | 2.6 |
| 12.0 | 4.7 | 3.9 |

[a] Including the experimental resolution.

[b] Excluding the experimental resolution.

residual nucleus. The width of the gaussians reflect the experimental energy resolution in combination with the intrinsic width of the level. The carbon data were processed first, since a comparison of this reaction with the more detailed study in our previous work [19] can be made, and thus serve as a confidence check. Furthermore, the experimental resolution can be obtained from this reaction, since the ground state is well isolated from excited states. With guidance from the carbon data, the beryllium data can be treated in an analogous way.

The carbon data at 0°–2° only extend up to the first few MeV, due to the limited momentum acceptance of our present setup (see Section 2). In this region, only the ground state peak is observed. At larger scattering angles, three peaking structures are clearly seen in the experimental data (Fig. 3; left panel). The first of these is associated with the $1^+$ ground state, in combination with the first excited $2^+$ state at $E_x = 0.95$ MeV, which could not be resolved from the ground state. The second peak is assigned mainly to the $2^-$ and $4^-$ states at $E_x = 4.46$ and 4.52 MeV, respectively. The third structure at about 8 MeV is interpreted as the sum of the $1^-$ isovector dipole (IVD; S = 0) and spin-isovector dipole (SIVD; S = 1) giant resonances, which from systematics are expected at this energy. In addition, a fourth gaussian was placed at $E_x = 12$ MeV, just to get a similar analysis as in Ref. [19]. To this end, also the 3-body break-up phase-space background used in that work was subtracted from the data before the fitting procedure. The parameters of the four gaussians are given in Table 1.

For each 1° angular bin, the strength of the four gaussians were fitted to the experimental energy spectra up to the maximum excitation energy. The result for a sample of the data is shown in Fig. 3 (left panel), where the gaussians are represented by solid lines. The sum of all the contributions (including the 3-body break-up phase-space) is shown as the solid line close to the experimental data points. As can be seen, the data are well described by the fitted curves up to the maximum excitation energy.

The angular distributions of the first two peaks are shown as filled circles in Fig. 4. As can be seen, the present results resemble well the data of Olsson et al. [19], shown as open circles in the same figure, although the present data have poorer statistics.

For the beryllium data, three gaussians were fitted at low excitation energy (see Fig. 3; right panel). The first one corresponds to the transition from the $J^\pi = \frac{3}{2}^-$; $T = \frac{1}{2}$ ground

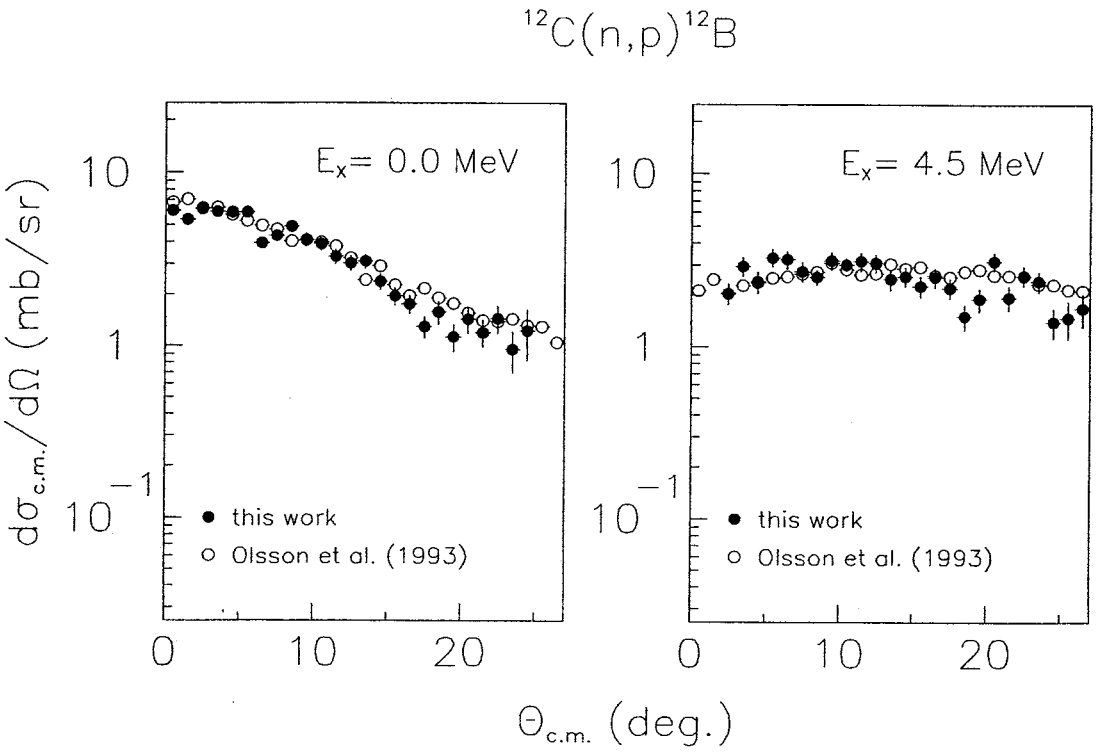


Fig. 4. Angular distributions for the first two gaussian peaks of the carbon data shown in Fig. 3 (filled circles) compared to the data at $E_n = 98$ MeV from Olsson et al. [19] (open circles).

Table 2
Parameters of the gaussian peaks used to fit the beryllium spectra in Fig. 3

| $E_x$ (MeV) | $\Gamma^a$ (MeV) | $\Gamma^b$ (MeV) |
|---|---|---|
| 0 | 2.7 | 0 |
| 2.7 | 2.7 | 0 |
| 7.1 | 4.3 | 3.3 |

[a] Including the experimental resolution.

[b] Excluding the experimental resolution.

state of $^9$Be to the $J^\pi = \frac{3}{2}^-$; $T = \frac{3}{2}$ ground state of $^9$Li. The second one is identified as the transition to the $J^\pi = \frac{1}{2}^-$ excited state at $E_x = 2.69$ MeV, which is probably the isobaric analogue of the $E_x = 16.98$ MeV state in $^9$Be [26] (see Fig. 1a). A third gaussian is introduced to represent the steep rise of a possible dipole resonance at about $E_x = 7$–$8$ MeV. The parameters of the gaussians are given in Table 2.

The strength of the three gaussians were fitted to the experimental data up to $E_x = 4$ MeV for the 0°–2° region and up to 8 MeV for $\theta > 2°$. The result for a sample of the data is shown in Fig. 3 (right panel). The gaussians are again shown as solid lines, while the sum of all contributions is represented by the solid line close to the experimental data points. Since the fitting was terminated already at $E_x = 8$ MeV, and the main interest in

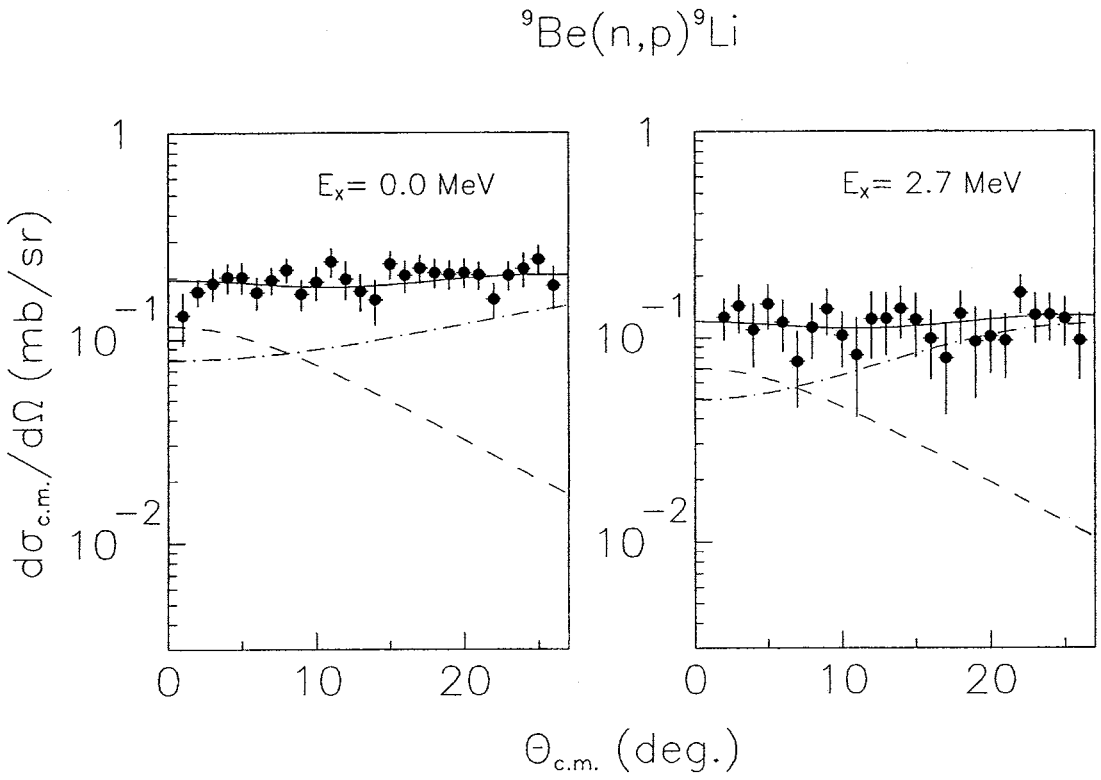


Fig. 5. Angular distributions for the first two gaussian peaks of the beryllium data shown in Fig. 3 (filled circles). Also included are the curves from DWBA calculations using OBDME's based on shell-model calculations and represent: GT (dashed) and $2^+$ (dash-dotted). The upper solid curve represents the sum of both contributions. The normalization for the different transitions is discussed in the text.

the present work is restricted to the ground-state transition, we found no reason to involve a subtraction of a phase-space continuum. As can be seen, the data are well described by the fitted curves up to about $E_x = 8$ MeV.

The angular distributions for the two peaks obtained in the fitting are shown as filled circles in Fig. 5. The error bars are the statistical errors combined with the uncertainties in the peak decomposition. We note that the distributions are similar in shape, i.e., both peaks show rather flat angular distributions.

The cross sections for these two transitions are, to our knowledge, the weakest ever measured in an (n,p) reaction experiment. Therefore, a possible contamination of background arising from *np* scattering in the MWPC foils could, in principle, severely distort the analysis of the ground state, which is of main interest here. Such a contamination would occur at large angles ($> 20°$), but should be separated by kinematics at small angles. This effect can be checked by displaying the small-angle double differential spectra down to, e.g., $E_x = -10$ MeV. For such a contamination one would expect non-zero cross section in the excitation-energy region below the ground state, separated by the $Q$-value difference and the kinematics. As can be seen in Fig. 3, this contamination is negligible for both data sets in the energy region of interest.

### 4.2. DWBA calculations

Angular distributions were calculated in the framework of the distorted-wave Born approximation (DWBA), using a model of $1p - 1h$ excitations. The reaction calculations were performed using the code DW81 [27], where contributions from the different particle-hole configurations are added coherently. The effective nucleon–nucleon (NN) force was represented by the energy- and density-dependent G-matrix at 100 MeV of Nakayama and Love [28]. This interaction is built on the Bonn potential [29], and takes nuclear medium effects into account.

The distorted waves were determined with the optical model. Parameters for both the $^9$Be + n and $^9$Li + p potentials were obtained from a systematic parametrization by Koning [30].

The single-particle wave functions used to calculate one-body density-matrix elements (OBDME) were obtained from $0\hbar\omega$ and $1\hbar\omega$ shell-model calculations for the positive- and negative-parity transitions, respectively, using the computer code OXBASH [31]. The positive-parity transitions were derived from the CK(POT) interaction [32] in the $p$ model-space, while the negative-parity ones were derived from the Millener–Kurath (MK) interaction [33] in the $sp$–$2sd$ model-space. The mass 9 nuclei were described by simple harmonic-oscillator radial wave functions, calculated with an oscillator constant of $b_0 = 1.44$ fm.

The ground state transition connects a $\frac{3}{2}^-$ initial to a $\frac{3}{2}^-$ final state and corresponds to spin transfers of $J^\pi = 0^+, 1^+, 2^+$, and $3^+$. The $J^\pi = 0^+$ transition gives by far the smallest contribution, roughly four orders of magnitude smaller than the other $J$ values. The GT transition ($J^\pi = 1^+$) dominates at small angles, while $J^\pi = 2^+$ and $3^+$ dominate further out. A least squares fitting of the calculated angular distributions to the experimental data was performed, as is shown in Fig. 5 (left panel). From the fitting procedure, it was found to be sufficient to include the GT (dashed line) and $J^\pi = 2^+$ (dot-dashed line) transitions to account for the data. The $J^\pi = 2^+$ and $J^\pi = 3^+$ distributions are very similar, and cannot be distinguished by such a fit. The GT transition had to be multiplied by 0.18, while a factor of 1.6 was used for the $2^+$ transition. The sum of the two contributions, shown as a solid line, describes the data points well.

The 2.7 MeV excited state is the result of a transition from a $\frac{3}{2}^-$ initial state to a $\frac{1}{2}^-$ final state, which means that only $1^+$ and $2^+$ transitions come into play. The shell-model calculation gives no state close to this excitation energy, and thus we have used the same $1^+$ and $2^+$ angular distributions as were used for the ground state. The result is shown in Fig. 5 (right panel), where it can be seen that the sum (solid line) of the $1^+$ (dashed line) and $2^+$ (dot-dashed line) contributions describes the data well. The factors needed to fit the data were 0.11 ($1^+$) and 1.01 ($2^+$), respectively.

The negative-parity transitions are expected to be of dipole character, and have $J^\pi = 0^-$, $1^-$, and $2^-$. Major contributions are expected from $1^-$ and $2^-$ transitions, while the $0^-$ transitions should be weak. The OXBASH calculation shows broad concentrations of $1^-$ strength around $E_x = 12$ MeV and $2^-$ strength at about $E_x = 7$–$8$ MeV. A similar trend, although at lower excitation energy and with smaller separation, was found in the previous

work on $^{12}$C(n,p) [19]. The steep rise seen in the spectrum above $\sim 5$ MeV (see Fig. 3; right panel), simulated in the decomposition by introducing the third gaussian, is identified as the concentration of $2^-$ strength found in the calculation.

To compare the shell-model calculations for the broad dipole states with the experimental data, we have made an attempt to bring the analysis one step further by calculating the full spectrum response. Thus, we have performed DWBA calculations for all the shell-model states resulting from the OXBASH calculation (including the $1^+$ and $2^+$ transitions). Excitation energy spectra for each angular bin were produced by adding the calculated double differential cross sections from each state, and folding with the experimental resolution of 2.7 MeV. It was found that the absolute magnitude of the dipole states is overpredicted by the model (about a factor of 3–5), and that the $1^-$ strength seems to appear at too low energy. It is, however, not uncommon that shell model calculations on a limited base falls short of reproducing the full degree of collectivity. As a result, the excitation energy and the absolute values of the cross sections might not be very well reproduced, although the shape makes sense. We have therefore taken ourselves the liberty to translate the calculated $1^-$ strength 4 MeV upwards, which results in a much improved description of the data.

In Fig. 6, we present the result for a few selected angles, after reduction of the calculated strengths to fit the experimental data at small angles. The reduction factors for the positive-parity states were kept the same as for the ground state, while factors of 0.18 and 0.32 were needed for the $1^-$ and $2^-$ distributions, respectively. As can be seen, the shape is well described over the experimental excitation energy range. The magnitude of the calculated spectra reproduces the experimental data reasonably well from 0° up to about 16°, while the data are overestimated at larger angles.

### 4.3. Gamow–Teller unit cross section

The proportionality between the 0° (p,n) cross section and the corresponding GT $\beta$ decay transition strength, $B_{\mathrm{GT}}$, has been discussed in detail by Taddeucci et al. [1], and this proportionality should be equally valid for (n,p) reactions [3]. Thus, the $^9$Be(n,p)$^9$Li reaction, where the $^9$Li residual nucleus is left in its $\frac{3}{2}^-$ ground state, is governed by the same matrix element as the inverse GT $\beta^-$ decay. The cross section of the (n,p) reaction can therefore be directly related to the $\beta$ decay strength. A factorised relation has been determined [1,34] for the cross section of GT transitions in charge-exchange reactions, valid at intermediate energies and in the limit of zero momentum transfer ($q = 0$) and zero energy loss ($\omega = E_x - Q = 0$),

$$\frac{d\sigma}{d\Omega}(q=0,\omega=0) = K(E_n,\omega=0)N^D(q=0,\omega=0)|J_{\sigma\tau}(q=0)|^2 B^{np}_{\mathrm{GT}}, \tag{2}$$

where $N^D$ is the ratio of the distorted- to plane-wave cross sections, and $J_{\sigma\tau}(q=0)$ is the volume integral of the central spin–isospin component $V_{\sigma\tau}$ of the effective NN interaction. $K$ is a kinematic factor given by

$$K(E_n,0) = \frac{E_i E_f}{(\pi\hbar^2c^2)^2}\frac{k_f}{k_i}. \tag{3}$$

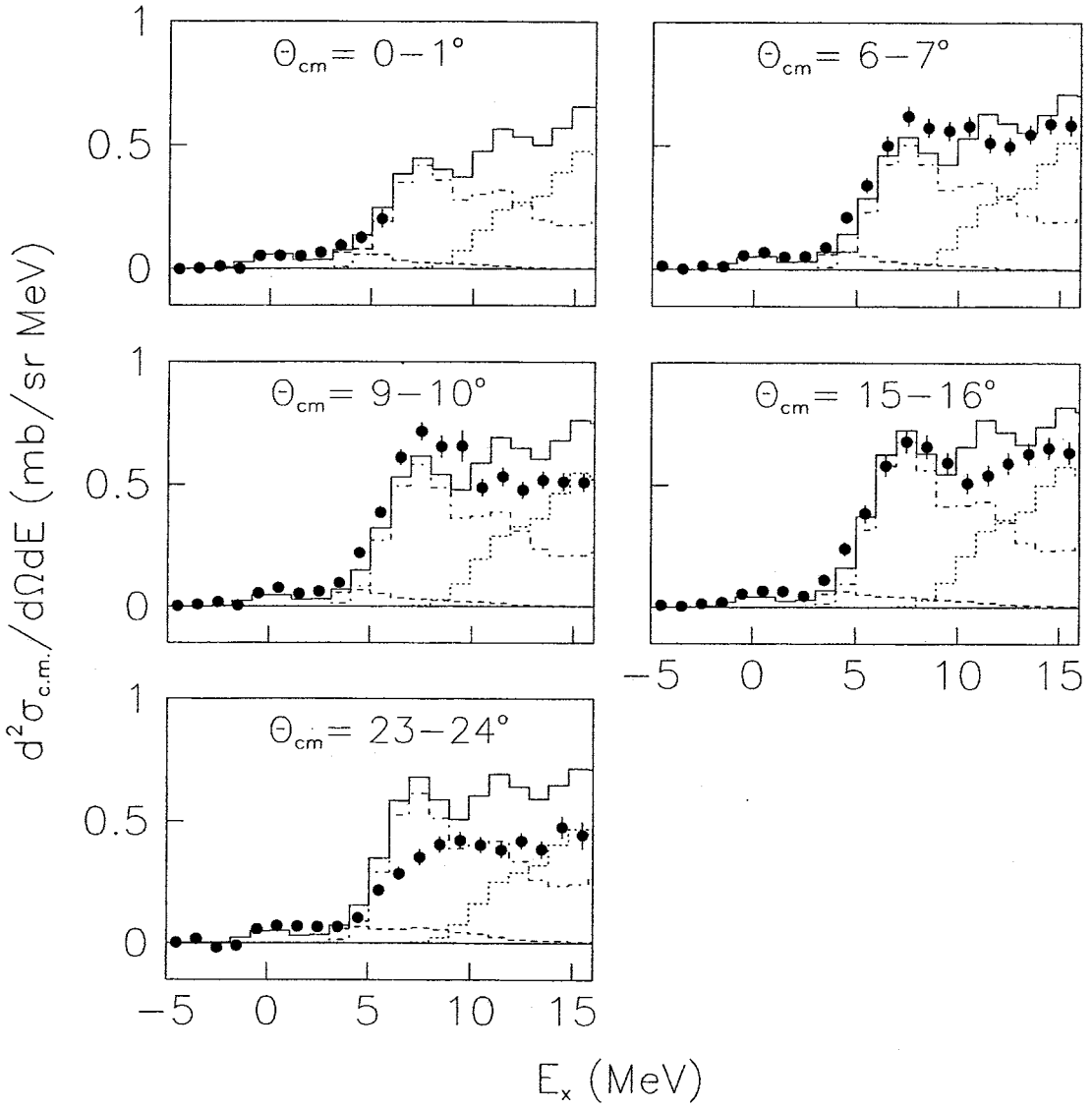


Fig. 6. Experimental double differential cross sections of the $^{9}$Be(n,p)$^{9}$Li reaction at $E_n = 96$ MeV projected into energy spectra with angular bins of 1°. The dashed, dotted and dot-dashed lines represent the DWBA calculations for $1^+ + 2^+$, $1^-$ and $2^-$ transitions, respectively. The solid line is the sum of these contributions. The normalization of the calculations is described in the text.

Using the definition of the unit cross section, $\hat{\sigma}$,

$$\hat{\sigma} = K(E_n, 0)N^D(0, 0)|J_{\sigma\tau}(0)|^2, \tag{4}$$

the expression given in Eq. (2) can be rewritten in terms of $\hat{\sigma}$ as

$$\hat{\sigma} = \frac{d\sigma}{d\Omega}(0, 0)/B_{\mathrm{GT}}^{np}. \tag{5}$$

The GT transition strength, $B_{\mathrm{GT}}^{np}$, is derived from the inverse $\beta$ decay using

$$\left(\frac{g_A}{g_V}\right)^2 B_{\mathrm{GT}}^{np} = \frac{2J_f + 1}{2J_i + 1}\frac{6166}{ft}, \tag{6}$$

Table 3
log $ft$ values of the $^9$Li($\beta^-$)$^9$Be $\beta$ decay leading to the ground state

| Author | | log $ft$ | $B_{GT}^{np}$ |
|---|---|---|---|
| Nyman et al. [9] | Measured | 5.32 | $0.019 \pm 0.002$ |
| Björnstad et al. [10] | Measured | 5.32 | $0.019 \pm 0.002$ |
| Langevin et al. [11][a] | Measured | 5.31 | $0.019 \pm 0.002$ |
| Chen et al. [12] | Measured | $5.12^{+0.01}_{-0.02}$ | $0.029 \pm 0.002$ |
| Alburger et al. [13] | Measured | $5.5 \pm 0.02$ | $0.012 \pm 0.006$ |
| Nefkens [14] | Measured | 5.23 | $0.023 \pm 0.006$ |
| Kumar [36] | Calculated | 5.46 | 0.013 |
| Barker [37] | Calculated | 5.32 | 0.019 |
| Cohen and Kurath [32] | Calculated | 5.12 | 0.029 |

[a] $B_{GT}$ taken from Ref. [38].

where $(g_A/g_V) = 1.260 \pm 0.008$ [1,35] and $J_{i(f)}$ refers to the total angular momentum of the target (residual) nucleus in the (n,p) reaction. With knowledge of the log $ft$-value of the $\beta$ decay, $B_{GT}^{np}$ can be deduced. Table 3 gives such values, both theoretical and experimental, found in the literature. Singh et al. [15] have recommended a log $ft$-value of 5.31 in their recent review, corresponding to a $B_{GT}$ of $0.019 \pm 0.002$, which we have adopted in this paper.

Obtaining $d\sigma(0,0)/d\Omega$ from the experimental cross section is done by correcting for the $q$ and $\omega$ dependences using DWBA calculations,

$$\frac{d\sigma}{d\Omega}(0,0) = \frac{[d\sigma(0,0)/d\Omega]_{\mathrm{DWBA}}}{[d\sigma(q,\omega)/d\Omega]_{\mathrm{DWBA}}}\left[\frac{d\sigma}{d\Omega}(q,\omega)\right]_{\mathrm{exp}}. \tag{7}$$

The first factor of Eq. (7) is determined using the ratio of two calculations, where the first one refers to a fictitious $1^+$ GT transition with $q = \omega = 0$, and the second one is the $1^+$ ground state transition at actual $q$ and $\omega$ presented in Section 4.2. Thus, we find an extrapolation factor of

$$\frac{[d\sigma(0,0)/d\Omega]_{\mathrm{DWBA}}}{[d\sigma(q,\omega)/d\Omega]_{\mathrm{DWBA}}} = \frac{0.769}{0.632} = 1.217. \tag{8}$$

The second factor of Eq. (7) is the experimental cross section at 0°. First, this is determined directly from the data, assuming all cross section at this angle being due to the GT transition. To obtain a cross section at 0°, we use the sum of the fitted $1^+$ and $2^+$ distributions shown as a solid line in the left panel of Fig. 5. This must, however, be considered as an upper limit of $\hat{\sigma}$, since also other multipolarities contribute to the cross section. We find $d\sigma(0°)/d\Omega = 0.195 \pm 0.016$ mb/sr, which after correction results in $d\sigma(0,0)/d\Omega = 0.237 \pm 0.019$ mb/sr and, with Eq. (5), gives

$$\hat{\sigma}_{\mathrm{max}} = 12.5 \pm 1.7 \text{ mb/sr}. \tag{9}$$

Second, we try to obtain a more realistic value of $\hat{\sigma}$ by taking contributions from other multipolarities into consideration. This can be done straightforwardly by using the $1^+$

contribution of Fig. 5 only. The cross section at 0° is $0.116 \pm 0.015$ mb/sr, which gives an extrapolated value of $d\sigma(0,0)/d\Omega = 0.141 \pm 0.018$ mb/sr. We then find a unit cross section

$$\hat{\sigma} = 7.4 \pm 1.2 \text{ mb/sr}, \tag{10}$$

where the error is dominated by the statistical uncertainty of the experimental data. The error in the extrapolation to $q = \omega = 0$ is difficult to estimate, but is expected to give an additional contribution of at most about 20%.

$B_{GT}$ can also be determined from the matrix elements of the OXBASH calculation. Since these matrix elements are used to calculate the cross section in DWBA, there is a direct link between strength and unit cross section. The calculated $B_{GT}$ is about a factor of five higher than the value found from experimental $\beta$ decay studies. By scaling the calculation to $B_{GT} = 0.019$, and extrapolating to $q = \omega = 0$, we find an intrinsic unit cross section of $\hat{\sigma} = 8.4$ mb/sr. This value agrees well, within the uncertainties, with the experimental one.

By using Eq. (4) and the experimentally determined $\hat{\sigma}$ value, it is possible to estimate the volume integral, $J_{\sigma\tau}(q = 0)$. The distortion factor $N^D$, calculated as the ratio of the DWBA to PWBA cross sections, was found to be 0.567. Thus, we get

$$|J_{\sigma\tau}(q = 0)| = 154 \pm 25 \text{ MeV fm}^3. \tag{11}$$

This is slightly lower, but within errors, compared to the value of $180 \pm 9$ MeV fm$^3$ found in previous work [19,28]. It should be noted, however, that the distortion factor is sensitive to the choice of optical potential parameters through the DWBA cross section, and the determination of $J_{\sigma\tau}$ is consequently also sensitive to these parameters. In contrast, the determination of $\hat{\sigma}$ is performed using a ratio of two distorted-wave cross sections, and is thus less sensitive to the particular optical model used.

## 5. Discussion

It has been found from the $^9$Be(p,n)$^9$B experiment [16], which was carried out at a beam energy of 135 MeV, that the GT unit cross section for the ground state transition is $\hat{\sigma} = 11.0 \pm 1.6$ mb/sr. This value was obtained, following the work of Mikolas et al. [38], by assuming that; (i) the cross section at 0° is directly proportional to $B_{GT}$, (ii) the $B_{GT}$ value for the ground state transition is 0.620, and (iii) 17% of the cross section is due to the Fermi component [16]. The extracted value is considerably higher than the one of the present work, but lower than the maximum value allowed by the experimental data, if all strength is considered as GT.

At $E_x = 14.6$ MeV in $^9$B, two states have been identified; one is a sharp state, the other is 0.6 MeV wide. The latter, with a cross section peaking at 0°, is assumed to be a member of the $T = \frac{3}{2}$ multiplet in the mass $A = 9$ system, and hence the isospin mirror reaction of the $^9$Be(n,p)$^9$Li$_{g.s.}$ reaction. Cross sections were given at four different momentum transfers, as is shown in Fig. 7 (open circles). The absolute magnitude is in fair agreement with our data, while the slope seems to be steeper. The reduced $\chi^2$ with respect to the trend

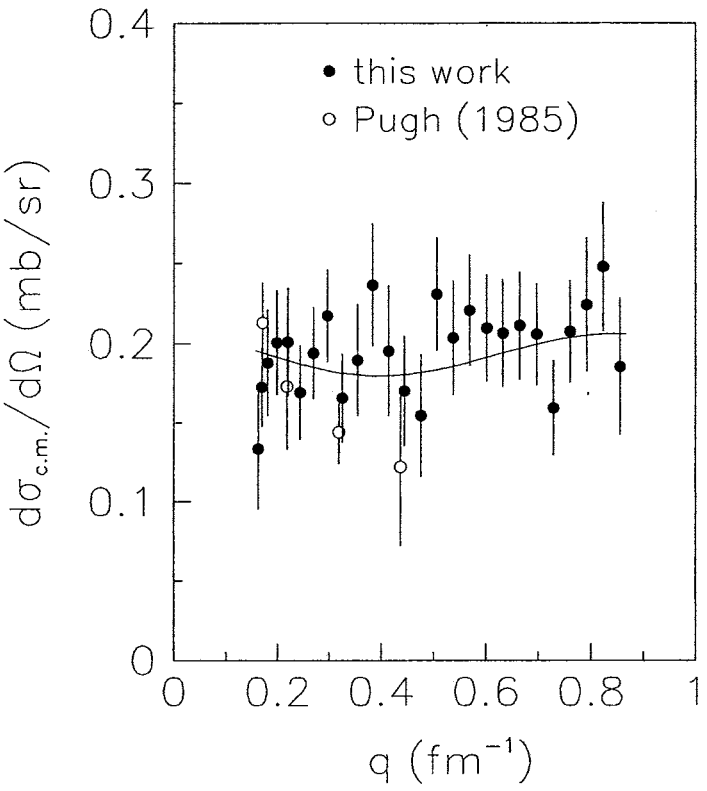


Fig. 7. Cross sections for the ground state transition of the $^{9}$Be(n,p)$^{9}$Li reaction as a function of momentum transfer, $q$. The solid line is the sum of the DWBA calculation for the $1^+$ and $2^+$ transitions shown in Fig. 5. Also included are data from the 14.6 MeV $T = \frac{3}{2}$ state of the $^{9}$Be(p,n)$^{9}$B reaction [16].

through our data (solid line) is about 2. We conclude that the (p,n) data, within the errors, are consistent with the present (n,p) data.

Recently, an analogue to the (n,p) charge-exchange reaction, using the (t,$^{3}$He) reaction, has been performed at NSCL using a 127 MeV/A triton beam [39]. A measured 0° cross section of $0.27 \pm 0.07$ mb/sr was found for the $^{9}$Be(t,$^{3}$He)$^{9}$Li reaction. This cross section is slightly larger than the (n,p) cross section at the same momentum transfer. This should, however, not be overinterpreted, because of the different distortions in the (n,p) and (t,$^{3}$He) reactions. Since there is only one datum point with a fairly high momentum transfer ($q = 0.156$ fm$^{-1}$), an extrapolation to $q = 0$ has not been carried out and, consequently, a GT unit cross section determination has not been attempted.

As was pointed out in the introduction, the Gamow–Teller unit cross section, determined from the (p,n) reaction, is significantly larger for a few light nuclei than a smooth trend through the data would indicate. The best example of this is the $A = 13$ system (see Fig. 1b). The first data on the $^{13}$C(p,n) reaction [40] showed consistent unit cross sections for the transitions to the $^{13}$N ground state ($T = \frac{1}{2}$) and to the $T = \frac{3}{2}$ state at $E_x = 15.1$ MeV, i.e., the isobaric analogue of the $^{13}$B and $^{13}$O ground states. For the latter transition, no direct $\beta$ decay data exist, but the $B_{GT}$ for the isospin (mirror) decays of $^{13}$O and $^{13}$B — which are almost identical — were used for the unit cross section determination.

The first measurement of the $^{13}$C(n,p) transition to the $^{13}$B ground state implied a

significantly different unit cross section than for its isospin analogue [7]. This motivated a new measurement of the $^{13}$C(p,n) reaction [8], which resulted in a unit cross section for a transition to the $T = \frac{3}{2}$ state consistent with that to its isospin mirror, i.e., the $^{13}$C(n,p)$^{13}$B$_{g.s.}$ reaction, but instead the ground state ($T = \frac{1}{2}$) transition deviates from the $T = \frac{3}{2}$ results.

In the present work, a similar investigation on the $A = 9$ system is reported. As can be seen in Fig. 1a, the level diagram looks very similar, but there are a few complications when comparing with the $A = 13$ system. First, the $^{9}$Be(p,n) data are of good quality only for the ground state transition, while the cross sections for the transition to the $T = \frac{3}{2}$ state have large uncertainties. Thus, a direct verification that the (p,n) and (n,p) transitions to the same isospin multiplet agree cannot be done with good precision. Instead, we can only conclude from Fig. 7 that the (p,n) data are compatible with the (n,p) data, within the (large) errors. For the same reason, a good comparison of the (p,n) transitions to $T = \frac{3}{2}$ and $T = \frac{1}{2}$ cannot be done, but instead we have had to compare the (p,n) ground state transition with the (n,p) transition to the $T = \frac{3}{2}$ multiplet. A second complication is that the $^{9}$B ground state is particle unstable, and breaks up to a proton and two alpha particles. Thus, its $\beta$ decay strength to the $^{9}$Be ground state is experimentally unknown, but has to be determined theoretically (see, e.g., Ref. [38]).

The result of this comparison is that the unit cross section derived from the (n,p) reaction is smaller than that from the (p,n) reaction. Both of them, however, follow the trend indicated by even nuclei of the respective reaction (see Fig. 8).

It is notable that for both the $A = 9$ and $A = 13$ systems, the $T = \frac{1}{2} \rightarrow T = \frac{1}{2}$ ground state transitions show evidence of Gamow–Teller unit cross sections about 30% stronger than for the $T = \frac{1}{2} \rightarrow T = \frac{3}{2}$ transitions. In both cases are the $T = \frac{1}{2} \rightarrow T = \frac{3}{2}$ transitions in (p,n) and (n,p) in agreement within their uncertainties. The $A = 9$ and $A = 13$ systems represent the only odd-mass cases where complete information is available. It would be very interesting to find out whether this picture is general for odd-mass nuclei.

An extensive study of the GT unit cross section from the (p,n) reaction on several nuclei as a function of mass has been conducted by Taddeucci et al. [1]. It is found from that study that the measured values of $\hat{\sigma}$ on odd nuclei are systematically larger than those of even nuclei. Extrapolation to masses where the GT unit cross section is not experimentally known can be established. This extrapolation, together with a reliable calculation of the corresponding cross section at $q = \omega = 0$, may be used to determine the $\beta$ decay strength between states that are not energetically accessible for $\beta$ decay [3]. Fig. 8a shows the systematic study of $\hat{\sigma}$ versus $A^{1/3}$ from the (p,n) reaction. Only statistical uncertainties are displayed. The systematic errors are more difficult to quantify; in some cases no systematic error is given. In the present experiment, the systematic error is estimated to be at most 20 %. It seems likely that the other data displayed in Fig. 8 have similar systematic uncertainties.

Due to the lack of experimental data, a systematic study of $\hat{\sigma}$ from the (n,p) reaction has not, until recently, been performed. Alford and Spicer [3] have made a review on nucleon charge-exchange reactions at intermediate energies and found that for the strong GT transitions in $^{6}$Li, $^{12}$C, and $^{13}$C, the unit cross sections for (n,p) and (p,n) agree within the

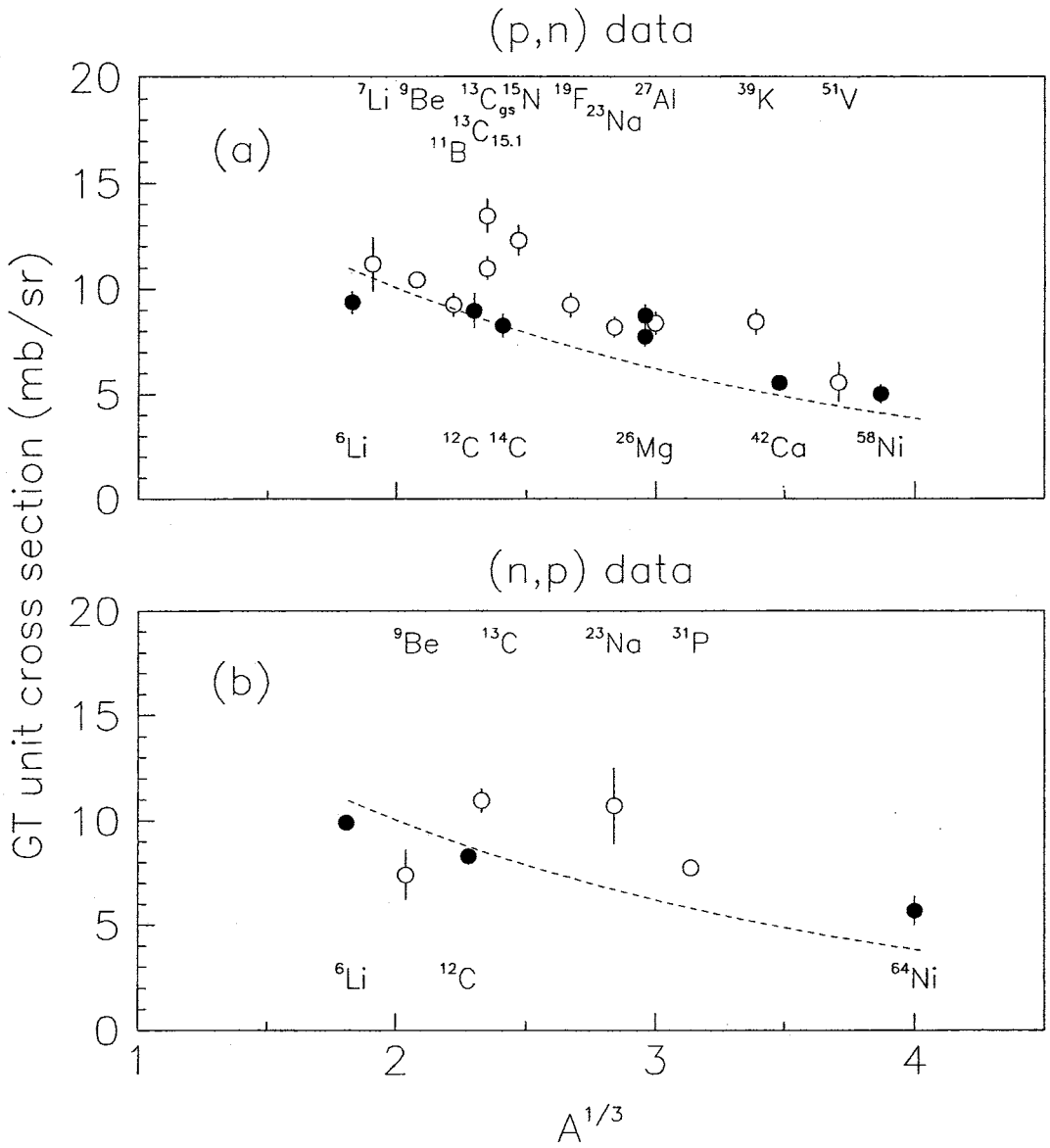


Fig. 8. Experimental GT unit cross sections: (a) from the (p,n) reaction, and (b) from the (n,p) reaction. Solid circles depict even nuclei and open circles odd nuclei. The dashed lines in both panels are the parameterizations of Taddeucci et al. [1]. The uncertainties given are statistical only.

experimental uncertainties. The measurement of $^{64}$Ni(n,p)$^{64}$Co, which has no direct (p,n) counterpart, is also in reasonable agreement with results of (p,n) measurements in the mass region $A = 60$. Sorensen et al., have made a systematic study of the energy dependence of $\hat{\sigma}$ of the same three nuclei as above [7], showing that it stays constant above 100 MeV, whilst it has a tendency of being smaller below 100 MeV for the carbon isotopes. In Fig. 8b, we present an extension of the experimental results, including $^{23}$Na(n,p)$^{23}$Ne [41], $^{31}$P(n,p)$^{31}$Si [42], and $^{9}$Be(n,p)$^{9}$Li.

Extending the systematics to lower masses makes the picture look slightly different. There are recent data on the $^{1}$H(n,p) reaction at the same energy as the present work, i.e., 96 MeV [43], and at 162 MeV [44]. In addition, there are data on the $^{1}$H(d,$^{2}$He)n reaction

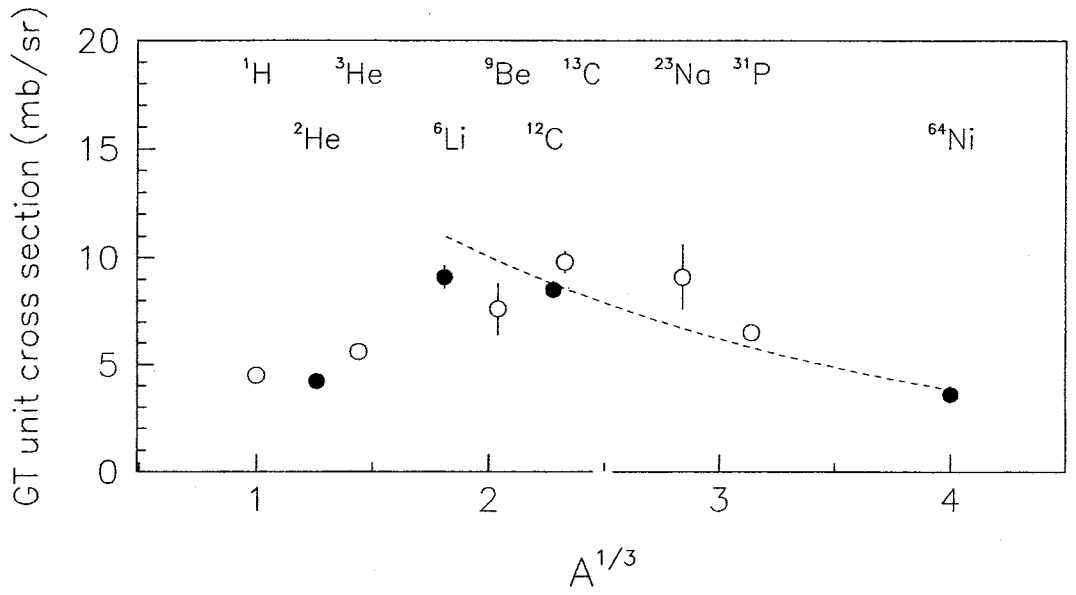


Fig. 9. Experimental GT unit cross sections from the (n,p) reaction, scaled to a c.m. energy of 100 MeV. Solid circles depict even nuclei and open circles odd nuclei. The dashed line is the parameterization of Taddeucci et al. [1].

at 200 MeV, i.e., 100 MeV per nucleon [45], which can be used to extract a $^2$He(n,p) cross section by reversing the kinematics and taking spin factors into account. Finally, there are data on the $^3$He(n,p)$^3$H [6] reaction at a much higher incident energy, $E_n = 288$ MeV. We have used the scaling of the unit cross sections suggested by Ling et al. [46], i.e., $\hat{\sigma}$ varies as $10^{0.0008E}$, to scale all measurements to 100 MeV c.m. energy for comparison. For $^1$H(n,p), the 162 MeV data were used because they are closer to 100 MeV c.m. energy (i.e., 200 MeV lab energy) than the 96 MeV data. The result is displayed in Fig. 9, where it can be seen that the unit cross section is significantly smaller for low masses. Why this is the case remains to be explained. It should be pointed out though that the distortion effects could be significantly different for different nuclear masses.

We want to point out that an extraction of the GT transition strength from experimental small-angle data is not straight forward if also other multipole transitions are present. This is most often the case for odd nuclei, which by necessity have $J^\pi \neq 0^+$ for the ground state. A careful calculation of the contribution from various transitions has to be performed in such cases. Furthermore, the experimental data have to cover a reasonable fraction of the angular distribution, to facilitate a decomposition into the different spin transfers and, specifically, to extract the GT part of the cross section close to 0°. We have shown in the present work that interpreting all cross section at 0° as being due to GT strength could lead to an overestimation of the unit cross section by 40%. One could speculate if such problems play a role for the discrepancies found between GT unit cross sections for even and odd nuclei. In addition, various choices of parameters used in the calculations might be an important factor for the discrepancies. A revision of all determined GT unit cross sections in a consistent manner might therefore be valuable.

## 6. Summary and conclusions

We have measured the double differential cross sections for the $^{9}$Be(n,p)$^{9}$Li reaction, using a magnetic spectrometer with position-sensitive detectors for the determination of the proton energy and emission angle. The data cover excitation energy and angular ranges of up to 20 MeV and 0°–27°, respectively. As a consistency check, the $^{12}$C(n,p)$^{12}$B reaction was also studied in the same angular and excitation-energy range. The data were normalised with respect to the backward-angle *np* scattering cross section and the previously published carbon data. A few gaussian peaks at known excitation energies were fitted to the experimental double differential cross section data. The angular distributions for the ground state and the first excited state were compared with results from DWBA calculations, using matrix elements from a shell-model calculation. At higher excitation energy, the experimental energy spectra were compared with calculated spectra for negative-parity transitions within the $sp$–$2sd$ shells.

The importance of a careful decomposition into various multipolarities has been shown, and it is speculated if this could be part of the explanation of the discrepancies found between unit cross sections for odd and even nuclei.

Using the unit cross section, we have estimated the volume integral of the spin-isospin part of the central NN interaction. A value of $J_{\sigma\tau} = 154 \pm 25$ MeV fm$^3$ was obtained.

The data for the ground state were used to determine a GT unit cross section of $\hat{\sigma} = 7.4 \pm 1.2$ mb/sr. This is in good agreement with the intrinsic value obtained from the calculations, but is considerably lower than that estimated from the $^{9}$Be(p,n)$^{9}$Li ground state reaction ($\hat{\sigma} = 11.0 \pm 1.6$ mb/sr). Thus, it seems as the $T = \frac{1}{2} \rightarrow T = \frac{3}{2}$ transitions are about 30% weaker than the $T = \frac{1}{2} \rightarrow T = \frac{1}{2}$ (ground-state) transition. This resembles the situation of the $A = 13$ system, where the $T = \frac{1}{2} \rightarrow T = \frac{3}{2}$ transition has a unit cross section of around 10–11 mb/sr, whilst the $T = \frac{1}{2} \rightarrow T = \frac{1}{2}$ (ground-state) transition has $\hat{\sigma} = 14.4 \pm 1.2$ mb/sr, i.e., also here the former is about 30% weaker. The puzzle which motivated the present work seems therefore to remain.

## Acknowledgements

The authors wish to thank the The Svedberg Laboratory staff for significant contributions in the construction of the equipment and during the measurements. One of the authors (SD) wishes to thank the Development and Promotion of Science and Technology Talents Project of Thailand for the financial support. This work was financially supported by the Swedish Natural Science Research Council.

## References

[1] T.N. Taddeucci, C.A. Goulding, T.A. Carey, R.C. Byrd, C.D. Goodman, C. Gaarde, J. Larsen, D. Horen, J. Rapaport, E. Sugarbaker, Nucl. Phys. A 469 (1987) 125, and references therein.
[2] J. Rapaport, E. Sugarbaker, Ann. Rev. Nucl. Part. Sci. 44 (1994) 109.
[3] W.P. Alford, B.M. Spicer, Adv. Nucl. Phys. 24 (1998) 1.

[4] T.-S.H. Lee, D.O. Riska, Phys. Rev. Lett. 70 (1993) 2237.
[5] C. Horowitz, H.O. Meyer, D.K. Griegel, Phys. Rev. C 49 (1994) 1337.
[6] A. Celler, S. Yen, W.P. Alford, R. Abegg, B.A. Brown, S. Burzynski, D. Frekers, O. Häusser, R. Helmer, R.S. Henderson, K. Hicks, K.P. Jackson, R. Jeppesen, C.A. Miller, M.A. Moinester, B.W. Pointon, A. Trudel, M. Vetterli, Phys. Rev. C 47 (1993) 1563.
[7] D.S. Sorensen, X. Aslanoglou, F.P. Brady, J.R. Drummond, R.C. Haight, C.R. Howell, N.S.P. King, A. Ling, P.W. Lisowski, B.K. Park, J. Rapaport, J.L. Romero, W. Tornow, J.L. Ullmann, Phys. Rev. C 45 (1992) R500.
[8] J.L. Mildenberger, W.P. Alford, A. Celler, O. Häusser, K.P. Jackson, B. Larson, B. Pointon, A. Trudel, M.C. Vetterli, S. Yen, Phys. Rev. C 43 (1991) 1777.
[9] G. Nyman, R.E. Azuma, P.G. Hansen, B. Jonson, P.O. Larsson, S. Mattsson, A. Richter, K. Riisager, O. Tengblad, K. Wilhelmsen, ISOLDE collaboration, Nucl. Phys. A 510 (1990) 189.
[10] T. Björnstad, H.Å. Gustafsson, P.G. Hansen, B. Jonson, V. Lindfors, S. Mattsson, A.M. Poskanzer, H.L. Ravn, Nucl. Phys. A 359 (1981) 1.
[11] M. Langevin, C. Détraz, D. Guillemaud, F. Naulin, M. Epherre, R. Klapisch, S.K.T. Mark, M. De Saint Simon, C. Thibault, F. Touchard, Nucl. Phys. A 366 (1981) 449.
[12] Y.S. Chen, T.A. Tombrello, R.W. Kavanagh, Nucl. Phys. 146 (1970) 136.
[13] D.E. Alburger, Phys. Rev. 132 (1963) 328.
[14] B.M.K. Nefkens, Phys. Rev. C 10 (1963) 243.
[15] B. Singh, J.L. Rodiguez, S.S.M. Wong, J.K. Tuli, Nucl. Data Sheets 84 (1998) 487.
[16] B. Pugh, Ph.D. Thesis, MIT, 1985, unpublished.
[17] H. Condé, S. Hultqvist, N. Olsson, T. Rönnqvist, R. Zorro, J. Blomgren, G. Tibell, A. Håkansson, O. Jonsson, A. Lindholm, L. Nilsson, P.-U. Renberg, A. Brockstedt, P. Ekström, M. Österlund, F.P. Brady, Z. Szeflinski, Nucl. Instr. Meth. A 292 (1990) 121.
[18] T. Rönnqvist, H. Condé, N. Olsson, R. Zorro, J. Blomgren, G. Tibell, O. Jonsson, L. Nilsson, P.-U. Renberg, S.Y. van der Werf, Phys. Rev. C 45 (1992) R496.
[19] N. Olsson, H. Condé, E. Ramström, T. Rönnqvist, R. Zorro, J. Blomgren, A. Håkansson, G. Tibell, O. Jonsson, L. Nilsson, P.-U. Renberg, A. Brockstedt, P. Ekström, M. Österlund, S.Y. van der Werf, D.J. Millener, G. Szeflinska, Z. Szeflinski, Nucl. Phys. A 559 (1993) 368.
[20] T. Rönnqvist, H. Condé, N. Olsson, E. Ramström, R. Zorro, J. Blomgren, A. Håkansson, A. Ringbom, G. Tibell, O. Jonsson, L. Nilsson, P.-U. Renberg, S.Y. van der Werf, W. Unkelbach, F.P. Brady, Nucl. Phys. A 563 (1993) 225.
[21] H. Condé, N. Olsson, E. Ramström, T. Rönnqvist, R. Zorro, J. Blomgren, A. Håkansson, G. Tibell, O. Jonsson, L. Nilsson, P.-U. Renberg, M. Österlund, W. Unkelbach, J. Wambach, S.Y. van der Werf, J. Ullmann, S.A. Wender, Nucl. Phys. A 545 (1992) 785.
[22] A. Ringbom, A. Håkansson, G. Tibell, R. Zorro, H. Condé, J. Blomgren, J. Nilsson, N. Olsson, E. Ramström, T. Rönnqvist, O. Jonsson, L. Nilsson, P.-U. Renberg, S.Y. van der Werf, Nucl. Phys. A 617 (1997) 316.
[23] R. Bonetti, C. Chiesa, Multistep direct reaction computer code, unpublished.
[24] E. Ramström, private communication.
[25] H. Feshbach, A. Kerman, S. Koonin, Ann. Phys. 125 (1980) 429.
[26] F. Ajzenberg-Selove, Nucl. Phys. A 490 (1988) 1.
[27] R. Schaefer, J. Raynal. Program DWBA70, unpublished; J.R. Comfort extended version DW81, unpublished.
[28] K. Nakayama, W.G. Love, Phys. Rev. C 38 (1988) 51.
[29] R. Machleidt, K. Holinde, Ch. Elster, Phys. Rep. 149 (1987) 1.
[30] A. Koning, private communication.
[31] B.A. Brown, A. Etchegoyen, W.D.M. Rae, Program OXBASH, MSUCL Report 524, 1988.
[32] S. Cohen, D. Kurath, Nucl. Phys. 73 (1965) 1.
[33] D.J. Millener, D. Kurath, Nucl. Phys. A 255 (1975) 315.

[34] F. Petrovich, W.G. Love, R.J. McCarthy, Phys. Rev. C 21 (1980) 1718.
[35] D.H. Wilkinson, Nucl. Phys. A 377 (1982) 474.
[36] N. Kumar, Nucl. Phys. A 225 (1975) 221.
[37] F.C. Barker, Nucl. Phys. 83 (1966) 418.
[38] D. Mikolas, B.A. Brown, W. Benenson, L.H. Harwod, E. Kashy, J.A. Nolen Jr., B. Sherrill, J. Stevenson, J.S. Winfield, Z.Q. Xie, R. Sherr, Phys. Rev. C 37 (1988) 766.
[39] I. Daito, H. Akimune, S.M. Austin, D. Bazin, G.P.A. Berg, J.A. Brown, B.S. Davids, Y. Fujita, H. Fujimura, M. Fujiwara, R. Hazama, T. Inomata, K. Ishibashi, J. Jaenecke, S. Nakayama, K. Pham, D.A. Roberts, B.M. Sherrill, M. Steiner, A. Tamii, M. Tanaka, H. Toyokawa, M. Yosoi, Phys. Lett. B 418 (1998) 27.
[40] C.D. Goodman, R.C. Byrd, I.J. Van-Heerden, T.A. Carey, D.J. Horen, J.S. Larsen, C. Gaarde, J. Rapaport, T.P. Welch, E. Sugarbaker, T.N. Taddeucci, Phys. Rev. Lett. 54 (1985) 877.
[41] B. Siebels, T.P. Gorringe, W.P. Alford, J. Bauer, J. Evans, S. El-Kateb, K.P. Jackson, A. Trudel, S. Yen, Phys. Rev. C 52 (1995) 1488.
[42] R.M. Sedlar, T.P. Gorringe, W.P. Alford, D.A. Beatty, J. Campbell, H.T. Fortune, P. Hui, D.A. Hutcheon, R.B. Ivie, K.P. Jackson, A.G. Ling, Z. Mao, M.G. McKinzie, B. Siebels, D.A. Smith, P. Walden, S. Yen, Phys. Rev. C 59 (1999) 789.
[43] J. Rahm, J. Blomgren, H. Condé, S. Dangtip, K. Elmgren, N. Olsson, T. Rönnqvist, R. Zorro, O. Jonsson, L. Nilsson, P.-U. Renberg, A. Ringbom, G. Tibell, S.Y. van der Werf, T.E.O. Ericson, B. Loiseau, submitted for publication.
[44] J. Rahm, J. Blomgren, H. Condé, S. Dangtip, K. Elmgren, N. Olsson, T. Rönnqvist, R. Zorro, A. Ringbom, G. Tibell, O. Jonsson, L. Nilsson, P.-U. Renberg, T.E.O. Ericson, B. Loiseau, Phys. Rev. C 57 (1998) 1077.
[45] T. Motobayashi, C. Perrin, J. Carbonell, C. Wilkin, S. Kox, F. Merchez, Nguyen Van Sen, D. Rebreyend, G. Guillaume, J. Arvieux, J. Yonnet, B. Bonin, A. Boudard, M. Garcon, J. Guillot, G. Gaillard, Phys. Lett. B 233 (1989) 69.
[46] A. Ling, X. Aslanoglou, F.P. Brady, R.W. Finlay, R.C. Haight, C.R. Howell, N.S.P. King, P.W. Lisowski, B.K. Park, J. Rapaport, J.L. Romero, D.S. Sorenson, W. Tornow, J.L. Ullmann, Phys. Rev. C 44 (1991) 2794.

# Appendix V

S0375-9474(00)00374-2/FLA AID:5622 Vol.00(0)
ELSEV2s 2000/08/03 Prn:4/09/2000; 10:29
Doctopic: Nuclear Structure and Dynamics

NPA5622

P.1 (1-20)
by:EL p. 1

ELSEVIER

Nuclear Physics A 00 (2000) 1–20

NUCLEAR PHYSICS A

www.elsevier.nl/locate/npe

# The $^{10,11}$B(n, p)$^{10,11}$Be reactions at $E_n = 96$ MeV

A. Ringbom [a,1], J. Blomgren [b,*], H. Condé [b], K. Elmgren [b], N. Olsson [b], J. Rahm [b], T. Rönnqvist [b], O. Jonsson [c], L. Nilsson [c], P.-U. Renberg [c], G. Tibell [a], Chr. Bargholtz [d], K. Fransson [d], K. Lindh [d], P.-E. Tegnér [d], P. Thörngren Engblom [a,d], S.Y. van der Werf [e]

[a] *Department of Radiation Sciences, Uppsala University, Box 535, S-75121 Uppsala, Sweden*
[b] *Department of Neutron Research, Uppsala University, Box 535, S-75121 Uppsala, Sweden*
[c] *The Svedberg Laboratory, Uppsala University, Box 533, S-75121 Uppsala, Sweden*
[d] *Department of Physics, Stockholm University, Box 6730, S-113 85 Stockholm, Sweden*
[e] *Kernfysisch Versneller Instituut, Zernikelaan 25, 9747 AA Groningen, The Netherlands*

Received 12 May 2000; revised 13 June 2000; accepted 9 August 2000

**Abstract**

Double-differential cross sections of the $^{10,11}$B(n, p)$^{10,11}$Be reactions have been measured at 96 MeV in the angular range 0°–30° for excitation energies up to 35 MeV. The spectra have been decomposed into different multipolarities using sample angular distributions calculated within the distorted-wave Born approximation. From the identified Gamow–Teller strength, $S_{\beta+}$ values were obtained for $^{10}$B and $^{11}$B. At higher excitation energies, the spectra are dominated by $L = 1$ strength in broad distributions with maxima around 22 and 12 MeV in $^{10}$B and $^{11}$B, respectively. 

*PACS:* 24.50.+g; 25.40.-h; 25.40.Kv; 27.20.+n
*Keywords:* NUCLEAR REACTION: $^{10}$B(n, p), $^{11}$B(n, p), $E = 96$ MeV; Measured $\sigma(E_p, \theta)$; DWBA calculations; Deduced Gamow–Teller strength; Dipole excitations

## 1. Introduction

Charge-exchange reactions have proven to be extremely valuable in the study of nuclear structure and, in particular, for investigations of the isovector components of nucleon–nucleus interactions. Most of the effort has been spent on studies of the Gamow–Teller (GT) resonance, which was in fact discovered in a (p, n) experiment at 45 MeV [1]. The GT resonance originates from $\Delta L = 0$ transitions within a major shell ($0\hbar\omega$), induced by the

* Corresponding author.
*E-mail address:* jan.blomgren@tsl.uu.se (J. Blomgren).
[1] Present address: Swedish Defense Research Establishment (FOA), S-17290 Stockholm, Sweden

0375-9474/00/$ – see front matter 
PII: S0375-9474(00)00374-2

$\sigma\tau$ operator, with change of both isospin and spin ($\Delta T = 1$, $\Delta S = 1$), which corresponds to the analogous $\beta$-decay. It has been shown [2,3] that the cross section at zero momentum transfer and zero energy loss is closely related to the $\beta$-decay strength and the volume integral of the central spin–isospin part of the nucleon–nucleon (N–N) interaction.

Up to now rather little information has been collected on spin-flip strengths other than the GT resonance, e.g., on spin–dipole transitions. Recent progress in shell-model calculations [4–6] and G-matrix representations of the N–N force [7,8] for use in distorted-wave Born approximation (DWBA) calculations, has resulted in powerful tools to distinguish the transition strengths of different multipolarities.

The Uppsala neutron beam facility has been used in extensive measurements of the (n, p) reaction at about 100 MeV on a series of nuclei, i.e., $^{9}$Be [9], $^{12}$C [10], $^{54,56}$Fe [11], $^{90}$Zr [12] and $^{208}$Pb [13], and, in addition, to study free n–p scattering, i.e., $^{1}$H(n, p) [14–17]. The wealth of spectroscopic information that could be extracted from the data on $^{9}$Be and $^{12}$C has inspired to continued studies of $p$-shell nuclei. In this paper, we report the results of an extensive investigation of the (n, p) reaction on $^{10}$B and $^{11}$B, covering a wide range both in excitation energy and scattering angle, with good statistics.

In both the $^{10}$B(n, p)$^{10}$Be and $^{11}$B(n, p)$^{11}$Be reactions, particular features of the nuclei involved might play a role. Only five stable odd–odd nuclei exist in nature, with $^{2}$H, $^{6}$Li and $^{10}$B being the lightest ones. $^{10}$B has its unpaired nucleons in the $p_{3/2}$ orbital and a ground-state spin and parity of $3^{+}$, and is thereby the only known stable nucleus which has a spin-stretched ground state. The (n, p) transition to the $0^{+}$ ground state of $^{10}$Be has been suggested as a good place to study tensor force effects in the nuclear interaction. An experiment dedicated to this aspect has recently been performed at Los Alamos [18].

The $^{11}$Be nucleus is the most studied one-neutron halo nucleus. Since the discovery of neutron halos in light nuclei with small neutron separation energies [19], a wealth of experimental techniques have been used to study the structure of these very neutron-rich nuclei. See, e.g., Ref. [20] for a review.

For Gamow–Teller transitions in nuclei, a simple and model independent sum rule can be derived for the difference in strength in the (p, n) and (n, p) reactions on the same target nucleus. This is the Ikeda sum rule, given by (summed over all states)

$$S_{\beta^-} - S_{\beta^+} = 3(N - Z). \tag{1}$$

For a derivation, see, e.g., Ref. [21]. It has been known for a long time that the Ikeda sum rule is exhausted to 50–70% in nuclei heavier than $A \approx 90$, whilst the observed strength for lighter nuclei is in better accordance with the sum rule, typically 70–100% [22]. The question of the missing GT strength has been given profound attention, both experimentally and theoretically. Since (p, n) data exist for both $^{10}$B and $^{11}$B, the corresponding (n, p) data could provide two more test cases.

In this paper we present double-differential cross sections for the $^{10,11}$B(n, p)$^{10,11}$Be reactions at 96 MeV. The experimental apparatus and procedure are described in Section 2, while the data reduction and the experimental results are presented in Section 3. Section 4 is devoted to analysis of the experimental proton spectra in terms of different multipole

contributions, which were obtained by a decomposition using calculated sample angular distributions. A summary and the conclusions are given in Section 5.

## 2. Experimental apparatus and procedure

The experiment presented in this paper was carried out at the (n, p) facility of The Svedberg Laboratory in Uppsala, Sweden. The equipment has been described in detail in a previous publication [23] and only a brief summary will be given here.

The layout of the experiment is shown in Fig. 1. Protons from the cyclotron impinged on the neutron production target from the left in the figure. The $96.3 \pm 0.5$ MeV neutrons were produced by the $^7$Li(p, n)$^7$Be reaction, using a 200 mg/cm$^2$ thick disc of lithium, enriched to 99.98% in $^7$Li. After the target the proton beam was deflected into a well-shielded beam dump. A narrow neutron beam in the forward direction was defined by a system of three collimators. The vacuum system was terminated with a 1 mm aluminium window after the first collimator. Charged particles produced in this window and along the collimator channel were deflected by a clearing magnet. The diameter of the neutron beam was about 7 cm at the (n, p) target position, 8 m from the neutron production target. With a 5.0 μA proton beam incident on a 200 mg/cm$^2$ thick $^7$Li target, the neutron yield was about $1.0 \times 10^6$ s$^{-1}$ within the solid angle defined by the collimators. The charged-particle contamination of the beam was about $10^{-5}$.

To improve the (n, p) reaction rate without impairing the energy resolution, a sandwiched multitarget system was used. It consisted of a stack of thin (n, p) target foils interspaced

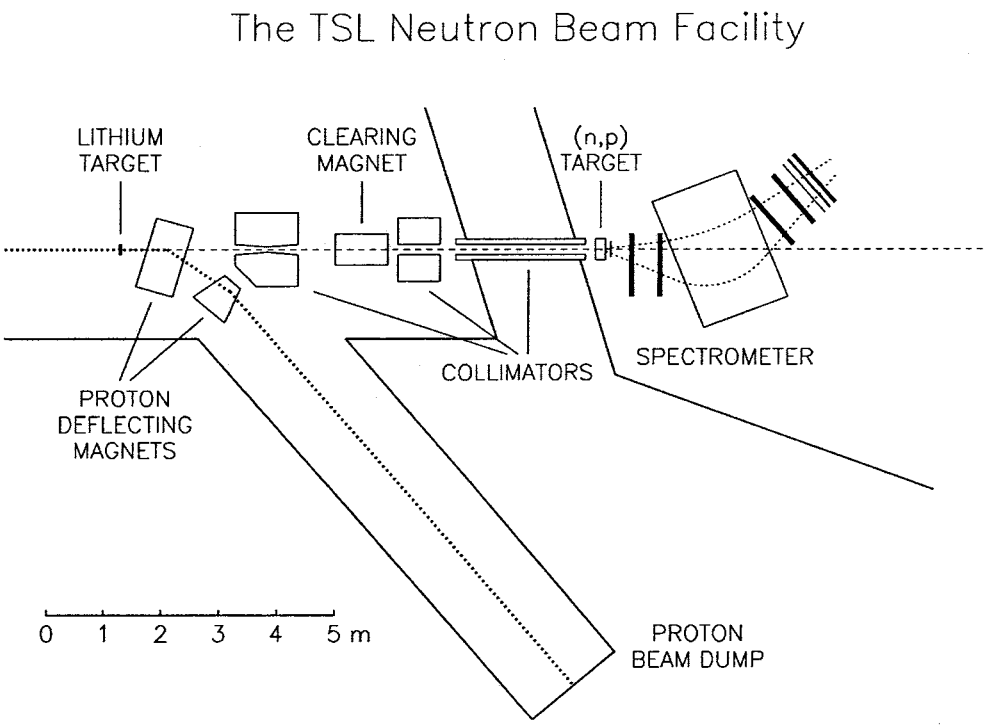


Fig. 1. The Uppsala (n, p) facility.

by multiwire proportional chambers (MWPC). In this way it was possible to determine in which foil the reaction occurred, so that corrections for the energy loss in the subsequent targets could be applied. The efficiency per chamber plane was in general above 99%. The first two MWPCs provided veto signals for rejection of charged particles contaminating the neutron beam.

For this experiment, a technique to produce very pure isotopically enriched boron targets was developed. Previously, targets for this kind of experiments have been manufactured by dissolving small amounts of styrene or carbowax into boron powder, which has subsequently been pressed to discs. These techniques have the disadvantage that they introduce hydrogen contaminations into the targets, which is a complication, because the $^{1}$H(n, p) cross section is an order of magnitude larger than any other cross section in the interesting region of the present experiment.

Our method has been described in a separate paper [24], and only a summary is given here. Isotopically enriched (more than 99%) $^{10}$B and $^{11}$B powder was mixed with water to a mud, which was dried on a polypropylene foil, serving as a backing. A second polypropylene layer was mounted to seal the boron target. The hydrogen contamination from these backing foils was about a factor three less than that obtained using the previous techniques, and it was corrected for by background measurements.

Two targets of $^{10}$B were mounted in the first two positions of the multitarget box. The thicknesses of the discs were 226 and 287 mg/cm$^2$. In the following positions three $^{11}$B targets with thicknesses of 243, 248 and 290 mg/cm$^2$, respectively, were mounted. In addition, a 102 mg/cm$^2$ $CH_2$ reference foil was placed in the last target position. This foil was used to normalize the $^{10,11}$B(n, p) cross sections to that of n–p scattering. To determine the instrumental background, spectra were recorded at all experimental settings with only polypropylene and $CH_2$ foils mounted in the multitarget box.

However, some targets deteriorated during the experiment, resulting in a gradual thickness increase at the lower parts of the targets. This was corrected for by analyzing small areas of each target separately. The reliability of this routine could be inspected by comparisons with a target that stayed intact during the entire run. The worsening of the resolution for part of the data could not be compensated though, resulting in a worse energy resolution than was obtained in the previous measurement of the $^{12}$C(n, p) reaction [10]. Furthermore, the deterioration of the targets caused an additional error in the corrections for energy loss in the downstream targets. This resulted in an uncertainty of the excitation energy scale of about $\pm 1$ MeV for the $^{10}$B(n, p) data. The uncertainty for $^{11}$B is smaller, since these targets were located downstream the $^{10}$B targets.

The momentum determination of the charged particles emitted from the reaction target was performed with a spectrometer consisting of a dipole magnet and four drift chambers, two in front of and two behind the magnet. The scattering angle was determined by the trajectory through the first two drift chambers. The detection efficiency of a single drift-chamber plane was about 98%. To reduce the multiple scattering of charged particles in air, the space between the first two drift chambers and the volume in the pole gap were filled with helium gas.

The data were taken with the spectrometer magnet at two different positions, covering the scattering angular ranges 0°–15° and 15°–30°, respectively. In the first position, magnetic fields of 0.8 and 1.0 T were used for the angular ranges 0°–8° and 8°–15°, respectively. A magnetic field of 0.7 T was used to cover the angular range 15°–30°. The energy resolution (FWHM) was about 3.5 MeV in the angular range 0°–15° and 4.5 MeV for the larger angles.

A trigger signal for the data acquisition system was generated by a triple coincidence between two large plastic scintillators, located behind the last drift chamber, and a thin scintillator, positioned immediately after the multitarget box. The neutron time-of-flight (TOF) was measured using pulses from the thin scintillator and the cyclotron RF as start and stop signals, respectively. This information was used to reject events from low-energy neutrons in the tail of the neutron spectrum. Together with information on the particle momentum, the pulse heights from the two large scintillators were used for particle identification, enabling separation of protons from other charged particles.

The data acquisition system consisted of a VME-bus configuration in conjunction with CAMAC and NIM electronic modules. For each event, the time information from the drift chambers and the MWPCs of the multitarget box, together with the linear signals from the scintillators and the neutron TOF, were stored on magnetic tape.

## 3. Data reduction and experimental results

The data were analyzed off line on an event-by-event basis. The accepted boron events were stored as relative double-differential cross sections in matrices with angular and energy bin widths of 1° and 0.5 MeV, respectively.

The background spectra, dominated by n–p scattering in the MWPC foils, were treated in a similar way. The resolution of the background spectra was about 30% better than for the $^{10,11}$B(n, p) data. The background was therefore folded with a gaussian distribution to obtain the same resolution as for the boron data, and were then subtracted after flux normalization.

The data from the $CH_2$ foil were treated in the same way as the boron data. A gaussian distribution was fitted to the proton peak in the energy spectrum for each angular bin. Differential cross sections were obtained by normalizing to n–p scattering data of a previous measurement [14].

Due to the finite width of the micropulses from the cyclotron (3–4 ns) the TOF rejection of low-energy neutrons was not complete. The remaining tail of low-energy neutrons was therefore subtracted from the boron spectra using an unfolding technique. The tail below the peak in the proton spectrum was divided into bins where the contents were compared to that of the total hydrogen spectrum. Scaled by this ratio, a shifted boron spectrum was subtracted from the full spectrum for each bin. The effect of this correction was small, being negligible below 10 MeV excitation energy and having its maximum at 30 MeV where it is about 10%.

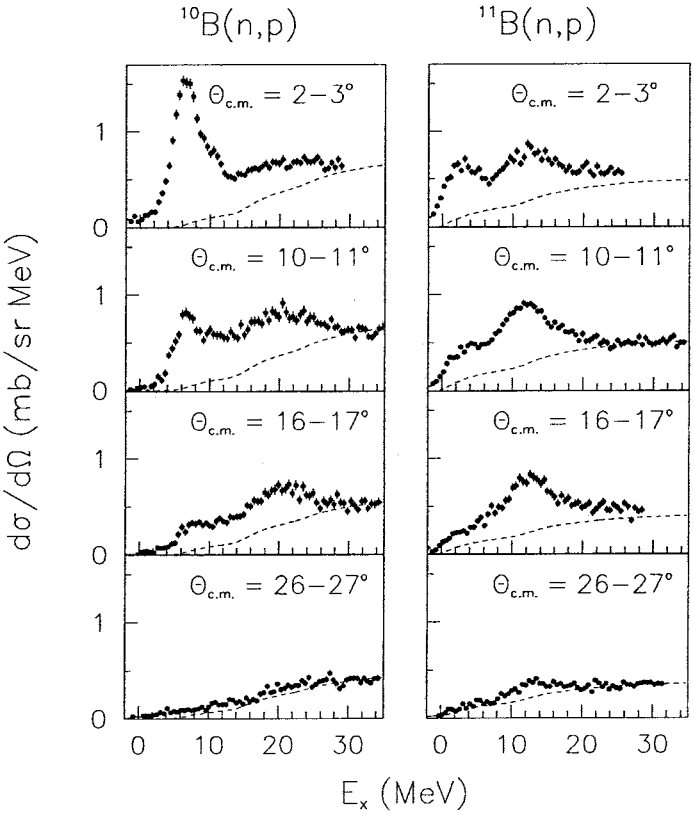


Fig. 2. Experimental double-differential cross sections of the $^{10}$B(n, p) and $^{11}$B(n, p) reactions at $E_n = 96$ MeV projected into energy spectra with angular bins of 1°. The dashed line is the calculated breakup continuum cross section, fitted to the experimental data in the excitation energy region 30–35 MeV.

Acceptance corrections were determined experimentally by making narrow software cuts in the vertical scattering angle to allow only trajectories almost parallel to the median plane, i.e., unperturbed by the pole faces of the magnet. By comparing energy spectra and angular distributions obtained with different vertical angle cuts, the required correction factors could be extracted.

Experimentally determined double-differential cross sections in the centre-of-mass (c.m.) system, grouped in 1° bins, are shown as filled circles in Fig. 2. The error bars represent statistical uncertainties. In addition, the cross section scale has a systematic uncertainty of about 10%, which is dominated by the 4% uncertainty in the n–p scattering cross sections, and a 5–10% uncertainty in the target thicknesses, caused by the previously mentioned deterioration of the targets. The data set, spanning the angular range 0°–30°, is for most angles complete up to about 35 MeV excitation energy (in $^{10,11}$Be).

## 4. Data analysis and discussion

The experimental cross section data are expected to consist of a mixture of resonances of different multipolarities and contributions from other reaction channels with at least one proton in the exit channel. In contrast to the studies of medium-weight and heavy

nuclei [11–13], multistep contributions are expected to be negligible because of the much lower level densities of these light nuclei. To extract the contribution from different multipolarities, a multipole decomposition was performed for each energy bin of the experimental data, both with and without adopting an underlying continuum, using sample angular distributions obtained from DWBA calculations. The underlying continuum was considered to originate mainly from (n, np) three-body break-up reactions.

In this section the treatment of the underlying continuum is described, followed by a description of the DWBA calculations. Furthermore, the method used to decompose the data into different multipolarities is presented, and the obtained $L = 0$ and $L = 1$ strengths are discussed.

### 4.1. Underlying continuum

A common way to treat the underlying continuum in this kind of reactions is to perform a calculation of the 3-body break-up phase space [10,25–27]. Generally, the cross section for one reaction channel can be described as

$$\frac{\mathrm{d}^2\sigma}{\mathrm{d}E\,\mathrm{d}\Omega} \propto PS \times |T_{\mathrm{if}}|^2, \tag{2}$$

where $PS$ is the phase-space factor and $T_{\mathrm{if}}$ is the transition amplitude. The simplest approach is to keep $|T_{\mathrm{if}}|^2$ constant, calculate the 3-body phase space for the (n, np) channel, which should be the dominating one, at least at low excitation, and normalize the cross section curve at the highest excitation energy. One difficulty with this method is that only one reaction channel is taken into account. The residual nucleus could, however, also be left in an excited state, and, in addition, several other reaction channels with protons in the final state open at excitation energies around 10–15 MeV. To take this into account, we used the method applied in the previous $^{12}$C(n, p) work [10]. In the $^{10}$B case we calculated the phase-space for the ground state and all relevant low-lying excited states. By adding these, weighted by the spectroscopic factors determined in an $(e, e'\mathrm{p})$ study [28], we believe that we get a fairly realistic description of the continuum. For $^{11}$B, 60% of the cross section was, more or less arbitrarily, assigned to the ground-state (n, np) reaction, and the rest was assumed to come from other reaction channels, simulated by calculating the phase-space for a fictitious three-body reaction with a $Q$-value corresponding to a threshold in the region $E_x = 11$–13 MeV. All calculations were performed assuming $|T_{\mathrm{if}}|^2 = 1$. The phase-space curves were folded with the experimental resolution, and fitted to data in the region $E_x = 30$–35 MeV. The result is shown in Fig. 2. The shape of the calculated phase-space distributions agrees well with data at the highest excitation energies. It should be pointed out that the gross features of these curves are not very sensitive to the details of the calculation.

### 4.2. DWBA calculations

Angular distributions were calculated in the framework of the distorted-wave Born approximation (DWBA), using a model of $1p$–$1h$ excitations. As described in Ref. [12],

normalized $p$–$h$ amplitudes were obtained from calculations based on normal mode excitations [29], which are the response to a simple tensor multipole operator acting on the ground state. The configuration space was restricted to $\leqslant 2\hbar\omega$ transitions, assuming ground state configurations based on $s$ and $p$ orbitals only.

The reaction calculations were performed using the code DW81 [30], where contributions from the different particle–hole configurations are added coherently. The effective nucleon–nucleon force was represented by the energy- and density-dependent G-matrix at 100 MeV according to Nakayama and Love [8]. This interaction is built on the Bonn potential [31], and takes nuclear medium effects into account.

The distorted waves were determined with the optical model. Parameters for the $^{10}$B + p potential were obtained by using data at 50 MeV [32], scaled to 96 MeV using systematics from $^{12}$C + p by Comfort and Karp [33]. The $^{11}$B + p potential parameters were taken from Ref. [34]. Adjustments for the ingoing $^{10,11}$B + n and outgoing $^{10,11}$Be + p channels were applied according to the isospin dependence of the global potential of Schwandt et al. [35].

The single-particle wave functions for the positive-parity transitions were calculated in a harmonic-oscillator potential well with an oscillator constant of $b_0 = 1.60$ fm for $^{10}$B, and $b_0 = 1.62$ fm for $^{11}$B. The negative-parity states were calculated using a Woods–Saxon potential with the parameters $r_0 = 1.41$ fm and $a = 0.65$ fm. The single-particle binding energies for the protons in $^{10}$Be were set to $-6.59$, $-8.59$ and $-24.00$ MeV for the $p_{3/2}$, $p_{1/2}$ and $0s_{1/2}$ orbits, respectively, while the corresponding energies for $^{11}$Be were $-11.23$, $-13.23$ and $-28.0$ MeV. These values were based on binding energies from neighboring nuclei. The binding energies for the neutron $1p$-orbits of $^{10}$Be were taken from experimental data on the $^{9}$Be(d,p)$^{10}$Be reaction [36], giving binding energies of $-6.82$ and $-3.0$ MeV for the $p_{3/2}$ and $p_{1/2}$ orbits, respectively. The unbound single-particle states were assigned a small binding energy to simplify the calculations. No bound, excited neutron orbits for $^{11}$Be exist.

Differential cross sections were calculated for several $J^\pi$ transitions with $L \leqslant 3$ in steps of 10 MeV up to 30 MeV excitation energy in the final nuclei $^{10}$Be and $^{11}$Be. By interpolating between these distributions, cross sections could be obtained at intermediate excitation energies. Examples of resulting angular distributions for $E_x = 0$ MeV are given in Fig. 3.

To reduce the number of degrees of freedom in the multipole decomposition, the calculated cross sections for the different $J^\pi$ values of each multipolarity $L$ were added (i.e. without renormalization of the different contributions), and these cross sections were used as sample angular distributions in the multipole decomposition. For $L = 0$ the GT $1^+$ distribution was used. Both non-spin-flip and spin-flip transitions were included, giving the following set of four angular distributions for the different multipolarities: Gamow–Teller (GT $J^\pi = 1^+$), dipole (non-spin-flip $1^-$, spin-flip $0^-$, $1^-$, and $2^-$), quadrupole (non-spin-flip $2^+$, spin-flip $2^+$, and $3^+$) and octupole (non-spin-flip $3^-$, spin-flip $2^-$, $3^-$, and $4^-$). Other combinations of $J^\pi$ were also tested, for instance an $L = J$ grouping of the angular distributions. No significant difference in the resulting strengths could be found using this set of angular distributions. The $2\hbar\omega$ monopole transitions ($0^+$ and $1^+$), are not expected to be excited to any extent in these light nuclei [10], and were therefore not included in the decomposition.

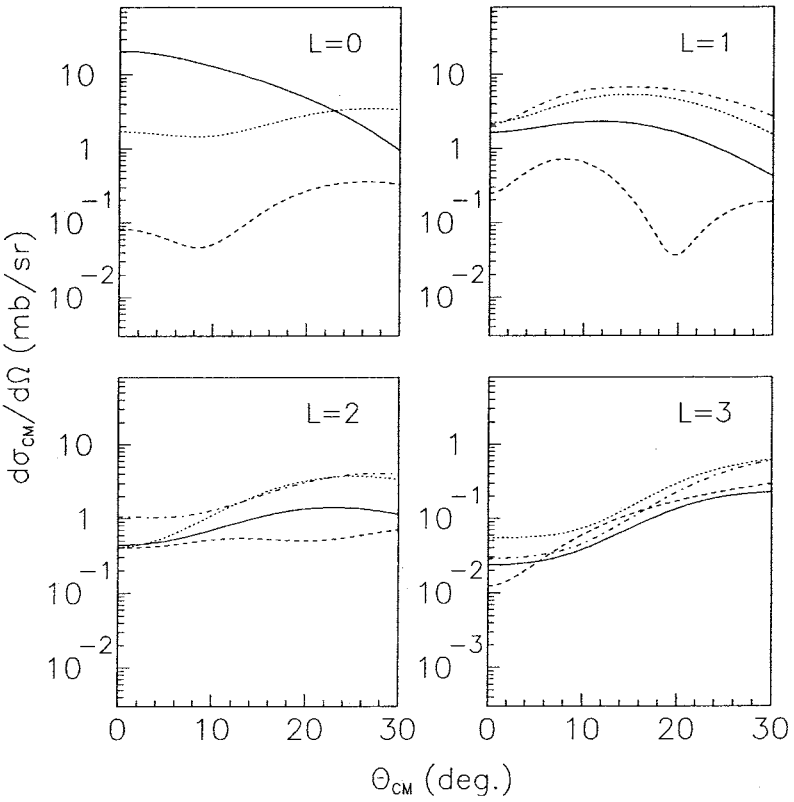


Fig. 3. Angular distributions from DWBA calculations, using the Nakayama–Love G-matrix, for $L = 0$, 1, 2 and 3 of the $^{11}$B(n, p) reaction at $E_n = 96$ MeV and at an excitation energy of 0 MeV. For $L = 0$, the different curves represent: $\Delta J = \Delta L = \Delta S = 0$, $0\hbar\omega$ (solid), $\Delta J = \Delta L = \Delta S = 0$, $2\hbar\omega$ (dotted), $\Delta J = \Delta L = 0$, $\Delta S = 1$, $2\hbar\omega$ (dot-dashed), For $L \leqslant 1$, the different curves represent: $J = L$, $\Delta S = 0$ (solid), $J = L$, $\Delta S = 1$ (dotted); $J = (L - 1)$, $\Delta S = 1$ (dashed); $J = (L + 1)$, $\Delta S = 1$ (dot-dashed). The parity is odd for odd $L$ and even for even $L$.

### *4.3. Multipole decomposition of experimental data*

Multipole decompositions of the $^{10}$B(n, p)$^{10}$Be and $^{11}$B(n, p)$^{11}$Be spectra up to an excitation energy of 30 MeV were performed, before and after subtraction of the phase-space continuum. For each 0.5 MeV energy bin the experimental angular distributions were described by

$$\left(\frac{d\sigma}{d\Omega}\right)_{exp} = \sum_L A_L \left(\frac{d\sigma}{d\Omega}\right)_L, \tag{3}$$

where $L$ represents the different multipolarities and $(d\sigma/d\Omega)_L$ denotes the calculated sample angular distributions, normalized to unity at the peak values. The coefficients $A_L$ were determined by a least squares fit to the data. These coefficients were set to zero whenever they became negative in the fitting.

The results of the multipole decomposition for $^{10}$B(n, p) and $^{11}$B(n, p) before subtraction of the (n, np) phase-space are shown in Fig. 4. Both nuclei show broad $L = 0$ distributions, peaking at around 6 and 3–4 MeV in $^{10}$Be and $^{11}$Be, respectively, but with a tail ranging all the way up to 30 MeV. The dipole ($L = 1$) distribution peaks at much higher excitation

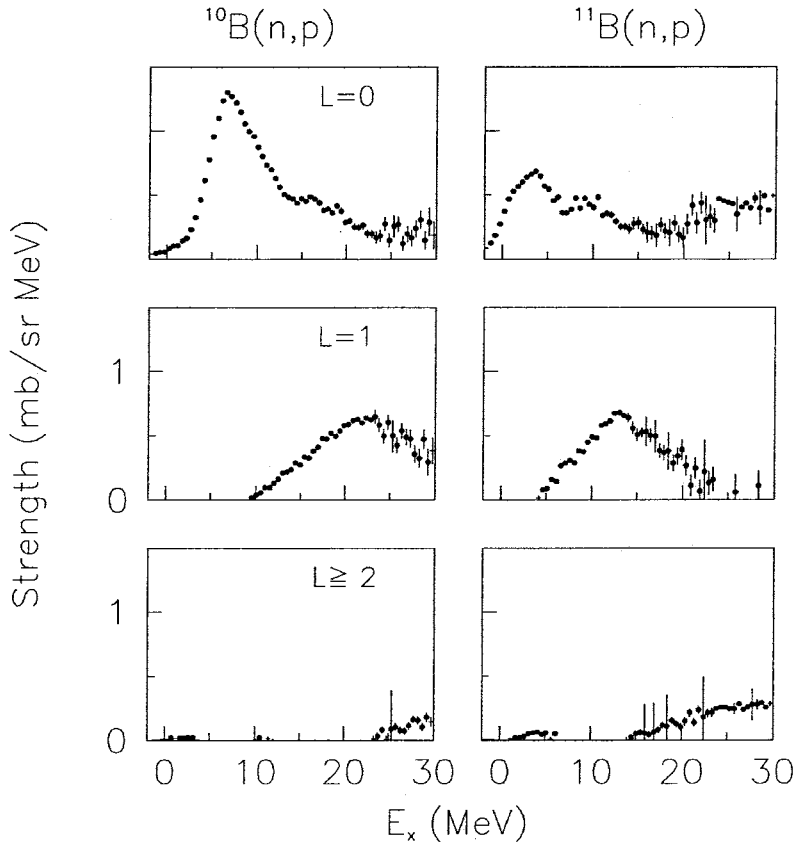


Fig. 4. Strength distributions for the $^{10,11}$B(n, p) reactions at $E_n = 96$ MeV as obtained from the multipole decomposition, without subtraction of the phase-space contribution. The strengths are shown at the angles where the angular distributions of the multipolarities have their maxima.

energy in $^{10}$Be than in $^{11}$Be (22 and 12 MeV, respectively). A small amount of strength corresponding to higher multipolarities are found in both nuclei.

The result of the decomposition after subtraction of the underlying continuum is shown in Fig. 5, where — as expected — the strengths at high excitation energies are reduced. The strength for $L \geqslant 2$ is almost completely removed, and the excitations of these nuclei are almost exclusively of $L = 0$ and $L = 1$ nature.

The quality of the fits in the multipole decomposition is illustrated in Fig. 6, showing experimental angular distributions for $E_x = 0$, 5, 10 and 20 MeV, together with the DWBA calculations. The contributions from the different multipolarities are shown, as well as the sum of the fit. As can be seen, the experimental data are generally very well fitted by the decomposition.

### 4.4. Gamow–Teller strength

The recorded spectra for the $^{11}$B(n, p)$^{11}$Be reaction can be compared with results from a $^{11}$B(d,$^2$He) measurement at $E_d = 70$ MeV (where $^2$He denotes two protons in a relative $^1S_0$ state) performed at RCNP, Osaka, Japan [37]. It is possible that at the rather low energy in the (d,$^2$He) experiment, 35 MeV/A, multistep processes are nonnegligible. It

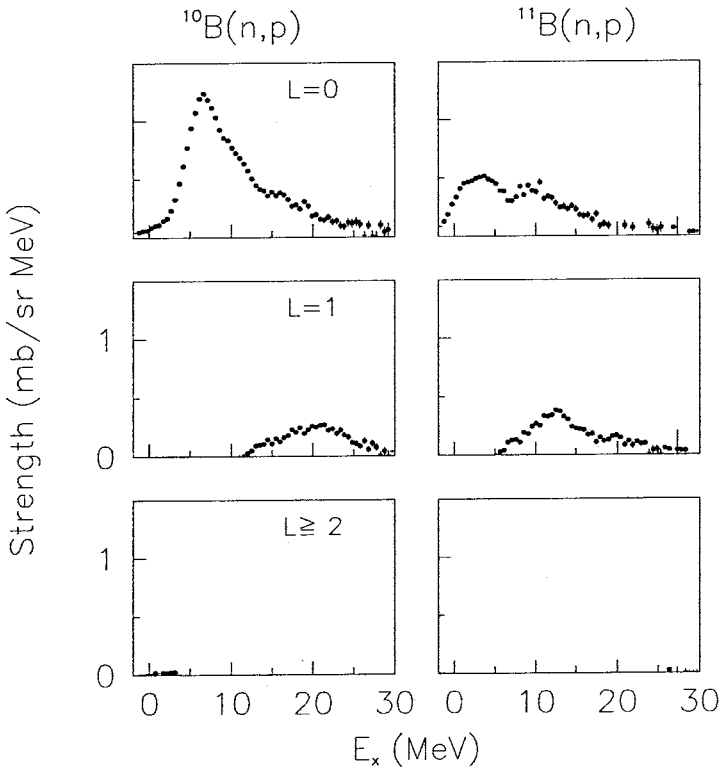


Fig. 5. Strength distributions for the $^{10,11}$B(n, p) reactions at $E_n = 96$ MeV as obtained from the multipole decomposition. The calculated 3-body phase-space contribution has been subtracted from the data. The strengths are shown at the angles where the angular distributions of the multipolarities have their maxima.

seems likely that such processes are less important in the (n, p) reaction at 100 MeV, and the reaction mechanism should also be better known than in the (d,$^2$He) case. The (d,$^2$He) reaction, on the other hand, is very selective for spin-flip strength, and the analysis identified three Gamow–Teller states below 4 MeV excitation energy. The GT-distribution observed in the present experiment is in agreement with these results, although the individual states cannot be resolved.

The only $^{10}$B(n, p)$^{10}$Be measurement conducted previously [18] was, as mentioned in Section 1, dedicated to the study of tensor effects in the transition to the $^{10}$Be ground state, which are strong in a different angular range than the present experiment. Accordingly, the smallest angle studied was 20°, which makes a direct comparison of data difficult. There exist, however, data on the $^{10}$B(p, n)$^{10}$C reaction at 186 MeV, measured at IUCF [38,39]. In this experiment, a large GT-peak was identified at 5.5 MeV, together with two broader distributions, centered at around 10 and 17 MeV, respectively. According to isospin symmetry, the excitation energy spectra of the (p, n) and (n, p) reactions should be the same to first order if the projectile energies are the same. In spite of the different energies of the present (n, p) and the IUCF (p, n) experiments, the results for the GT transitions are in reasonably good agreement.

A factorized expression has been derived [2,3] for the cross section of GT transitions in charge-exchange reactions, valid at intermediate energies and in the limit of zero

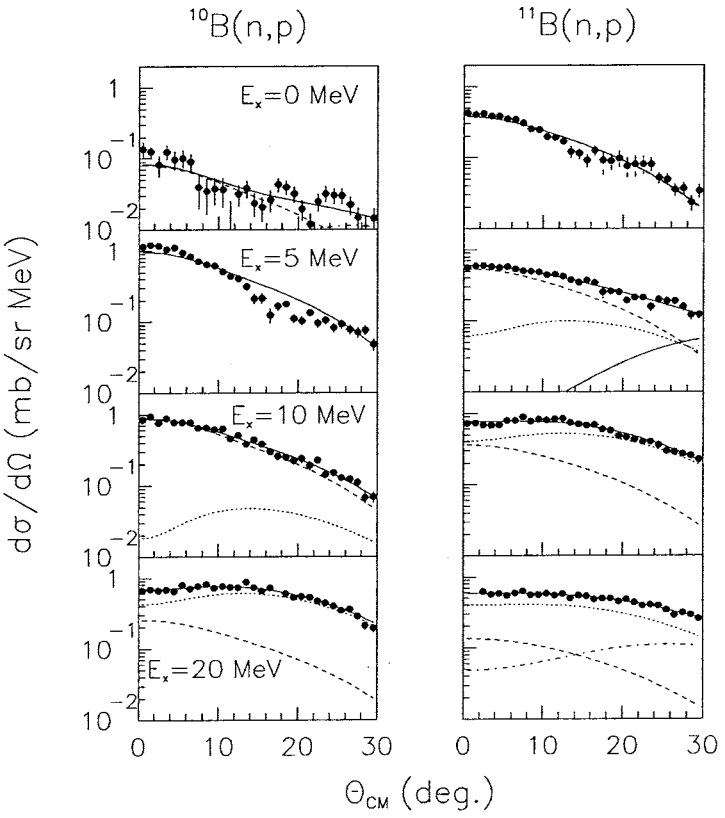


Fig. 6. Experimental double-differential cross sections of the $^{10,11}$B(n, p) reactions at $E_n = 96$ MeV projected into angular distributions with energy bins of 0.5 MeV (filled circles). Data are shown at excitation energies 0, 5, 10 and 20 MeV. No phase-space contribution has been subtracted. The curves represent the fitted angular distributions $L = 0$ (dashed), $L = 1$ (dotted), $L = 2$ (dot-dashed) and $L = 3$ (solid). The sum is drawn as a solid line close to the data points. A single solid line means that data can be described by $L = 0$ alone.

momentum transfer $q$ and zero energy loss ($\omega = E_x - Q_{\text{g.s.}}$),

$$\frac{\mathrm{d}\sigma}{\mathrm{d}\Omega}(q=0,\omega=0) = K(E_n,\omega=0)N^{\mathrm{D}}(q=0,\omega=0)\left|J_{\sigma\tau}(q=0)\right|^2 B_{\mathrm{GT}}^{np}, \tag{4}$$

where $N^{\mathrm{D}}$ is the ratio of the distorted-wave to plane-wave cross sections, $J_{\sigma\tau}(0)$ is the volume integral of the central spin–isospin component $V_{\sigma\tau}$ of the effective N–N interaction, and $B_{\mathrm{GT}}^{np}$ is the GT transition strength. $K$ is a kinematic factor given by

$$K(E_n,0) = \frac{E_{\mathrm{i}}E_{\mathrm{f}}}{(\pi\hbar^2c^2)^2}\frac{k_{\mathrm{f}}}{k_{\mathrm{i}}}. \tag{5}$$

The product of the first three factors in Eq. (4) is called the unit cross section, $\hat{\sigma}$,

$$\hat{\sigma} = K(E_n,0)N^{\mathrm{D}}(0,0)\left|J_{\sigma\tau}(0)\right|^2, \tag{6}$$

and thus

$$\frac{\mathrm{d}\sigma}{\mathrm{d}\Omega}(0,0) = \hat{\sigma}\,B_{\mathrm{GT}}^{np}, \tag{7}$$

where $\mathrm{d}\sigma/\mathrm{d}\Omega(0,0)$ is obtained from the experimental cross section by correcting for the $q$ and $\omega$ dependence using DWBA calculations,

$$\frac{d\sigma}{d\Omega}(0,0) = \frac{[d\sigma/d\Omega(q,\omega)]_{exp}}{[d\sigma/d\Omega(q,\omega)]_{DWBA}} \left[\frac{d\sigma}{d\Omega}(0,0)\right]_{DWBA}. \quad (8)$$

This means that if $B_{GT}^{np}$ is known from the corresponding $\beta$-decay, the unit cross sections can be determined from the experiment. In the present cases, where the GT transitions go to excited states in the final nuclei, this information is not available. On the other hand, the unit cross section can be calculated to reasonable precision using Eq. (6), if $J_{\sigma\tau}(0)$ is known. This is especially true for light nuclei, where distortion effects are quite small.

The distortion factors were calculated as the DWBA/PWBA cross section ratios, and were found to be 0.414 and 0.450 for $^{10}$B and $^{11}$B, respectively. Using $J_{\sigma\tau}(0) = 180$ MeV fm$^3$ [10], one obtains a unit cross section of 7.6 mb/sr for $^{10}$B, and 8.4 mb/sr for $^{11}$B. This is in accordance with systematics from experimentally determined (n, p) unit cross sections for other light nuclei [9,27], which all are in the region 8–9 mb/sr at this neutron energy. The error in the unit cross section, mainly caused by the uncertainty in the optical potential, was estimated to be ± 10%.

Using these unit cross sections, the Gamow–Teller strengths were determined, according to Eqs. (7) and (8). The result is displayed in column 4 of Table 1, for three excitation energy regions. The experimentally determined cross section is given in column 2, followed by the cross section extrapolated to $q = \omega = 0$ in column 3. All strengths were determined using data where the phase-space continuum was subtracted.

If the results are compared with corresponding (p, n) data, a comparison with the model-independent Ikeda sum can be made. The analysis of the $^{10}$B(p, n)$^{10}$C measurement discussed above results in a GT strength of $S_{\beta-} = 1.9 \pm 0.2$ sum rule units up to 20 MeV of excitation [38]. We then get $S_{\beta-} - S_{\beta+} = (1.9 \pm 0.2) - (1.74 \pm 0.18) = 0.2 \pm 0.3$, which is compatible with the Ikeda sum rule strength of 0.

The $^{11}$B(p, n)$^{11}$C reaction has been studied by Taddeucci et al. [40] in the energy range 160–795 MeV. An experimental strength of $S_{\beta-} = 2.56 \pm 0.07$ up to an excitation

Table 1
Zero-degree cross sections and Gamow–Teller strength (column 4) in three excitation energy regions, for the $^{10,11}$B(n, p) reactions at 96 MeV. Column 2 gives the $L = 0$ cross section and column 3 the cross section extrapolated to $q = \omega = 0$. The unit-cross sections ($\hat{\sigma}$) used in the calculations are also given

| $E_x$-range (MeV) | $(d\sigma/d\Omega)_{exp}$ (mb/sr) | $(d\sigma/d\Omega)$ (mb/sr) at $q = \omega = 0$ | $B_{GT}^{np}$ |
|---|---|---|---|
| | $^{10}$B(n, p) ($\hat{\sigma} = 7.6$ mb/sr) | | |
| $\leqslant 10$ | 7.18 ± 0.03 | 7.89 ± 0.03 | 1.04 ± 0.11 |
| $\leqslant 20$ | 11.23 ± 0.05 | 13.22 ± 0.06 | 1.74 ± 0.18 |
| $\leqslant 30$ | 12.22 ± 0.10 | 14.99 ± 0.12 | 1.97 ± 0.21 |
| | $^{11}$B(n, p) ($\hat{\sigma} = 8.4$ mb/sr) | | |
| $\leqslant 10$ | 4.73 ± 0.04 | 6.26 ± 0.05 | 0.75 ± 0.08 |
| $\leqslant 20$ | 6.77 ± 0.07 | 9.89 ± 0.10 | 1.18 ± 0.13 |
| $\leqslant 30$ | 7.06 ± 0.12 | 10.73 ± 0.18 | 1.28 ± 0.15 |

energy of 13.8 MeV was obtained in that experiment. It seems highly likely, however, that significant additional Gamow–Teller strength might reside at higher excitation energies, making a comparison with the Ikeda sum rule unreliable.

Recently, Daito et al. have made a pioneering investigation of the (t, $^3$He) reaction at 127 MeV/$A$ as a probe of Gamow–Teller strength [41]. With their technique, an energy resolution of 780 keV (FWHM) has been reached, i.e. significantly better than in the present work. On the other hand, their study was limited to 0° and therefore their identification of the final states could not be supported by angular distributions.

In their work, a general trend of proportionality between the 0° cross section and known $B$(GT) values from beta decay was observed, using the experimental cross sections of the (t,$^3$He) reaction on $^9$Be, $^{12}$C and $^{13}$C in combination with information from the literature on ground state beta decay of the residual nuclei.

The Gamow–Teller strength was also studied in $^{10}$B and $^{11}$B. For the latter, structure calculations have indicated a summed $B$(GT) of 0.73 for the three states at 0.3, 2.7 and 3.8 MeV excitation energy [42]. Daito et al. found only $0.47 \pm 0.08$ for the summed strength, and speculated whether this could be due to a neutron halo effect originating from a poor overlap of the wave functions of the $^{11}$B ground state and the final states in $^{11}$Be. In the present work, an integration of the Gamow–Teller strength up to 6 MeV, i.e. covering the same range in excitation energy as the three states above, results in a summed strength of $B(\mathrm{GT}) = 0.58 \pm 0.06$, i.e. also lower than the theory prediction.

### 4.5. Dipole strength

The excitation energy spectra (Fig. 2) and the results from the multipole decomposition (Figs. 4 and 5) show that there are broad distributions of dipole strength centered around excitation energies of 22 and 12 MeV in $^{10}$B and $^{11}$B, respectively. By construction, the normal modes described in Section 4.2 exhaust the full strength of the associated operator that is contained in the particle–hole basis used. To estimate the fraction of dipole strength exhausted in the experiment, we simply summed the $A_L$ coefficients of the 0.5 MeV energy bins (without renormalization) from the multipole decomposition, up to an excitation energy of 30 MeV. The fractions of strength obtained for the full and continuum subtracted data are given in the third and fifth column of Table 2, respectively. The errors are due to the statistics of the data and the decomposition procedure. As can be seen in the table, only about 50% of the predicted total dipole strength is exhausted in both nuclei before subtraction of the continuum. After subtraction of the underlying continuum, around 20% of the strength is left. This should be compared with the results obtained for $^{12}$C [10], where 130% and 75% of the normal mode strength were seen, before and after continuum subtraction, respectively.

The present data for dipole excitations can be compared with the results from the $^{10}$B(p, n)$^{10}$C reaction at $E_p = 186$ MeV [39]. This is presented in Fig. 7, where data for $\theta^{pn}_{\mathrm{CM}} = 11°$ and $\theta^{np}_{\mathrm{CM}} = 16°$ are plotted together. The chosen angles correspond to approximately the same momentum transfers for the two reactions. The (p, n) spectrum has

Table 2
Result of the multipole decomposition for the $L = 1$ strength for the total (left part) as well as for the continuum-subtracted data (right part). The second and fourth columns show the observed energy-integrated cross section in the region $E_x = 0$–30 MeV. The third and fifth columns give the corresponding ratios between the observed cross section and that of the normal-mode (NM) calculations. Only statistical errors are given

| | Total data | | Continuum-subtracted data | |
|---|---|---|---|---|
| | $(d\sigma/d\Omega)_{exp}$ (mb/sr) | $(d\sigma/d\Omega)_{exp}/(d\sigma/d\Omega)_{NM}$ (%) | $(d\sigma/d\Omega)_{exp}$ (mb/sr) | $(d\sigma/d\Omega)_{exp}/(d\sigma/d\Omega)_{NM}$ (%) |
| $^{10}$B | 8.35±0.15 | 43±1 | 2.71±0.06 | 14±1 |
| $^{11}$B | 7.46±0.24 | 53±2 | 3.62±0.10 | 26±1 |

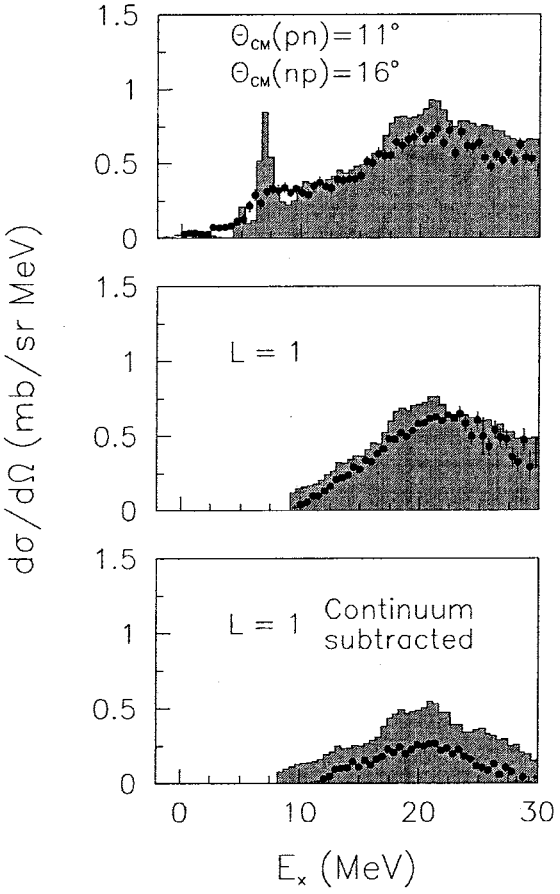


Fig. 7. A comparison between the present $^{10}$B(n, p)$^{10}$Be data at $E_n = 96$ MeV (filled circles) and data for the $^{10}$B(p, n)$^{10}$C reaction at $E_p = 186$ MeV [39] (shaded areas). The (p, n) data have been shifted upwards in excitation energy by 1.5 MeV, to get better agreement between the GT peaks in the two data sets. The top panel shows measured differential cross sections, compared at the same momentum transfer. In the lower two panels, the results of the multipole decomposition for $L = 1$ are displayed.

been adjusted 1.5 MeV upwards in energy to get better agreement between the positions of the GT peaks in the two data sets. This difference in excitation energy might be due to the target deterioration problem in our experiment, described in Section 2. Taking the different resolutions into account, the data look similar, both in shape and on an absolute scale. The results from the multipole decompositions for $L = 1$ are also compared in Fig. 7. The differences between the strength distributions after subtraction of the continuum are to a large extent due to the different treatments of this background. The (p, n) data extend to much higher excitation energies, which means that a more accurate fit of the calculated background is possible. The prescription used in the (p, n) analysis resulted in a smaller background subtraction, which explains the differences. It is possible that the continuum in our case has been overestimated, causing a somewhat too large reduction in strength.

It has been suggested that halo nuclei could have a dipole component at very low excitation energy [43]. This can be understood in a simple, hydrodynamical model. Besides the well known giant dipole resonance (GDR) — which is an out-of-phase oscillation of protons versus neutrons — there could be a mode where the halo neutron oscillates versus the core. The excitation energy of this mode must be very low, because the restoring force is rather weak, due to the low density of the halo. The experimental status of this mode is still not satisfactorily resolved, although indications of soft dipole strength have been reported in Coulomb breakup experiments [44,45] and in a pion double charge-exchange experiment [46].

The identification of a soft dipole is difficult in the present experiment. An E1 excitation ($1^-$) built on the $^{11}$Be ground state ($1/2^+$) would have spin and parity of $1/2^-$ or $3/2^-$. The $^{11}$B ground state has a $3/2^-$ configuration, and hence the transitions from the $^{11}$B ground state to a soft dipole in $^{11}$Be can be $0^+$, $1^+$, $2^+$ or $3^+$. The transition quantum numbers $1^+$ and $2^+$ are also valid for transitions to the first excited state of $^{11}$Be ($1/2^-$), which is strongly excited. If there is at all a soft dipole in $^{11}$Be, it is possibly hidden by this strong excitation.

An interesting observation in the $^{11}$B(d,$^2$He) experiment discussed above [37], was that the centroid of the dipole distribution, situated at $E_x \approx 10$ MeV, was 2 MeV lower in excitation energy compared to what would be expected for a nonhalo nucleus. This result was interpreted as support for a halo structure, based on a comparison of two structure calculations. A recent calculation assuming a halo [47] displays this downward shift, while a standard structure calculation [4] without halo does not reproduce this particular feature. In addition, the summed spin-flip dipole strength for $^{11}$Be was found to be 40% larger than in neighboring nonhalo nuclei. Also in this case, the structure calculation assuming a halo agrees better with these data. Recently, transitions from $^{11}$B to $^{11}$Be have been studied by electron-induced pion production [48]. In this publication, evidence for dipole strength shifted to lower excitation energies than expected for a nonhalo nucleus were presented, based on comparisons with Hartree–Fock calculations [47].

The observed centroid of the dipole distribution lies about 2 MeV higher in excitation energy in the present measurement compared to the $^{11}$B(d,$^2$He) data. Since the (n, p) reaction excites both spin-flip and non-spin-flip transitions, the position of the dipole distributions cannot be compared directly. It is possible that non-spin-flip IVD transitions

moves the dipole centroid to higher energies. This is supported by results from the $^{12}$C measurement [10], in which a peak dominated by SIVD $2^-$ was found at lower excitation energy than the corresponding $1^-$ state, which contains both $\Delta S = 1$ and $\Delta S = 0$ transitions. In view of this fact, the dipole distributions in the two experiments do not contradict each other. Furthermore, the structure calculation for the non-spin-flip case by Hoshino et al. [47], does not display a clear shift in excitation energy for a halo nucleus compared to a nonhalo nucleus that is seen in the spin-flip case.

The model-independent energy-weighted sum rule (EWSR) of the E1 strength depends only on the number of neutrons and protons. The non-energy-weighted sum of E1 strength (NEWSR), however, increases with the nuclear radius, so that the effect of a halo is to increase the total E1 strength. This requires part of the strength to be moved to lower excitation energy in order to conserve the EWSR [49]. For $^{11}$Li — the best studied halo nucleus, both experimentally and theoretically — calculations [50] have predicted about 10% of the EWSR (corresponding to 30% of the NEWSR) at very low energy. Other studies have revealed similar features [51,52], and in addition found the total E1 strength to increase with about 50% compared to neighboring nonhalo nuclei.

In the present experiment, we find no evidence of such an increase in non-energy-weighted E1 strength. In fact, we find significantly less than in the neighboring $^{12}$C nucleus. However, dipole and spin–dipole strength cannot be distinguished by a differential (n, p) cross section measurement alone, and the spin-flip transitions are stronger in magnitude than non-spin-flip at this energy.

## 5. Summary and conclusions

In this work double-differential cross sections of the $^{10,11}$B(n, p)$^{10,11}$Be reactions have been measured in the excitation energy and angular regions 0–35 MeV and 0°–30°, respectively, using a magnetic spectrometer with position-sensitive detectors for the determination of the proton energy and emission angle. The data were normalized to the backward-angle n–p scattering cross section. The analysis was performed in terms of multipole transitions and a continuum distribution. The latter was estimated from a simple calculation of the phase space for a number of knockout reaction channels, fitted to the experimental data at high excitation energy. A multipole decomposition of the experimental energy spectra was performed, using sample angular distributions calculated within the DWBA, using normal-mode excitations. From this analysis the energy-integrated cross section and the fraction of the sum rule strength exhausted for each multipolarity could be determined.

The obtained 0° cross sections for the Gamow–Teller transitions were used to extract the GT strength. This strength could be used for a full test of the Ikeda sum rule, using unit cross sections based on the DWBA calculations. In the $^{10}$B case, a sum-rule strength compatible with the theoretical value of 0 was obtained, while for $^{11}$B, the (p, n) data do not extend to a sufficiently high excitation energy to make a comparison meaningful.

The summed Gamow–Teller strength of three low-lying states in the $^{11}$B(t,$^{3}$He)$^{11}$Be reaction has recently been found to be significantly lower than predicted by structure calculations, and it has been discussed whether this strength deficit could be due to halo effects in the residual $^{11}$Be nucleus. The Gamow–Teller strength found in the present experiment is in agreement with the (t,$^{3}$He) result.

Dipole strengths were found in broad peaks around excitation energies of 22 and 12 MeV for $^{10}$B and $^{11}$B, respectively. A significantly smaller part of the sum-rule dipole strength is exhausted in these nuclei compared to a previous $^{12}$C(n, p) measurement. A soft dipole excitation at low excitation energy, and a downward shift in excitation energy of the dipole strength have been suggested for halo nuclei. In neither case, we can provide evidence. The possible presence of a soft dipole is hidden under a strong excitation of the first excited state in $^{11}$Be, and no downward shift in excitation energy of the dipole strength was observed, in contrast to a recent $^{11}$B(d,$^{2}$He) measurement [37].

## Acknowledgements

The authors wish to thank The Svedberg Laboratory staff for significant contributions in the construction of the equipment and during the measurements. This work was financially supported by the Swedish Natural Science Research Council.

## References

[1] R.R. Doering, A. Galonsky, D.M. Patterson, G.F. Bertsch, Phys. Rev. Lett. 35 (1975) 1691.
[2] F. Petrovich, W.G. Love, R.J. McCarthy, Phys. Rev. C 21 (1980) 1718.
[3] T.N. Taddeucci, C.A. Goulding, T.A. Carey, R.C. Byrd, C.D. Goodman, C. Gaarde, J. Larsen, D. Horen, J. Rapaport, E. Sugarbaker, Nucl. Phys. A 469 (1987) 125.
[4] D.J. Millener, D. Kurath, Nucl. Phys. A 255 (1975) 315.
[5] E.K. Warburton, D.J. Millener, Phys. Rev. C 39 (1989) 1120.
[6] E.K. Warburton, B.A. Brown, Phys. Rev. C 46 (1992) 923.
[7] H.V. von Geramb, in: H.O. Meyer (Ed.), The Interaction Between Medium Energy Nucleons in Nuclei, New York, AIP, 1983, p. 44.
[8] K. Nakayama, W.G. Love, Phys. Rev. C 38 (1988) 51.
[9] S. Dangtip, J. Blomgren, N. Olsson, H. Condé, K. Elmgren, J. Rahm, A. Ringbom, G. Tibell, O. Jonsson, L. Nilsson, P.-U. Renberg, S.Y. van der Werf, Nucl. Phys. A 677 (2000) 3.
[10] N. Olsson, H. Condé, E. Ramström, T. Rönnqvist, R. Zorro, J. Blomgren, A. Håkansson, G. Tibell, O. Jonsson, L. Nilsson, P.-U. Renberg, A. Brockstedt, P. Ekström, M. Österlund, S.Y. van der Werf, D.J. Millener, G. Szeflinska, Z. Szeflinski, Nucl. Phys. A 559 (1993) 368.
[11] T. Rönnqvist, H. Condé, N. Olsson, E. Ramström, R. Zorro, J. Blomgren, A. Håkansson, A. Ringbom, G. Tibell, O. Jonsson, L. Nilsson, P.-U. Renberg, S.Y. van der Werf, W. Unkelbach, F.P. Brady, Nucl. Phys. A 563 (1993) 225.
[12] H. Condé, N. Olsson, E. Ramström, T. Rönnqvist, R. Zorro, J. Blomgren, A. Håkansson, G. Tibell, O. Jonsson, L. Nilsson, P.-U. Renberg, M. Österlund, W. Unkelbach, J. Wambach, S.Y. van der Werf, J. Ullmann, S.A. Wender, Nucl. Phys. A 545 (1992) 785.
[13] A. Ringbom, A. Håkansson, G. Tibell, R. Zorro, J. Blomgren, H. Condé, J. Rahm, N. Olsson, E. Ramström, T. Rönnqvist, O. Jonsson, L. Nilsson, P.-U. Renberg, S.Y. van der Werf, H. Lenske, Nucl. Phys. A 617 (1997) 316.

[14] T. Rönnqvist, H. Condé, N. Olsson, R. Zorro, J. Blomgren, G. Tibell, O. Jonsson, L. Nilsson, P.-U. Renberg, S.Y. van der Werf, Phys. Rev. C 45 (1992) R496.

[15] T.E.O. Ericson, B. Loiseau, J. Nilsson, N. Olsson, J. Blomgren, H. Condé, K. Elmgren, O. Jonsson, L. Nilsson, P.-U. Renberg, A. Ringbom, T. Rönnqvist, G. Tibell, R. Zorro, Phys. Rev. Lett. 75 (1995) 1046.

[16] J. Rahm, J. Blomgren, H. Condé, S. Dangtip, K. Elmgren, N. Olsson, T. Rönnqvist, R. Zorro, O. Jonsson, L. Nilsson, P.-U. Renberg, A. Ringbom, G. Tibell, S.Y. van der Werf, T.E.O. Ericson, B. Loiseau, submitted for publication.

[17] J. Rahm, J. Blomgren, H. Condé, S. Dangtip, K. Elmgren, N. Olsson, T. Rönnqvist, R. Zorro, A. Ringbom, G. Tibell, O. Jonsson, L. Nilsson, P.-U. Renberg, T.E.O. Ericson, B. Loiseau, Phys. Rev. C 57 (1998) 1077.

[18] D.S. Sorenson, J.L. Ullman, R.A. Lindgren, A. Ling, J. Rapaport, B.K. Park, R.C. Haight, F.P. Brady, J.L. Romero, N.S.P. King, B.L. Clausen, H. Baghaei, C. Wuegt, in preparation.

[19] I. Tanihata, H. Hamagaki, O. Hashimoto, Y. Shida, N. Yoshikawa, K. Sugimoto, O. Yamakawa, T. Kobayashi, N. Takahashi, Phys. Rev. Lett. 55 (1985) 2676.

[20] I. Tanihata, Nucl. Phys. A 522 (1991) 275c.

[21] M.C. Vetterli, O. Häusser, R. Abegg, W.P. Alford, A. Celler, D. Frekers, R. Helmer, R. Henderson, K.H. Hicks, K.P. Jackson, R.G. Jeppesen, C.A. Miller, K. Raywood, S. Yen, Phys. Rev. C 40 (1989) 559.

[22] F. Osterfeld, in: J. Speth (Ed.), Electric and Magnetic Giant Resonances in Nuclei, International Review of Nuclear Physics, Vol. 7, World Scientific, Singapore, 1991.

[23] H. Condé, S. Hultqvist, N. Olsson, T. Rönnqvist, R. Zorro, J. Blomgren, G. Tibell, A. Håkansson, O. Jonsson, A. Lindholm, L. Nilsson, P.-U. Renberg, A. Brockstedt, P. Ekström, M. Österlund, F.P. Brady, Z. Szeflinski, Nucl. Instrum. Methods A 292 (1990) 121.

[24] J. Blomgren, L. Einarsson, Int. Nucl. Target Develop. Soc. Newsl. 22 (1995) 13.

[25] F.P. Brady, G.A. Needham, J.L. Ullmann, C.M. Castaneda, T.D. Ford, N.S.P. King, J.L. Romero, M.L. Webb, V.R. Brown, C.H. Poppe, J. Phys. G. 10 (1984) 363.

[26] F.P. Brady, T.D. Ford, G.A. Needham, J.L. Romero, D.S. Sorenson, C.M. Castaneda, J.R. Drummond, E.L. Hjort, B. McEachern, N.S.P. King, D.J. Millener, Phys. Rev. C 43 (1991) 2284.

[27] D.S. Sorenson, PhD thesis, University of California, Davis, CA, 1991, Los Alamos National Laboratory Report LA-12061-T.

[28] K. Nakamura, S. Hirimatsu, T. Kamae, H. Muramatsu, Nucl. Phys. A 296 (1978) 431.

[29] A. Bohr, B. Mottelson, Nuclear Structure, Vol. 2, Benjamin, 1969.

[30] R. Schaeffer, J. Raynal, Program DWBA70 (unpublished); J.R. Comfort, extended version DW81 (unpublished).

[31] R. Machleidt, K. Holinde, Ch. Elster, Phys. Rep. 149 (1987) 1.

[32] G.T.A. Squier, A.R. Johnston, E.W. Spiers, S.A. Harbison, N.M. Stewart, Nucl. Phys. A 141 (1970) 158.

[33] J.R. Comfort, B.C. Karp, Phys. Rev. C 21 (1980) 2162.

[34] A.J. Houdayer, T.Y. Li, S.K. Mark, Can. J. Phys. 48 (1970) 765.

[35] P. Schwandt, H.O. Meyer, W.W. Jacobs, A.D. Bacher, S.E. Vigdor, M.D. Kaitchuck, T.R. Donoghue, Phys. Rev. C 26 (1982) 55.

[36] F. Ajzenberg-Selove, Nucl. Phys. A 490 (1988) 1.

[37] H. Sakai, H. Okamura, S. Ishida, H. Okuno, N. Fukunishi, H. Sagawa, A. Okihana, Y. Nagai, K. Takeda, T. Toriyama, A. Yoshida, Phys. Lett. B 302 (1993) 7.

[38] L. Wang, X. Yang, J. Rapaport, C.D. Goodman, C.C. Foster, Y. Wang, R.A. Lindgren, E. Sugarbaker, D. Marchlenski, S. de Lucia, B. Luther, L. Rybarcyk, T.N. Taddeucci, B.K. Park, Phys. Rev. C 47 (1993) 2123.

[39] X. Yang, L. Wang, J. Rapaport, C.D. Goodman, C.C. Foster, Y. Wang, E. Sugarbaker, D. Marchlenski, S. de Lucia, B. Luther, L. Rybarcyk, T.N. Taddeucci, B.K. Park, Phys. Rev. C 52 (1995) 2535.
[40] T.N. Taddeucci, R.C. Byrd, T.A. Carey, D.E. Ciskowski, C.C. Foster, C. Gaarde, C.D. Goodman, E. Gülmez, W. Huang, D.J. Horen, J. Larsen, D. Marchlenski, J.B. McClelland, D. Prout, J. Rapaport, L.J. Rybarcyk, E. Sugarbaker, I.J. Van Heerden, C.A. Whitten Jr, Phys. Rev. C 42 (1990) 935.
[41] I. Daito, H. Akimune, Sam M. Austin, D. Bazin, G.P.A. Berg, J.A. Brown, B.S. Davis, Y. Fujita, H. Fujimura, M. Fujiwara, R. Hazama, T. Inomata, K. Ishibashi, J. Jänecke, S. Nakayama, K. Pham, D.A. Roberts, B.M. Sherrill, M. Steiner, A. Tamii, M. Tanaka, H. Tokoyawa, M. Yosoi, Phys. Lett. B 418 (1998) 27.
[42] S. Cohen, D. Kurath, Nucl. Phys. 73 (1965) 1.
[43] P.G. Hansen, B. Jonson, Europhys. Lett. 4 (1987) 409.
[44] T. Kobayashi, S. Shimoura, I. Tanihata, K. Katori, K. Matsuta, T. Minamisono, K. Sugimoto, W. Muller, D.L. Olson, T.J.M. Symons, H. Wieman, Phys. Lett. B 82 (1989) 232.
[45] D. Sackett, K. Ieki, A. Galonsky, C.A. Bertulani, H. Esbensen, J.J. Kruse, W.G. Lynch, D.J. Morrissey, N.A. Orr, B.M. Sherrill, H. Schulz, A. Sustich, J.A. Winger, F. Deak, A. Horvath, A. Kiss, Z. Seres, J.J. Kolata, R.E. Warner, D.L. Humphrey, Phys. Rev. C 48 (1993) 118.
[46] T. Kobayashi, Nucl. Phys. A 538 (1992) 343c.
[47] T. Hoshino, H. Sagawa, A. Arima, Nucl. Phys. A 523 (1991) 228.
[48] T. Yamaya, M. Saitoh, H. Yamazaki, T. Taniuchi, K. Shoda, H. Tsubota, Phys. Rev. C 51 (1995) 493.
[49] K. Riisager, A.S. Jensen, P. Møller, Nucl. Phys. A 548 (1992) 393.
[50] Y. Suzuki, Y. Tosaka, Nucl. Phys. A 517 (1990) 599.
[51] G. Bertsch, J. Foxwell, Phys. Rev. C 41 (1990) 1300.
[52] H. Esbensen, G. Bertsch, Nucl. Phys. A 542 (1992) 310.

# Appendix VI

ELSEVIER Nuclear Instruments and Methods in Physics Research A 452 (2000) 484–504

NUCLEAR INSTRUMENTS & METHODS IN PHYSICS RESEARCH Section A

www.elsevier.nl/locate/nima

# A facility for measurements of nuclear cross sections for fast neutron cancer therapy

S. Dangtip[a], A. Ataç[a], B. Bergenwall[a], J. Blomgren[a], K. Elmgren[a], C. Johansson[a], J. Klug[a], N. Olsson[a,*], G. Alm Carlsson[b], J. Söderberg[b], O. Jonsson[c], L. Nilsson[c], P.-U. Renberg[c], P. Nadel-Turonski[d], C. Le Brun[e], F.-R. Lecolley[e], J.-F. Lecolley[e], C. Varignon[e], Ph. Eudes[f], F. Haddad[f], M. Kerveno[f], T. Kirchner[f], C. Lebrun[f]

[a]*Department of Neutron Research, Uppsala University, Box 535, S-75121 Uppsala, Sweden*
[b]*Department of Radiology and Radiation Physics, Linköping University, S-58185 Linköping, Sweden*
[c]*The Svedberg Laboratory, Uppsala University, Box 533, S-75121 Uppsala, Sweden*
[d]*Department of Radiation Sciences, Uppsala University, Box 535, S-75121 Uppsala, Sweden*
[e]*LPC, ISMRA et Université de Caen, CNRS/IN2P3, 14050 Caen Cedex, France*
[f]*SUBATECH, Université de Nantes, CNRS/IN2P3, 44070 Nantes Cedex 03, France*

Received 29 March 2000; accepted 6 April 2000

**Abstract**

A facility for measurements of neutron-induced double-differential light-ion production cross-sections, for application within, e.g., fast neutron cancer therapy, is described. The central detection elements are three-detector telescopes consisting of two silicon detectors and a CsI crystal. Use of $\Delta E$–$\Delta E$–$E$ techniques allows good particle identification for p, d, t, $^3$He and alpha particles over an energy range from a few MeV up to 100 MeV. Active plastic scintillator collimators are used to define the telescope solid angle. Measurements can be performed using up to eight telescopes at 20° intervals simultaneously, thus covering a wide angular range. The performance of the equipment is illustrated using experimental data taken with a carbon target at $E_n = 95$ MeV. Distortions of the measured charged-particle spectra due to energy and particle losses in the target are corrected using a newly developed computer code. Results from such correction calculations are presented. 

*PACS:* 29.30.Ep; 29.40.Wk; 29.40.Mc; 25.40. – h

*Keywords:* Charged particle spectrometer array; Nuclear reactions

## 1. Introduction

Today, about half of all cancer patients in the western countries are treated with ionizing radiation. A majority of these undergo treatment with bremsstrahlung photon and electron beams, which are weakly ionizing. Not all tumours respond positively to this kind of radiation. It has been claimed that a large number of patients could benefit from therapy with more densely ionizing radiation [1,2].

* Corresponding author. Tel.: + 46-18-471-3043.
*E-mail address:* nils.olsson@tsl.uu.se (N. Olsson).

0168-9002/00/$ - see front matter 
PII: S0168-9002(00)00455-1

Cancer therapy with fast neutrons employs the fact that neutrons, interacting with tissue, give rise to a sizeable component of radiation with high linear energy transfer (LET), which has been shown to be of great value for the treatment of some specific, slowly growing, tumours. During the last two decades, fast neutron therapy has been modernized and better optimized by, e.g., higher energies (up to 70 MeV), and is now employed at about 20 centres around the world. The method has gained renewed interest in recent years after successful treatments of, among others, salivary gland tumours, which are not accessible for surgery. Results of treatments of other kinds of tumours, e.g., prostatic cancer and some tumours of the head and neck region, have been more difficult to interpret [3–8].

Thus, cancer therapy with fast neutrons has an interesting potential as treatment alternative for tumours that do not respond to low LET radiation. To investigate this potential fully, the dose delivery has to be known with the same precision as is common in photon therapy. To achieve this, the fundamental cross-sections converting neutrons into ionizing charged particles have to be determined.

It is important to realize that for each incoming neutron with a specific energy, a multitude of charged particles can be created in tissue: protons, deuterons, tritons, $^{3}$He and alpha particles, as well as carbon, nitrogen and oxygen recoils, etc., each with its characteristic energy and angular distribution, which in turn are different for different nuclei. It is these charged particles that are responsible for the ionization, which causes damage on the cellular level. The conversion from neutrons to charged particles proceeds via the microscopic, nuclear cross-sections for each reaction channel. Unfortunately, the energy region of several tens of MeV is difficult to describe with simple theories and, in addition, the data base is very meagre. In this energy region, compound nuclear processes, direct processes and intermediate, or pre-compound, processes are all important, and nuclear reaction models must take into account all these processes and their variation with energy. Most evaluated data bases were intended for use in the development of nuclear fission and fusion energy sources, and have a 20 MeV upper energy limit. This makes it difficult to estimate correctly the dose given by modern neutron therapy beams, which extend up to 70 MeV, and to plan and optimize the radiation therapy. A substantial improvement in the knowledge of fundamental nuclear data is therefore needed for a better understanding of the processes occurring on the cellular level.

During 1987–1992, a cross-disciplinary Coordinated Research Programme (CRP) on "Nuclear Data Needed for Neutron Therapy" was organized by the IAEA [9]. The purpose was to identify which fundamental data are of highest relevance for the development of fast neutron therapy. The CRP gave highest priority to new measurements of the following data: (1) Double-differential light-ion production cross-sections and kerma factors for the most important elements in tissue, i.e., carbon, nitrogen, oxygen and calcium, up to about 80 MeV. (2) Differential cross-sections for elastic and inelastic neutron scattering from carbon and oxygen at, e.g., 30, 50 and 80 MeV. These data are needed to improve theoretical model calculations, and this need has repeatedly been emphasized [10,11].

Interest in the information on charged particles emitted in reactions induced by neutrons is not limited to the medical community. Such information is also of relevance for other applications, like transmutation of nuclear waste and cosmic-ray-induced effects in aviation electronics.

In transmutation applications, the proposed technologies involve high-energy neutrons created in proton-induced spallation of a heavy target element. The NEA nuclear science committee [12,13] has indicated cross-section measurements for the (n,xp) reaction in a number of nuclei, e.g., $^{56}$Fe,$^{58}$Ni, $^{208}$Pb, $^{232}$Th, and $^{238}$U, in the energy range 20–200 MeV as one of the high priorities among their nuclear data requests for this application.

The importance of cosmic radiation effects in aircraft electronics has recently been highlighted (see e.g. Refs. [14–16] and references therein). At commercial flight altitudes, as well as at sea level, the most important particle radiation is due to neutrons, created in the atmosphere by spallation of nitrogen and oxygen nuclei, induced by cosmic-ray protons. When, e.g., an electronic memory

circuit is exposed to neutron radiation, charged particles can be produced in a nuclear reaction. The released charge can cause a flip of the memory content in a bit, which is called a single-event upset (SEU). To get a deeper understanding of these phenomena, more detailed cross-section information on neutron-induced charged-particle production at intermediate energies is needed.

To fulfill the needs of better nuclear data for fast neutron cancer therapy, as well as for other applications, we have built and tested a new experimental set-up, MEDLEY, dedicated for measurements of double-differential neutron-induced light-ion production cross-sections. Employing MEDLEY together with the unique quasi-monoenergetic neutron beam facility at The Svedberg Laboratory (TSL) in Uppsala [17], it is possible to measure such cross-sections for production of protons, deuterons, tritons, $^3$He and alpha particles in relevant nuclei. MEDLEY is superior to several similar existing arrays, due to its larger energy and angular coverage, and it can preferably be used in an energy region of greatest relevance for the mentioned applications, i.e., up to 100 MeV.

There are, or have been, very few facilities available, which can be used for such measurements. The UC Davis [18] set-up had three telescopes, each consisting of three detector elements. Measurements of protons, deuterons, tritons, $^3$He and alpha particles from carbon [19], nitrogen and oxygen [20] were carried out at 27.4, 39.7 and 60.7 MeV. In the case of carbon, data are extensive in the forward direction, but more scarce in the backward, while for nitrogen and oxygen, data only extend out to 65°, which makes kerma factor calculations rather ambiguous [10,21].

The four telescopes at Louvain-la-Neuve each consists of two detectors. Measurements of the same light ions have been performed between 30 and 75 MeV for carbon [22–25], between 25 and 65 MeV for oxygen [26–28], and up to 65 MeV for aluminium [29], all with large angular coverage. The UC Davis and Louvain-la-Neuve data show considerable discrepancies, especially for oxygen [20,26–28] in the low-energy domain.

In the Tohoku facility, the telescopes consisted of two elements. Measurements of protons and deuterons were carried out at forward angles with carbon and aluminium targets at 64.5 and 75 MeV [30]. However, the low-energy cut-off was very high, since the experiment was conducted in air.

In this article, the MEDLEY facility and its performance is described in some detail. Section 2 is devoted to the experimental set-up, i.e., the neutron beam production, scattering chamber, configuration of detector telescopes, electronics and data acquisition system. In Section 3, data reduction procedures and results from a test measurement are presented. Corrections for energy and particle losses in the target are discussed in Section 4, and finally, a summary and the conclusions are presented in Section 5.

## 2. Experimental set-up and techniques

### 2.1. TSL neutron beam facility

The neutron beam facility at the The Svedberg Laboratory (TSL) has been described in detail in a previous publication [17], and an updated presentation is underway [31]. Therefore, only a short description will be given here. An overview of the facility is shown in Fig. 1. A proton beam from the cyclotron is used to produce neutrons through the $^7$Li(p,n)$^7$Be reaction. The lithium targets are typically 2–15 mm thick and enriched to 99.98% in $^7$Li. The produced neutron beam is shaped and

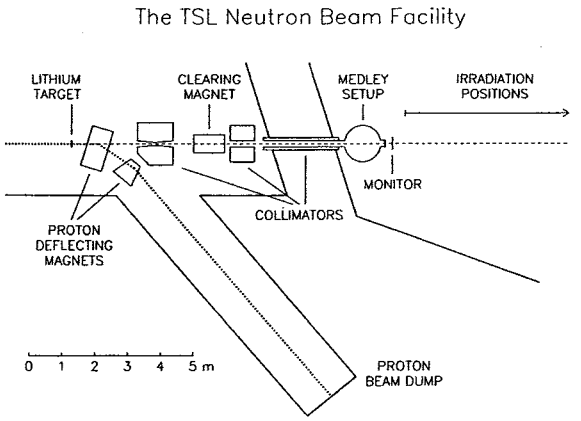


Fig. 1. Overview of the Uppsala neutron beam facility, showing the neutron production system, the proton beam dump, the neutron collimation, and the position of the MEDLEY set-up.

delivered to the experimental area through a system of collimators. Charged particles produced in the collimation system are deflected by a clearing magnet. The remaining proton beam, after the neutron production target, is bent out of the neutron beam by two dipole magnets into a well-shielded beam dump tunnel. At the end of the 8 m long tunnel, the beam is dumped in a lead-shielded water-cooled graphite Faraday cup, which is also used to measure the proton beam current.

The experimental area is situated at about 8 m from the neutron production target. The beam size at the reaction target is 7 cm in diameter. The neutron intensity in the experimental hall, with a 100 MeV proton beam current of 5 μA on a 4 mm thick Li target, is about $3 \times 10^4$ n $s^{-1}$ $cm^{-2}$.

The relative neutron beam intensity is monitored by the integrated proton beam current at the beam dump, and by thin film breakdown counters (TFBC) [32], mounted in the neutron beam, measuring the number of neutron-induced fissions in $^{238}U$.

A prominent feature of the neutron beam facility is the good shielding between the beam dump and the experimental area, which gives very low background around the detectors. Furthermore, the long distance between the neutron source and the reaction target allows the use of time-of-flight (TOF) techniques to reject low-energy neutrons. In a typical neutron-energy spectrum [17], shown in Fig. 2, about 50% of the neutrons are in the full-energy peak, while the rest forms a low-energy neutron tail, which can be suppressed by TOF techniques. It should be emphasized that the width of the neutron peak seen in Fig. 2 includes the limited resolution of the used detection system; in reality the peak has a width (FWHM) of the order of 1 MeV for a typical Li-target thickness of 4 mm.

Another characteristic is the 25 m long neutron beam line in the experimental area, which makes several irradiation positions available. In addition to the MEDLEY set-up, the neutron beam can be simultaneously used in several other experiments, e.g., studies of neutron elastic scattering, testing of single event upsets in electronic devices, dosimetry development, and fission cross-section measurements, thus providing an efficient use of the beam.

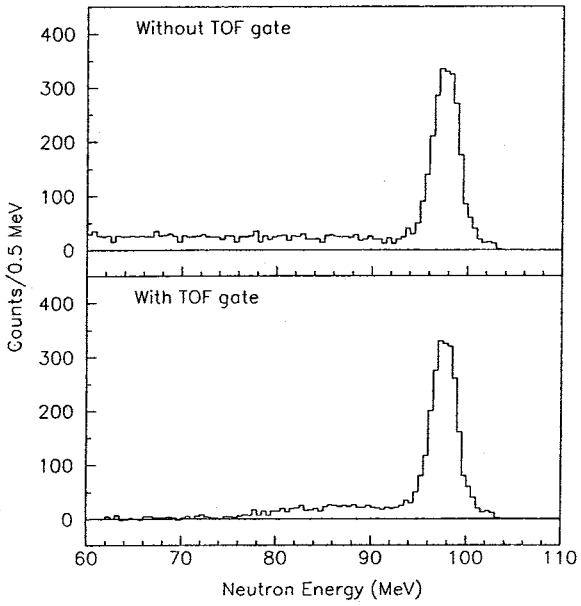


Fig. 2. Typical neutron energy spectrum from the $^7Li(p,n)$ reaction at $E_p = 100$ MeV and at 0°, as determined with a magnetic spectrometer [17]. The upper panel shows the full neutron spectrum from 60 to 100 MeV, while the lower panel illustrates the effect of TOF suppression of low-energy neutrons.

### 2.2. Scattering chamber

The MEDLEY detector set-up is installed in a cylindrical scattering chamber, positioned directly after the last neutron collimator (see Fig. 1). The chamber is about 100 cm in diameter and has a height of about 24 cm. There are four large ports; two in the neutron beam line and two on the sides perpendicular to the beam. The first two ports are used for beam transport, and the others for a turbo vacuum pump and a calibration source holder, respectively.

Fig. 3 shows the arrangement inside the vacuum chamber. The reaction target is located at the centre of the chamber. Since the neutron beam has a diameter of 7 cm, it is not practical, or even possible, to use a standard target ladder design. Instead, the target is mounted in a thin aluminium target frame, using thin threads. The target frame is large enough (20 cm wide by 14 cm high) to allow free passage of the neutron beam. Three target frames, which can be moved into or out of the neutron beam, are available at present. The

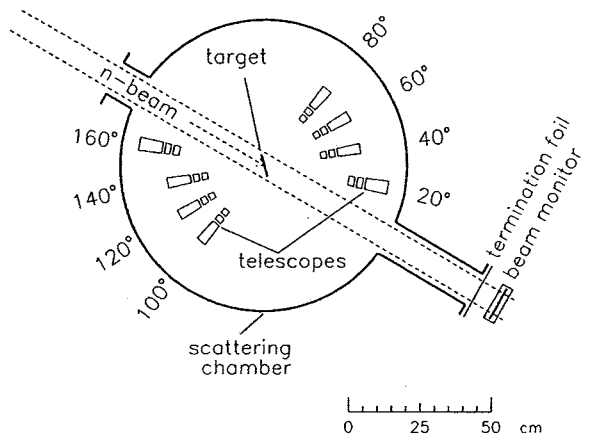


Fig. 3. Arrangement of the eight MEDLEY telescopes inside the 1 m diameter vacuum chamber. The target under study is located at the centre of the chamber. The TFBC neutron monitor is shown at about 50 cm downstream the chamber. The scale is approximate.

reaction targets typically have diameters of 20–25 mm, which is a compromise between reasonable count rate and angular resolution.

A $^{241}$Am alpha source, which can be used for calibration and adjustment of the electronics, is attached onto a metal rod in one of the chamber ports. When not in use, the source can be fully retracted so that the emitted alpha particles do not interfere with the detectors.

Eight detector telescopes are mounted in the chamber. They are placed at 20° intervals, covering scattering angles from 20° to 160° simultaneously. The telescopes are mounted in two sets, one on each side of the beam, covering the forward and backward hemispheres, respectively. The detector elements of each telescope are mounted in an aluminium housing, which in turn is mounted on a radial rail. The position of the telescope housing on the rail is adjustable, so that the target-to-detector distance can be varied between 15 and 28 cm. At the most forward and backward angles, the telescopes are typically placed at 28 cm distance from the target to avoid beam interference, while at other angles the distance is around 20 cm. The centre of the telescopes is at the same height as the beam axis and the centre of the target.

All the telescope rails are fixed onto a turnable plate at the bottom of the chamber. This plate is joined to a cylindrical vacuum feedthrough, which on the outside, below the chamber, has an indicator and a scale. In this way, the telescopes can be precisely positioned at the desired scattering angles.

This feature is used in the energy calibration of the telescopes. At forward angles, reasonably sharp peaks, corresponding to low-lying states in the residual nuclei, are present in (n,p) and (n,d) reaction spectra, and the energy of these peaks can be calculated to high precision. By rotating the plate, the forward and backward sets of telescopes can be interchanged, thus allowing also the backward telescopes to be calibrated by such reactions.

During experiments, the chamber is under vacuum in the range of $10^{-5}$ mbar or better. The vacuum is terminated at the exit port with a 0.1 mm thick stainless steel foil, which is located about 40 cm from the inner wall of the chamber (see Fig. 3).

All operations inside the vacuum chamber, i.e., movement of the target frames, insertion or retraction of the alpha source, or rotation of the telescope table, can be made without breaking the vacuum. Signal and bias cables for all detectors are brought out of the chamber via connectors mounted in the cylindrical feedthrough assembly at the bottom of the chamber.

### 2.3. Detector telescopes

It is important to obtain good separation between the different kinds of particles. This has to be done over a large dynamic range, i.e., from a few MeV alpha particles to 100 MeV protons, which corresponds to a range in $dE/dx$ of about 200. The $\Delta E - E$ technique can be used only if the incident particle has sufficiently high energy to penetrate the $\Delta E$ detector, and thus to be registered in the $E$ detector. Furthermore, the fraction of energy loss in the $\Delta E$ detector must be large enough to yield non-overlapping energy loss distributions for the various particle types. We found in our preliminary studies that a telescope consisting of two $\Delta E$ detectors and one thick $E$ detector, in which the total energy of the most energetic charged particle can be absorbed, would give a sufficient dynamic range.

The $\Delta E$ detectors are fully depleted standard silicon surface barrier detectors from ORTEC. The front $\Delta E$ detectors ($\Delta E_1$) are either 50 or 60 μm

thick, while the second ones ($\Delta E_2$) are 400 or 500 μm. They all have a sensitive area of 450 mm$^2$.

As $E$ detectors, we use CsI(Tl) crystals, since they possess several superior properties, e.g., high light conversion yield and high density, which makes them very efficient as stopping medium for various charged particles. Furthermore, the crystals are only slightly hygroscopic and relatively easy to handle. Although CsI(Tl) has a significant ion-charge and mass dependence in its scintillation response (see, e.g., Refs. [33,34]), this dependence is expected to be rather small within the limited range of light particles considered here.

The $E$ detectors have a total length of 50 mm. The first 30 mm of the crystals, which is a sufficient thickness to stop 100 MeV protons, is made cylindrical with a diameter of 40 mm. The remaining 20 mm is tapered to 18 mm diameter to match the size of the readout system. The 40 mm diameter was chosen so that particles produced at the edge of a 25 mm diameter target at the closest target-to-detector distance (15 cm to the first $\Delta E$ detector), passing through the edge of the second $\Delta E$ detector, can still be measured safely in the CsI $E$ detector. All the $E$ detectors are made window-less to avoid dead layer effects [18], which cause loss of energy, and thus a discontinuity in the linear correspondence between incident and measured energy.

Photodiodes (PD) of the Hamamatsu S3204-03 $18 \times 18$ mm$^2$ model were chosen to read out the light from the CsI(Tl) crystals. The spectral response function of a PD matches well the emission spectrum of the crystal, and they are very compact and thus well suited for an application where space is limited. Furthermore, PDs show excellent linearity and temperature stability. However, one drawback with PDs is the lack of internal gain, which means that at very low energy (keV region), electronic noise will outperform the detector. In the energy region of interest here (a few MeV and above), this problem is less important. The CsI(Tl) crystals were manufactured and assembled with the PDs by Crismatec in France.

To get a well-defined acceptance, collimators are needed in front of the telescopes. However, the presence of a collimator, thick enough to stop 100 MeV protons, can cause particles to scatter or react before reaching the first detector, and thus necessitate complicated correction calculations. To avoid such complications, we have instead chosen to employ thin, active collimators, where the signal from a hit is used to veto the related event.

The collimators are made from plastic scintillators, having a $40 \times 40$ mm$^2$ square shape and a thickness of 1 mm. The thickness is chosen to get reasonable pulse height also for the most penetrating particles (100 MeV protons). Each collimator has a 19 mm diameter hole at the centre, and is aligned concentrically with the telescope axis. The light produced in the scintillator is guided through a plexiglass light guide, which is bent 90°, to a 10 mm diameter photomultiplier tube (PMT). The PMT is of the Hamamatsu R1635 type, with fairly high gain ($1.1 \times 10^6$), low dark current (0.03 mA) and fast rise time (0.8 ns). The hybrid assembly (Hamamatsu H3164-10), with integrated PMT, base and voltage divider chain, is used due to its compactness. The whole collimator arrangement is fixed to the telescope housing.

A schematic view of the detector arrangement for a telescope is shown in Fig. 4. For a typical 25 mm diameter target, the average angular acceptance (or opening angle) is about 6° for most of the telescopes, and slightly less than 5° for the most forward and backward ones, due to their longer target-to-detector distance.

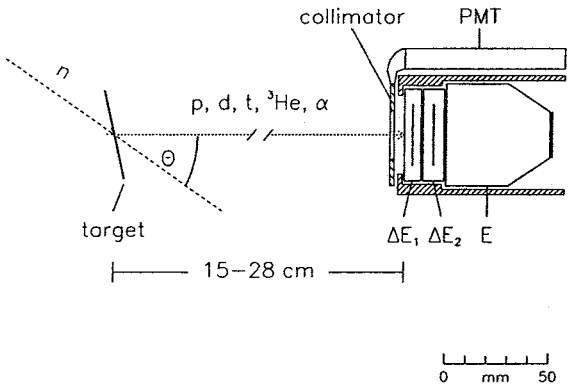


Fig. 4. Detailed sketch of one of the telescopes, showing the $\Delta E_1$ (50 or 60 μm Si) and $\Delta E_2$ (400 or 500 μm Si) detectors, as well as the CsI(Tl) $E$ detector. Also shown is the telescope housing and the collimator, which is placed in front of the telescope, with its PM tube on the top of the telescope housing.

### 2.4. Electronics

All telescope detector signals are processed by preamplifiers, placed close to the detectors, immediately outside the vacuum chamber. The remaining signal handling takes place in a distant counting room using standard electronic units.

The charge-sensitive preamplifiers are of the hybrid CAEN A422 model, which offers good $S/N$ ratio, fairly fast rise time (40–70 ns), proper energy sensitivity and a relatively low price. These preamplifier cards can also be optimized for various detector capacitances. Furthermore, the small dimensions of the $3.8 \times 3.3$ cm 14-pin single in-line package allow a very compact housing for all 24 preamplifier cards. They are mounted four by four on six mother cards, which provide bias voltages, connections to BNC contacts, etc. All six mother cards are housed in a single box, which is mounted just below the vacuum chamber.

For each detector, the output signal is processed by the preamplifier and two output signals are generated; energy ($E$) and timing ($T$). The $E$ branch is further amplified and shaped, and the pulse height is registered by an ADC. The gate for the ADC is derived from a MASTER signal (see below). The other branch ($T$) is utilized only for the thin ($\Delta E_1$) and thick ($\Delta E_2$) silicon detectors, since the $T$ signal from the CsI ($E$) detector has too slow rise time (a few μs) to be useful. The T signal is amplified by a fast amplifier ($\times 10$) and then fed to a constant fraction discriminator (CFD), where two standard output signals are generated. The first output is used to create the MASTER signal, while the second is used as stop signal of a TDC. The presence of a signal at the TDC is also used to identify which telescope, and which silicon detector of that telescope, generated the MASTER signal.

The threshold of the $T$ signal at the CFD is chosen in such a way that it is significantly below the smallest expected pulse height, i.e., from high-energy protons, at least for one of the $\Delta E_1$ or $\Delta E_2$ detectors. This is illustrated in Fig. 5, which shows the pulse height (in MeV) versus energy for protons in the silicon detectors. This criterion ensures that there will always be a timing signal, and a MASTER signal, when a particle is detected. On the other hand, the threshold must be set reasonably well above the experimentally observed detector noise level. The values used are around 1.0 and 0.5 MeV for the $\Delta E_1$ and $\Delta E_2$ detectors, respectively. These settings have worked well during the test experiments.

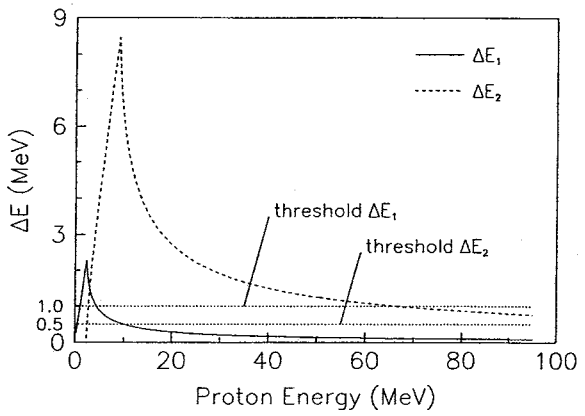


Fig. 5. Calculated proton energy loss in 50 μm (full curve) and 400 μm (dashed curve) $\Delta E$ silicon detectors, respectively, as a function of energy. The sharp peaks of the curves correspond to the punch-through energies. The thresholds applied to the timing signals of these detectors are shown as dotted lines.

The collimator signals from the PMTs are amplified by fast amplifiers ($\times 10$) in the experimental hall, and then fed directly to charge-sensitive ADCs (QDCs) for registration. A low-energy cut, corresponding to an energy loss well below that of the least ionizing particles, i.e., 100 MeV protons, is applied to the QDC spectra in the off-line analysis. All registrations above this cut are used to reject the corresponding events, thus ensuring that the accepted particles passed the collimator hole.

For each telescope, a logic OR between the $T$ signals of the $\Delta E_1$ and $\Delta E_2$ detectors is used to define an event for that telescope. These OR signals are fed to a hit pattern unit to redundantly register which telescope triggered the event, which simplifies the off-line analysis. The logic event signal from each telescope is further ORed with the corresponding signals from all other telescopes. This secondary OR logic defines the MASTER signal, which announces the presence of an event in the system, and that the event should be read out. The MASTER signal is also used to: (i) gate all energy signals (ADCs and QDCs), (ii) start the TDC units, and (iii) gate the hit pattern unit.

The RF signal from the cyclotron is used as the TOF reference signal, and is recorded as a stop signal in one of the TDCs, as is the $T$ signal from all the silicon detectors. The MASTER signal is used as common start for all TDC channels. The time between two consecutive RF signals or beam bursts, i.e., the timing window, is about 58 ns at 95 MeV.

Since the count rate is rather low, it takes long time to identify in the on-line monitoring whether the TOF peak is reasonably well centred within the timing window. For this reason, an additional RF signal, with an added delay of about 30 ns, is also recorded. In this way, a TOF peak is always ensured to be seen in at least one of the TOF windows.

The number of events from each telescope is recorded by a scaler unit. This information is used to monitor the performance and stability of the telescopes and the electronics. The number of master gate pulses, both with and without computer busy veto, is registered to monitor the dead time of the data acquisition system. The dead time is typically in the order of a few %, and never above 15%. The unit also records the relative neutron beam intensity from both the integrated proton beam current at the beam dump and the TFBC neutron monitor.

### 2.5. Data acquisition

Data are recorded on an event-by-event basis using SVEDAQ, a general purpose data acquisition system employed at the TSL [35]. Data are read out through a CAMAC branch highway and sent to a VME-based event builder. From the event builder system, data are split into two independent branches; to tape and to on-line analysis, the latter with lower priority. A SUN workstation is used for on-line sorting, monitoring and control. Typical on-line spectra that can be displayed are pulse heights from all detectors, TOF, two-dimensional plots of pulse height of $\Delta E_1$ versus $\Delta E_2$, $\Delta E_2$ versus $E$, and TOF versus the different pulse heights. The other data stream is sent to an Exabyte tape station for recording. An additional tape station can be set up as backup.

## 3. Experimental tests, data analysis and results

To investigate the characteristics of the MEDLEY set-up, we have performed a measurement of light-ion production in carbon induced by 95 MeV neutrons. All eight telescopes were employed in the experiment, and these data are used here to illustrate the analysis procedure and the performance of the equipment. Most of the measurements were performed before the installation of the collimators, but this is of minor importance for the conclusions drawn in the present paper.

The main data acquisition was done with a 22 mm diameter by 0.5 mm thick carbon target with natural isotopic composition. Background runs were performed by moving the target frame out of the beam. In addition, a 25 mm diameter by 1.0 mm thick $CH_2$ target was used for absolute normalization purposes, utilizing the well-known np scattering cross-section. In the middle of the data taking period, the telescope table was rotated to interchange the telescopes in the forward and backward directions. The series of targets was then repeated again. The various runs were normalized to the same incident neutron fluence using the integrated proton beam current and the number of fissions in the TFBC monitor.

Data analysis is done on an event-by-event basis, where the data are first sorted into separate files for each telescope. By generating two-dimensional plots of the pulse height of the $\Delta E_1$ versus $\Delta E_2$ and $\Delta E_2$ versus $E$ detectors, respectively, each event can be assigned a particle identification (ID), and the data are further separated into files for each kind of particle. Using pulse height information from the alpha particle source in the thin silicon detector, calculated maximum energy losses of various particles in both silicon detectors, and pulse heights in the CsI detector for particles with known energy loss in the silicon detectors, as well as energies of resolved states in the $^{12}C$(n,p) and (n,d) reactions, energy calibration of all detectors can be performed. With this information at hand, the pulse height can be converted into energy loss for each particle in each detector. Adding the energy losses in the three detectors gives the incident energy for each particle. A two-dimensional plot of particle energy versus neutron flight time is used to identify

particles associated with the main neutron peak, while those induced by low-energy neutrons are rejected.

After these steps of event-by-event operations, the data are sorted into histograms, thus showing particle emission energy spectra. The procedures so far are applied in the same way to both the signal (target-in) and the background (target-out) runs. On histogram basis, the background is subtracted from the signal, after normalization to the same neutron beam fluence.

The $CH_2$ data are treated in a similar way. After proper subtraction of target-out and $^{12}C(n,xp)$ background contributions, the cross-section per count can be determined from the np scattering peak, using data previously taken at a similar energy [36]. The normalization coefficient is then applied to the carbon data to get the absolute cross-section.

Each of the steps in the analysis procedure will be described in some detail in this section.

### 3.1. Particle identification

The $\Delta E - \Delta E$ or $\Delta E - E$ technique is used to identify light reaction products, i.e., protons, deuterons, tritons, $^3$He and alpha particles. Fig. 6 shows typical (a) $\Delta E_1$–$\Delta E_2$ and (b) $\Delta E_2$–$E$ scatter plots, respectively, from 95 MeV neutron-induced light-ion production reactions in carbon at 20°. Particles which stop in the $\Delta E_2$ detector are shown in Fig. 6a, while those stopping in the ($E$) detector appear in Fig. 6b. The separation between different particles is very good, which makes the assignment of particle ID a straight forward procedure. Two-dimensional contours are applied to the scatter plot for each particle type. Examples of such contours for protons are shown as solid lines enclosing the proton bands in the figure.

An interesting feature of the present facility, which can also be seen in the scatter plot in Fig. 6a, is the very low energy cut-off of the system. The threshold achieved with the telescopes here is about

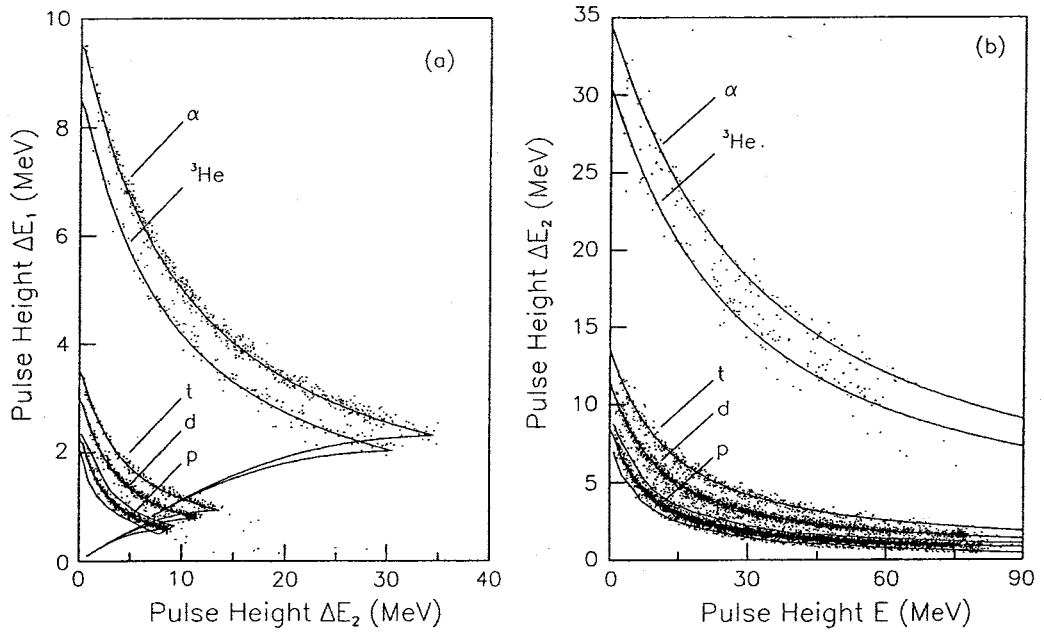


Fig. 6. Two-dimensional scatter plots of (a) the 60 μm $\Delta E_1$ versus the 500 μm $\Delta E_2$ detector pulse heights, and (b) the $\Delta E_2$ versus $E$ detector pulse heights. The data are obtained at 20°, using a carbon target bombarded with 95 MeV neutrons. The solid lines through the middle of each band show the expected behaviour from an energy loss calculation. The contours around the proton bands illustrate how proton events are selected from the data.

2–3 MeV for the hydrogen isotopes and about 9 MeV for the helium isotopes. The threshold for the sum of the helium isotopes (dominated by alpha particles) can be pushed further down to 3.5 MeV, since the various hydrogen isotopes deposit at most about 3 MeV in the $\Delta E_1$ detector.

### 3.2. Energy calibration

The second step in the data reduction is to convert the detector pulse height into energy for all detectors. This is done following a rather complex procedure, in which various sources of information are used.

The $\Delta E_1$ and $\Delta E_2$ silicon detectors are calibrated by determining the pulse height for the various particles at the point where they start to punch through the detectors, i.e., at the left- and right-hand end-points, respectively, of the bands in Fig. 6a. The corresponding energies are calculated using the detector thicknesses given by the manufacturer, and stopping power data from Andersen and Ziegler [37–39]. The result of such calculations are then fitted to the experimental data, as shown in Fig. 6a, where the calculations are represented by solid lines centred at the data bands. Assuming a linear correspondence between pulse height and energy in the silicon detectors, which is appropriate for this application, the method gives several calibration points for each detector. The $\Delta E_1$ detectors are further calibrated and checked using the 5.48 MeV alpha particles from the $^{241}$Am source stopping in these detectors.

The assumption of linear correspondence between pulse height and energy is not necessarily valid for the CsI detectors. An attempt was therefore made to determine this relation experimentally, with the aid of the collected data. For each detected particle, the energy losses in the silicon detectors are well known according to the procedure above. Since the energy loss for a certain type of particle is a single-valued function of the particle energy, the latter can be calculated from the measured energy loss, and thus the energy deposited in the CsI detector can be calculated. By plotting this calculated energy versus the measured pulse height, bands correlating energy and pulse height are obtained. This is shown for protons, deuterons, tritons and alpha particles in Fig. 7a–d, respectively. As can be seen, the bands are narrow close to the origin, while they rapidly become wider for higher energies, also with a relative measure.

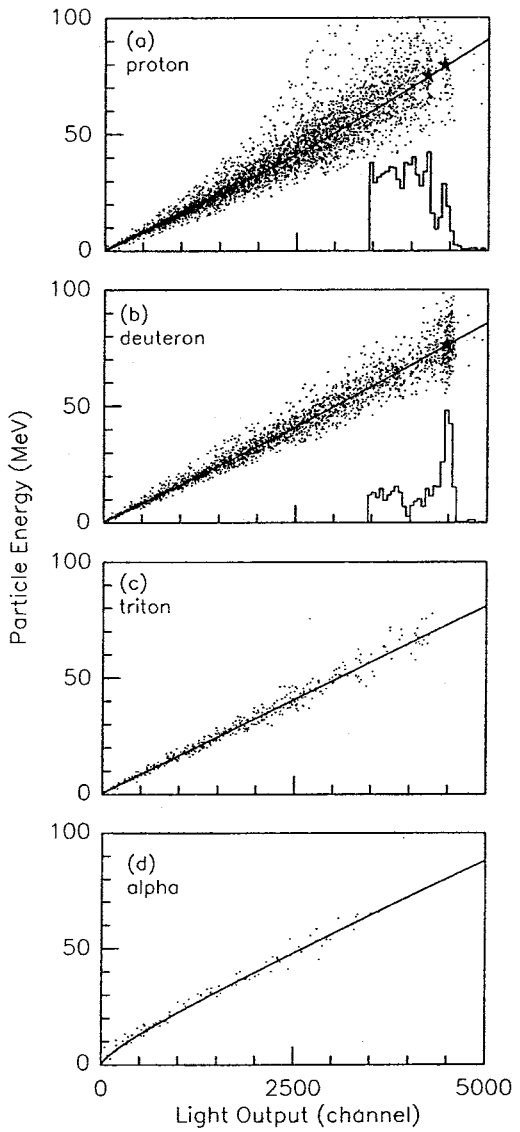


Fig. 7. Scatter plot of energy deposited in a CsI(Tl) detector, as calculated from the measured energy loss in the silicon detectors, versus the corresponding light output for (a) protons, (b) deuterons, (c) tritons and (d) alpha particles. For protons and deuterons, spectra with peaks corresponding to transitions to low-lying states are shown in the insets. The corresponding energies, as calculated from reaction kinematics, are represented by stars in the scatter plots. The solid lines are the final calibration curves after fitting of Eqs. (2) and (3) to the data.

The reason for this is that the energy loss at high energies is small, and thus the calculated energy becomes more uncertain. It can also be seen that the bands become more narrow with increasing mass and charge of the particles, which is the result of the larger energy loss for those particles.

Fortunately, the data also contain some precise information at high energy, i.e., the distinct peaks corresponding to ground-state and low excitation-energy transitions in the $^{12}C(n,p)^{12}B$ and $^{12}C(n,d)^{11}B$ reactions, as shown in the insets in Fig. 7a and b, respectively. The energy of these peaks can be calculated from the neutron energy and the reaction kinematics, taking the energy loss in the carbon target and in the silicon detectors into account. The result is shown as stars in Fig. 7a and b, which thus provide good calibration points at high energy for protons and deuterons, i.e., the cases showing the widest bands.

To be useful in the analysis, these experimental calibration data have to be expressed in a simple, analytical way. The response of CsI detectors to ions is most often expressed using the well-established formula [33,34]

$$L = a_0 + a_1\left(E - a_2 Az^2 \ln\left[\frac{E + a_2 Az^2}{a_2 Az^2}\right]\right) \quad (1)$$

where $L$ is the light output (pulse height); $a_0$, $a_1$, and $a_2$ are experimentally determined constants; $E$ the incident particle energy; $A$ the atomic mass of the incident particle; and $z$ the charge of the incident particle. Eq. (1) follows from the well-known Birk's formula [40], which relates $dL/dx$ to $dE/dx$, and includes quenching effects (for a derivation, see, e.g., Refs. [34,41]).

Eq. (1) relates the energy to light output, $L(E)$, while the opposite is wanted, i.e., $E(L)$. Several analytical expressions of $E(L)$ that approximate Eq. (1) have been suggested, and we have here adopted [42]

$$E = a + bL + c\ln(1 + dL) \quad (2)$$

where $a$, $b$, $c$ and $d$ are constants determined by fitting to the data. This formula gives a bending at low energy, which corresponds to quenching effects at very dense ionization. In our data, this effect is only seen for alpha particles, which thus can be represented using Eq. (2) (see Fig. 7d, solid line). For the hydrogen isotopes, low-energy quenching is not seen at all; instead there seems to be a decreasing scintillation efficiency at high energy, i.e., at low ionization. Such an effect has been observed also by Twenhöfel et al. [43]. To represent the calibration of the hydrogen isotopes, we used an expression with a linear and a quadratic term, i.e.,

$$E = a + bL + c(bL)^2. \quad (3)$$

The linear parameter $b$, and the fraction of quadratic dependence $c$, were obtained by fitting to the experimental data, including the well-determined high-energy points from the proton and deuteron spectra. It was found that $c$ is independent of the specific detector, and seems to be a function of the particle type only. Thus, $c$ was kept fixed in the analysis to the following average values: $c = 0.0030$ for protons, $c = 0.0014$ for deuterons, and $c = 0$ for tritons, i.e., the tritons are well described by a linear term only. The corresponding fits are shown as solid lines in Fig. 7a–c.

The high-energy proton and deuteron points (the stars in Fig. 7a and b) provide a cross-check of the correctness of the assumed silicon detector thicknesses, as given by the manufacturer. Even a very small error in the thickness (a few %) would make the two sources of information, i.e., the energies calculated from the peaks (stars) and from the energy loss in the $\Delta E_1$ and $\Delta E_2$ detectors (bands), incompatible.

The final calibration curves used in the analysis are summarized in Fig. 8. It is obvious from this figure that the deviation from a linear response is small for hydrogen and helium ions in the 0–100 MeV range. It is also obvious that this deviation goes in opposite directions for the two elements. Similar effects have been reported in, e.g., Refs. [43,44].

### 3.3. Matching of spectra

Each telescope consists of three individual detectors, and in most cases the charged particle is detected in more than one detector. The total energy for each emitted particle is obtained by adding the energies from the relevant detectors, as determined from the pulse heights using the calibration

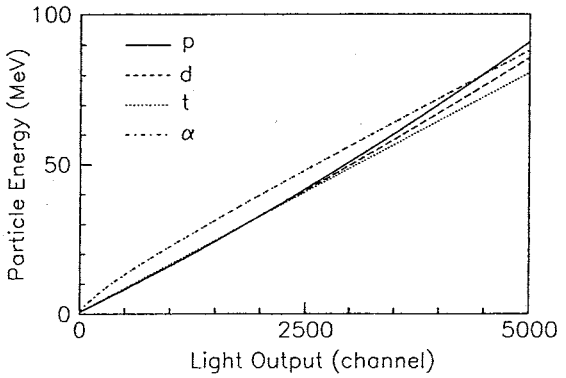


Fig. 8. Experimentally determined energy calibration for the CsI(Tl) detectors. The lines represent protons (solid line), deuterons (dashed line), tritons (dotted line), and alpha particles (dot-dashed line).

procedures discussed above. The energy spectra will thus be based on events where the particle has stopped either in the $\Delta E_2$ detector or in the CsI. In the case of $^3$He and alpha particles, also particles which have stopped in the $\Delta E_1$ detector can be considered.

Generally, a problem arises for particles that just penetrate the $\Delta E_2$ detector and barely enter the CsI, but lose too little energy in the latter to be detected. Such particles will be misinterpreted as having stopped in the second silicon detector, but since they have punched through, they will be registered with a slightly lower energy than that for particles having maximum energy and still stopping. Such events will be found along the line from the punch-through point to the origin in Fig. 6a. The result for the full energy spectra is that there will be events missing in the first bins of the CsI part of the spectrum, and these events will instead show up just below the punch-through energy of the $\Delta E_2$ detector. It should be pointed out, however, that the total number of events is still correctly conserved.

This effect is of serious concern if the detectors are manufactured with windows, since these act as dead layers without registration of energy loss. In the present case, the energy loss in detector windows can be neglected, since the silicon detectors have extremely thin windows and the CsI detectors are manufactured without windows. There is, however, another effect that has to be taken into account. It arises from the electronic thresholds of the ORTEC 413 ADCs, which are typically set to about 0.5% of the full ADC range. For the $\Delta E_1$ and $\Delta E_2$ silicon detectors, the full energy ranges are about 10 and 40 MeV, respectively, while for the CsI detector it is about 100 MeV. This corresponds to thresholds of about 0.05, 0.2, and 0.5 MeV, respectively. Thus, the effect of the threshold is more pronounced for the CsI detector than for the others. As a result, particles with residual energy below 0.5 MeV reaching the CsI detector are not recorded in that detector, while particles of higher energy are registered with their full residual energy. However, because of the limited resolution at low energy (see below), the effect will not show up as a sharp discontinuity, but rather be somewhat washed out.

The matching is illustrated for protons (a) and deuterons (b) in Fig. 9. The histograms show spectra measured with a telescope consisting of $\Delta E_1$ and $\Delta E_2$ silicon detectors (60 and 500 μm for protons; 50 and 400 μm for deuterons) and a CsI(Tl) $E$ detector. The dashed lines represent particles that stopped in the $\Delta E_2$ detector, the dotted lines those that gave good energy information in the CsI detector, and the solid lines represent all data. To improve the statistics at low energies, no low-energy neutron rejection is applied. The punch-through energy of the $\Delta E_2$ detector is calculated to be 8.8 and 10.5 MeV for protons and deuterons, respectively, and a small discontinuity, as discussed above, can be seen around these energies. Since the total number of events is conserved, a small redistribution of events can be applied to correct for the discontinuity, resulting in a smooth behaviour of the spectra also in the matching region.

It should be pointed out that the fact that the discontinuity is small reflects that we have good control over the energy calibration. Even small errors in the calibration would show up as clearly visible discontinuities in the matching region.

### 3.4. Energy resolution

The energy resolution of each individual detector has been checked using a 5.48 MeV alpha source. It was found to be about 60, 45 and 500 keV (FWHM)

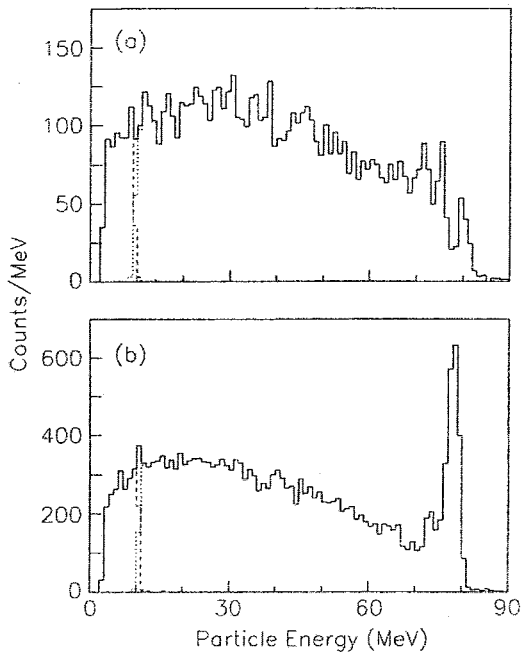


Fig. 9. Histograms showing energy spectra of (a) protons and (b) deuterons. Dashed lines represent particles stopping in the $\Delta E_2$ detector, dotted lines those giving energy information also in the CsI detector, and solid lines are all data. No low-energy neutron rejection is applied.

for the $\Delta E_1$, $\Delta E_2$, and $E$ detectors, respectively. Typical spectra for the three types of detectors are shown in Fig. 10a–c. The low-energy tails seen for the silicon detectors in Fig. 10 probably arise from energy loss in an epoxy ring at the edge of the detectors, applied to fix the silicon wafer to the detector can. The fraction of events found in this tail is about 17% in the case of the thin detector (Fig. 10a) and 4% for the thick one (Fig. 10b). These percentages agree, at least qualitatively, with estimates of the fraction of the detector surface covered by the epoxy. The problems caused by the epoxy ring are removed by the recent installation of active collimators.

For the silicon detectors, the resolution is about a factor of two worse than in the measurements performed by the manufacturer with an optimized system, but is fully acceptable for the purpose here. The resolution of the CsI(Tl) detector for the source of alpha particles might appear poor ( $\sim 9\%$), but one should keep in mind that to deposit 5 MeV in

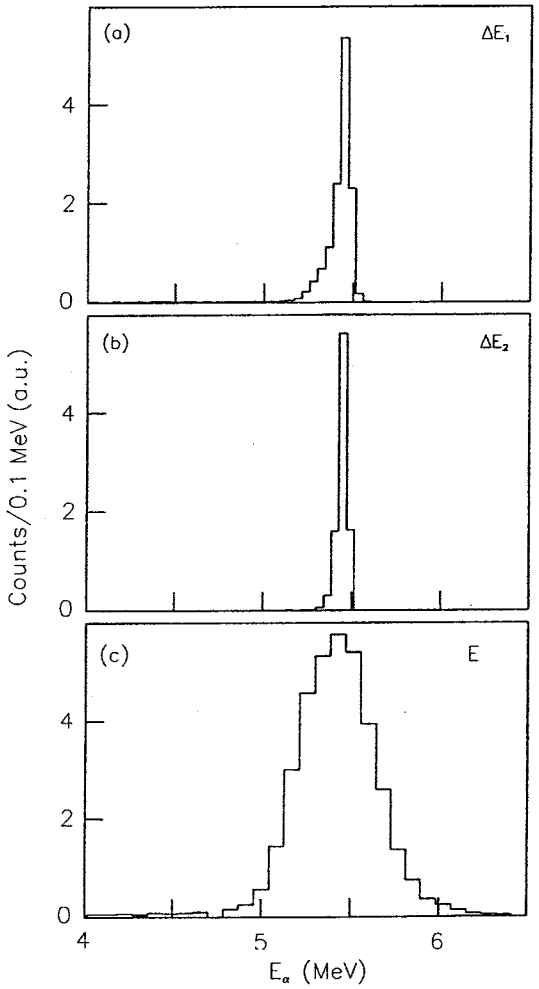


Fig. 10. Measured energy spectra for alpha particles from the $^{241}$Am source (5.48 MeV). (a) $\Delta E_1$ detector (60 μm silicon), (b) $\Delta E_2$ detector (500 μm silicon), and (c) $E$ detector (3 cm CsI).

the CsI, the alpha particle must have an energy of almost 40 MeV when entering the telescope, and thus the relative resolution for such a particle is of course higher. For particles of higher energies, the relative resolution of the CsI detectors is expected to be much better (about 2% at 80 MeV).

The energy resolution of a full telescope can be studied by adding the calibrated pulse heights from all three detectors. With the 95 MeV neutron beam, having a main peak width of 0.9 MeV (FWHM), on a 0.5 mm thick carbon target, the observed overall energy resolution in the 20° telescope is 2.0 and 2.3

MeV for the $^{12}C(n,p)^{12}B_{gs}$ and $^{12}C(n,d)^{11}B_{gs}$ reactions, respectively. By subtracting the width of the neutron peak (0.9 MeV) and the energy loss in the target (0.7 and 1.2 MeV for protons and deuterons, respectively), the intrinsic energy resolution of the telescope is about 1.7 MeV for both particle types at the highest energies (about 80 MeV).

### 3.5. Low-energy neutron rejection

Before rejection of low-energy neutrons, the neutron TOF has to be constructed. The TDC registers the time difference between the MASTER signal and the cyclotron RF. Using the information on which telescope, and which detector of that telescope, generated the MASTER signal, the TDC data can be assigned to every event.

The measured TOF is the sum of the flight times for the neutron and the charged particle. Since the energy and mass of the charged particle are determined with the telescope, its flight time over the known target-to-detector distance can be calculated. Subtraction of the charged-particle flight time from the total TOF then yields the neutron TOF.

After the neutron TOF information is assigned to every event, it is possible to create a two-dimensional plot of the neutron TOF versus charged-particle energy. Fig. 11a shows an example of such a plot for protons from the $^{12}C(n,xp)$ reaction. The horizontal dark band in the upper part of the figure represents particles associated with the full-energy neutrons. This band shows up as a clear peak in Fig. 11b, which is the projection onto the TOF axis.

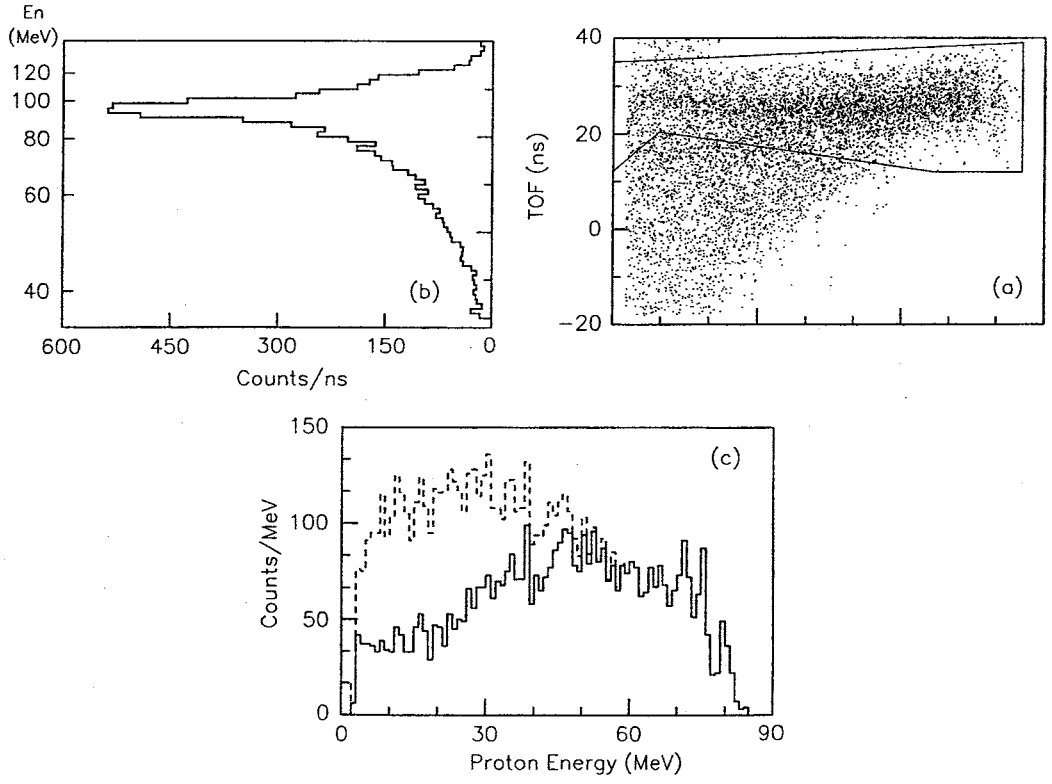


Fig. 11. Two-dimensional scatter plot of neutron TOF versus proton energy for the $^{12}C(n,xp)$ reaction at 20° and at $E_n = 95$ MeV. Neutrons corresponding to the full-energy peak appear as a horizontal band. A selection of protons associated with the neutron peak is illustrated with the full line contour. (b) Neutron TOF spectrum as projected from the scatter plot. (c) Proton energy spectra as projected from the scatter plot. Dashed histogram represents all data and solid histogram those events that fall within the neutron peak contour.

The width of the peak (FWHM) is about 6–7 ns, which includes the contribution from the duration of the cyclotron beam pulse (typically 2–4 ns).

Due to the fact that the highest-energy protons produce the smallest signals in the silicon detectors, the timing fluctuations are larger at these energies, and thus the band in Fig. 11a is wider at the high-energy end. Furthermore, the band shows some bending, which reflects walk effects of the CFD unit. This does not pose a problem, since the selection of protons associated with the full-energy neutrons can be made by a two-dimensional contour enclosing the band, as is shown by the solid line in Fig. 11a. This contour can be further tightened to minimize the contribution to the spectrum from low-energy neutrons. Protons that satisfy the selection criterion are projected onto the energy axis and shown as the solid histogram in Fig. 11c. It can be compared with the corresponding proton spectrum created by neutrons of all energies, which is shown as the dashed histogram in the same figure. The difference between the two spectra is due to events induced by low-energy neutrons.

A similar example for the $^{12}C(n, xd)$ reaction is shown in Fig. 12a–c. In this case, for which the silicon detector pulse heights are slightly larger, the walk is smaller and thus the width of the main neutron peak is smaller, i.e., less than 5 ns. Subtracting the contribution from the beam pulse width, indicates that the intrinsic time resolution of the detection system is of the order of 2–4 ns.

It should be pointed out that although the definition of the full-energy peak in the TOF spectra is relatively wide, and may cover neutrons from 75 to 80 MeV and above, only a small fraction of these neutrons comes from below the 1 MeV wide main peak (see Section 2.1).

Furthermore, the high repetition rate of the beam pulses, which at 95 MeV limits the TOF window to 58 ns, causes a wrap-around problem. Thus, it is not possible to distinguish 95 MeV neutrons from those of about 20 MeV created by

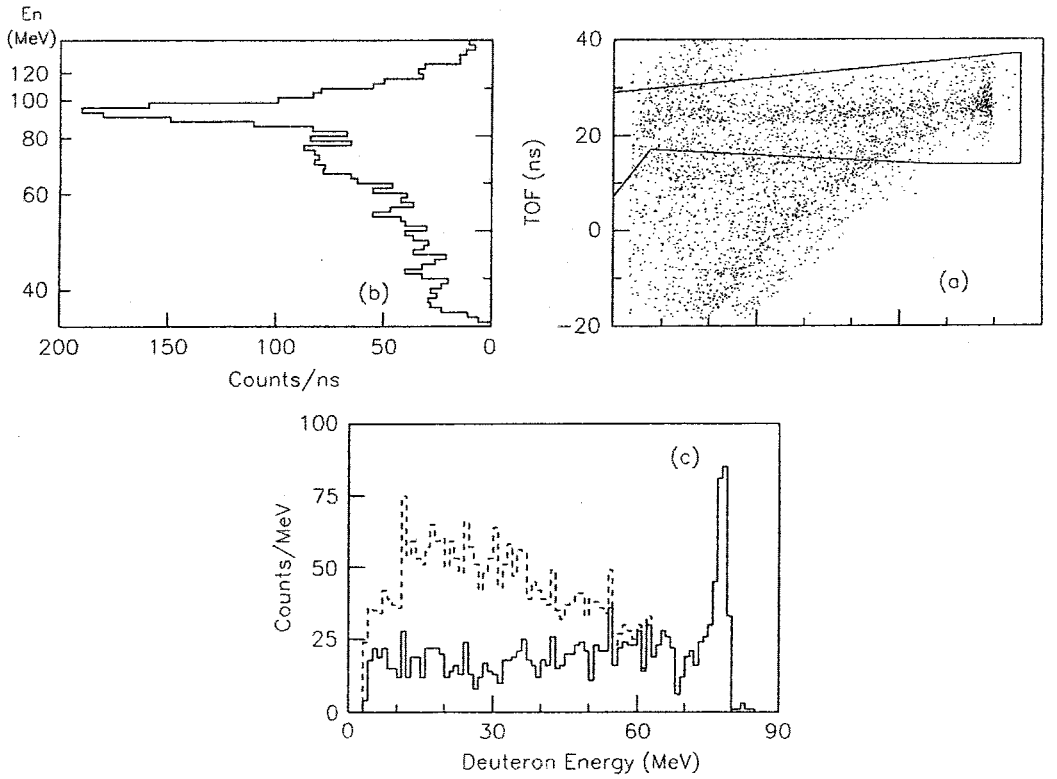


Fig. 12. Same as Fig. 11, but for the $^{12}C(n, xd)$ reaction.

the previous beam burst, since the latter have the same TOF when the 58 ns is subtracted. This can be seen in Figs. 11a and 12a, where the scatter pattern at the lower left corner continues at the upper left corner, where it is seen to interfere with the full-energy neutron band. In the general case, this problem can only be solved by increasing the time separation of beam bursts. Installation of a beam-kicker system, where only one pulse out of two, three, etc., is allowed to reach the target, is presently under consideration at the TSL.

For the present application, the problem is more limited. For the reactions under study here, the $Q$-values are typically of the order of 15 MeV. This makes 20 MeV neutrons rather inefficient in creating particles, since reaction channels for emission of charged particles open slowly close to threshold. Thus, a small correction can be applied to the data by estimating the contribution from wrap-around neutrons using the (weak) tail outside the main neutron band, i.e., using the events found in the upper left corner of Figs. 11a and 12a.

### 3.6. Background subtraction

Up to this point the data have been treated on event-by-event basis. Thus, to each event is assigned the particle type and the energy at the entrance to the telescope. In addition, the neutron TOF is assigned to each event, and those that fall outside the main neutron peak are rejected. For the remaining analysis procedures, data are sorted into different histograms according to the particle type. The histograms reflect the energy distributions of the different particles at the various telescope angles, i.e., the relative double-differential light-ion production spectra.

The background (target-out) runs, which are analysed in the same way as the signal (target-in) runs in the event-by-event stage, are normalized to the same neutron fluence as the signal runs, corrected for data acquisition dead time differences, and then subtracted on histogram basis.

The background is dominated by protons, mainly going in the forward direction, thus affecting mostly the 20° telescope. These protons are believed to arise from neutrons in the beam halo, reacting in the beam tube wall at the chamber

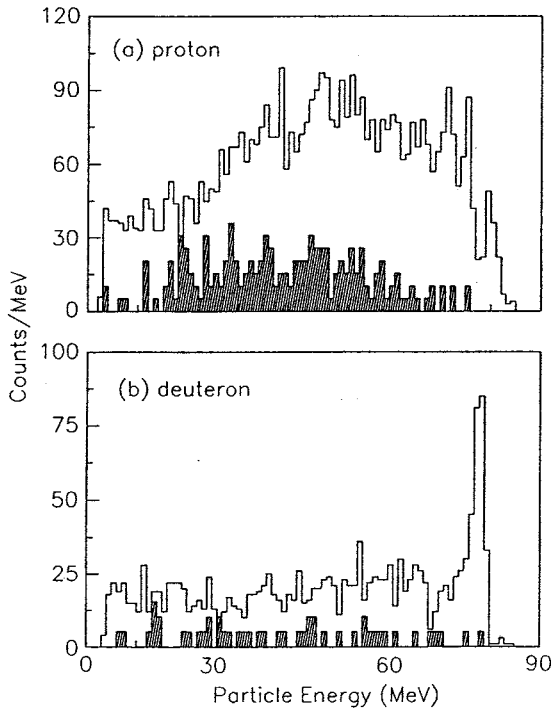


Fig. 13. Target-out background (hatched area) for the final (a) $^{12}C(n,xp)$ and (b) $^{12}C(n,xd)$ data at 20° and at $E_n = 95$ MeV (open histograms).

entrance. For the 20° telescope the signal-to-background ratios are about 5:1 and 7:1 for protons and deuterons, respectively. In the case of alpha particles, the background is negligible. Fig. 13a and b illustrates observed typical proton and deuteron background spectra, respectively. Corresponding signal data, before background subtraction, are also shown for comparison. The newly installed active collimators reduce the mentioned relative background for both protons and deuterons by about a factor of three, thus giving a signal-to-background ratio of 15–20:1 for the used 0.5 mm carbon target.

### 3.7. Absolute cross-section normalization

Absolute, double-differential cross-sections are obtained from the measured data using a comparison with the number of recoil protons emerging from a hydrogenuous target, and assuming that the np scattering cross-section is well known. The latter

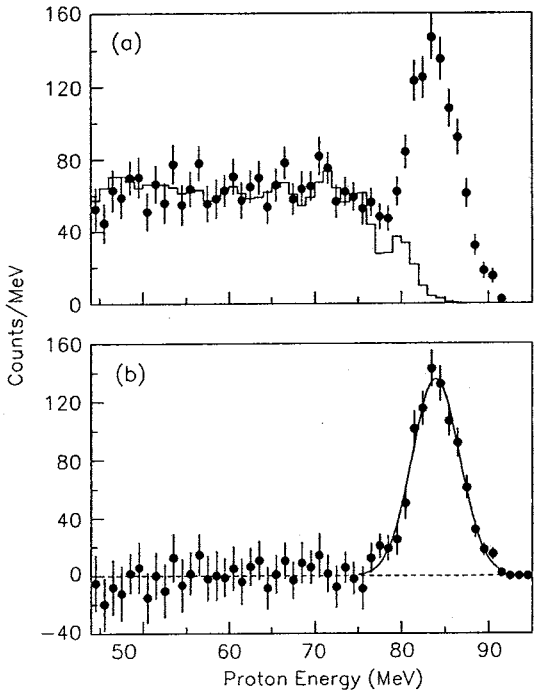


Fig. 14. (a) Protons emitted from a 1.0 mm thick $CH_2$ target at $E_n = 95$ MeV detected by the 20° telescope (filled circles). A normalized spectrum for a pure carbon target is shown as a histogram. (b) The difference between the two spectra, corresponding to free np scattering. A Gaussian distribution has been fitted to the peak.

has been measured at 96 MeV in a previous experiment at TSL [36], and the absolute precision is believed to be better than 2%.

The recoil proton peak is observed at forward angles using a 1.0 mm thick by 25 mm diameter $CH_2$ target. After proper subtraction of the $^{12}C(n, xp)$ and target-out contributions, a pure recoil proton spectrum is obtained. This is illustrated in Fig. 14, where the upper panel shows the $CH_2$ spectrum at 20° (filled circles) and the corresponding contribution from a pure carbon target (histogram). The resolution of the $CH_2$ spectrum is worse than that for the pure carbon target, since the $CH_2$ data were collected using a $^7Li$ target twice as thick. The carbon spectrum has therefore been folded with a Gaussian resolution function to achieve approximately the same resolution as the $CH_2$ data. The lower panel shows the subtracted spectrum, where essentially only the np scattering peak remains. The width of the peak (6 MeV FWHM) is dominated by kinematic effects due to the solid angle of the telescope (about 5.5 MeV), but has also contributions from the width of the neutron peak (about 1.8 MeV), the energy loss of protons in the $CH_2$ target (of the order of 0.6 MeV), and the energy resolution of the telescope (about 2 MeV).

As can be seen in the figure, the number of counts in the peak, $N_H$, can easily be extracted. From this number, one can calculate the cross-section per count for hydrogen, $\sigma_H/N_H$, which is used to calculate the corresponding quantity, $\sigma_x/N_x$ for the target under study ($x$):

$$\frac{\sigma_x}{N_x} = \left(\frac{\sigma_H}{N_H}\right)\frac{2M_x}{M_{CH_2}}\frac{t_{CH_2}}{t_x}\frac{\Phi_{CH_2}}{\Phi_x}\frac{\Omega_{CH_2}}{\Omega_x}, \tag{4}$$

where $M$ is the molecular mass, $t$ is the target thickness (mg/cm$^2$), $\Phi$ is the relative neutron beam fluence (n/cm$^2$) as determined by the monitors, and $\Omega$ is the solid angle from the target to the telescope (sr).

In the present carbon experiment, the studied element is present also in the $CH_2$ target, and events originating from carbon relative to those of np scattering readily provide a direct measure; thus leaving the relative beam intensity determination as redundant information.

The procedure described can only be used at forward angles, i.e., $\theta = 20$–$40°$. At larger angles the np scattering peak becomes wider, and it is not as clear to determine the peak content. Thus, only the most forward telescopes (and the most backward; after turning the telescope table) can be cross-section normalized in this way. For the telescopes at other scattering angles, the same intrinsic efficiency is assumed. Furthermore, it is assumed that the energy dependence of the intrinsic efficiency of the CsI(Tl) crystals is small in the energy range of interest here. This assumption is supported by studies from other work [31].

We estimate the uncertainty in the absolute normalization to be about 3.5%, with contributions of 2% from the np cross-section, about 2% from the target thickness, and about 2% from the uncertainty in the relative neutron fluence.

## 4. Corrections

In measurements employing a low-intensity secondary beam, such as a neutron beam, relatively thick reaction targets have to be used to obtain a reasonable count rate. However, using a thick target results in distortions of the energy spectra, because of the energy loss within the target itself. At low energies, this could even mean that some of the particles are lost, since they have too small an energy to escape from the target. Some light can be shed on this problem by using, e.g., two different target thicknesses: a thicker one to obtain good statistics for high-energy particles, having small energy losses, and a thinner one for low-energy particles, especially alpha particles, that are subject to large energy losses. To determine the true double-differential cross-sections, the measured spectra have in any case to be corrected for these effects.

As a first step in such a correction scheme, we have developed a Monte Carlo code, CONNECT, to simulate the experimental set-up, taking the geometry and most of the relevant physics into account. In the CONNECT code, particles, sampled from a given energy distribution, are followed through the target and detection system. On their way, they undergo scattering from atomic electrons, which causes them to lose energy. This is a statistical process, resulting in a straggling distribution around the expected energy loss. If a nuclear reaction occurs, the primary particle is considered to be lost. More details about the code can be found in Ref. [45].

Thus, starting from a known, "true" energy distribution, CONNECT will generate a spectrum that can be compared with the experimental data. What we want, however, is the opposite: to generate the true spectrum from the measured distribution. This can be done in several ways, and once a "true" spectrum is generated, it can be checked by running CONNECT and compared with data. Several iterations might be needed to obtain good agreement.

To correct the measured data for energy loss in the target, a code module, CRAWL, has been written. The code is based on a stripping technique, similar to the one described in Ref. [46]. CRAWL makes use of calculated energy-loss and straggling distributions for particles created at any point in the target, and for each energy bin $i$ with mean energy $E_i$, within which particles are created. We call these distributions the response function, $R_i(E)$. Thus, $R_i(E)$ is the spectrum seen by the detector after creation of nearly mono-energetic particles of energy $E_i$, and shows an essentially rectangular distribution, caused by the target energy loss, with a diffuseness at the low-energy side reflecting the straggling.

The true spectrum is obtained by unfolding the measured one, using the response function. Starting at the highest-energy bin, $n$, of the true spectrum, the response function, which extends also to lower energy bins ($n-1$, $n-2$, ...), is calculated and fitted to bin $n$ of the experimental spectrum. The content, $c_n$, of the distribution is assigned to bin $n$ of the true spectrum, and the distribution is subtracted from the experimental spectrum. The procedure is repeated for bin $n-1$ of the true spectrum, and continues further down in energy. At the end, the experimental spectrum, $S_{\mathrm{exp}}$, is thus represented by

$$S_{\mathrm{exp}}(E) = \sum_{i=1}^{n} c_i R_i(E) \tag{5}$$

where the coefficients $c_i$ are the bin contents of the true spectrum. At a certain point, particles are created at such a low energy that those emerging from the first layers of the target cannot penetrate fully and thus cannot escape the target. This is also corrected for, and leads to breaking of the conservation of number of particles. To lower the sensitivity to statistical variations of the experimental data, the spectra are slightly smoothed using a spline-fit method before running CRAWL.

To get an estimate of the error in the true spectrum, 100 "experimental" spectra are sampled within the standard deviation of the data. As indicated above, the content of energy bin $i$ is correlated to that of energy bin $i-1$, $i-2$, ..., and so on, and this is taken into account in the sampling. The stripping technique is applied, and from the 100 estimates of the true spectrum, a calculation of the error is performed.

Also other methods have been used to attack the problem of energy and particle loss in the target. Rezentes et al. [45] use a matrix-inversion technique to solve a Fredholm equation of the first kind, and their code is a development of the

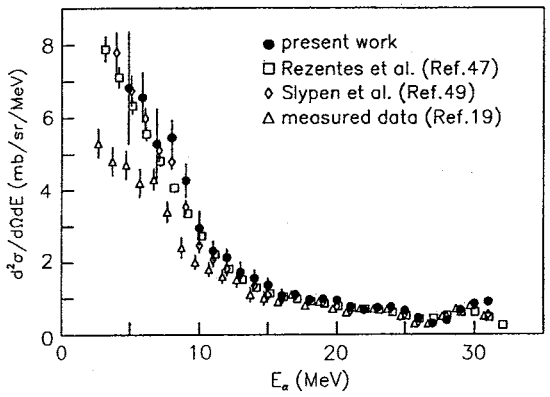


Fig. 15. Results of various approaches to correct alpha particle spectra for energy and particle loss within the target. The present results are shown as filled circles, while those of Refs. [47] and [49] are shown as open squares and open diamonds, respectively. The experimental data (triangles) are from the $^{12}C(n, x\alpha)$ reaction, measured at 20° and at 39.7 MeV neutron energy, using a 4.1 mg/cm$^2$ thick polystyrene (CH) target [19].

previous work of Johnson et al. [48]. Slypen et al. [49] perform a Monte Carlo simulation of the experimental set-up and calculate the mean energy deposited in the target, the energy after the target, and the active fraction of the target, i.e., the fraction in which created particles can penetrate and escape. From the simulation, correction factors are determined, and then applied to the experimental data.

The three mentioned methods have been compared by performing correction calculations for alpha particles from the $^{12}C(n, x\alpha)$ reaction in a 4.1 mg/cm$^2$ polystyrene target at $E_n = 39.7$ MeV and at an angle of 20°. The data are from an experiment conducted at UC Davis [19]. The result is shown in Fig. 15. As can be seen, the spectrum using CRAWL is slightly higher than the others, but all three codes agree well within the errors. The corrected spectrum of Rezentes et al. [47] shows considerably smaller errors, probably reflecting the more pronounced smoothing used by that group, while the errors of Slypen et al. [49] are in between.

## 5. Summary and conclusions

In this paper, we have presented the new MEDLEY facility, intended for measurements of neutron-induced double-differential light-ion production cross-sections for fast neutron cancer therapy and other applications, such as accelerator-driven transmutation technologies and studies of single-event upsets (SEU) in, e.g., computer electronics. The facility consists of eight particle telescopes, mounted in a large scattering chamber. Each telescope is composed of two $\Delta E$ silicon detectors and one CsI(Tl) $E$ detector with photodiode readout. The telescopes are also equipped with active collimators in the form of thin plastic scintillators, coupled to small photomultiplier tubes. The facility can be used to acquire data with very good particle separation, wide energy and angular coverage, low energy threshold, and good energy resolution. In addition, the timing properties allow suppression of events from the low-energy neutron tail.

We have performed an experiment on neutron-induced light-ion production from carbon at 95 MeV. The data have been used to illustrate the performance of the facility, and also to determine the response of the CsI(Tl) detectors for various light particles. It was found that the hydrogen isotopes do not show quenching of light output at low energies; instead a small loss of light output was seen at several tens of MeV.

Computer codes have been developed to simulate the experimental set-up, and to provide corrections to the data for loss of energy and particles within the target itself.

To conclude, the MEDLEY facility at TSL can be used to extend the scarce data base to higher energies, i.e., up to 100 MeV. It can also be used to measure light-ion production spectra with good precision and energy continuity, down to lower energies than is often the case. It is expected that the MEDLEY set-up can contribute in resolving considerable discrepancies found, e.g., between the UC Davis [20] and Louvain-la-Neuve [26–28] data in the low-energy domain.

## Acknowledgements

The authors wish to thank the The Svedberg Laboratory staff for significant contributions to the construction of the equipment, the development of data acquisiton software, and for careful cyclotron

operation during the measurements. The authors would also like to thank Mr. Sture Hultqvist and Mr. Ove Johansson from Gammadata AB for valuable contributions to the mechanical and electronic developments. Thanks are also due to Drs. Isabelle Slypen and Juan Romero for supplying us with their correction calculations.

This work was financially supported by the Swedish Cancer Foundation, the Swedish Natural Science Research Council, Göran Gustafsson Foundation, and the Development and Promotion of Science and Technology Talents Project of Thailand.

## References

[1] A. Wambersie, P. Pihet, H.G. Menzel, Radiat. Prot. Dosim. 31 (1990) 421.
[2] M. Tubiana, J. Dutreix, A. Wambersie, Introduction to Radiobiology, Taylor & Francis, London, 1990.
[3] A. Wambersie, F. Richard, N. Breteau, Acta Oncol. 33 (1994) 261.
[4] W. Duncan, Acta Oncol. 33 (1994) 299.
[5] V. Budach, Strahlenther. Onkol. 167 (1991) 677.
[6] T.W. Griffin, Critical Rev. Oncol./Hematol. 13 (1992) 17.
[7] M. Catterall, R.D. Errington, Int. J. Radiat. Oncol. Biol. Phys. 13 (1987) 1313.
[8] T.W. Griffin, T.F. Pajak, G.E. Laramore, W. Duncan, M.P. Richter, F.R. Hendrickson, M.H. Maor, Int. J. Radiat. Oncol. Biol. Phys. 15 (1988) 1085.
[9] R.M. White, J.J. Broerse, P.M. DeLuca Jr., G. Dietze, R.C. Haight, K. Kawashima, H.G. Menzel, N. Olsson, A. Wambersie, Radiat. Prot. Dosim. 44 (1992) 11.
[10] M.B. Chadwick, P.M. DeLuca Jr., R.C. Haight, Radiat. Prot. Dosim. 70 (1997) 1.
[11] P.M. DeLuca Jr., A. Wambersie, R.S. Caswell, ICRU News, June 1996, p. 14.
[12] A.J. Koning, T. Fukahori, A. Hasegawa, Intermediate energy data: final report and recommendations for follow-up, NEA Report, NEA/NSC/WPEC/DOC 1998, p. 187.
[13] A.J. Koning, J.-P. Delaroche, O. Bersillon, Nucl. Instr. and Meth. A 414 (1998) 49.
[14] Y. Tosaka, H. Kanata, T. Itakura, S. Satoh, IEEE Trans. Nucl. Sci. NS-46 (1999) 774.
[15] J.F. Ziegler, IBM J. Res. Dev. 40 (1996) 19.
[16] H.H.K. Tang, IBM J. Res. Dev. 40 (1996) 91.
[17] H. Condé, S. Hultqvist, N. Olsson, T. Rönnqvist, R. Zorro, J. Blomgren, G. Tibell, A. Håkansson, O. Jonsson, A. Lindholm, L. Nilsson, P.-U. Renberg, A. Brockstedt, P. Ekström, M. Österlund, F.P. Brady, Z. Szeflinski, Nucl. Instr. and Meth. A 292 (1990) 121.
[18] T.S. Subramanian, J.L. Romero, F.P. Brady, Nucl. Instr. and Meth. 174 (1980) 475.
[19] T.S. Subramanian, J.L. Romero, F.P. Brady, J.W. Watson, D.H. Fitzgerald, R. Garrett, G.A. Needham, J.L. Ullmann, C.I. Zanelli, D.J. Brenner, R.E. Prael, Phys. Rev. C 28 (1983) 521.
[20] T.S. Subramanian, J.L. Romero, F.P. Brady, D.H. Fitzgerald, R. Garrett, G.A. Needham, J.L. Ullmann, J.W. Watson, C.I. Zanelli, D.J. Brenner, R.E. Prael, Phys. Rev. C 34 (1986) 1580.
[21] M.B. Chadwick, P.G. Young, Nucl. Sci. Eng. 123 (1996) 1.
[22] I. Slypen, S. Benck, V. Corcalciuc, J.P. Meulders, Radiat. Prot. Dosim. 70 (1997) 21.
[23] I. Slypen, V. Corcalciuc, J.P. Meulders, M.B. Chadwick, Phys. Rev. C 53 (1996) 1309.
[24] I. Slypen, V. Corcalciuc, J.P. Meulders, Phys. Rev. C 51 (1995) 1303.
[25] I. Slypen, V. Corcalciuc, A. Ninane, J.P. Meulders, Nucl. Instr. and Meth. A 337 (1994) 431.
[26] S. Benck, I. Slypen, J.P. Meulders, V. Corcalciuc, Eur. Phys. J. A 3 (1998) 149.
[27] S. Benck, I. Slypen, J.P. Meulders, V. Corcalciuc, Eur. Phys. J. A 3 (1998) 159.
[28] S. Benck, I. Slypen, J.P. Meulders, V. Corcalciuc, Phys. Med. Biol. 43 (1998) 3427.
[29] S. Benck, I. Slypen, J.P. Meulders, V. Corcalciuc, M.B. Chadwick, P.G.Young, A.J. Koning, Phys. Rev. C 58 (1998) 1558.
[30] Y. Nauchi, M. Baba, T. Sanami, M. Ibaraki, T. Iwasaki, N. Hirakawa, S. Tanaka, S. Meigo, H. Nakashima, H. Takada, T. Nakamura, Y. Watanabe, J. Nucl. Sci. Tech. 36 (1999) 143.
[31] J. Klug, J. Blomgren, A. Ataç, B. Bergenwall, S. Dangtip, K. Elmgren, C. Johansson, N. Olsson, J. Rahm, O. Jonsson, L. Nilsson, P.-U. Renberg, P. Nadel-Turonski, A. Ringbom, A. Oberstedt, F. Tovesson, C. Le Brun, J.-F. Lecolley, F.-R. Lecolley, M. Louvel, N. Marie, C. Schweitzer, C. Varignon, Ph. Eudes, F. Haddad, M. Kerveno, T. Kirchner, C. Lebrun, L. Stuttgé, I. Slypen, A. Prokofiev, A. Smirnov, R. Michel, S. Neumann, U. Herpers, to be published.
[32] A.N. Smirnov, V.P. Eismont, A.V. Prokofyev, Radiat. Meas. 25 (1995) 151.
[33] V.V. Avdeichikov, L. Bergholt, M. Guttormsen, J.E. Taylor, L. Westerberg, B. Jakobsson, W. Klamra, Yu. A. Murin, Nucl. Instr. and Meth. A 349 (1994) 216.
[34] D. Horn, G.C. Ball, A. Galindo-Uribarri, E. Hagberg, R.B. Walker, R. Laforest, J. Pouliot, Nucl. Instr. and Meth. A 320 (1992) 273.
[35] T. Sundqvist, J. Nyberg, TSL Progress Report 1996–1997, p. 21.
[36] J. Rahm, J. Blomgren, H. Condé, S. Dangtip, K. Elmgren, N. Olsson, T. Rönnqvist, R. Zorro, O. Jonsson, L. Nilsson, P.-U. Renberg, A. Ringbom, G. Tibell, S.Y. van der Werf, T.E.O. Ericson, B. Loiseau, submitted to Phys. Rev. C.
[37] H.H. Andersen, J.F. Ziegler, Hydrogen stopping Powers and Ranges in all Elements, Pergamon Press, Elmsfor, New York, 1977.

[38] J.F. Ziegler, Helium: Stopping Powers and Ranges in all Elemental Matter, Pergamon Press, Elmsfor, New York, 1977.
[39] J.F. Ziegler, J.P. Biersack, U. Littmark, The Stopping and Range of Ions in Solids, Pergamon Press, Elmsfor, New York, 1985.
[40] J.B. Birks, The Theory and Practice of Scintillation Counting, Pergamon, New York, 1964, p. 465.
[41] Y. Larochelle, L. Beaulieu, B. Djerroud, D. Doré, P. Gendron, E. Jalbert, R. Laforest, J. Pouliot, R. Roy, M. Samri, C. St-Pierre, Nucl. Instr. and Meth. A 348 (1994) 167.
[42] D.W. Stracener, D.G. Sarantites, L.G. Sobotka, J. Elson, J.T. Hood, Z. Majka, V. Abenante, A. Chbihi, D.C. Hensley, Nucl. Instr. and Meth. A 294 (1990) 485.
[43] C.J.W. Twenhöfel, P.F. Box, P. Schotanus, T.M.V. Bootsma, G.J. van Nieuwenhuizen, P. Decowski, R. Kamermans, Nucl. Instr. and Meth. B 51 (1990) 58.
[44] R.J. Meijer, A. van den Brink, E.A. Bakkum, P. Decowski, K.A. Griffioen, R. Kamermans, Nucl. Instr. and Meth. A 256 (1987) 521.
[45] S. Dangtip, J. Söderberg, Linköping University Report #88, ISRN ULi-RAD-R-88, 1998.
[46] G.F. Knoll, Radiation Detection and Measurement, 2nd Edition, Wiley, New York, 1989, p. 674.
[47] P.S. Rezentes, J.L. Romero, C.M. Castaneda, Nucl. Instr. and Meth. A 361 (1995) 574.
[48] M.L. Johnson, J.L. Romero, T.S. Subramanian, F.P. Brady, Nucl. Instr. and Meth. A 169 (1980) 179.
[49] I. Slypen, V. Corcalciuc, J.P. Meulders, Nucl. Instr. and Meth. B 88 (1994) 275.

# Appendix VII

# Partial and total kerma coefficients for carbon deduced from experimental double-differential cross sections at 95 MeV

S Dangtip[1], N Olsson[1], A Ataç[1], B Bergenwall[1], J Blomgren[1], K Elmgren[1], C Johansson[1], J Klug[1], G Alm Carlsson[2], J Söderberg[2], P Nadel-Turonski[3], O Jonsson[4], L Nilsson[4], P-U Renberg[4], J-F Lecolley[5], F-R Lecolley[5], C Varignon[5], M Kerveno[6], F Haddad[6] and T Kirchner[6]

1) Department of Neutron Research, Uppsala University,
Box 525, S-75120 Uppsala, Sweden
2) Department of Radiology and Radiation Physics, Linköping University,
S-58185, Linköping, Sweden
3) Department of Radiation Sciences, Uppsala University,
Box 535, S-75121 Uppsala, Sweden
4) The Svedberg Laboratory, Uppsala University, Box 533, S-75121 Uppsala, Sweden
5) LPC, ISMRA et Université de Caen, CNRS/IN2P3, 14050 Caen Cedex, France
6) SUBATECH, Université de Nantes, CNRS/IN2P3, 44070 Nantes Cedex 03, France

August 11, 2000

**Abstract:** Double-differential cross sections of inclusive proton, deuteron and triton production induced by 95 MeV neutrons on carbon have been measured. Eight particle telescopes were used, covering the angular range 20° – 160°. The various charged particles were identified using $\Delta E - \Delta E - E$ techniques. Integrated production cross sections, as well as partial kerma coefficients, are determined from the data. It is found that the proton kerma coefficient is 35% higher than that of a recent evaluation, leading to a total kerma coefficient that is about 25% higher. This supports a trend observed for similar data below 73 MeV.

## 1 Introduction

During recent years there has been an increasing demand on improved knowledge of dosimetry for neutrons in the several tens to hundreds MeV region. The reason is mainly the interest in fast neutron cancer therapy, since this modality has been shown to be beneficial for some tumour types that do not respond positively to conventional therapy. In addition, radiation protection for, e.g., air crews and personnel at accelerator laboratories or installations, has become an increasingly important issue.

A coordinated research program (CRP), organized by the IAEA, expressed that, with the exception of hydrogen, sufficiently accurate data for use in fast neutron therapy do not yet exist to allow neutron therapy to reach its full potential (White *et al.* 1992, Broerse *et al.* 1997). High priority was given by the CRP to new measurements of double-differential charged-particle production cross sections and kerma coefficients for the most important elements in tissue, i.e., carbon, oxygen, nitrogen and calcium. Similar needs have repeatedly been emphasized (DeLuca *et al.* 1996, Chadwick *et al.* 1997). Double-differential data have recently been presented by Louvain-la-Neuve (Benck *et al.* 1998, Slypen *et al.* 2000) up to 73 MeV, and with the present work we have started to extend them further up to almost 100 MeV, a region where essentially no experimental data at all existed before. Such data are important to validate evaluations, in which complete sets of data are obtained by combining experimental and theoretical information. The most recent evaluation (Chadwick *et al.* 1999) can be considered as state-of-the-art in this context.

To fulfill the goal of better nuclear data for neutron therapy and radiation protection, we have constructed a new experimental setup, MEDLEY, at the The Svedberg Laboratory (TSL) neutron beam facility in Uppsala. In this work, we present neutron-induced double-differential cross sections for production of hydrogen isotopes in carbon at $E_n = 95$ MeV, and from these data we extract partial kerma coefficients as well as an estimate of the total kerma coefficient at this energy. We consider the results as preliminary, since the data have limited statistics and were mainly acquired to characterize the MEDLEY setup. Nevertheless, the findings are of great interest and the lack of good statistics is not important for the integral quantities, i.e., total production cross sections and kerma coefficients.

The experimental setup and the neutron facility are briefly described in section 2, while the data reduction procedures are discussed in section 3. Double-differential emission spectra of protons, deuterons and tritons, as well as differential and integrated cross sections and partial and total kerma coefficients, are presented and discussed in section 4. Finally, the conclusions of this work are given in section 5.

# 2 Experimental setup and procedures

The measurements were performed using the MEDLEY detector setup (Dangtip *et al.* 2000) at the neutron beam facility (Condé *et al.* 1990, Klug *et al.* 2000) of TSL in Uppsala. Protons from the Gustaf Werner cyclotron impinge on a 4 mm thick lithium disc, enriched to 99.98% in $^7$Li. Neutrons are produced by the $^7$Li(p,n)$^7$Be reaction, which gives a $95.0 \pm 0.5$ MeV full-energy peak and a rather flat low-energy continuum. After the neutron production target, the proton beam is bent into a beam dump, where the integrated charge can be measured. The neutron beam is delivered to MEDLEY, about 9 m downstream the lithium target,

through a system of collimators.

MEDLEY consists of eight detector telescopes, mounted in a 1 m diameter scattering chamber, which is kept under vacuum during the measurements. The vacuum is terminated at the beam exit port with a 0.1 mm stainless steel foil, located about 40 cm from the inner wall of the chamber. The target under study is mounted in the centre of the chamber. The telescopes are positioned at 20° intervals, covering the range $20° - 160°$ simultaneously. The 20° and 160° telescopes were placed at a distance of 28 cm from the carbon target to avoid interference of the neutron beam with these telescopes, while the rest of the telescopes were placed at a distance of 20 cm. The telescopes are arranged in two sets, one in the forward and the other in the backward hemisphere. The two sets can be interchanged without breaking of the vacuum. Each telescope consists of a $\Delta E - \Delta E - E$ detector arrangement, with 50 or 60 $\mu$m and 400 or 500 $\mu$m $\Delta E$ silicon detectors, having an active area of 450 mm$^2$, and a 30 mm thick by 40 mm diameter CsI(Tl) $E$ detector. The latter has an additional thickness of 20 mm, which is tapered to 18 mm in diameter to match the photodiode readout system.

All detector signals are processed by charge-sensitive preamplifiers, and output signals are generated for energy (E) and timing (T). The E branch is further amplified and shaped, and the pulse height is registered by an ADC. Time definition is obtained by feeding the T signals to constant fraction discriminators. The T branch is utilized only for the silicon detectors, since the T signal from the CsI(Tl) detector has too slow rise time (a few $\mu$s) to be useful. For each telescope, a logic OR between the T signals from the silicon detectors are used to define an event for that telescope. A MASTER signal, triggering the data acquisition system, is created by a logic OR between all eight telescopes. The RF signal from the cyclotron is used as the time-of-flight (TOF) reference signal, and is recorded as a stop signal in one of the TDCs, as are the T signals from all the silicon detectors. The MASTER signal is used as common start for all TDC channels. The time between two consecutive RF signals, and thus between two beam bursts, is about 58 ns at 95 MeV. Data are recorded on an event-by-event basis using SVEDAQ, a general purpose data acquisition system employed at TSL (Sundqvist and Nyberg 1997). Data are split into two independent branches, one for on-line monitoring and the other to tape for subsequent analysis. The dead time of the system is typically a few per cent.

The relative neutron beam intensity is monitored by integrating the proton beam current in the beam dump, and by measuring the number of neutron-induced fissions in $^{238}$U with a thin film breakdown counter (TFBC) (Prokofiev *et al.* 1999). The results of the two methods were in good agreement.

The main data acquisition was done with two different carbon targets of natural isotopic composition, using about 18 hours of beam time for each. The targets have dimensions of 25 mm in diameter by 0.15 mm thick and 22 mm in diameter by 0.5 mm thick, respectively. The former was used to minimize the necessary energy loss corrections at low particle energy, while the latter gave good statistics

at high energy. In addition, a 25 mm diameter by 1 mm thick $CH_2$ target was used for absolute cross section normalization, employing the well-known *np* scattering cross section. Background runs were performed without any target in the neutron beam. In the middle of the data taking period, the forward and backward sets of telescopes were interchanged, and the series of targets were repeated. The various runs were normalized to the same incident neutron fluence using the integrated proton beam current and the number of fissions in the TFBC monitor.

# 3 Data reduction

Data analysis is performed on an event-by-event basis, where the data are first sorted into separate files for each telescope. By generating two-dimensional plots of the pulse height of the $\Delta E_1$ versus $\Delta E_2$ and $\Delta E_2$ versus $E$ detectors, respectively, each event can be assigned a particle-type identification, and the data are further separated into files for each kind of particle. A two-dimensional plot of particle energy versus neutron flight time is used to identify particles associated with the main neutron peak, while those induced by low-energy tail neutrons are rejected.

Energy calibration (Dangtip *et al.* 2000) of the silicon detectors is performed by determining the pulse height for the various particles at the point where they punch through the detectors, with the assumption of linear correspondence between pulse height and energy. Alpha particles from a $^{241}$Am source are used to check the calibration curve for the first, thin $\Delta E$ detector. For the CsI detectors, the linear response assumption is no longer valid, and the calibration curve is determined for each particle type by plotting the calculated energy, derived from the energy deposited in the second silicon $\Delta E$ detector and standard stopping power data, versus the measured pulse height. The obtained calibration is checked by comparing with pulse heights of resolved states in $^{12}$C(n,p) and (n,d) reactions, for which the energies are known. Adding the energy losses in the three detectors gives the incident energy for each charged particle.

After these steps of event-by-event operations, the data are sorted into histograms reflecting the particle emission energy spectra, i.e., the relative double-differential cross sections. The energy bin width of the histograms is 1 MeV. The same procedure is applied to both the signal (target in) and the background (target out) runs. After normalization to the same neutron fluence, the background runs are subtracted from the signal ones.

The $CH_2$ data are treated in a similar way. After proper subtraction of target-out and $^{12}$C(n,xp) background contributions, the cross section per count and incident neutron is determined from the *np* scattering peak, using data previously published at a similar energy (Rönnqvist *et al.* 1992, Olsson *et al.* 2000). This normalization coefficient is then applied to the carbon histograms to obtain the absolute cross section. The uncertainty in the absolute cross section determination

is estimated to be about 3.5% (Dangtip *et al.* 2000).

Because of the finite thickness of the reaction targets, the particle spectra are slightly distorted due to energy losses within the target itself. Correction factors for such distortions, which can be considerable at the lowest particle energies, were calculated using a Monte Carlo code (Slypen *et al.* 1994). The corrected data from the two different target thicknesses show no systematic differences. This fact is taken as a verification that the correction calculations are under good control.

# 4 Experimental results and discussion

## 4.1 Cross sections

### 4.1.1 Double-differential cross sections

Because of the limited statistics obtained in this preliminary experiment, the final double differential cross sections for production of protons, deuterons and tritons at an incident neutron energy of 95 MeV are presented using rather wide energy bins, i.e., 2 MeV for the energy range 3 – 15 MeV and 8 MeV for the region above 15 MeV. The binning is identical to that used in the recent evaluation (Chadwick *et al.* 1999), which facilitates a comparison between the experiment and the evaluation.

Double differential cross sections for proton and deuteron production at angles of 20°, 40°, 80° and 120° are shown in Figs. 1 and 2, respectively. Data obtained with the 0.5 mm thick target are shown as filled circles and those with the 0.15 mm thick target as open circles. The error bars represent a combination of statistical errors and uncertainties in the correction procedure, with the latter dominating at the lowest energies. As can be seen, the low-energy threshold for protons is about 3−4 MeV, while it is slightly higher for deuterons. The solid histograms represent the evaluation (Chadwick *et al.* 1999). Since the evaluation is not tabulated at 95 MeV, a linear interpolation between 90 and 100 MeV was made for each bin.

For both types of particles, the spectra show a monotonically decreasing trend with energy for angles larger than 40°. This is what would be expected for particle emission after statistical equilibrium of the absorbed projectile energy, and the measured spectra are well described by the evaluation. However, at forward angles the spectra deviate from this behaviour by showing a marked structure at high energy. In the case of deuterons, this can be easily understood as direct (n,d) proton pick-up reactions, leaving the residual nucleus in the ground state or in a low-lying excited state. This is well described by the evaluation, although the interpolation between 90 and 100 MeV smears out the ground-state peak.

For protons, a broad bump is observed at 20° in the mid-energy region, and the experimental data are about a factor of two higher than the evaluation. This deviation, although smaller, is observed also at 40°, but at lower energy. A similar behaviour is seen also in the corresponding Louvain-la-Neuve data at 72.8 MeV

(Slypen *et al.* 1995). The origin of this effect could be a strong component of a direct, or semi-direct, reaction mechanism. Quasi-elastic scattering, i.e., scattering of the projectile neutron from a target proton, is not expected to play a major role at the low incident energy of the present experiment, but would cause a forward-peaked, broad bump, that decrease in energy with increasing scattering angle, in accordance with the present data. Other mechanisms of preequilibrium reactions could also be involved. The dotted curves represent a calculation (Chadwick 2000) for the $^{12}$C(p,xp) reaction at 96 MeV with a new Monte Carlo preequilibrium model (Blann and Chadwick 1998). This calculation gives a better account of the forward-angle data, although the cross section is slightly underestimated at low energy and large angles. This is not surprising, since the model does not yet include equilibrium emission, and is therefore not expected to be reliable below about $15 - 20$ MeV.

The triton emission spectra are decreasing with energy at all angles. The statistics is slightly worse than that for the deuterons. No evaluated spectra for comparison are available.

### 4.1.2 Differential and integrated cross sections

Integrated cross sections are obtained as a two-fold integral of the double-differential data over energy and angle, i.e.,

$$\sigma = \int\int \frac{d^2\sigma}{d\Omega dE}(\theta, E)\, d\Omega\, dE. \tag{1}$$

The integration can be performed either over energy or angle first. In this work we used both ways, to get a consistency check of the procedures used.

Thus, energy-differential cross sections were determined by first integrating over the scattering angle $\theta$,

$$\frac{d\sigma}{dE}(E_i) = \int \frac{d^2\sigma}{d\Omega dE}(\theta, E_i)\, d\Omega. \tag{2}$$

To this end, Legendre polynomial expansions were fitted to the data for each energy bin $i$. The cross sections from both target thicknesses were used for these fits. At the highest energy bins the angular distributions are rather steep, which calls for a polynomial of high order. To avoid overparameterisation in those cases, some artificial points, with large errors, had to be added at large angles to smoothly guide the fit. This procedure has negligible consequencies for the integrated cross sections.

The resulting energy-differential cross sections for production of protons, deuterons and tritons are shown as filled circles in Fig. 3. Also shown are the corresponding proton and deuteron spectra from the evaluation (solid line). As can be seen, the experimental data are remarkedly well described by the evaluation, with

the exception of the mid-energy range for protons discussed above, and at somewhat lower energy for deuterons. Also shown is the preequilibrium calculation for protons, which describes the mid-energy range well.

Integrated cross sections were obtained simply by summing over all energy bins,

$$\sigma = \sum \frac{d\sigma}{dE}(E_i)\ \Delta E_i, \tag{3}$$

where $\Delta E_i$ is the width of the $i$-th energy bin. Because of the low-energy threshold, only the experimental data from 5 MeV and upwards were taken into consideration. The integrated cross sections obtained with this method are given in the first row of Table 1.

Table 1: Cross sections for charged-particle production in $^{12}$C + n reactions at 95 MeV. The errors given for the measured data in the first and second rows are due to counting statistics and the energy-loss correction, while for the average (third row) a systematic error of 9% is also included.

| Cross section (mb) | Protons | Deuterons | Tritons |
|---|---|---|---|
| $\sigma_{\text{meas}}$ (from eqs. 2 and 3) | $164.8 \pm 3.1$ | $70.1 \pm 1.5$ | $21.2 \pm 0.8$ |
| $\sigma_{\text{meas}}$ (from eqs. 4 and 5) | $167.9 \pm 3.5$ | $71.2 \pm 2.1$ | $23.6 \pm 1.3$ |
| $\sigma_{\text{meas}}$ (average; total errors) | $166.4 \pm 15.4$ | $70.6 \pm 6.7$ | $22.5 \pm 2.4$ |
| $\sigma_{\text{extrap}}$ (Chadwick *et al.* 1999) | $39.1 \pm 3.9$ | $19.5 \pm 2.0$ | $7.0 \pm 1.4$ |
| $\boldsymbol{\sigma}$ | **205.5±15.9** | **90.1±7.0** | **29.5±2.8** |

Angle-differential cross sections were obtained by first summing the data over all energy bins for each angle,

$$\frac{d\sigma}{d\Omega}(\theta) = \sum \frac{d^2\sigma}{d\Omega dE}(\theta, E_i)\ \Delta E_i. \tag{4}$$

Cross sections from the evaluation were used for the two lowest energy bins, as described below. The angular distributions for protons, deuterons and tritons, for both the thick (filled circles) and thin (open circles) targets, are shown in Fig. 4. The solid lines represent the corresponding quantity from the evaluation. As can be seen, the experimental proton data show a stronger forward peaking than the cross sections from the evaluation, while the deuteron distribution is well described at forward angles. On the other hand, the experimental data are higher than the evaluation above 60° in this case.

Integrated cross sections were obtained by fitting Legendre polynomials to the experimental angular distributions,

$$\sigma = \int \frac{d\sigma}{d\Omega}(\theta)\, d\Omega, \tag{5}$$

as is indicated by the dashed lines in Fig. 4. In these cases, the polynomial order could be kept reasonably low while achieving a good fit. Similar fits were performed to the experimental data only, i.e., to angular distributions of data above 5 MeV. The result of these fits are presented in the second row of Table 1.

The cross sections determined with the two methods agree within the statistical errors. The first method gives slightly smaller errors, which is caused by the artificial information introduced in the Legendre polynomial fitting. For the average of the two methods, given in the third row of Table 1, we keep the more correct statistical errors from the second method, and add in quadrature a systematic error of 9% (see below). To extrapolate to zero energy, cross sections from the evaluation were used for the two lowest bins, i.e., $0-3$ MeV and $3-5$ MeV. Since no evaluation exists for tritons, the proton distribution, scaled by a factor of 0.18 to fit the data in the $7-30$ MeV range, was used for extrapolation in this case (dashed histogram in Fig. 3). The extrapolated cross sections ($0-5$ MeV) are given in the fourth row of Table 1. An error of 10% has been assigned to the extrapolated cross section for protons and deuterons, while the lack of calculated data for tritons suggests a larger uncertainty, i.e., 20%. As our final cross section results, given in the last row of Table 1, we take the average values of the two methods of analysis (third row), and add the extrapolated cross sections (fourth row). The errors of the final cross sections are obtained by adding the corresponding errors in quadrature. We note that the measured fraction of the total cross sections is around 80%, which is considerably more than in the work of Louvain-la-Neuve (Slypen *et al.* 2000). The reason is that we have a lower threshold, especially for deuterons and tritons, and that the present measurement gives spectra that extend to much higher charged particle energy.

Fig. 5 shows integrated cross sections for protons, deuterons and tritons from the present work (filled circles), Louvain-la-Neuve (open circles) (Slypen *et al.* 2000) and UC Davis (open squares) (Subramanian *et al.* 1983), as well as the evaluation (solid lines) (Chadwick *et al.* 1999). The new points at 95 MeV fit nicely into the trends given by the lower-energy data. Furthermore, the Louvain-la-Neuve and the present data are systematically higher than the evaluation for all energies, especially for protons.

## 4.2 Kerma coefficients

Partial neutron kerma coefficients, i.e., the kerma for production of a specific charged particle per unit neutron fluence, can be obtained directly from the measured microscopic cross sections, using a two-fold integral of the energy-weighted

double-differential cross section over energy and angle,

$$k_\Phi = N \iint E \, \frac{d^2\sigma}{d\Omega dE}(\theta, E) \, d\Omega \, dE, \tag{6}$$

where $N$ is the number of target nuclei per unit mass.

Adding these partial kerma coefficients, including also values for particles not measured in the present work, gives an estimate of the total kerma coefficient for carbon at 95 MeV. No experimental kerma determination at such a high energy has been obtained previously.

### 4.2.1 Partial kerma coefficients

As was the case for the integrated cross sections, the two-fold integration was performed in two ways. First, the angle-integrated energy distributions determined according to eq. 2 were used to calculate the partial kerma coefficients through

$$k_\Phi = N \sum E_i \left( \int \frac{d^2\sigma}{d\Omega dE}(\theta, E_i) \, d\Omega \right) \Delta E_i = N \sum E_i \, \frac{d\sigma}{dE}(E_i) \, \Delta E_i, \tag{7}$$

where $i$ denotes the energy bin number and $E_i$ is the mean energy of the bin. The result of this analysis, for energy bins from 5 MeV and upwards, is given in the first row of Table 2.

Table 2: Partial kerma coefficients for charged-particle production in $^{12}$C + n reactions at 95 MeV. The errors given for the measured data in the first and second rows are due to counting statistics and the energy-loss correction, while for the average (third row) a systematic error of 6% is also included.

| Kerma coefficient (fGy m$^2$) | Protons | Deuterons | Tritons |
|---|---|---|---|
| $k_{\Phi,\mathrm{meas}}$ (from eq. 7) | $4.29 \pm 0.10$ | $1.78 \pm 0.04$ | $0.38 \pm 0.02$ |
| $k_{\Phi,\mathrm{meas}}$ (from eq. 8) | $4.34 \pm 0.12$ | $1.72 \pm 0.07$ | $0.36 \pm 0.02$ |
| $k_{\Phi,\mathrm{meas}}$ (average; total errors) | $4.32 \pm 0.29$ | $1.75 \pm 0.13$ | $0.37 \pm 0.03$ |
| $k_{\Phi,\mathrm{extrap}}$ (Chadwick *et al.* 1999) | $0.08 \pm 0.008$ | $0.04 \pm 0.004$ | $0.02 \pm 0.004$ |
| $\boldsymbol{k_\Phi}$ | **4.40±0.29** | **1.79±0.13** | **0.39±0.03** |

Second, the double-differential data for each angle were summed with respect to the energy bins, after multiplication with the mean bin energy, $E_i$, and the bin width, $\Delta E_i$. Only data above 5 MeV were taken into consideration. The obtained angular distributions were subsequently fitted with Legendre polynomials

to obtain the kerma coefficients. Thus, the procedure followed was

$$k_\Phi = N \int \left( \sum E_i \, \frac{d^2\sigma}{d\Omega dE}(\theta, E_i) \, \Delta E_i \right) d\Omega, \tag{8}$$

and the result is given in the second row of Table 2.

Also for the kerma, the two methods give consistent results within the errors. For energies below 5 MeV we used evaluated data (Chadwick *et al.* 1999) to obtain an extrapolation to zero energy. Final partial kerma coefficients for protons, deuterons and tritons, as given in the last row of Table 2, are obtained by adding the average of the measured values from the two methods of analysis (third row) and the extrapolated values (fourth row). Because of the energy weighting in the calculation of kerma coefficients, the extrapolated data only account for $2-5\%$, and thus the values given can be considered to be fully experimental.

The partial kerma coefficients are shown in Fig. 6 (filled circles) together with corresponding data at lower energy from Louvain-la-Neuve (open circles) (Slypen *et al.* 2000) and UC Davis (open squares) (Romero *et al.* 1985). As for the integral cross sections, the new data at 95 MeV fit well into the trends of the lower energy kerma coefficients. The evaluation (solid line) is close to the deuteron data, although slightly low, while it seriously underestimates the kerma coefficient for protons. The deviation increases with energy from about 40 MeV, and amounts to 35% at 95 MeV.

### 4.2.2 Total kerma coefficient

To get an estimate of the total kerma coefficient for carbon at 95 MeV, the partial coefficients for protons, deuterons and tritons from Table 2 were added to the corresponding values for alpha particles, $A > 4$ recoils and elastic recoils of the evaluation (Chadwick *et al.* 1999). Since the systematic errors for the three measured particles are not independent, they were added linearily, while the statistical errors were added in quadrature. The partial kerma coefficents taken from the evaluation were assigned errors of 10%, which were also added linearily for this portion. The total error was obtained by quadratically adding the errors of the experimental and evaluation parts. In this way we obtain a total kerma coefficient of $k_\Phi = 8.59 \pm 0.46$ fGy m$^2$. The various contributions are given in Table 3, where it can be seen that the present experiment accounts for 77% of the total kerma coefficient.

The present result is plotted in Fig 7, together with other determinations from microscopic cross sections (filled symbols) (Romero *et al.* 1985, Slypen *et al.* 2000) as well as from integral measurements (open symbols) (Schuhmacher *et al.* 1992, Schrewe *et al.* 1992, 1995, 2000). The recent evaluation (Chadwick *et al.* 1999) is also shown. For the integral measurements, only data above 30 MeV have been included. The experimental data are well described by the evaluation up to about 40 MeV, where a deviation starts. The integral measurements, which agree

Table 3: Estimate of the total kerma coefficient for $^{12}C$ + n at 95 MeV.

| Energy transfer by | $k_\Phi$ (fGy m$^2$) | $\sum k_\Phi$ (fGy m$^2$) |
|---|---|---|
| Protons (present work) | $4.40 \pm 0.29$ | |
| Deuterons (present work) | $1.79 \pm 0.13$ | |
| Tritons (present work) | $0.39 \pm 0.03$ | $6.58 \pm 0.42$ |
| Alpha particles (Chadwick *et al.* 1999) | $1.37 \pm 0.14$ | |
| $A > 4$ recoils (Chadwick *et al.* 1999) | $0.51 \pm 0.05$ | |
| Elastic recoils (Chadwick *et al.* 1999) | $0.13 \pm 0.01$ | $2.01 \pm 0.20$ |
| Total kerma coefficient | | **8.59±0.46** |

well with the evaluation, are systematically lower than the microscopic ones in the $50 - 70$ MeV region. In fact, the microscopic data can be well described by a straight line between 40 and 100 MeV, as is indicated by the dashed line in the figure. The present kerma coefficient at 95 MeV is about 25% higher than the corresponding value of the evaluation.

## 4.3 Systematic errors

In addition to errors due to counting statistics and to the target-related energy-loss corrections, several sources of systematic errors come into play. The normalization of signal and background runs, as well as those with the $CH_2$ target, to the same neutron fluence, is estimated to have an accuracy of 2%, based on the fluctuations between the two methods used. The absolute normalization using *np* scattering is believed to be accurate to within 3.5% (Dangtip *et al.* 2000).

There is a finite probability that a charged particle stopping in a CsI detector undergoes a nuclear reaction before coming to rest. In such a reaction, energy is lost or transfered to other (charged or uncharged) particles. This normally means a loss of light, and consequently the particle will be registered at too low energy in the spectrum, or being totally lost. In the former case, the integrated cross section will not be affected while the kerma will, because of the distortion of the spectrum. However, in the latter case both the cross section and the kerma will be reduced. Based on total reaction cross section data (Carlson 1996), we estimate these effects to be less than 3% in the energy region of interest here.

The TOF gate, applied to the data to cut out only neutrons related to the main peak of the incident neutron spectrum, has a finite width in accordance with the finite time resolution, and thus the data contain a small fraction of events caused by the low-energy neutron tail. By applying TOF gates with various widths, we

have estimated that the maximum amount of such events is about 7%. These are not evenly distributed over the spectrum; the effect is at maximum at low charged particle energy, while it is absent at the highest energies. Thus, the kerma determinations will, because of the energy weighting, be less affected than the cross sections, and we estimate the uncertainty in this case to be half of that for cross sections, i.e., 3.5%.

To conclude, we estimate, by adding the various contributions in quadrature, the total systematic error to be 9% for the integrated cross sections and about 6% for the kerma determinations.

# 5 Conclusions

In the present work, double-differential cross sections of inclusive proton, deuteron and triton production, induced by 95 MeV neutrons on carbon, have been measured. The measurements were performed with a recently installed experimental setup, MEDLEY, which consists of eight three-detector particle telescopes, mounted in a 1 m diameter scattering chamber. The data cover the angular range $20° - 160°$ and secondary particle energies from $3 - 4$ MeV and upwards.

It is found that the proton spectra have a higher cross section in the mid- to high-energy range at forward angles compared to a recent evaluation (Chadwick *et al.* 1999). This feature is probably caused by a stronger component of direct reaction mechanisms, e.g., quasi-elastic scattering, and leads, because of the energy weighting, to a partial kerma coefficient that is 35% higher. Since protons give a large contribution to the total kerma, our value, $k_\Phi = 8.59 \pm 0.46$ fGy m$^2$, is about 25% higher than that given in the evaluation. Our data, both concerning cross sections and kerma coefficients, support a trend observed for similar data below 73 MeV (Slypen *et al.* 2000).

In the nearest future, we will analyse recently taken carbon data, which have better statistics than in the present experiment, with the objective to obtain smaller errors, and also cross sections and kerma coefficients for production of helium isotopes. With the better statistics, it will also be possible to extract data in the $60 - 95$ MeV energy range, by employing the low-energy neutron tail with other TOF gates (Benck *et al.* 1998, Slypen *et al.* 2000). Thus, the 95 MeV data will be directly connected to the lower-energy data of Louvain-la-Neuve.

The next experiment will be devoted to similar measurements on oxygen. These measurements are considered important, since large discrepancies between different measurements exist for this nucleus (Chadwick *et al.* 1999). Furthermore, good data on oxygen will as well facilitate a determination of the carbon/oxygen kerma ratio, which is of great use in dosimetric applications.

New data at an even higher energy, e.g., 150 MeV, is of high priority to better understand the evolution of various reaction mechanisms with neutron energy, and ultimately to resolve the problems of increasing discrepancy between data

and theory with increasing energy. Such a measurement is being planned at TSL in Uppsala.

The authors wish to thank the The Svedberg Laboratory staff for significant contributions to the construction of the equipment, the development of the data acquisition software, and for careful cyclotron operation during the measurements. The authors would also like to thank Mr. Sture Hultqvist and Mr. Ove Johansson from Gammadata AB for valuable contributions to the mechanical and electronics development. Thanks are also due to Dr. Isabelle Slypen for supplying us with the correction calculations, and to Dr. Mark Chadwick for fruitful discussions and for making results from his new preequilibrium Monte Carlo code available prior to publication.

This work was financially supported by the Göran Gustafsson Foundation, Swedish Cancer Foundation, Swedish Natural Science Research Council, and the Development and Promotion of Science and Technology Talents Project of Thailand.

# References

Benck S, Slypen I, Meulders J P and Corcalciuc V 1998 Experimental double-differential cross sections and derived kerma factors for oxygen at incident neutron energies from reaction thresholds to 65 MeV *Phys. Med. Biol.* **43** 3427–47

Blann M and Chadwick M B 1998 New precompound decay model: Angular distributions *Phys. Rev.* C **57** 233–43.

Broerse J J, DeLuca P M, Jr., Dietze G, Height R C, Hiraoka T, Kawashima K, Kocherov N, Menzel H G, Olsson N, Wambersie A, White R M and Zoetelief J 1997 Nuclear data for neutron therapy: Status and future needs, *IAEA-TECDOC-992*

Carlson R F 1996 Proton-nucleus total reaction cross sections and total cross sections up to 1 GeV *Atomic Data and Nuclear Data Tables* **63** 93–116

Chadwick M B, DeLuca P M, Jr. and Haight R C 1997 Nuclear data needs for neutron therapy and radiation protection *Radiat. Prot. Dosim.* **70** 1–12

Chadwick M B, Barschall H H, Caswell R S, DeLuca P M, Jr., Hale G M, Jones D T L, MacFarlane R E, Meulders J P, Schuhmacher H, Schrewe U J, Wambersie A and Young P G 1999 A consistent set of neutron kerma coefficients from thermal to 150 MeV for biologically important materials *Med. Phys.* **26** 974–91;
*ICRU Report 63* Nuclear data for neutron and proton radiotherapy and

for radiation protection (International Commission on Radiation Units and Measurements, Bethseda, MD, 2000)

Chadwick M B 2000 private communication

Condé H, Hultqvist S, Olsson N, Rönnqvist T, Zorro R, Blomgren J, Tibell G, Håkansson A, Jonsson O, Lindholm A, Nilsson L, Renberg P-U, Brockstedt A, Ekström P, Österlund M, Brady F P and Szeflinski Z 1990 A facility for studies of neutron induced reactions in the 50 – 200 MeV range *Nucl. Instr. Meth.* A **292** 121–8

Dangtip S, Ataç A, Bergenwall B, Blomgren J, Elmgren K, Johansson C, Klug J, Olsson N, Alm Carlsson G, Söderberg J, Nadel-Turonski P, Jonsson O, Nilsson L, Renberg P-U, Le Brun C, Lecolley J F, Lecolley F R, Varignon C, Eudes Ph, Haddad F, Kerveno M, Kirchner T and Lebrun C 2000 A facility for measurements of nuclear cross sections for fast neutron cancer therapy *Nucl. Instr. Meth.* A (in press)

DeLuca P M, Jr., Wambersie A and Caswell R S 1996 Nuclear data needed for fast neutron and proton radiation therapy *ICRU News June 1996* 14–18

Klug J, Blomgren J, Ataç A, Bergenwall B, Dangtip S, Elmgren K, Johansson C, Olsson N, Rahm J, Jonsson O, Nilsson L, Renberg P-U, Nadel-Turonski P, Ringbom A, Oberstedt A, Tovesson F, Le Brun C, Lecolley J-F, Lecolley F-R, Louvel M, Marie N, Schweitzer C, Varignon C, Eudes Ph, Haddad F, Kerveno M, Kirchner T, Lebrun C, Stuttgé L, Slypen I, Prokofiev A, Smirnov A, Michel R, Neumann S and Herpers U 2000 SCANDAL - A facility for elastic neutron scattering studies in the 50 – 130 MeV range (to be published)

Olsson N, Blomgren J, Condé H, Dangtip S, Elmgren K, Rahm J, Rönnqvist T, Zorro R, Jonsson O, Nilsson L, Renberg P-U, Ringbom A, Tibell G, Ericson T E O and Loiseau B 2000 Uppsala neutron-proton scattering measurements and the $\pi NN$ coupling constant, *Physica Scripta* T **87** 7–13

Prokofiev A V, Smirnov A N and Renberg P-U 1999 A monitor for intermediate-energy neutrons based on thin film breakdown counters *Report TSL/ISV-99-0203* Uppsala University (unpublished)

Romero J L, Brady F P and Subramanian T S 1985 Neutron induced charged particle spectra and kerma from 25 to 60 MeV *Proc. Int. Conf. on Nuclear Data for Basic and Applied Science (Santa Fe, New Mexico, 13–17 May 1985)* pp 687–99

Rönnqvist T, Condé H, Olsson N, Zorro R, Blomgren J, Tibell G, Jonsson O, Nilsson L, Renberg P-U and van der Werf S Y 1992 Backward angle n-p differential cross sections at 96 MeV *Phys. Rev.* C **45** R496–9

Schrewe U J, Brede H J, Gerdung S, Nolte R, Pihet P, Schmelzbach P and Schuhmacher H 1992 Determination of kerma factors of A-150 plastic and carbon at neutron energies between 45 and 66 MeV *Radiat. Prot. Dosim.* **44** 21–4

Schrewe U J, Newhauser W D, Brede H J, Dangendorf V, DeLuca P M, Jr., Gerdung S, Nolte R, Schmelzbach P and Schuhmacher H 1995 Measurement of neutron kerma factors in C and O: Neutron energy range of 20 MeV to 70 MeV *Radiat. Prot. Dosim.* **61** 275–80

Schrewe U J 2000 Experimental kerma coefficients and dose distributions of C, N, O, Mg, Al, Si, Fe, Zr, A-150 plastic, $Al_2O_3$, AlN, $SiO_2$ and $ZrO_2$ for neutron energies up to 66 MeV *Phys. Med. Biol.* **45** 651–83

Schuhmacher H, Brede H J, Henneck R, Kunz A, Menzel H G, Meulders J P, Pihet P and Schrewe U J 1992 Measurement of neutron kerma factors for carbon and A-150 plastic at neutron energies of 26.3 MeV and 37.8 MeV *Phys. Med. Biol.* **37** 1265–81

Slypen I, Corcalciuc V and Meulders J P 1994 Geometry and energy loss features of charged particle production in fast-neutron induced reaction *Nucl. Instr. Meth.* B **88** 275–81

Slypen I, Corcalciuc V and Meulders J P 1995 Proton and deuteron production in neutron-induced reactions on carbon at $E_n$ = 42.5, 62.7, and 72.8 MeV *Phys. Rev.* C **51** 1303–11

Slypen I, Benck S, Meulders J and Corcalciuc V P 2000 Experimental partial and total kerma coefficients for carbon deduced from microscopic cross sections at incident neutron energies below 75 MeV *Phys. Med. Biol.* **45** 577–97

Subramanian T S, Romero J L, Brady F P, Watson J W, Fitzgerald D H, Garrett R, Needham G A, Ullmann J L, Zanelli C I, Brenner D J and Prael R E 1983 Double differential inclusive hydrogen and helium spectra from neutron-induced reactions on carbon at 27.4, 39.7 and 60.7 MeV *Phys. Rev.* C **28** 521–8

Sundqvist T and Nyberg J 1997 SVEDAQ Data acquisition *TSL Progress Report 1996–1997* p 21 (unpublished)

White R M, Broerse J J, DeLuca P M, Jr., Dietze G, Haight R C, Kawashima K, Menzel H G, Olsson N and Wambersie A 1992 Status of nuclear data for use in neutron therapy *Radiat. Prot. Dosim.* **44** 11–20

# Figure captions

1. Double-differential cross sections at $\theta$ = 20°, 40°, 80° and 120° for the $^{12}$C(n,xp) reaction at 95 MeV. Filled and open circles correspond to measurements using a 0.5 mm and 0.15 mm thick target, respectively. Solid histograms represent evaluated data (Chadwick *et al.* 1999), and dotted curves are from a preequilibrium calculation of the $^{12}$C(p,xp) reaction (Chadwick 2000).

2. Same as Fig. 1 but for the $^{12}$C(n,xd) reaction.

3. Angle-integrated energy distributions for protons, deuterons and tritons from the $^{12}$C(n,x) reaction at 95 MeV (filled circles). Solid histograms represent evaluated data (Chadwick *et al.* 1999), and the dotted curve is from a preequilibrium calculation of the $^{12}$C(p,xp) reaction (Chadwick 2000). The dashed histogram is the evaluation for protons, scaled by a factor of 0.18 to fit the triton data in the 7 – 30 MeV range.

4. Energy-integrated angular distributions for protons, deuterons and tritons from the $^{12}$C(n,x) reaction at 95 MeV. Filled and open circles correspond to measurements using a 0.5 mm and 0.15 mm thick target, respectively. Solid curves represent evaluated data (Chadwick *et al.* 1999), and dashed curves are Legendre polynomial fits to the experimental data.

5. Integrated cross sections for production of protons, deuterons and tritons in carbon versus incident neutron energy. The filled circles represent the present work, open circles are from Louvain-la-Neuve (Slypen *et al.* 2000) and open squares from UC Davis (Subramanian *et al.* 1983). Solid curves represent evaluated data (Chadwick *et al.* 1999).

6. Partial kerma coefficients for production of protons, deuterons and tritons in carbon versus incident neutron energy. The filled circles represent the present work, open circles are from Louvain-la-Neuve (Slypen *et al.* 2000) and open squares from UC Davis (Subramanian *et al.* 1983). Solid curves represent evaluated data (Chadwick *et al.* 1999).

7. Total kerma coefficients for the $^{12}$C + n reaction versus incident neutron energy. The various symbols are explained in the figure. The dashed line is an eye-guide to the data from microscopic measurements in the region 40 – 100 MeV.

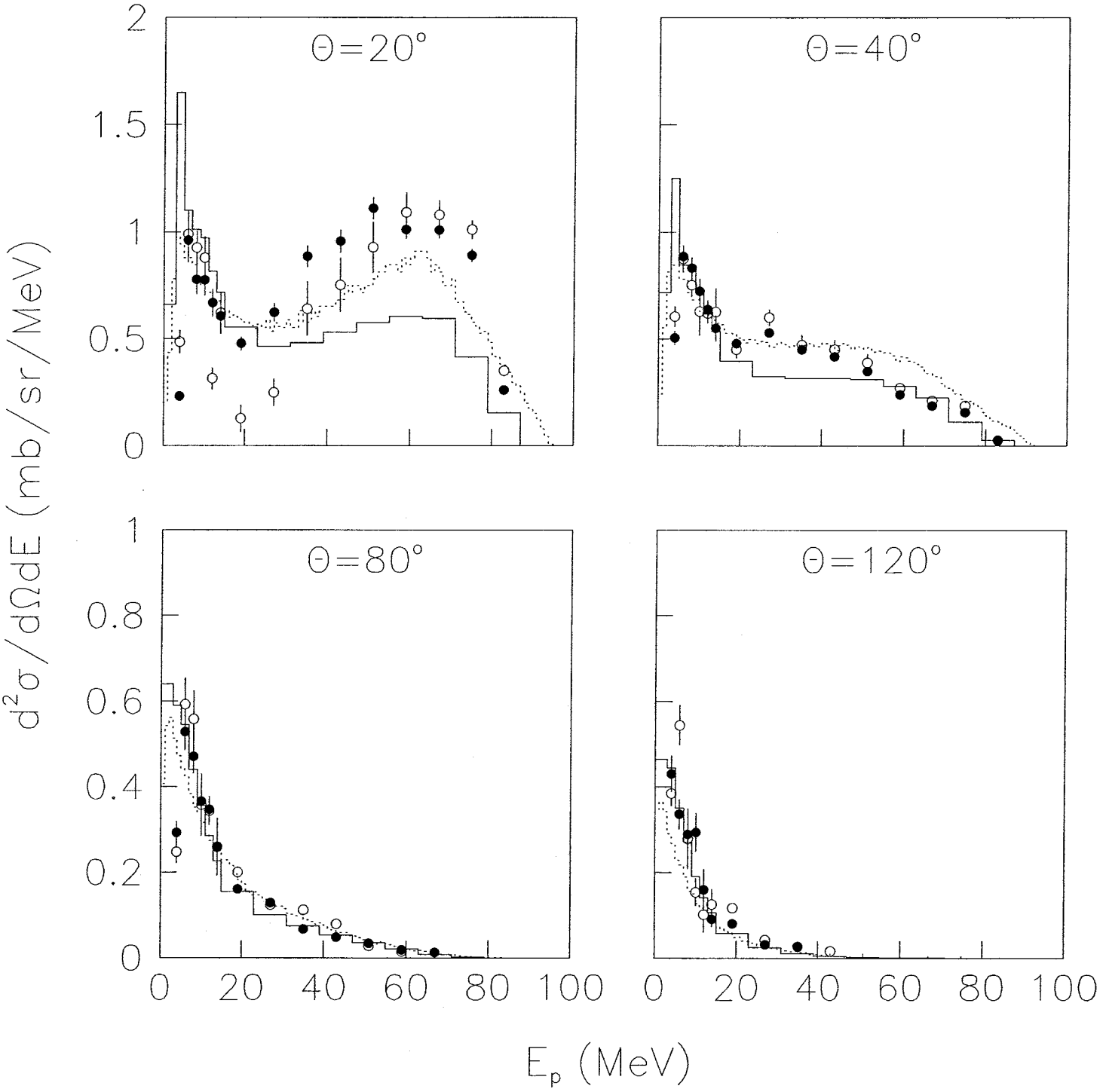
Θ=20°
Θ=40°
Θ=80°
Θ=120°
$d^2\sigma/d\Omega dE$ (mb/sr/MeV)
$E_p$ (MeV)
0
0.2
0.4
0.6
0.8
1
0.5
1.5
2
0
20
40
60
80
100

Fig. 1

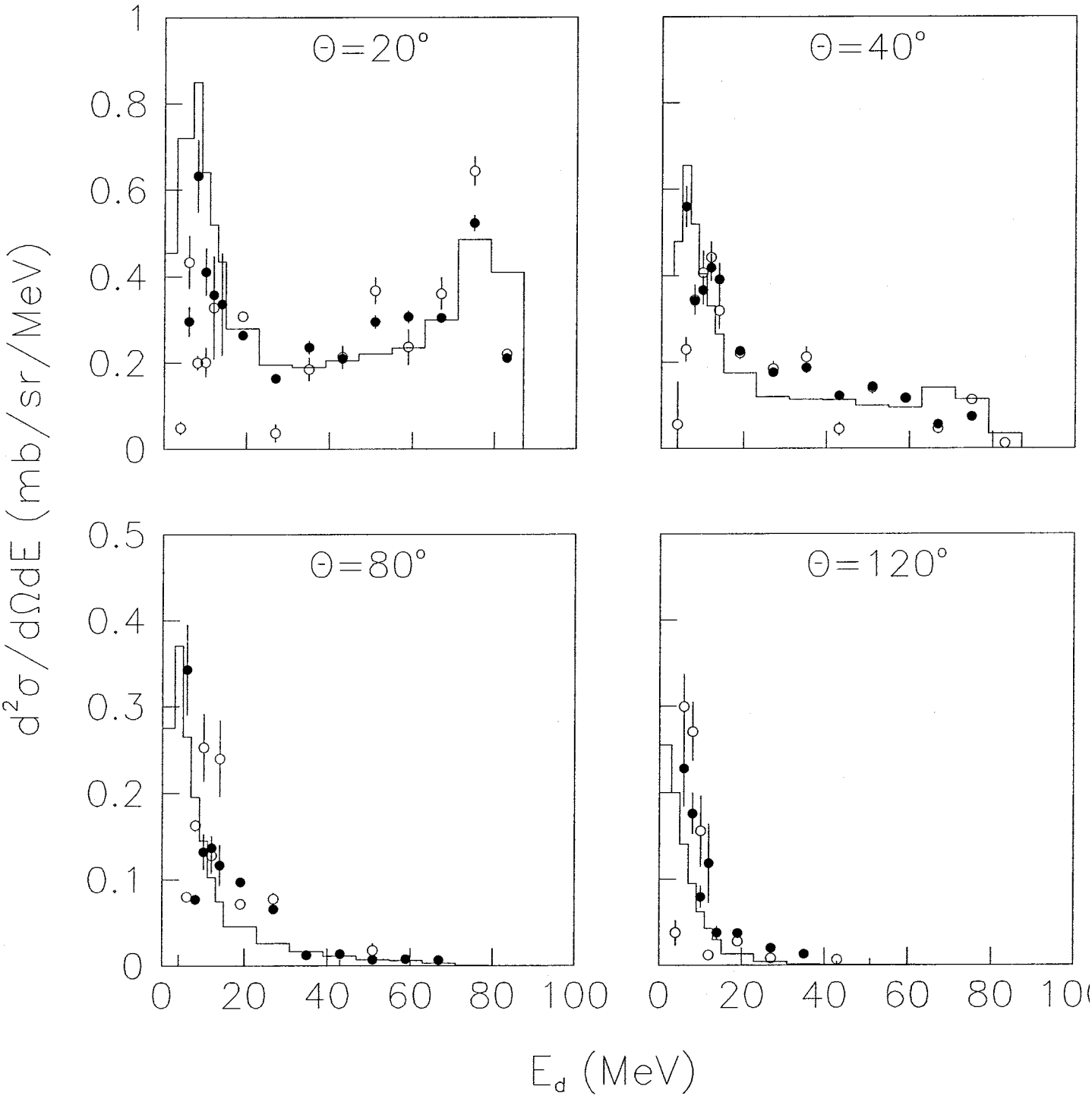
Θ=20°
Θ=40°
Θ=80°
Θ=120°
d²σ/dΩdE (mb/sr/MeV)
E_d (MeV)
0
0.2
0.4
0.6
0.8
1
0.1
0.3
0.5
0
20
40
60
80
100

Fig. 2

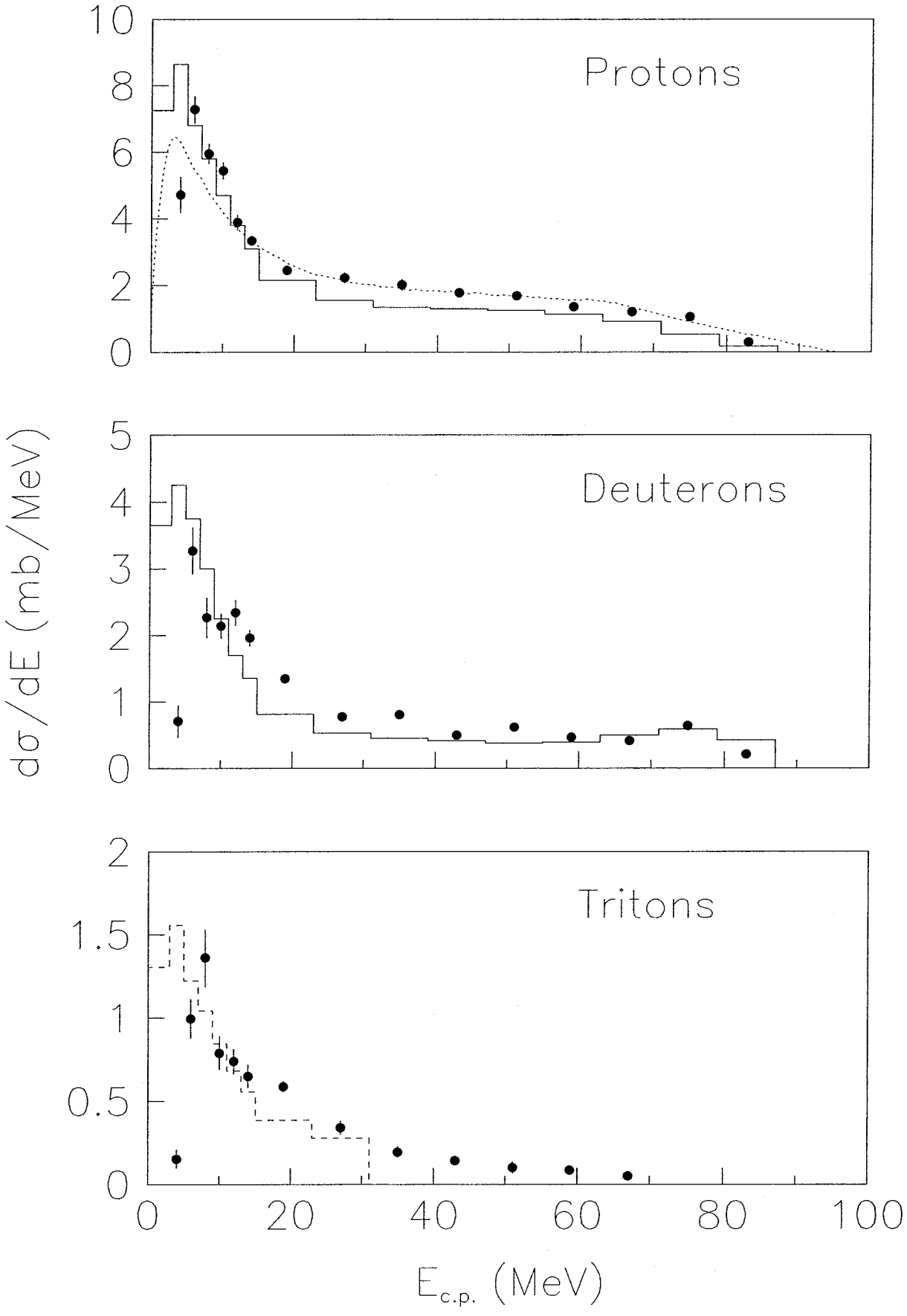
Protons
Deuterons
Tritons
dσ/dE (mb/MeV)
E c.p. (MeV)
0
2
4
6
8
10
1
3
5
0.5
1.5
20
40
60
80
100

Fig. 3.

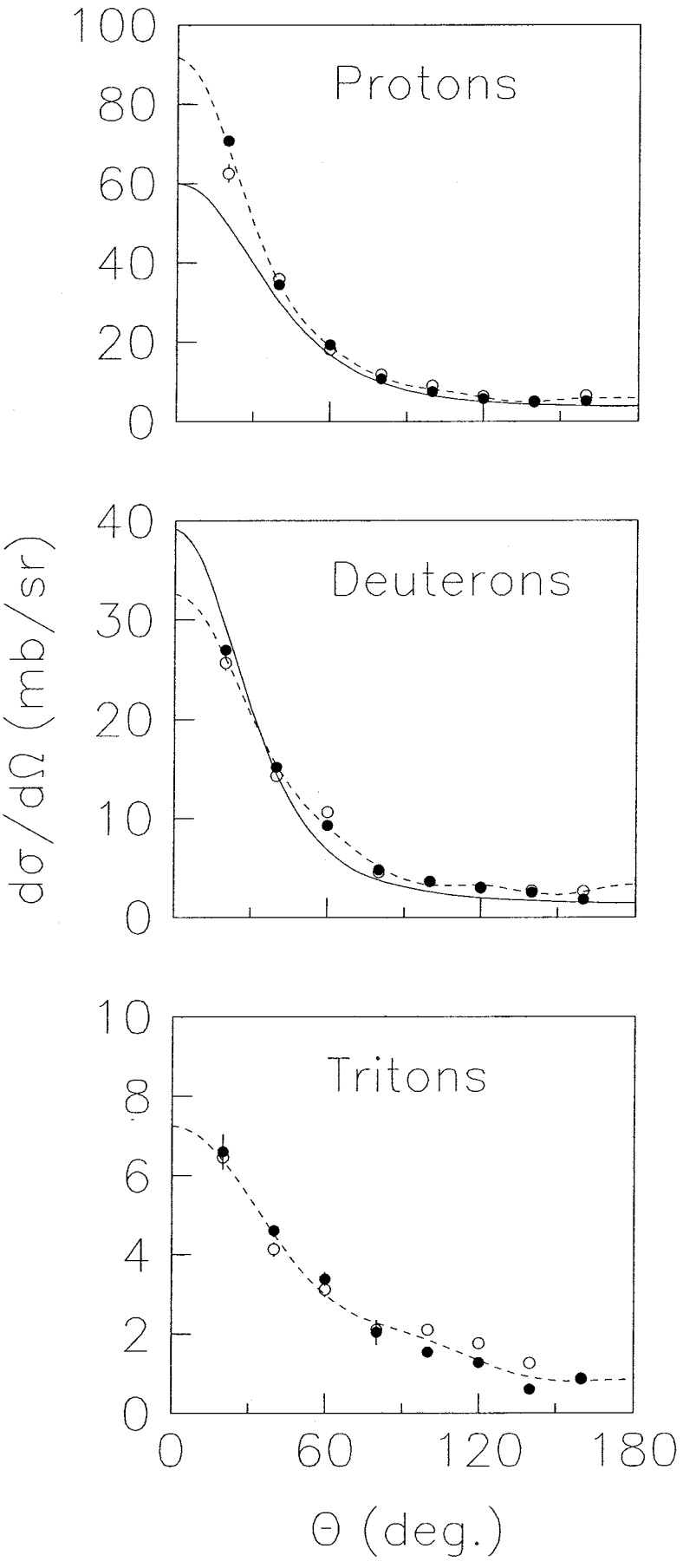
Protons
Deuterons
Tritons
dσ/dΩ (mb/sr)
Θ (deg.)
100
80
60
40
20
0
40
30
20
10
0
10
8
6
4
2
0
0
60
120
180

Fig. 4.

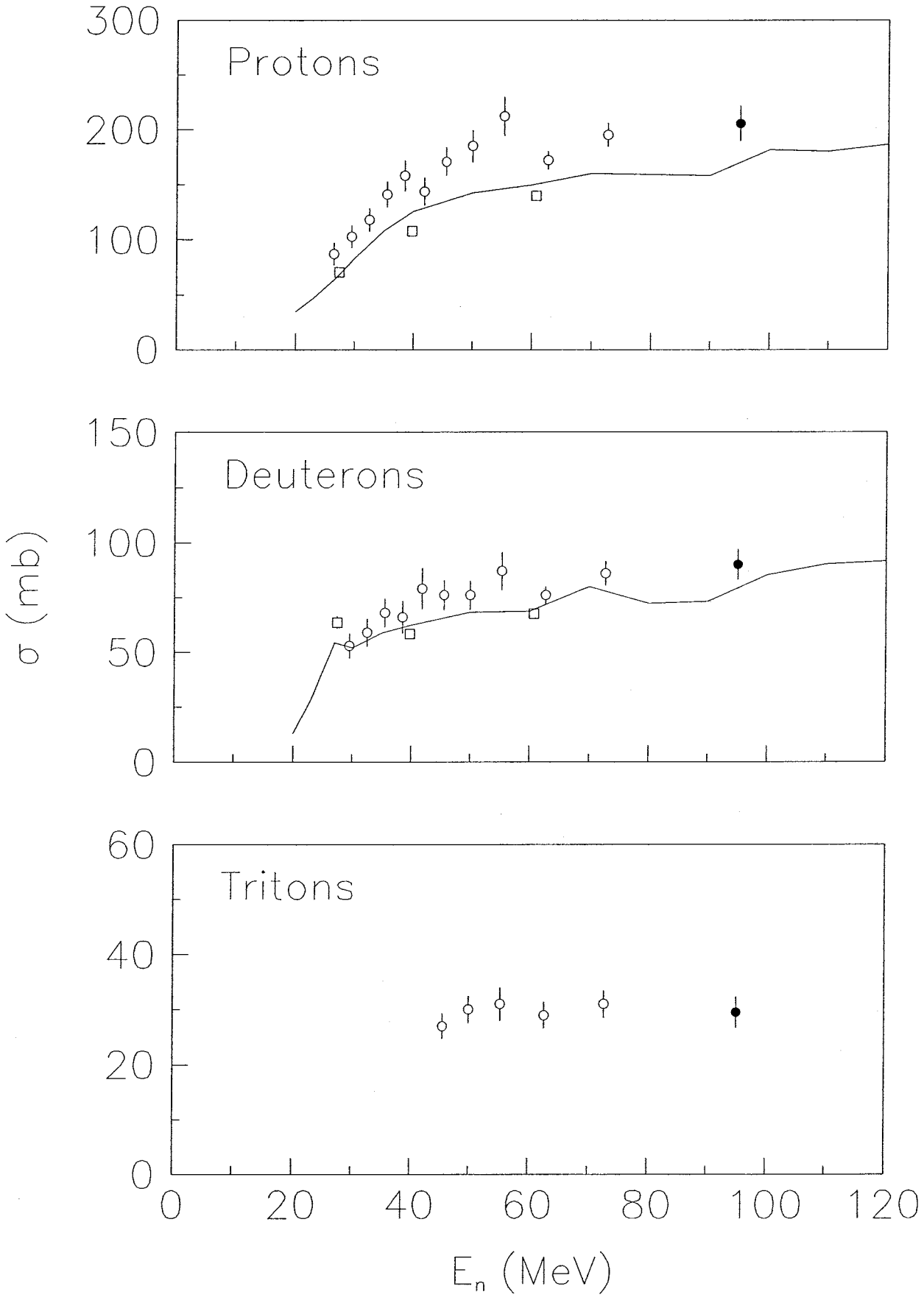
Protons
Deuterons
Tritons
σ (mb)
$E_n$ (MeV)
300
200
100
0
150
100
50
0
60
40
20
0
0
20
40
60
80
100
120

Fig. 5.

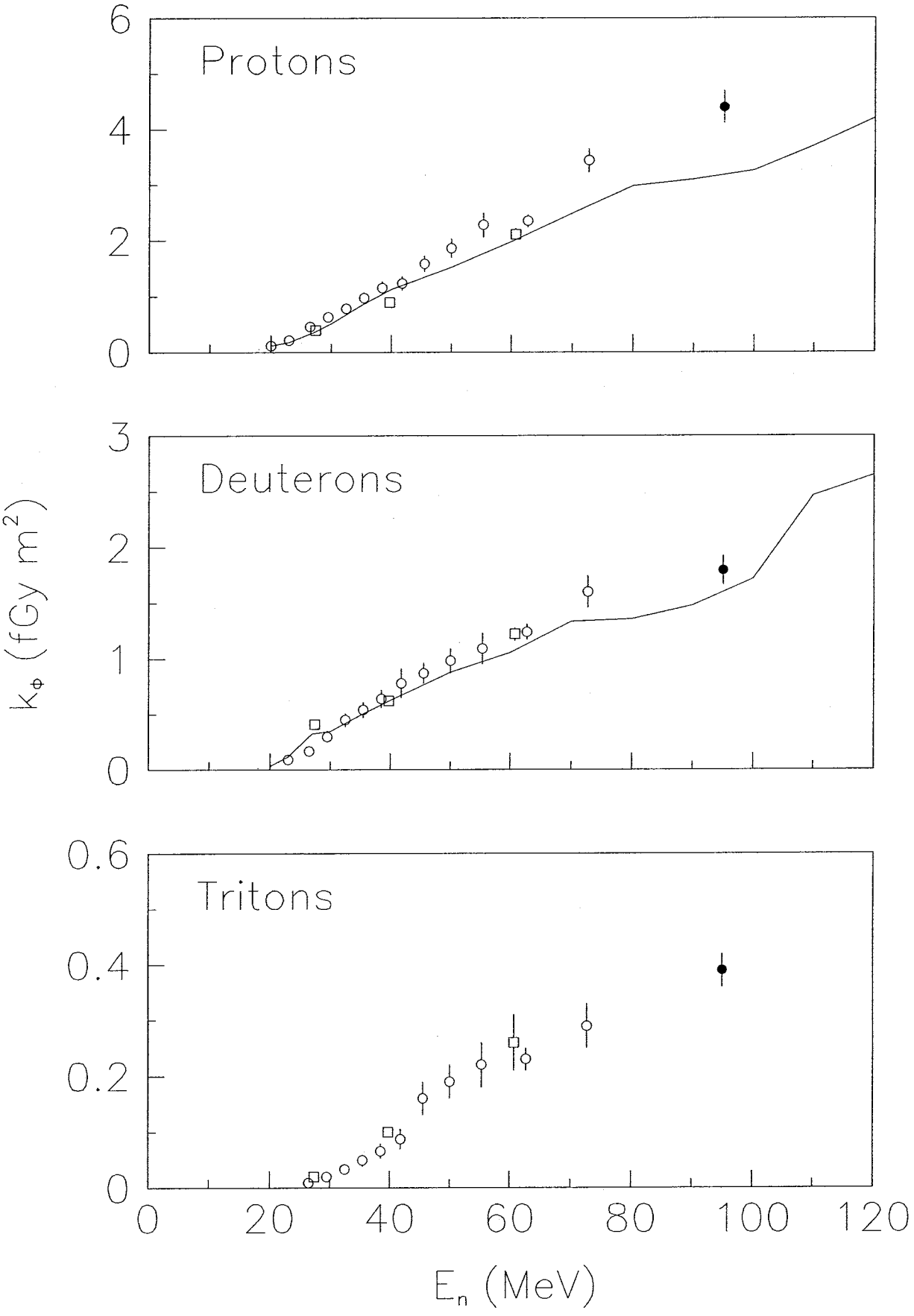
Protons
Deuterons
Tritons
$k_\Phi$ (fGy m$^2$)
$E_n$ (MeV)
0
2
4
6
1
3
0.2
0.4
0.6
20
40
60
80
100
120

Fig. 6.

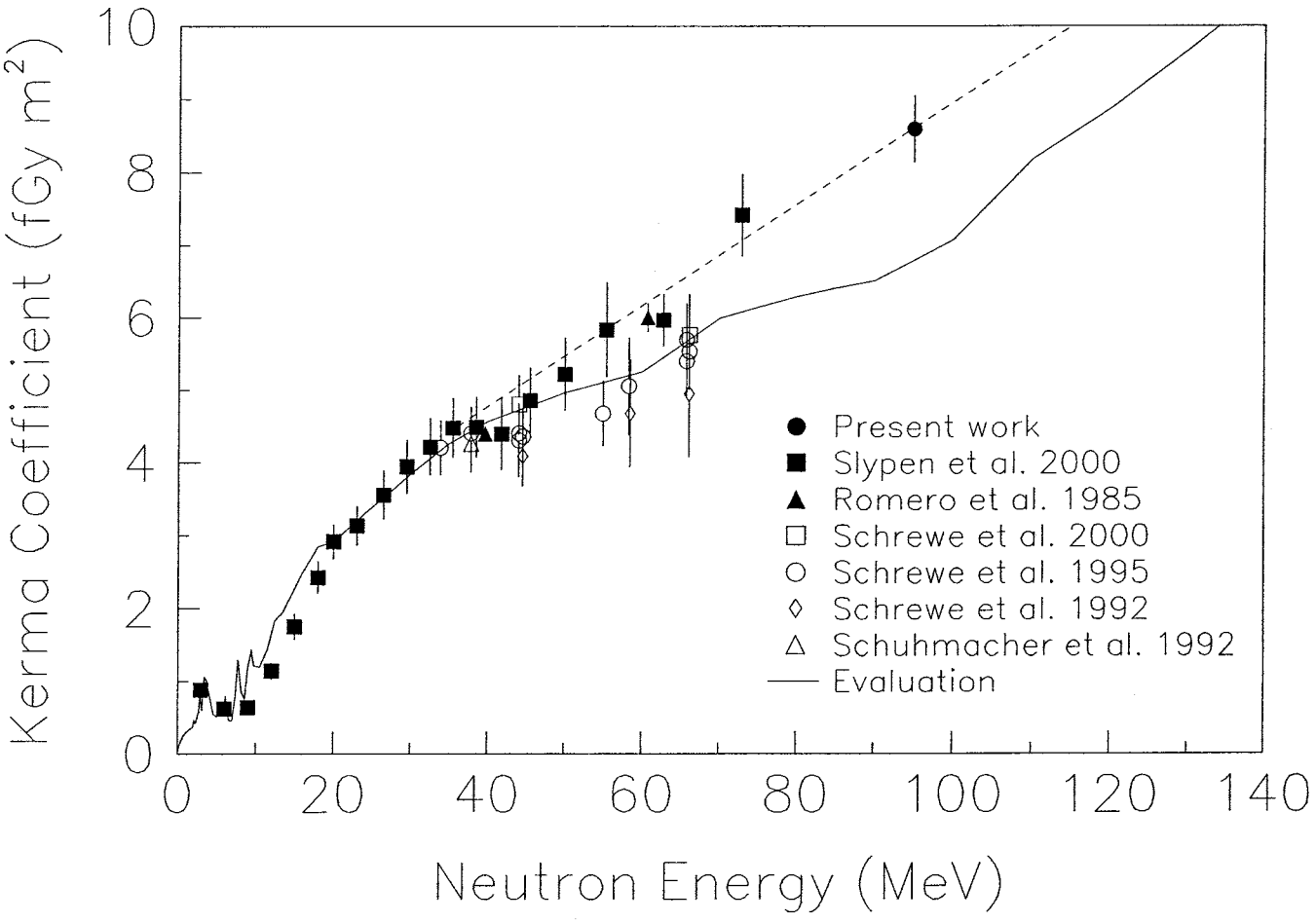
Kerma Coefficient (fGy m$^2$)
10
8
6
4
2
0
0
20
40
60
80
100
120
140
Neutron Energy (MeV)
Present work
Slypen et al. 2000
Romero et al. 1985
Schrewe et al. 2000
Schrewe et al. 1995
Schrewe et al. 1992
Schuhmacher et al. 1992
Evaluation

Fig. 7.

# Appendix VIII

For Official Use

NEA/SEN/NSC/WPEC(2000)2

OECD
OCDE
PARIS

Organisation de Coopération et de Développement Economiques
Organisation for Economic Co-operation and Development

OLIS : 22-Aug-2000
Dist. : 23-Aug-2000

Or. Eng.

NUCLEAR ENERGY AGENCY
NUCLEAR SCIENCE COMMITTEE

# Working Party on International Evaluation Co-operation

# SUMMARY RECORD OF THE TWELFTH MEETING

**Japan Atomic Energy Research Institute (JAERI)**
**20-21 June 2000**

94463



NEA/SEN/NSC/WPEC(2000)2
For Official Use
Or. Eng.

# Working Party on International Evaluation Co-operation

## Summary Record of the Twelfth Meeting

Japan Atomic Energy Research Institute (JAERI), Tokai-Mura, Japan, 20 - 21 June 2000

## Introduction

The local organiser, A. Hasegawa, welcomed the delegates. The chairman, C. Dunford, opened the meeting and introduced T. Osugi, group leader in JAERI for nuclear transmutation systems and vice chairman of the NEA Nuclear Science Committee. T. Osugi welcomed the participants and informed them of the great importance that JAERI attached to the WPEC effort.

## Adoption of the Agenda

The proposed agenda was adopted without modifications.

## Approval of the Summary Record of the Eleventh WPEC Meeting

The summary record (NEA/SEN/NSC/WPEC(99)2) of the eleventh meeting of the Working Party was approved without corrections.

## Brief progress reports and discussion of the plans for each of the projects

*JENDL*

A. Hasegawa presented the status of the JENDL project. Work on the third revision of the JENDL-3 general-purpose file was well advanced and the JENDL-3.3 library would be issued in FY2001. The main features of the new library are the inclusion of covariance information for the major elements and isotopes, addition of extra gamma-ray production data, adoption of isotope evaluation policy, rather than natural element evaluation policy, and updated or modified evaluations for a number of important isotopes.

Among the JENDL special purpose files could be mentioned the update and release of the High Energy files, the PKA/KERMA file, and the Photonuclear data file in FY2000, and the release, material-by-material, of the Actinide file in FY2001. The latter file has been developed in co-operation with Russian evaluators through the ISTC project.

*FENDL*

D. Muir presented the IAEA FENDL project. Since the release of the FENDL-2 library in mid 1998, the main emphasis of the project has been on data validation and maintenance. The latest FENDL meeting, held in Obninsk in June 1999, concentrated on the validation of the activation, decay and dosimetry libraries. An improved activation sublibrary, called FENDL-2.1, will be issued as a result of this meeting. The IAEA NDS had also developed an interactive plotting facility called "FENDL in Pictures", using HTML and generated GIF pictures.

The IAEA CRP on "Compilation and Evaluation of Photonuclear Data for Application" had been completed and a draft version of the final report, entitled "Handbook on photonuclear data for applications", was distributed.

*JEFF*

R. Jacqmin gave an overview of the status of the JEFF-3 project. A test version of the JEFF-3 general-purpose library had been produced in mid 1999. This library had then been processed using a different version of NJOY with subsequent correction of identified inconsistencies in the file. The benchmark testing will start in July 2000 and will continue for approximately one and a half years, before the file can be released to a wider audience.

Work on the JEFF-3 special purpose files had also started. The EFF project had contributed the latest version of the activation file (EAF-99) and the compilation of the decay data and fission yield libraries were well advanced. The compilation of the JEFF-3 intermediate energy file will start in 2001 when the TALYS code system will be available.

*CENDL*

Liu Tingjin informed WPEC of the status of the CENDL project. The CENDL-3 library, containing about 200 nuclides, will be completed in 2000. About 95 of the 133 planned evaluations in the general-purpose file have been completed so far. The work on the special purpose libraries continued and good progress has been made especially for the fission yield, photonuclear and prompt gamma-ray data.

The validation of the CENDL-2.1 library had continued in 1999. The library had been tested with the heavy water benchmark assemblies ZEEP-1, -2 and -3. The results were compared with similar calculations performed with ENDF/B-VI and WIMS-D libraries. The results for CENDL-2.1 were very good, having the same trends as ENDF/B-VI, but opposite trends to the WIMS-D library.

*ENDF*

C. Dunford reported on the progress achieved to date concerning the ENDF project. Release 7 of the ENDF/B-VI library had been completed in April 2000. The release contained mainly new fission product evaluations together with new evaluations for Bi-209 and Cm isotopes. Release 8 will be reviewed at the next CSEWG meeting in November 2000. This release will also mainly contain new fission product evaluations. CSEWG is looking into the possibility of preparing an ENDF/B-VII library in the time frame of about 3 to 5 years when the revised neutron standards should be available.

Three results from data validation studies were reported. The first concerned a new LANL critical assembly, ZEUS, which has an intermediate energy spectrum. The results with ENDF/B-VI release 4 using MCNP show an over-prediction of $k_{eff}$ by about 0.5%. The second concerned the latest $^{235}U$

evaluation from ORNL, which showed 0.3 - 1.0 % lower criticality for fast and intermediate energy systems compared to previous $^{235}U$ evaluations. The new ORNL $^{233}U$ evaluation seems to have eliminated the previous under-prediction of $k_{eff}$ for thermal systems.

*Evaluation efforts in Korea*

J. Chang presented the status of nuclear data evaluation activities in Korea. These activities had started in 1997 with a total staff of 12 persons (8 regular and 4 temporary staff). Seven (7) staff members mainly devoted their efforts to evaluations, four (4) to processing and one (1) to computer operations. The evaluation efforts were devoted to fission products for burn-up credit of spent fuel, to intermediate energy data for accelerator driven systems, to charged particle data for medical applications, and to photonuclear data for different applications. The processing of evaluated data covered applications libraries such as WIMS-D, ORIGEN-2 and MCNP libraries for reactor operations, CASMO-3 and HELIOS libraries for reactor core design and MATXS library for PWR pressure vessel and dosimetry applications.

## A report on the experimental activities

A. Carlson gave an overview of the US nuclear data measurement program. The group at ANL, headed by D. Smith, has made collaborative measurements using facilities both at JAERI, Japan and at IRMM, Belgium. A rather large effort is devoted to neutron activation cross-sections and a proposal for a formation of a WPEC subgroup on this subject was presented. Among the neutron data activities at the LANSCE facility mentioned were total cross-section measurements for 31 elements and isotopes from 5 to 560 MeV, gamma-ray production cross sections for oxygen, $^{235}U$, $^{238}U$ and $^{239}Pu$, (n,charged-particle) measurements for silicon, $^{59}Co$, and $^{92,94,96}Mo$, and the installation of a new array of high-resolution gamma-ray detectors called FIGARO. The measurements at the University of Massachusetts, Lowell, covered total cross sections for $^{27}Al$, $^{159}Tb$, $^{169}Tm$, and $^{235}U$, and inelastic scattering or gamma-production cross-sections for $^{169}Tm$ and $^{159}Tb$. The NIST nuclear data activities included collaborative measurements with Ohio University and LANL of the hydrogen scattering cross-section at 10 MeV neutron energy, and preparations for measurements of iron non-elastic cross sections. Neutron spectra for the Be(p,n), B(d,n), Be(d,n) and Al(d,n) reactions have been measured at Ohio University with the Van de Graaff accelerator. Also at that facility, measurements of the n, p, and $\alpha$ particles produced from $^{6}Li$ and $^{10}B$ ions incident on $^{27}Al$ and $^{28}Si$ targets have been made to provide level density and spin cut-off information. At ORNL, linac measurements focused on resonance parameter determination have been made of $^{233}U$ fission, $^{27}Al$ capture, chlorine transmission and capture, and silicon capture. Neutron capture and transmission measurements on Zr, Nb, Mo, Sm, Nd, Ho, Er, Tm, Hf, and W had been performed at the RPI linac. Significant improvements to the linac are now underway and should be completed this fall.

H. Weigmann presented the measurements performed at IRMM, as well as at Uppsala University, Sweden, and University of Hannover, Germany. The total and capture cross-sections of $^{99}Tc$ and $^{237}Np$, high resolution inelastic scattering cross-section of Fe and $^{208}Pb$ and capture cross-sections of Pb, Bi, $^{232}Th$ and Kr-isotopes had been measured at the Gelina accelerator. A group at IRMM had also studied Doppler broadening of neutron resonances. The Van de Graaff accelerator had mainly been used for measurements of activation and inelastic scattering cross-sections and fission fragment yields and cross-sections. The efforts at Uppsala University covered mainly n-p and elastic neutron scattering as well as (n,xp) and (n, charged-particle) cross-section measurements for ADS applications. The group at Hannover used a number of European and US accelerators to measure activation cross-sections at intermediate energies and the production of radioactive isotopes by protons.

M. Salvatores complemented the European picture by mentioning some additional important measurement projects. The projects mentioned were the EC sponsored HINDAS intermediate energy data

measurement co-operation on Fe, Pb and U, the new nTOF facility at CERN and the French GEDEON project. M. Salvatores also highlighted the need to report on integral data measurements at WPEC meetings, as the results from these integral experiments are often used to validate evaluated data files.

M. Baba presented the Japanese nuclear data measurement activities. Fission neutron spectra of $^{232}$Th, $^{233}$U and $^{238}$U were measured at Tohoku University, as well as neutron elastic scattering cross-sections and double differential cross-sections at 55 to 75 MeV. The (n,p) cross-section on hydrogen had also been measured at 14.1 MeV. Capture cross-sections at low energies were measured at Kyoto University, at Tokyo Institute of Technology and at JNC. Activation cross-sections in the fast neutron range were reported from JAERI FNS, Nagoya University and Osaka University. In the high energy region there had been neutron production measurements at KEK in collaboration with both JAERI and Kyushu University. Riken and JAERI had co-operated with Tohoku University on activation and elastic scattering data experiments in the energy region above 20 MeV.

Liu Tingjin reported on the nuclear data measurements completed in 1999 in China. The following three areas had been covered:

- neutron double differential cross-sections on $^{9}$Be and $^{6,7}$Li had been measured at Peking University and at China Institute of Atomic Energy (CIAE) respectively,
- activation cross-sections at Peking, Sichuan and Lanzhou Universities, and
- fission product yields from $^{235}$U at CIAE.

The WPEC discussed the new measurement facility nTOF under construction at CERN. M. Salvatores forwarded a request from the nTOF scientific programme committee to the WPEC to provide a list of experts that could be consulted in the measurement proposal review process. **The WPEC agreed to establish such a list of experts and to send it to the chairman of the nTOF scientific programme committee**, H. Flocard. The WPEC discussed also the possibilities for non-European measurement groups to use the nTOF facility. **M. Salvatores was asked to find out the conditions and costs for such external groups to have access to the facility.**

## Reports from the chairs of the longer term activities

*Subgroup A (Nuclear Model Codes)*

The WPEC chairman presented the subgroup status report and a proposal for a workshop on nuclear model codes to be held in connection with the next WPEC meeting. The aim of the workshop would be to exchange information with other groups developing nuclear model codes and to clearly define the long-term goal of the present subgroup.

The WPEC felt that the subgroup should put more emphasis on the modularity and standardisation of the different codes under development to facilitate exchange of subroutines. The subgroup co-ordinators were **requested to more clearly specify their short- and long-term goals** and to **clarify the relationship between the subgroup and IAEA projects**, such as the RIPL project. **The WPEC endorsed the proposed workshop** on "Nuclear Reaction Statistical Models and Code Development" and would request NEA support for its organisation.

*Subgroup B (Formats and Processing)*

The WPEC discussed the scope and working methods of the subgroup. It was felt that the subgroup was presently acting mainly as a mailbox for format proposals and that there was a need to have constructive discussions between the evaluation projects before finally submitting proposals to the CSEWG format subcommittee. **The Working Party suggested that A. Trkov, IAEA, take the leading role in this subgroup** and be responsible for the circulation and discussion of format proposals before their final submission to CSEWG.

The WPEC also discussed the maintenance and continued development of the NJOY processing code. This code has evolved into the standard processing code for evaluated nuclear data libraries and was extensively used by all of the participating evaluation projects. **The WPEC expressed concern about the future development of the NJOY code,** considering the importance of the code, and would investigate possibilities to improve the situation.

*Subgroup C (High Priority Request List)*

The NEA Secretariat presented the status of the subgroup. Some work had been recorded but no new request list had been produced. The following three specific activities had been decided at the last WPEC meeting:

- Update the present, rather extensive, request list with information on activities going on in relation to items in the list,
- Reduce the present list to a real high priority request list, and
- Establish an internationally agreed high priority request list for ATW/ADS type of systems.

The work presented at the meeting covered a French effort to establish a request list based on the validation of the JEF-2.2 library and the presentation of a revised Japanese High Priority Request List. A synthesis report of the French activity would be issued within a couple of months.

The WPEC noted that the main support for the high priority request list was to be found in Europe and Japan. It was thus suggested, in order to have an active discussion within the group, to assign a co-ordinator from one of these two regions. **It was agreed to ask T. Fukahori, Japan,** to take the leading role in this subgroup.

**The WPEC confirmed the work programme mentioned above,** as decided at the last meeting.

## Discussion on the status of ongoing and closing subgroups

*Subgroup 6 (Delayed Neutron Data)*

The NEA Secretariat had received the draft final report from the subgroup co-ordinator, A. d'Angelo, in the beginning of December 1999. The report had then been peer-reviewed by J. Rowlands, whose comments had been intensively discussed by the subgroup during the first half of 2000. The main issue was the final recommendation for the delayed neutron data and associated uncertainty of $^{238}$U, for which inconsistent data sets existed.

**The WPEC decided that the report should not try to conclude on the $^{238}$U data,** but rather highlight the discrepancy and leave the issue to be solved at a later stage. **The report should be published before the end of August 2000.**

*Subgroup 7 (Nuclear Data Standards)*

The subgroup co-ordinator, A. Carlson, presented the progress. Most of the progress has been on the database. He informed the WPEC that the work to produce the new standard evaluations would take longer than initially foreseen. This was due both to the time needed to finalise on-going important experiments and also to develop new improved tools for understanding the small uncertainties, which can result from simultaneous evaluation and R-matrix analyses. An IAEA CRP would be started in support of this subgroup which will initially investigate corrections or algorithms used in standard error propagation in simultaneous evaluation or R-matrix analyses.

**The WPEC endorsed the future programme of work** of the subgroup and expressed its appreciation of the supportive IAEA CRP activity.

*Subgroup 9 (Fission Neutron Spectra)*

The WPEC took note of the progress report provided by the subgroup chairman, D. Madland. The work seemed to advance according to schedule and **a draft final report was expected for the next WPEC meeting.**

*Subgroup 10 (Fission Product Inelastic Scattering)*

Following recent discussions with the subgroup co-ordinator, M. Kawai, the WPEC was informed that 70 per-cent of the final report had been written. The remaining 30 per-cent concerned mainly the integral validation of the results. This work would be undertaken in the second half of 2000.

**The WPEC agreed to extend the subgroup for one last year**. G. Rimpault and R. Jacqmin were assigned to be reviewers of the report and they would also be responsible for defining the deadline for the final report.

*Subgroup 11 (Resonance Region of $^{52}Cr$, $^{56}Fe$, and $^{58}Ni$)*

C. Nordborg informed the working party that F. Fröhner had agreed to produce a final report before the end of 2000. The WPEC felt that the most important goal, that of including the resonance parameters in the evaluated data libraries, had been achieved and would welcome a document describing the work performed. **It was agreed to prolong the subgroup for one last year**, pending the final report.

*Subgroup 14 (Processing and Validation of Intermediate Energy Evaluated Data Files)*

A. Koning had distributed the draft final report of the subgroup well before the meeting. The WPEC assigned M. Chadwick and T. Fukahori to review the report before publication. T. Fukahori informed the working party that he had already sent his comments to A. Koning. M. Chadwick would be asked to provide his comments before mid August 2000, **with the goal of having the report published by the end of September 2000.**

## Discussion of proposals for formation of new subgroups

*Neutron Activation Cross Section Measurements from Threshold to 20 MeV for the Validation of Nuclear Models and their parameters*

H. Weigmann presented a proposal by A. Plompen for co-operation between groups that measure activation cross-sections and that also validate nuclear model calculations.

The WPEC felt that the project should not be limited to 20 MeV, as there was presently a very strong interest in the intermediate energy region. In addition, it would be useful to include in the proposal a list of isotopes and energies at which the measurements would be performed, as well as a list of existing measurements. The need to co-ordinate this activity with the IAEA RIPL project was stressed and the relation between the two projects should be clearly defined. Japanese representation in the subgroup should also be specified.

**The WPEC approved the establishment of the subgroup on condition that a revised proposal be issued before end of August 2000,** taking into account the above mentioned comments and suggestions.

*Evaluation, Processing and Practical Use of Covariance Data for the Group-Constant Adjustment*

T. Kawano presented a proposal to start a subgroup on the evaluation, processing and practical use of covariance data in evaluated data libraries. The objectives of the subgroup would be to:

- Develop methods for covariance evaluation,
- Investigate the problems related to the processing of the covariance data, and
- Perform the adjustment of nuclear data with covariance files.

The WPEC expressed strong interest in the proposal, but felt that the scope was somewhat too ambitious and could probably not be completed within the outlined time-schedule. It was suggested to reduce the scope to cover only evaluation methodology and processing of the covariance information, with special emphasis on the resolved and unresolved resonance regions.

**It was agreed that a revised proposal should be produced. This proposal would be reviewed at the next meeting of WPEC.** Some preparatory work, within the reduced scope of the subgroup, could, in the meantime, be undertaken.

## Any other business

A discussion of the recent ENDF/B-VI (release 5) evaluation of U-235 was held. The discussion was initiated by a paper on the benchmark testing of this isotope presented at the Physor2000 conference by the group at Stuttgart University. The paper contained statements such as: "For LWR UOX fuel, however, there is too strong under-prediction of $k_{eff}$ if ENDF/B-VI release 5 for U235 is used. Since no clear dependence of the under-prediction on enrichment can be observed (except for highly enriched systems), one could conclude that the problem lies in the U-235 cross-section itself" and "the results are not acceptable neither for design calculations nor for criticality safety." It is not clear which data ($^{235}U$, $^{238}U$, oxygen or other cross sections) might be responsible for the observed effect.

As this information was too recent for a constructive discussion at this meeting, it was agreed that **the JEFF community would investigate the problem further and report back to WPEC when the complete picture concerning the U-235 was clearer.**

## Time and place of next meeting

Following an invitation from the US delegation, it was decided to hold the next meeting of the Working Party in Santa Fe, USA, in April 12-13, 2001.

# ANNEX 1

## Subgroups Status

### Shorter term subgroups

| | Topic | Co-ordinator | Status in June 2000 |
|---|---|---|---|
| 1 | $^{52}$Cr, $^{56}$Fe & $^{58}$Ni data | C.Y. Fu, USA | Published |
| 2 | Covariance files for Fe | H. Vonach, Austria | Published |
| 3 | Thermal actinide data | H. Tellier, France<br>H. Weigmann, Geel | Published |
| 4 | $^{238}$U capture and inelastic data | M. Baba, Japan | Published |
| 5 | $^{239}$Pu fission cross-section | E. Fort, France | Published |
| *6* | ***Delayed Neutron Data*** | ***A. d'Angelo, Italy*** | ***Modifications to final report before end Aug. 2000*** |
| *7* | ***Nuclear Data Standards*** | ***A. Carlson, USA*** | ***Ongoing*** |
| 8 | Minor Actinide Data | T. Nakagawa,<br>H. Takano, Japan | Published |
| *9* | ***Fission Neutron Spectra*** | ***D. Madland, USA*** | ***Ongoing, to be completed in 2001*** |
| *10* | ***Fission Product Inelastic Scattering*** | ***M. Kawai, Japan*** | ***Final report well before next meeting*** |
| *11* | ***Resonance Region of $^{52}$Cr, $^{56}$Fe, and $^{58}$Ni*** | ***F. Fröhner, Germany*** | ***Final report before end 2000*** |
| 12 | Nuclear Model Validation | M. Chadwick, USA | Published |
| 13 | Intermediate Energy Nuclear Data Evaluation | A. Koning, Holland,<br>T. Fukahori, Japan | Published |
| *14* | ***Processing & validation of intermediate energy data files*** | ***A. Koning, Holland*** | ***Ongoing review of final report; Publication by Sept. 2000*** |
| 15 | Self-shielding treatment in the unresolved resonance region | F. Fröhner, Germany | Published |
| 16 | Nuclear Level Densities for $^{52}$Cr, $^{56}$Fe & $^{58}$Ni | M. Chadwick, USA | Published. |
| 17 | Fission Product Cross-sections for Fast Reactors | H. Gruppelaar, Holland | Published |
| 18 | Epithermal capture of $^{235}$U | C. Lubitz, USA | Published |
| *19* | ***Activation cross-sections*** | ***A. Plompen, IRMM*** | ***Approved; proposal to be updated*** |
| *20* | ***Evaluation and processing of covariance data*** | ***T. Kawano, Japan*** | ***Revised proposal to be reviewed at the next WPEC meeting*** |

## Longer term subgroups

| | | | |
|---|---|---|---|
| *A.* | *Nuclear Model Codes* | *M. Chadwick, USA*<br>*A. Koning, Holland* | *Clarification of goals needed; workshop to be organised* |
| *B.* | *Formats and Processing* | *A. Trkov, IAEA*[*] | *Revision of working methods needed* |
| *C.* | *High Priority Request List* | *T. Fukahori, Japan*[*] | *New version to be compiled* |

[*] Proposed at the WPEC meeting. To be confirmed

## ANNEX 2

**List of Participants at the Twelfth WPEC meeting**
**Japan Atomic Energy Agency (JAERI), Tokai-Mura, Japan, 20 - 21 June 2000**

WPEC Members:

| | | |
|---|---|---|
| C. Dunford | USA | (Chairman/ENDF) |
| C. Nordborg | NEA | (Secretary) |
| M. Baba | Japan | (JENDL) |
| A. Carlson | USA | (ENDF) |
| E. Cheng | USA | (ENDF) |
| R. Forrest | UK | (JEFF) |
| A. Hasegawa | Japan | (JENDL) |
| R. Jacqmin | France | (JEFF) |
| D. Muir | IAEA | (FENDL) |
| M. Salvatores | France | (ex. chairman) |
| K. Shibata | Japan | (JENDL) |
| Liu Tingjin | China | (CENDL) |
| H. Weigmann | IRMM | (JEFF) |
| T. Yoshida | Japan | (JENDL) |

WPEC Observers:

| | |
|---|---|
| J. Chang | Korea |
| T. Kawano | Japan |

## ANNEX 3

**Documents presented at the Twelfth Working Group Meeting**
**Japan Atomic Energy Agency (JAERI), Tokai-Mura, Japan, 20 - 21 June 2000**

| | |
|---|---|
| IEC-209 | Present status of JENDL project; A. Hasegawa |
| IEC-210 | Progress report on the Fusion Evaluated Nuclear Data Library (FENDL); M. Herman and D. Muir |
| IEC-211 | Handbook on photonuclear data for applications; IAEA-TECDOC-Draft No. 3 |
| IEC-212 | Status of Nuclear Data Evaluation Activity in KAERI; J. Chang |
| IEC-213 | Status of the JEFF-3 project; R. Jacqmin |
| IEC-214 | The Present Status of CENDL-3; Liu Tingjin |
| IEC-215 | Cross-section Evaluation Working Group Highlights; C.L. Dunford. |
| IEC-216 | U.S. Nuclear Data Measurement Activities; A. Carlson |
| IEC-217 | Experimental Activities at IRMM; H. Weigmann |
| IEC-218 | Status Report for NEA/WPEC Nuclear Model Code Activity; M.B. Chadwick and A. Koning |
| IEC-219 | Draft Proposal for a Workshop on Nuclear Reaction Statistical Models and Code Development |
| IEC-220 | Subgroup B: Formats and Processing, Status Report; R.W. Roussin |
| IEC-221 | Japanese High Priority Request List; T. Fukahori and A. Hasegawa |
| IEC-222 | Status report from subgroup 6 and subgroup C; E-mail from R. McKnight |
| IEC-223 | Status Report of Subgroup 7 to the NEANSC WPEC: Nuclear Data Standards Evaluation; A. Carlson |
| IEC-224 | Subgroup 9 Status Report: Fission Neutron Spectra; D. Madland |
| IEC-225 | Processing and validation of intermediate energy evaluated data files: Draft final report for subgroup 14; A.J. Koning |
| IEC-226 | WPEC Subgroup Proposal: Neutron Activation Cross-Section Measurements; A. Plompen |
| IEC-227 | WPEC Subgroup Proposal: Evaluation and Processing of Covariance Data; T. Kawano |

# Appendix IX

INDC/P(00)-15
Distr.: G

# Minutes of the 23rd Meeting of the International Nuclear Data Committee

## IAEA, Vienna, Austria

## 24 - 26 May 2000

A.L. Nichols
INDC Executive Secretary
AEA Technology, Harwell
Oxon, OX11 0QJ, UK

June 2000

# Executive Summary

The International Nuclear Data Committee (INDC) meets regularly to provide expert advice and guidance to the International Atomic Energy Agency in the field of nuclear data, and to assist the Nuclear Data Section (NDS) in the formulation of programme plans. Because of the new timetable, in which the IAEA programme and budget is prepared in even-numbered years, the 23rd meeting of the INDC was convened at IAEA Headquarters in Vienna, Austria, from 24-26 May 2000, one year after the previous meeting (instead of the normal two-year spacing). In order to reduce costs, a meeting of three days was held instead of the usual five.

At the request of the Agency, the Section's performance was not reviewed. This was because this topic is now reviewed by the PPAS process. The 23rd meeting focused on a plenary discussion of the data development activities being considered in the NDS for initiation in the 2002-2003 biennium. These discussions examined in detail several potential Co-ordinated Research Projects (CRPs) of interest to IAEA Member States. Two CRPs, in particular, were highly recommended:

- Production and decay data for therapeutic radioisotopes; and
- Improved neutron standards cross sections for light elements.

Two smaller-scale (non-CRP) data development projects were also highly recommended:

- New international reactor dosimetry file, IRDF-2000; and
- Data needs for societal applications.

Following the review of data development plans, two working groups were formed, namely, Working Group 1 on "Nuclear Data Dissemination and Co-ordination", and Working Group 2 on "Technology Transfer and Training".

At the request of the meeting attendees, the working groups also met in plenary, in order to permit participation of the full membership. The conclusions and recommendations of the working groups are given in the main report. Conclusions of particular note are as follows:

- Data network co-ordination by the NDS is extremely important, and efforts must continue in the collection of numerical data and improvement of user services;
- The traditional programme of nuclear data workshops organised jointly with ICTP, Trieste, should be expanded to the level of 5 weeks of training each year; and
- Active NDS participation in the Technical Co-operation Programme, to improve data access and to encourage more effective use of the data, is warmly applauded.

The INDC emphasises that the NDS provides an excellent and essential service to all Member States in a cost-effective manner. Evidence grows of the increasing adoption of electronic means of data and information transfer (rather than postal transmission of magnetic media and hardcopy). The NDS continues to play a pivotal role in this rapidly-emerging technology as the primary international co-ordinator of nuclear data centre networks.

Richard A. Meyer
Chairman
International Nuclear Data Committee

June 2000

# CONTENTS

# WORKING GROUP REPORTS

## WORKING GROUP 1: Nuclear Data Dissemination and Coordination

The WG discussions were held in plenary session.

J. Boldeman (Chair)
A.L. Nichols (Secretary)

The Working Group discussed the most recent activities of the NDS with respect to their dissemination and coordination roles.

- CINDA has been issued in CD-ROM form, with the regular booklet; the INDC believes that hard copies remain important and both forms should be produced, but with greater emphasis placed on CD-ROMs;

- EXFOR represents a primary product of the Nuclear Reaction Data Centre Network, coordinated by the NDS; the INDC acknowledges the excellence of this work and applauds on-going efforts to develop more user-friendly software to interrogate these files;

- The NDS plays an active role in the accumulation of Evaluated Data Libraries from other sources and this important activity must continue;

- Significant improvements continue to be made by NDS staff to facilitate data-user services. These welcome modifications are associated with electronic hardware, Web servers and graphical software. The INDC looks forward to the continuation of these efforts towards maintaining a leading presence in communications technology [for example, DVD-ROM or other high-density storage media, coupled to data centres through the Internet];

- NDS statistical quantification of nuclear data usage reveals the increased adoption of CD-ROMs and access to IAEA-NDS Web site. At the next meeting the INDC would welcome the presentation of equivalent data from other nuclear data centres (e.g., NEA Data Bank, U.S. National Nuclear Data Centre); and

- INDC members consider data network coordination extremely important and stress that this major NDS activity must be maintained.

## WORKING GROUP 2: Technology Transfer and Training

The WG discussions were held in plenary session.

M.A. Lone (Chair)
A.L. Nichols (Secretary)

### Workshops

- INDC encourages NDS to organise timely and appropriate workshops in conjunction with ICTP, Trieste.

- IAEA/ICTP workshops should be run in an open manner, to encourage the attendance of new workers/advanced students from developed countries as well as attendees from developing countries.

- INDC strongly endorses the Section's plan to offer 5 weeks of nuclear data workshop training each year in cooperation with ICTP, Trieste. In particular, the overall plan of offering a 5-week workshop on reactor related data in the even numbered years and 2 weeks of training in data for science and technology plus 3 weeks of nuclear structure data related training in the odd-numbered years is well balanced and appropriate.

- INDC strongly endorses initiation of the new series of IAEA/ICTP Workshops on Nuclear Structure and Decay Data (NSDD). There is an urgent need to hold the first Workshop in 2001 to train young scientists in the state-of-the-art NSDD evaluation methods. This would reverse the present trend of diminishing expertise in many fields of applications, including medical, material analysis and safeguards.

- INDC suggests that NDS develop a mechanism for formal feedback from workshop attendees to help in continual improvement of Workshop contents and operation.

- INDC recommends the formulation of the following workshops:

  (i) Nuclear Data for Science and Technology: Nuclear Analytical Techniques;

  (ii) Repeat of Online Access to Nuclear Data; and

  (iii) Repeat of LINUX Operating Systems.

### Technical Co-operation

- INDC recognises the excellent work of the NDS over the previous year with respect to technology transfer through the data services programme (utilization of Ghana Research Reactor-1; mirror site in Latin America).

- INDC notes that specific initiatives may be funded through the Technical Co-operation Programme. Specific suggestions were noted as possibilities for implementation within the TC framework:

(i) PC-server, Albania;

(ii) Pressure vessel workshop (aging and dosimetry), Prague; and

(iii) Other possible mirror sites.

- INDC strongly supports continued active participation of the NDS in the Agency's TC programme for technology transfer of Nuclear Data Services.

- INDC recognises and appreciates the significant technology transfer components of the NDS programme such as research contracts, workshops and visits of professionals from developing countries.

# FULL REPORT

23rd INDC MEETING
*IAEA Headquarters, Vienna, 24 - 26 May 2000*

## 1. Opening

D.W. Muir (Head, IAEA Nuclear Data Section) welcomed INDC members only one year after their previous meeting. The biennial review and budget assessments within the IAEA have been adjusted from odd to even years, necessitating this 3-day INDC meeting only one year after the 22nd INDC meeting. Emphasis would be placed on work programmes to be possibly undertaken by the Nuclear Data Section (NDS) from 2002 onwards. Since a detailed review of previous NDS work was carried out one year ago, only a relatively brief description would be given of the progress made in 1999 (although a full report had been prepared (INDC(NDS)-414)). The Section expressed its gratitude to Committee member M.A. Lone for providing much needed assistance with the preparations for this INDC meeting.

Various significant changes in personnel were noted:

- R.A. Meyer (INDC Chairman) retires at the end of 2000. His good efforts over five years were highly praised, particularly his ability to forge strong links with senior IAEA management;
- D. Muir (Head, IAEA-NDS) will retire before the next INDC meeting (in 2002);
- P. Oblozinsky (Deputy Head, IAEA-NDS) resigned in March 2000 and has moved to NNDC, Brookhaven National Laboratory; and
- A. Trkov (new Deputy Head, IAEA-NDS) has recently replaced P. Oblozinsky.

Other changes are envisaged during the course of the next two years, including the retirement of specific INDC members and the nomination and appointment of new representatives. Regular replacement of members of the INDC has been a specification that has been neglected in recent years, and this issue will be addressed in an imminent review of the Terms of Reference of the INDC.

Both J. Morales (IAEA-TC Department) and D.D. Sood (IAEA-Director of Division of Physical and Chemical Sciences) attended to listen and respond to the discussion of specific items of the agenda (TC projects within item B.2, and the wide-ranging debate on proposed NDS work programmes within item C.1, respectively). The INDC welcomed their attendance and thanked them for their key roles in support of these activities.

## 2. Chairman's Remarks

The INDC Chairman had noted the desire to focus the limited time of the INDC on the various NDS proposals for work beyond 2001 (including possible Coordinated Research Programmes (CRPs) and data development projects). While NDS staff would present progress reports covering 1999 (summarised below), the committee discussions would focus on the new and reformulated proposals for CRPs, other data development activities, data dissemination and user training (see Agenda, Appendix 1).

After some debate, INDC members agreed unanimously that all working group activities should be conducted in plenary session. Only two detailed reviews were judged to be necessary at this level:

- Nuclear Data Dissemination and Coordination; and
- Technology Transfer and Training.

Detailed debate would also focus on the various proposals for new work programmes that could begin in 2002/2003 (as outlined in INDC/P(00)-1).

Actions from the 22nd INDC meeting were considered (see Appendix 2). A number of these actions are designed to promote good communications between specific individuals and are judged to be continuous/on-going. Other actions are strongly linked with the activities of the NEA Data Bank and need to be pursued together by the two Agencies. Actions that arose during the course of the 23rd INDC meeting are listed in Appendix 3.

## 3. Nuclear Data Section Review: INDC(NDS)–414

### 3.1. Budget and Staffing

Both the budget and staffing levels will remain stable in 2000 and 2001, with 10 professionals and 8 support staff, and total costs of approximately $2.2M per annum. There has been increased activity in the development and implementation of Technical Cooperation projects, and more NDS resources have been directed towards workshops and other training initiatives.

During the previous two years there has been a significant increase in the number of documents made accessible through the IAEA-NDS Web site, and downloaded directly by users in Member States. The net result has been a reduction in the cost of printing hardcopies.

Staff had devoted considerable time responding to the demands of the PPAS (performance assessment) of the Department of Nuclear Sciences and Applications (NA), and providing the necessary briefing material. D. Muir noted that there had been an unusually high level of turnover of professional staff (90%) in NDS between May 1996 and May 2000.

The Terms of Reference of the INDC will have to be revised within the next year by D. Muir and R. Meyer (**ACTION**). While the PPAS of NA did not question the important role of the committee, the need to rotate the membership had been suggested. A redrafting of the Terms of Reference is envisaged, with an overhaul of the appointment and renewal procedures for INDC members.

### 3.2. Operations

The Computer Operations unit had been involved in the following activities during 1999:

- Completion of the Latin American "mirror" project;
- Introduction of Compaq Alpha Server DS20 to replace the AS2100 as the primary NDS server; and
- Placement of NDS Alpha and Ethernet LAN inside a new firewall.

These developments are a continuation of work plans outlined at the 22nd INDC meeting, and their successful completion was applauded.

The Institute IPEN in Sao Paulo, Brazil was chosen as the location for the Latin American mirror server, and a regional workshop was held on 20-24 March 2000 to introduce new users to the Nuclear Data Online Services – Argentina, Brazil, Chile, Columbia, Cuba, Ecuador, Mexico, Paraguay, Peru and Venezuela. This extremely successful initiative was funded through an IAEA Technical Cooperation project.

Nuclear data requests through NDS had been monitored and revealed a significant increase in the accessing of nuclear data files and reports via the Web site. An increase of 30% occurred in 1999 compared with 1998, and this trend is expected to continue in future years. NDS also expects a wider use of CD-ROMs for data distribution.

### 3.3. Nuclear Data Programmes

Specific items were discussed in detail:

- CINDA 2001: Extension of the neutron data bibliography to include charged-particle nuclear data and photonuclear data (to be completed in 2002);
- EXFOR: Include data from SIGMABASE (data base for ion-beam analysis);
- Use EXFOR as an archive for papers published in Phys. Rev. C. The Web version of all relevant articles has a hyperlink to the related EXFOR entry which may contain numerical data not included in the printed version; and
- NDS continues to maintain an updated library of data files and programs with the recent addition of JENDL-3.2, ENDF/B-VI Release 6, PCNuDat and other acquisitions.

Eight Coordinated Research Projects (CRPs) were at various stages of study (or completed) during 1999-2000:

| | |
|---|---|
| • Fission Yield Data (neutron-induced below 20 MeV) | completed 1998 (TECDOC pending) |
| • Photon Production Data | completed 1999 |
| • Charged Particle Cross Sections for Medical Radioisotope Production | completed 2000 |
| • Photonuclear Data | completed 2000 |
| • Fission Yield Data for Transmutation of Minor Actinides | on-going |
| • Update of x- and γ-ray Decay Data Standards for Detector Calibration | on-going |
| • Nuclear Model Parameter Library: Testing (RIPL-2) | on-going |
| • Database for Prompt γ-ray Neutron Activation Analysis | on-going |

Further Coordinated Research Projects are in the process of being started:

- Nuclear Data for Th-U Fuel Cycle to start in 2001
- Transport Simulation of Photon/Electron Radiotherapy to start in 2001

INDC members endorsed the evolution of CRPs through the combined efforts of NDS/INDC review processes. Deliverables are an important feature of these high-quality work programmes, and the procedures adopted to furnish these definitive products should be maintained.

NDS proposals were considered in detail by the INDC, including the reformulation of the approved CRP addressing Nuclear Data for the Production of Therapeutic Radioisotopes. All of the newly-proposed work programmes were classified and prioritised by the INDC after extensive debate in plenary session, and could become new tasks in 2002-2003 (depending on budget constraints). Detailed descriptions of all proposals, as presented for discussion, are given in Appendix 5. Summary opinions of the INDC are given in the 'Comments' column of the Table below:

**RECOMMENDED CRPs & OTHER DATA DEVELOPMENT PROJECTS**

| No | Title | Method | Comments |
|---|---|---|---|
| 1 | Nuclear Data for Production of Therapeutic Radioisotopes | CRP | Endorsed by INDC-22; **highly recommended by INDC-23** |
| 2 | Improved Standards Cross Sections for Light Elements | CRP | Endorsed by INDC-22; **highly recommended by INDC-23** |
| 3 | Modular Library of Standardised Subroutines for Calculation of Cross Sections | CRP | Reformulated: liaise with NEA-WPEC |
| 4 | ACE Format Applications Package of Evaluated Data Libraries including ACE File Transformation and Plotting Utility | CRP | New: **recommended by INDC-23** |
| 1 | New International Reactor Dosimetry File IRDF-2000. | CM/RC | Reformulated: **highly recommended by INDC-23** |
| 2 | Nuclear Reaction Data Base for Accelerator Applications | RC/CM/ AGM | Reformulated: **recommended by INDC-23** |
| 3 | Support of Data Needs for General Societal Applications of Nuclear and Related Technologies | CM/TCM | Reformulated: **highly recommended by INDC-23** |
| 4 | Nuclear Data for Actinides | CM/TCM | Endorsed by INDC-22; **recommended by INDC-23** |

**Points of particular note from the INDC discussions:**

***CRP Proposal #3: Modular Library of Standardised Subroutines for Calculation of Cross Sections***

A WPEC Subgroup is already looking at advances in nuclear model codes (Chadwick, Koning and others) through the Nuclear Science Committee of the NEA. Thus, the NDS needs to liaise with NEA-WPEC members and ensure that work in this area is shared rather than duplicated. The INDC recommends that the NDS work together with the membership of the NEA-WPEC to develop a clearer plan for inter-Agency cooperation in the field of nuclear model codes (**ACTION**).

***Data Development Project Proposal #2: Nuclear Reaction Data Base for Accelerator Applications***

This work programme has significant long-term impact and was discussed extensively. While judged unanimously to be extremely important, the exact form of the activity was felt to be much less clear at the present time.

The evolution of a CRP was judged to be premature, although the IAEA should appreciate the significance of this work in a nuclear context. Under these circumstances, the following statement was prepared and endorsed by the INDC:

> "The Member States of the IAEA have expressed the view that they wish the Agency to be forward looking and not too immersed in past nuclear developments. This view applies to the Nuclear Data Section.
>
> Presently, world uranium resources that can be mined economically amount to slightly more than 3.6 million tons. If the current usage rate of almost 70,000 tons per year continues into the future, nuclear power will be limited to a further 50 years without a new initiative. Future possibilities include accelerator-driven nuclear energy systems and the thorium fuel cycle.
>
> It is imperative that the NDS anticipates these developments and encourages the generation and provision of appropriate nuclear data to ensure that these new initiatives are pursued with the utmost efficiency. The NDS must provide assistance to 'Get to the Future First.'"

***Data Development Proposal #4: Nuclear Data for Actinides***

After an extensive and wide-ranging debate, members focused on whether this proposal should be formulated as a CRP or through a series of technical meetings (i.e., as a data development project). The majority decision was to pursue this need as a data development project to cover Pu, Am and Cm nuclides. Such an approach would ensure that any future CRP in this field would be highly focused and effective.

### 3.4. Technology Transfer

Technical Cooperation (TC) Projects had included assistance in the utilisation of the Ghana Research Reactor-1, and creation of the Latin American "mirror" site. Other opportunities have arisen for future NDS involvement in TC initiatives, particularly a PC server for nuclear data services in Albania and possible mirror site(s) in Asia. An associated workshop is also proposed near Prague in 2001 on Pressure Vessel Performance – ageing and dosimetry.

NDS staff have organised a series of 5-week workshops in conjunction with ICTP, Trieste:

- Nuclear Data for Science and Technology: Medical Physics, 4-15 October 1999;
- Nuclear Reaction Data and Nuclear Reactors: Physics, Design and Safety;

  13 March – 14 April 2000;
- Nuclear Data for Science and Technology: Accelerator-Driven Waste Incineration, 2001; and
- Nuclear Reaction Data and Nuclear Reactors: Nuclear Structure and Decay Data Evaluation, 2001 (approval pending),

  as well as shorter Vienna-based workshops:

- Advanced Nuclear Data Online Services, 29 November – 3 December 1999; and
- Installation and Use of Linux for Nuclear and Atomic Data Computation on Personal Computers, 13-17 December 1999.

The INDC fully supported the involvement of NDS staff in the technology transfer activities undertaken through TC sponsorship and the workshop system. All of the workshops had been well attended, and are essential in maintaining the necessary technical expertise for reactor design and development and other nuclear applications.

## 4. Committee Business

INDC maintained full plenary status during the three days of the 23rd meeting. Two working group sessions were instigated in which the statements and recommendations encompassed the full membership of the INDC. Both summary reports can be found at the beginning of this document.

## 5. Additional Considerations

### 5.1. Advisory Group Meeting on Long Range Needs for Nuclear Data for Applications, 28 November – 1 December 2000

The provisional technical sessions have been formulated by J.W. Boldeman. INDC members judge the Advisory Group Meeting to be extremely important in the evolution of new ideas (and the formulation of nuclear data needs). Specialist input has provided an appropriate forum for such a critical technical meeting:

- New reactor concepts and actinide incineration;
- Accelerator-driven energy systems;
- Nuclear safeguards and related applications;
- Nuclear data for medical applications;
- Nuclear data for astrophysics and space applications; and
- Nuclear data for material and environmental science.

### 5.2. ND2001: Nuclear Data for Science and Technology, Tsukuba, Japan, 7-12 October 2001

A. Hasegawa described the programme of this regular international nuclear data conference, to be held at Tsukuba, Japan. Topics include:

- Nuclear structure and decay data;
- Experimental facilities and measurements;
- Basic nuclear theory;
- Evaluation of nuclear reaction data;
- Evaluated data libraries;
- Processing, testing and verification;
- Fission technology;
- Fusion technology; and
- Standards and dosimetry.

## 6. Other Business

The next INDC meeting is expected to be held in May 2002, at the beginning of the next budget preparation cycle. INDC members will be kept informed of developments. (**ACTION**).

**Appendix 1**

# Final Agenda

## 23rd INDC Meeting
## Vienna, 24-26 May 2000
IAEA , Meeting Room C07-IV

**Wednesday, 24 May**

| | | |
|---|---|---|
| **09:15- 9:35** | **Registration** | *(IAEA desk-Rotunda)* |
| **9:45-11:15** | **A. Opening** | *(Plenary, room C07-IV)* |

- Opening statements
- Statements of INDC members
- Announcements
- Introductions
- Adoption of Agenda
- Adoption of Minutes of the 22nd Meeting

| | | |
|---|---|---|
| **11:15 – 12:00** | **B. Section Review** | *(Plenary, room C07-IV)* |

B.1 Budget, Staffing and Agency Thrust (2000-2001)

- Budget 2000-2001
- PPAS, SAGNA, Major Programmes
- AGM 2000

**12:00 – 13:00** **Lunch**

**13:00 – 16:00** B.2 Nuclear Data Section Activities (1999)

- Computer operations
- Data dissemination
- Network co-ordination
- Nuclear data development
- Technical Co-operation
- Training and workshops

**16:00 – 18:00** **C. Program Review and Suggested Actions (2002-2003)**

C.1 Nuclear Data Development *(Plenary, room C07-IV)*
(Proposals 1-8)

(to be continued on Thursday)

**Thursday, 25 May**

**C. Program Review and Suggested Actions for Future**
*(Plenary, room C07-IV)*

**08:30 – 09:30** C.1 Nuclear Data Development *(Plenary, room C07-IV)*
(Proposals 1-8, continued from Wednesday)

**09:30 – 11:00** C.2 Data dissemination and International co-ordination (WG1)
*(Plenary)*

**11:00 – 12:30** C.3 Training and technical co-operation (WG2)
*(Plenary)*

**12:30 – 13:30** **Lunch**

**13:45 – 17:30** **D. Production of Final Product** *(Plenary, room C07-IV)*

D.1 Discussion of area conclusions
D.2 Drafting of WG reports

**Friday, 26 May**

**08:45 - 16:00** **E. Summary and Concluding Activities** *(Plenary, room C07-IV)*

E.1 Presentation and discussion of WG reports
E.2 Other business
E.3 Adjournment